GDAŃSK UNIVERSITY OF TECHNOLOGY

The author of the doctoral dissertation: Kirill Fedorov
Scientific discipline: Chemical Sciences

DOCTORAL DISSERTATION

Title of doctoral dissertation: Degradation of organic water pollutants using hybrid cavitation-based advanced chemical processes.

Title of doctoral dissertation (in Polish): Degradacja organicznych zanieczyszczeń wody z zastosowaniem hybrydowych zaawansowanych procesów chemicznych wykorzystujących zjawisko kawitacji.

Supervisor:
PhD, D.Sc., Eng. Grzegorz Boczkaj, Professor (Associate).

Gdańsk, 2026

GDAŃSK UNIVERSITY OF TECHNOLOGY

STATEMENT

The author of the doctoral dissertation: Kirill Fedorov

I, the undersigned, declare that I am aware that in accordance with the provisions of Art. 27 (1) and (2) of the Act of 4th February 1994 on Copyright and Related Rights (Journal of Laws of 2021, item 1062), the university may use my doctoral dissertation entitled:
"Degradation of organic water pollutants using hybrid cavitation-based advanced chemical processes"
for scientific or didactic purposes.[1]

Gdańsk, ...
signature of the PhD student

Aware of criminal liability for violations of the Act of 4th February 1994 on Copyright and Related Rights and disciplinary actions set out in the Law on Higher Education and Science (Journal of Laws 2021, item 478), as well as civil liability, I declare, that the submitted doctoral dissertation is my own work.

I declare, that the submitted doctoral dissertation is my own work performed under and in cooperation with the supervision of prof. dr hab. inż. Grzegorz Boczkaj.

This submitted doctoral dissertation has never before been the basis of an official procedure associated with the awarding of a PhD degree.

All the information contained in the above thesis which is derived from written and electronic sources is documented in a list of relevant literature in accordance with Art. 34 of the Copyright and Related Rights Act.

I confirm that this doctoral dissertation is identical to the attached electronic version.

Gdańsk, ...
signature of the PhD student

I, the undersigned, agree to include an electronic version of the above doctoral dissertation in the open, institutional, digital repository of Gdańsk University of Technology.

Gdańsk, ...
signature of the PhD student

[1] Art 27. 1. Educational institutions and entities referred to in art. 7 sec. 1 points 1, 2 and 4–8 of the Act of 20 July 2018 – Law on Higher Education and Science, may use the disseminated works in the original and in translation for the purposes of illustrating the content provided for didactic purposes or in order to conduct research activities, and to reproduce for this purpose disseminated minor works or fragments of larger works.

2. If the works are made available to the public in such a way that everyone can have access to them at the place and time selected by them, as referred to in para. 1, is allowed only for a limited group of people learning, teaching or conducting research, identified by the entities listed in paragraph 1.

GDAŃSK UNIVERSITY OF TECHNOLOGY

DESCRIPTION OF DOCTORAL DISSERTATION

The Author of the doctoral dissertation: Kirill Fedorov

Title of doctoral dissertation: Degradation of organic water pollutants using hybrid cavitation-based advanced chemical processes.

Title of doctoral dissertation in Polish: Degradacja organicznych zanieczyszczeń wody z zastosowaniem hybrydowych zaawansowanych procesów chemicznych wykorzystujących zjawisko kawitacji.

Language of doctoral dissertation: English

Supervisor: PhD, D.Sc., Eng. Grzegorz Boczkaj, Professor (Associate).

Date of doctoral defense:

Keywords of doctoral dissertation in Polish: kawitacja, AOPs, ARPs, kawitacja hydrodynamiczna, kawitacja akustyczna, degradacja, utlenianie, rodniki

Keywords of doctoral dissertation in English: cavitation, AOPs, ARPs, hydrodynamic cavitation, acoustic cavitation, degradation, oxidation, radicals.

Summary of doctoral dissertation in English

This doctoral thesis investigates hybrid cavitation-based advanced chemical processes for the degradation of organic pollutants in aqueous conditions. Initially, hybrid processes combining acoustic (AC) or hydrodynamic cavitation (HC) with ozone- and sulfate radical-based advanced oxidation processes (AOPs) were developed and evaluated towards the degradation of BTEXs and 1,4-dioxane. Then HC was integrated with the emerging sulfite/UV advanced reduction process (ARPs) to degrade halogen-containing organic pollutant - clofibric acid (CLA). The effect of solution pH, reagent (radicals precursor)/pollutant molar ratio and common inorganic anions was studied. Radical quenching experiments were performed to determine the predominant radical species responsible for the degradation of pollutants. Based on the reaction intermediates identified in GC-MS and HPLC-UV-DAD, the degradation pathways of pollutants were proposed. The findings demonstrated the key role of cavitation in the hybrid processes performing activation and intensifying the AOPs as well as ARPs leading to high synergistic effect. In the case of HC/ARP, the presence of the reductive species was confirmed and their reactivity with CLA was supported by theoretical calculations - revealing enhanced generation of reductive species and reduced scavenging effect of dissolved oxygen on sulfite/UV when coupled with HC.

Streszczenie rozprawy w języku Polskim

Niniejsza rozprawa doktorska dotyczy badań nad hybrydowymi, kawitacyjnymi zaawansowanymi procesami chemicznymi do degradacji organicznych zanieczyszczeń w warunkach wodnych. Opracowano i oceniono procesy hybrydowe łączące kawitację akustyczną (AC) lub hydrodynamiczną (HC) z zaawansowanymi procesami utleniania (AOPs) opartymi na ozonie lub rodnikach siarczanowych, które zastosowano do degradacji związków z grupy BTEX oraz 1,4-dioksanu. Następnie HC zintegrowano z zaawansowanym procesem redukcyjnym (ARP) anion siarczynowy/UV w celu degradacji halogenowanego zanieczyszczenia organicznego - kwasu klofibrynowego (CLA). Zbadano wpływ pH roztworu, molowego stosunku prekursora rodników do zanieczyszczenia oraz obecności anionów nieorganicznych. Dominujące formy rodnikowe określeno na podstawie eksperymentów wygaszania. Na podstawie produktów pośrednich zidentyfikowanych metodami GC-MS i HPLC-UV-DAD zaproponowano ścieżki degradacji zanieczyszczeń. Uzyskane wyniki badań wykazały kluczową rolę kawitacji w aktywacji reagentów oraz intensyfikacji zarówno AOPs i ARPs, prowadząc do wysokiego efektu synergistycznego. W układzie HC/ARP potwierdzono obecność reaktywnych form redukcyjnych, a ich reaktywność względem CLA poparto obliczeniami teoretycznymi, ujawniając zwiększoną generację form redukcyjnych oraz ograniczenie wygaszania rodników przez rozpuszczony tlen w procesie anion siarczynowy/UV sprzężonym z HC.

Acknowledgements

I would like to express my deep gratitude to my supervisor Prof. Grzegorz Boczkaj, who once gave me a chance to begin my scientific journey at Gdansk University of Technology. His patient guidance, expertise and support helped me to grow as a researcher and finish this study. I appreciate his constant encouragement during these years and the time we spent discussing various research questions. Looking back, it was a long journey full of curiosity, discovers and obstacles, which constitutes a special period in my life.

I would also like to extend my thanks to the people from the laboratory who contributed to this work. I want to thank Michał Gągol, who introduced me to the operation in the hydrodynamic cavitation reactor and Maksymilian Plata-Gryl for his help whenever I had problems with GC-FID. I owe special thanks to my colleague Elvana Çako, with whom I started my PhD and developed new skills together. I am thankful to the members of our laboratory for their assistance as well as sharing ideas and skills.

I am grateful to Gdansk University of Technology for providing research environment. In particular, I thank the staff of the Faculty of Chemistry and the Faculty of Civil and Environmental Engineering as well as the main library branch in Nanotechnology Centre Building, where this work was written. I also express my gratitude to the Doctoral School for help and financial support. Besides, I would like to acknowledge the financial support from the National Science Centre (Warsaw, Poland), which made the presented work possible.

A special thanks go to my family, to my dearest mother.

Table of Contents

List of Figures

List of Tables

Abbreviations and Acronyms

AC	-	acoustic cavitation
ANOVA	-	analysis of variance
AOPs	-	advanced oxidation processes
APIs	-	active pharmaceutical ingredients
ARPs	-	advanced reduction processes
BOD	-	biochemical oxygen demand
BTEX	-	benzene, toluene, ethylbenzene, o-xylene
CCD	-	central composite design
CLA	-	clofibric acid
CLF	-	chloroform
COD	-	chemical oxygen demand
DFT	-	density functional theory
DFUS	-	dual-frequency ultrasound
DLLME	-	dispersive liquid-liquid microextraction
DO	-	dissolved oxygen
DOC	-	dissolved organic carbon
DOM	-	dissolved organic matter
EGDF	-	ethylene glycol diformate
EPR	-	electron paramagnetic resonance
Eq.	-	equation
Fig.	-	figure
GC-FID	-	gas chromatography with flame ionization detector
GC-MS	-	gas chromatography-mass spectrometry
HA	-	humic acids
HC	-	hydrodynamic cavitation
HOMO	-	highest occupied molecular orbital
HPLC-UV-DAD	-	high-performance liquid chromatography with ultraviolet-diode array detector
IPA	-	isopropyl alcohol
LUMO	-	lowest unoccupied molecular orbital
MeOH	-	methanol
NHE	-	normal hydrogen electrode

PAHs	-	polycyclic aromatic hydrocarbons
p-BQ	-	para-benzoquinone
PFAS	-	per- and polyfluoroalkyl substances
PhOH	-	phenol
PMS	-	peroxymonosulfate
POPs	-	persistent organic pollutants
PS	-	persulfate
ROSs	-	reactive oxygen species
RSM	-	response surface methodology
SFUS	-	single-frequency ultrasound
SPC	-	sodium percarbonate
SR-AOPs	-	sulfate anion radical-based advanced oxidation processes
TBA	-	*tert*-butyl alcohol
TOC	-	total organic carbon
US	-	ultrasound/ultrasounds
USEPA	-	the United States Environmental Protection Agency
UV	-	ultraviolet
VOCs	-	volatile organic compounds
WWTPs	-	wastewater treatment plants
ZVI	-	zero valent iron

1. Literature review

1.1. Introduction to wastewater treatment methods

The global demand in safe and clean water is increasing with rapid industrialization and the growing number of human populations. The issue of water scarcity is also worthened with the detection of chemical pollutants in various environmental water bodies, such as surface and groundwaters. In this sense, exploring efficient methods of water treatment and wastewater reuse is critical to ensure long-term access to safe water. Due to the high content of pollutants, industrial wastewaters pose a significant risk to human health and environment. The adverse effect, usually represented by toxicity may differ depending on the source of wastewater and chemical composition. Consequently, wastewaters constituted by biodegradable substances can be easily treated for reuse, whereas the wastewaters i.e., effluents from industrial sectors, such as steel production require more complex treatment. For instance, the wastewaters generated from sugar industry can be effectively treated by initial filtration, sedimentation followed by a biological treatment [1]. In the case of coke oven wastewaters from steel manufacturing sites, the load of contaminants is comprised of highly toxic phenol, cyanide and ammonia [2]. Conventional treatment strategies include sand filtration, chemical neutralization and activated sludge process. However, these methods are insufficient to completely degrade the pollutants and meet effluent standards.

To increase the effectiveness, additional methods, such as adsorption, precipitation, coagulation, electrolysis and ozonation are frequently employed in the treatment of coke wastewaters. Hence, it is clear that the composition and toxicity of wastewaters is dependent on the industry sector and the appropriate treatment strategies may include a wide variety of methods. In order to meet the criteria of discharge standards, wastewaters undergo decontamination in wastewater treatment plants (WWTPs) through four purification levels. The initial preliminary step involves the elimination of unwanted debris, floating solids and suspended particles from the effluent. Then, the effluent proceeds to the primary level, where the part of suspended particles and organic matter are precipitated. In the secondary treatment level, the residual suspended solids, biodegradable organic and nutrients (e.g., nitrogen, phosphorus) are removed *via* biological processes. Finally, specific water pollutants persistent to biological methods are

removed at the tertiary level. In this level, the pre-treated effluent containing non-biodegradable pollutants undergo purification using advanced treatment methods prior to discharge or reuse. The tertiary level treatment is also employed to prevent the secondary pollution, which can be caused by the incomplete mineralization of pollutants or formation of salts.

Nowadays, wastewater treatment strategies involve a multitude of methods the sequential or combined operation of which can provide the effective decontamination of wastewaters. Based on the type of action, these methods can be classified as physical, chemical and biological. The physical methods utilize physical and mechanical forces for wastewater treatment. The processes, such as sedimentation, screening, aeration, filtration and flotation are amongst the most commonly used physical wastewater treatment methods. Biological methods are based on the removal of water pollutants using biological processes under aerobic and anaerobic conditions, such as activated sludge and anaerobic digestion. The chemical methods employ chemical transformations to remove water pollutants which are induced by the addition of reagents. These methods include chlorination, ozonation, adsorption, coagulation, neutralization, ion exchange and advanced chemical processes.

1.2. Physical methods

1.2.1. Screening

As an initial step of the preliminary level of treatment, screening represent a simple method that plays an important role in preparation of the wastewater for the further levels. The aim of screening is to eliminate large solids and coarse suspended matters, which can be plastics, fibers, rags, paper waste. By removing the unfavorable substances, the screening method ensures the safety of the subsequent levels of treatment protecting the equipment from mechanical damages and clogging. Considering the structure and required filtration level, the screening is categorized into coarse, fine and micro fine screen. The size of openings in coarse screen exceeds 6 mm and is applied for separation of large solids and floating matter from wastewater. The separation is conducted in mechanically cleaned bar screens, reciprocating rake screens and catenary screens. Owing to the opening size in the range of 0.01-0.1 mm, the fine screening is employed to separate smaller solid particles dispersed and, thereby, preparing wastewater for primary treatment levels. The equipment like rotating drum screen

and traveling water screens are considered as effective solutions of fine screening. The micro fine screening with opening sizes in the range of 0.001-0.3 mm is primarily applied for the preparation of the secondary effluent for tertiary treatment levels. In this method, wastewater is forced to flow into a central drum equipped with filter media, which capture the highly dispersed particles by physical blocking in well-defined apertures [3]. Using the micro fine screening installation with opening size of 0.02 mm, 75-85% of solids were removed providing a consistent effluent concentration of 0.005 g/L. In order to prevent the accumulation and clogging, the separated solids should be removed from the screens frequently. The collected solid waste should be disposed properly by burying, incineration or grinding.

1.2.2. Sedimentation

The physical method of sedimentation is a fundamental unit operation in wastewater treatment. The method is based on the sedimentation induced by the gravitational force and allows to effectively isolate remaining suspended solids and organic matter. In WWTPs, the effluent from the preliminary level of treatment undergoes the removal of grit – sand, gravel, insoluble salts and other discrete inorganic particles larger than 0.21 mm [4]. The grit removal is carried out in horizontal flow grit chamber, aeration grit chamber or vortex flow grit chamber depending on the application scale and effluent characteristics. After removing heavy particles, the wastewater flows into the sedimentation tanks, i.e., primary and secondary settling tanks. The primary settling tanks are connected along with the frit chamber and target light organic matter. In this stage, the settling proceeds at lower flow velocity and the concentration of particles as well as their size distribution is lower as the sludge in primary settling tanks is not activated. On the other hand, the secondary settling tanks are incorporated with biological treatment methods, specifically, for separation of heavy biological sludge from wastewater. Installed after mixers and activation tanks, secondary settling tanks operate at higher concentration of particles with a wide range of size distribution [5]. As the layer of settled particles thickens, the sludge (e.g., biomass) is removed for disposal or returned to the biological reactor. By assuring the effective removal of precipitated solid waste, the sedimentation reduces the failure risk of the exploited equipment. Additionally, it decreases the turbidity and contamination load of the wastewater for the subsequent secondary and tertiary level of treatment. Owing to its simple operation concept with low energy demand, sedimentation represents

an important component of sustainable wastewater treatment strategies. It is performed in horizontal flow, solid contact and inclined surface sedimentation tanks [6]. Taking into account the factors affecting the sedimentation (e.g., temperature, flow velocity and time of settlement), more comprehensive modifications of settling tanks is designed with assistance of computational methods.

1.2.3. Flotation

Originated from mineral processing, flotation represents a unique physical method that operates in three phases: gaseous, liquid and solid. The concept of flotation is based on capture of light solid particles (or oil droplets) using gaseous bubbles and subsequent isolation in flotation tanks. In wastewater treatment, the introduced gas bubbles may adhere to the solid particles by electrical attraction, chemical adsorption or being physical trapped and transport them to the surface. The floated waste is accumulated at the surface of the flotation chamber forming a layer which is removed by skimming. Hydrophobic particles solids as well as suspended liquids, including oils and grease are easily isolated by flotation, and its separation effectiveness can be improved towards other pollutants. In particular, the separation can be improved by adding flocculants and coagulants that promote the aggregation of particles. Based on the method used to generate the gaseous bubbles, two categories of flotation can be distinguished: dispersed-air and dissolved-air flotation. In dispersed-air flotation, the air flow is introduced using diffuser installed at the bottom of the floatation column at atmospheric pressure. In this method, the size of generated bubbles reaches 1000 μm and the residence time is in the range of 4-6 min [7]. In the case of dissolved-air flotation, the air is saturated in wastewater under elevated pressure (i.e., 2.06-2.76 bar) and the air is released as minute bubbles after pressure recover. The residence time in dissolved-air flotation is approx. 30 min and the size of generated bubbles ranges from 10 to 120 μm. The application of flotation in WWTPs allows to remove smaller organic matter, light particles and oil droplets at shorter retention time. Currently, flotation is an essential part of WTTPs dealing with effluents of petrochemical industry [8], mineral processing [9], pulp and paper production [10,11]. Moreover, flotation is recently involved in wastewater treatment technologies addressing water pollution caused by microplastics and antibiotics [12].

1.2.4. Aeration

Aeration is another physical method adopted in WWTPs that utilize gaseous phase for the removal of dissolved pollutants and gaseous contaminants. This method is based on the absorption and circulation of air or pure oxygen over the water body to accelerate the mass transfer and remove the dissolved pollutants. The main operation principle of aeration is to increase the content of dissolved oxygen (DO) in wastewater and generation of highly-dispersive gaseous bubbles and promotes desorption of dissolved gases (e.g., CO_2, H_2S), volatile organic compounds (VOCs) [13]. In addition, aeration provides DO necessary for the sustainable growth of microorganisms exploited in biological processes. Depending on the approach used to increase the level of DO, the aeration can be natural and artificial. The natural aeration is accomplished by atmospheric diffusion and photosynthesis of plants. The artificial aeration refers to the increase contact area in water-air interface and intensifying the air absorption by mixing. The artificial aeration can be achieved using: 1. Surface aerators, which utilize mechanical energy to break down water into droplets using paddle wheel aerators, spiral aerators, pump-sprayers, vertical pump aerator; 2. Bubbling aerators that release air bubbles in water using the propeller-aspirator pump and submersible aerators; 3. Gravity aerators, such as weir aerator and circular stepped cascade aerators where the water flows over the ladder steps [14]. The effectiveness of aeration systems is measured by oxygen transfer rate, which rely on the quantification of oxygen mass transferred into the water body per a unit of time. Aeration is energy-intensive and consumes from 50% to 90% of electric power supplied to WWTPs demanding 0.18-0.8 kWh/m^3 [15]. The assessment of economic feasibility, particularly, electric energy consumption along with aeration performance is crucial when comparing different aeration systems. Hence, aeration efficiency showing oxygen transfer rate at electric power consumption can be useful when comparing the aeration systems. The aeration efficiency of gravity aerators, specifically, observed in circular stepped cascades was in the range of 2.16-2.70 kgO_2/kWh, while it was in the range of 1.1-3.3 kgO_2/kWh and 1.34-1.48 kgO_2/kWh in case of paddlewheel aerators and vertical pump sprayers, respectively [14,16]. Insufficient aeration is associated with low concentration of DO, which is detrimental to the quality of the effluent. In such a scenario, the growth of microorganism necessary for the biological treatment is inhibited and proliferation of filamentous bacteria and expansion of a sludge in aeration tank [17]. This suggests that the control and

optimization of aeration is vital to ensure high treatment efficiency of pollutants, lower energy consumption and overall operating cost.

1.2.5. Adsorption

The separation of water pollutants can also be accomplished by adsorption onto the surface of solid substrates. In WWTPs, adsorption occurs in the liquid-solid system, whereat the pollutant substrate is accumulated at the interface of the adsorbent. The adsorption processes are often employed to effectively separate and remove dissolved water pollutants remaining after biological treatment and chemical oxidation. Moreover, the adsorptive methods are capable to capture trace heavy metals (e.g., Cd, Cr, Hg) from wastewater, which can be recovered for further utilization. Since adsorption can be performed using readily available materials in reactors of versatile design, the adsorptive methods of water purification are recognized as economically and technically feasible. The process of adsorption in WWTPs is conducted in batch or continuous reactor systems using packed-bed columns, which are suitable for large-scale water purification at short time operation. The selection of an appropriate adsorbent involves the assessment of the adsorbent's capacity and effectiveness towards the target pollutant at given concentration level and conditions. The interaction between the pollutant and adsorbent surface can be established through weak physical forces, such as van der Waals forces, which imply a reversable process. In this case, the adsorption is classified as physisorption. On the other hand, the molecule of the pollutant can interact with the adsorbent resulting in the formation of stronger chemical bonds. This type of adsorption is often irreversible and called chemisorption. The industrial application of adsorbents requires widespread abundance, stability, developed surface morphology and high specific surface area. Activated carbon is a universal adsorbent widely applied in various industries including wastewater treatment. The dominance of activated carbon over other commercial adsorbents is reasoned by the increased adsorption capacity, non-toxicity, selectivity and thermal stability throughout the multiple cycles of regeneration. Moreover, adsorption on activated carbon was recommended by the US Environmental Protection Agency (USEPA) for the removal of toxic organic pollutants from drinking water. This was motivated by the inadequate effectiveness of conventional water treatment methods based on biological processes towards complex pharmaceutical contaminants. Thus, it was demonstrated that 73-84% of acetaminophen, 74-86% of carbamazepine and 90-96% of triclosan can be effectively removed by activated carbon in both granular

(GAC) and powdered (PAC) forms. Being produced via simple carbonization followed by activation, both forms activated carbon offer high surface area (i.e., 600-2000 m^2/g) and high pore volumes, which are beneficial for the adsorptive removal of water pollutants. Recently, increasing number of studies report the preparation of low-cost carbonaceous adsorbents from plant waste and sewage sludge. The obtained adsorbents exhibited high capacity for the adsorption of metals, such as Cu^{2+}, Ni^{2+}, Pb^{2+} and dyes, including methylene blue, indigo carmine and acid brown. Nevertheless, the commercial activated carbon is considered expensive mainly due to the energy intensive preparation method that involves a calcination at about 900 ºC. Therefore, commonly available, low-cost adsorbents, such as natural zeolites, activated alumina and silica-gel are of great potential in industrial use. Naturally occurring zeolites are hydrated aluminosilicate minerals characterized with large specific surface area, high thermal stability and ion exchange capacity. The primary building block of zeolites are tetrahedrons containing Si or Al atom in the center [18,19]. Such coordination leads to the negative charge in the zeolite framework, which is compensated by other cations located in the micropores of the framework. In wastewater treatment, natural and synthetic zeolites are used for the removal of dissolved ammonia (NH_4^+) and heavy metals through the ion exchange interaction. For instance, natural clinoptilolite zeolite can effectively remove NH_4^+ with an adsorption capacity of 2-30 mg/g releasing environmentally acceptable cations, e.g., Na^+, K^+, Ca^{2+}. Natural clinoptilolite was also found effective for the removal of heavy metals, such as Pb^{2+}, Cd^{2+} and Cr^{3+} demonstrating the adsorption capacity of 0.234-0.345 meq/mg, 0.12-0.18 meq/mg and 0.237 meq/mg, respectively [19]. The increased uptake of a metal ion from wastewater systems is varied depending on the utilized zeolite. In particular, clinoptilolite shows high selectivity towards Pb^{2+} and Sr^{2+}, while scolecite-based zeolite effectively adsorbs Cu^{2+} and Zn^{2+}[20,21]. Zeolites and its modified variations are being also investigated for the adsorptive removal of organic contaminants [22], dyes [23] and other water constituents, such as humic acids and inorganic anions [24,25]. It's worth to note that natural diatomite and clinoptilolite tested for the removal of naphthalene, *o*-xylene and toluene exhibited negligible sorption of naphthalene from water [22]. However, the adsorptive removal of the studied pollutants was correspondingly increased to 71%, 60% and 30%, respectively, for diatomite upon the surface modification using diphenyldichlorosilane. In the case of the modified clinoptilolite the adsorption of naphthalene, *o*-xylene and toluene were 51%, 30% and 16%, respectively. Unlike the ion exchange interaction, the mechanism behind the enhanced adsorption in

the modified zeolites was due to the increased affinity to aromatic compounds. This was enabled by the modification of zeolites using chlorosilane containing aromatic moieties. Besides carbon-based adsorbents and zeolites, activated alumina and silica-gel are also frequently involved in wastewater treatment. Hence, activated alumina also known as amorphous aluminum oxide is often used for the treatment of fluoro-containing wastewater [26]. Although adsorption on activated alumina is capable to ensure high extend of defluorination at low cost, the effective fluoride uptake occurs at narrow pH range. Thus, the maximum fluoride removal of 1450 mg/kg was observed at pH 7 during the treatment of F^- solution with initial 13.8 mg/L with 4 g/L of activated alumina [27]. It was proposed that the lower defluorination efficiency at lower pH < 7 was due to the formation of soluble Al-F complexes, while HO^- compete with F^- for ion exchange at basic pH. To improve the adsorption capacity, the surface and morphology of activated alumina is modified through physical and chemical treatment, including functionalization and impregnation of metals [26]. The novel composites with improved affinity to the target pollutant along with large specific surface area are continuously developed throughout the decades. However, the cost of preparation which may involve energy-intensive steps of calcination as well as the need in expensive noble metals. Therefore, various low-cost and environmentally safe materials abundant in nature are recently tested as a potential adsorbent in wastewater treatment. These non-conventional adsorbents mainly derive from a biomass produced from agriculture and forestry, namely, corn straw, rice husk, cellulose, chitosan, sawdust [28].

1.3. Biological treatment methods

1.3.1. Aerobic processes

Biological treatment methods represent an essential and energy-intensive stage of conventional WWTPs that accounts over 60% of the total energy consumption. In this stage, biodegradable and suspended organic matter are degraded exploiting the activity of microorganisms. Taking into account that the effectiveness of these methods is based on metabolic processes and cell synthesis of living microorganisms, the effect of operating parameters, such as temperature, pH, the presence or absence of oxygen, toxic compounds and elements is significant. Hence, the optimization of these parameters is crucial for the development and maintenance of the microbial community. Depending on the involvement of the

molecular oxygen, biological methods are classified into aerobic and anaerobic processes. In aerobic process, the degradation of organic pollutants, NH_4^+ as well as NH_3 proceeds in the presence of oxygen as electron acceptor. The oxidation of the organic matter proceeds in the presence of microorganism (e.g., *Achromobacter*, *Beggiatoa*, *Flavobacterium*) releasing carbon dioxide (CO_2) and water as the final product. In the case of NH_4^+, NH_3, the oxidative transformations are known as nitrification, which is commonly facilitated by *Nitrobacter* and *Nitrosomonas* to yield nitrate ions (NO_3^-). Subsequently, NO_3^- can be further reduced to molecular nitrogen (N_2) during the denitrification process. The effectiveness of these transformations is measured by biochemical oxygen demand (BOD) – a parameter that indicate the content of molecular oxygen consumed by microorganisms to proceed the biological decomposition the organic matter. Hence, a considerable reduction of the BOD implies a higher extend of degradation of organic pollutants.

In the aerobic processes the biomass containing the microorganism can be suspended in the volume of the effluent or attached to the surface. Specifically, a portion of microorganisms can be placed in aeration tank and mixed with the effluent received from the primary clarifier. To maintain the aerobic conditions and ensure the growth of the suspended microorganism, a stream of air or pure oxygen are supplied. After achieving the target extend of the degradation efficiency, the mixture is passed to the settling tank where the biomass is separated as a sludge. The sludge containing the active microorganism can be used for another cycle of aerobic process, which is known as activated sludge process. In combination with primary treatment methods (e.g., sedimentation, floatation), activated sludge process is capable to attain 90% of BOD reduction from wastewaters. Nevertheless, high energy cost due to the required step of aeration remains as the main drawback of activated sludge process. Application of tricking filters for the biological treatment of wastewaters is considered more economically viable. In this aerobic process, the wastewaters are flowed through the cylindrical tanks packed with materials, such as small rocks, plastics and ceramics. The population of microorganisms is attached onto these materials and the organic matter along with ammonia are biodegraded as the wastewater trickles along the filter. Besides the lower cost, the installation for tricking filters is compact and easy in operation. In addition, the utilized microorganisms possess resistance to shock loads of contaminants. As compared to activated sludge process, tricking filters are insufficient to provide a high level of BOD reduction when treating high volume flows of wastewater. Therefore, the application of tricking filters is preferred in

WWTPs of smaller communities or certain industries. Rotating biological contactors represent another solution of anaerobic processes in biological treatment of wastewaters. In this, the film of microorganisms is attached on a series of closely spaced circular discs. The disks are that is submerged in 40% above the surface of wastewater. When exposed to air, the microorganism consume oxygen and contact with organic pollutants inside the wastewater. Similar to tricking filters, the application of rotating biological contactors is preferred for small decentralized WWTPs and the utilized microorganisms are stable against shock loadings. Moreover, the usage of discs and simple design make this approach free of clogging, which may occur in filter nozzles in tricking filters installations.

1.3.2. Anaerobic processes

These processes of biological treatment are conducted in oxygen-free conditions with utilization of anaerobic microorganisms. Since O_2 is detrimental to the most of those microorganisms, the atoms of sulfur (S) and CO_2 serve as final electron acceptors in the system. The microorganisms convert the organic content of the wastewater into hydrogen (H_2), CO_2 and methane (CH_4), which represent a potential source of energy accounting over 80% of the generated biogas [29]. The anaerobic processes are capable to remove 90% of the organic content and significantly reduce the formation of a sludge as compared to aerobic processes [30]. Therefore, anaerobic digestion is not only an effective wastewater treatment tool, but also a viable approach of energy recovery. This is due to the fact that anaerobic processes offer economic benefits from low sludge disposal cost and energy production from the captured CH_4. Specifically, CH_4 can be burned on site to produce heat for biological processes or stored for generation of electricity, while the digested sludge can be further utilized as a biofertilizer [31].

Considering CH_4 as a final product, the process of anaerobic digestion of organic matter can be studied as chemical transformations steps of methanogenic fermentation. Hence, the anaerobic processes consist of three transformations steps that occur simultaneously conducted in the presence of different microorganisms and yielding different products. The initial step is hydrolysis or liquefaction, in which complex organic macromolecules and polymers are fragmented into low molecular organics, such as dimers and monomers [32,33]. For example, proteins can be hydrolyzed into amino acids, while polysaccharides into monosaccharides, which can be metabolized by anaerobic microorganisms. The step of hydrolysis is also responsible for the conversion of insoluble organic

matter into smaller molecules with the help of extracellular enzymes, such as protease, cellulase and lipase [34,35]. The impact of hydrolysis significantly affects the biodegradation in the subsequent steps. Low molecular compounds generated during hydrolysis are further converted into short chain organic acids, alcohols, CO_2 and H_2 during the step of acidogenesis. The products of acidogenesis are strictly dependent on the type of microbes and conditions. Carboxylic acids are mainly produced as a result of metabolism of *Bifidobacterium*, *Clostridium* and *Lactobacillus*, while acetogenic bacteria, such as *Syntrobacter wolini* and *Syntrphomonas wolfei* hydrogen are known to produce hydrogen, acetate ion (CH_3COO^-) and CO_2 [36,37]. The final step of the anaerobic digestion is named methanogenesis, in which CH_4 is formed as a final product. Since CH_4 can be produced from various precursor compounds depending on the nutritional requirements of microorganisms, three different routes of methanogenesis can be distinguished. Hence, methanogens, such as *Methanomicrobiales*, *Methanopyrales* and *Methanocellales* can consume CO_2 and H_2 to produce CH_4 and H_2O [38]. On the other hand, *Methanosarcinales* are capable to decompose acetic acid into CH_4 and CO_2, while ethanol can be consumed by *Methanobacteriales* to yield CH_4, CO_2 and water [35,38].

The growth of the microorganism responsible for CH_4 production - methanogens is much slower than that of acid-forming bacteria [30]. Therefore, the reactors designed for anaerobic processes are aimed to balance the bacterial community, optimize the process parameters and molecular composition for the effective methanogenesis. For this, various types of biological reactors were developed to ensure an efficient biomass retention and anaerobic digestion of the organic substrate. In particular, up-flow anaerobic sludge blanket (UASB) is amongst the most popular bioreactors for anaerobic processes, in which the active biomass is dispersed in the form of flocculent mass or granules [30]. In UASB reactors, the wastewater is supplied from the bottom and removed from above, where the biomass is transported by the upward velocity to contact substrate. The three-phase separator placed on the top of the reactor is used to separate sludge blanket containing biomass from treated effluent and collect biogas [29]. In continuously-stirred tank reactors (CSTR) the active biomass contacts the substrate in wastewaters under stirring conditions [39]. Anaerobic treatment in CSTR implies the continuous introduction and the removal of the wastewater without solids or in the form of suspension from the tank. During the process, the growth of microorganisms in the reactor is designed to compensate the colony removed with the effluent. This means that the concentration of the active biomass and substrate

is equal in properly designed CSTR. Another configuration of anaerobic reactors involves the use of filtration media, typically composed of ceramic and plastic materials. Application of anaerobic filters minimize the washout of the active biomass, while the treated effluent along with biogas are removed from above. This approach is relatively simple in design and operation, doesn't require stirring and exhibits high effectiveness at high organic loadings. However, this approach requires large size reactors due to packing materials and suffer from clogging of filter nozzles [40].

1.4. Chemical treatment methods

1.4.1. Chlorination

Disinfection of the treated wastewater is the last barrier in protection of human health and the environment [41]. The process of chlorination is universally practiced disinfection method designed to inactivate pathological bacteria and, thereby, preventing the infectious diseases. Except the broad-spectrum disinfection performance, the worldwide application of chlorination was reasoned also due to its low-cost and moderate contact time. The chlorination is based on the supplying and distribution of chlorine in the volume of the treated wastewater, where chlorine is converted into hypochlorous acid (HClO) as follows [42]:

$$Cl_2 + H_2O \rightarrow HClO + HCl \qquad 1.1$$

Lately, the gaseous chlorine was replaced with other viable alternatives, such as sodium hypochlorite (NaClO) and calcium hypochlorite ($Ca(OCl)_2$) [42]. The usage of these salts brought simplicity in operation and reduced safety concerns inherent when transporting and storing the gaseous chlorine. For instance, $Ca(OCl)_2$ containing 70% of available chlorine is solid and stable under dry storage. These three chlorination agents are strong oxidizing agents and capable to react with biological molecules, such as proteins, peptides, lipids and amino acids. However, their microbicidal activity is still under debate. The antimicrobial impact is suggested to occur due to the inhibition of essential enzymatic reactions within the cell as well as protein denaturation [43]. The neutral molecule of HClO easily diffuse inside the bacterial cells causing the damage of the membrane components and disruption of the synthesis of essential proteins [44]. The disinfection using HClO is reported to effectively inactivate *Escherichia coli* and *Pseudomonas spp* [44,45]. In the case of NaClO, its effectiveness is verified towards various

pathogens, including Ebola virus, murine norovirus and SARS-CoV-2 [46]. Because of this, NaClO is commonly used for sanitation and disinfection agent in hospitals, households and swimming pools. Nevertheless, some microorganisms (e.g., *Giardia lamblia cysts*, *Cryptosporidium parvum oocysts*) are resistant to chlorine-assisted disinfection and capable to develop adaptive response to the oxidative stress [42,47]. Another disadvantage of chlorination is the formation of disinfection by-products (DBPs), which possess high carcinogenic and mutagenic properties to human and other organisms [41]. The issue arose from the reaction of chlorine with dissolved organic matter (DOM) and represent the main disadvantage of the chlorination. Specifically, the interaction of chlorine with organic substances (e.g., humic and fulvic acids) through oxidation and substitution may results in the formation of trihalomethanes (THMs). With general formula of CHX_3 with X representing an atom of Cl and Br, THMs include chloroform, bromoform, bromodichloromethane and dibromochloromethane [48]. On the other hand, the chlorination processes are commonly associated with the occurrence of haloacetic acids (HAAs), which are more hydrophilic and less volatile than THMs. As a product of chlorine substitution on β-carbon of acetic acid, HAAs include monochloroacetic acid (MCAA), dichloroacetic acid (DCAA) and trichloroacetic acid (TCAA) [48]. Taking into account that DOM as the precursor consist of biopolymers, protein-like substances, humic and fulvic acids, DBPs can also include haloaromatics (i.e., halophenols, halohydroxybenzaldehydes, halohydroquinones and halopyrroles) [49]. These haloaromatics demonstrated higher toxicity compared to aliphatic HAAs and potentially cause tumor development in mice through the intracellular generation of ROSs [49,50]. In order to decrease the health and environmental risks caused by DBPs, the level of THMs and HAA5 (i.e., MCAA, DCAA, TCAA, bromoacetic and dibromoacetic acids) in disinfected wastewaters is strictly regulated. Thus, the highest level of HAA5 and total THMs allowed in drinking water is 0.06 mg/L and 0.08 mg/L, respectively, as recommended by USEPA [51]. To achieve lower content of DBPs and comply with the continuously stringent guidelines, several strategies were adapted. Since, DBPs are the unintended products derived from naturally-occurring materials and other organic substances, the wastewaters are preliminary treated to eliminate the precursors before chlorination. For this, the steps of sedimentation, enhanced coagulation, adsorption on activated carbon and membrane filtration can be located prior to disinfection [42]. Alternatively, the disinfection can be performed using chloramines, which prevent the formation of THMs [43]. Moreover, the

formation of DBPs can be eliminated using more effective ozonation and UV irradiation for disinfection purposes.

1.4.2. Ozonation

Although ozone (O_3) is less abundant as disinfectant than chlorine, the ozonation was the initial method of disinfection applied in drinking water treatment starting from 1906, in France [52]. Then, with the establishment of O_3 generation approaches (e.g., phosphorous contact, silent discharge, electrochemical reactions), the ozonation found its widespread application in global. Nowadays, O_3 disinfection is also implemented in municipal wastewater treatment facilities, where O_3 is generated on-site *via* a high-voltage corona discharge or UV light irradiation [53,54]. Owing to high oxidation potential of 2.07 V, O_3 is a powerful oxidant that directly reacts with organic substances, selectively attacking aromatics and unsaturated functional groups [53,55]. Specifically, O_3 interacts with olefins, sulfides, neutral amines and other electron-rich moieties with a greater rate constant [56]. Reacting with HO^- ions, O_3 is decomposed in water yielding hydroxyl ($HO^\bullet$) radicals as a product of radical reactions described in Eqs. 1.2-1.6. These transformations are relevant at circumneutral conditions and proceed slowly compared to basic pH levels.

$$O_3 + HO^- \rightarrow HO_2^{\bullet -} + O_2 \quad 1.2$$

$$HO_2^{\bullet -} + O_3 \rightarrow HO^\bullet + O_2 + O_2^{\bullet -} \quad 1.3$$

$$O_2^{\bullet -} + O_3 \rightarrow O_3^{\bullet -} + O_2 \quad 1.4$$

$$O_3^{\bullet -} + H^+ \leftrightarrow HO_3^\bullet \quad \text{pH} \leq 8 \quad 1.5$$

$$HO_3^\bullet \rightarrow HO^\bullet + O_2 \quad 1.6$$

The above features allow ozonation to achieve effective decolorization, odor and taste removal in the treated water as well as inactivation of pathogens. Application of O_3 can effectively inactivate a broad spectrum of microorganisms, including *Giardia* and *Cryptosporidium parvum*, which are resistant to other disinfection methods [47]. It was demonstrated that the inactivation of *Cryptosporidium parvum* using chlorine required 5000 mg*min/L, while 5 mg*min/L of O_3 was sufficient to achieve the same disinfection level. Similarly, ozonation required 100 times less concentration and contact time to inactivate 99% of *Escherichia coli* as compared to chlorination [53].

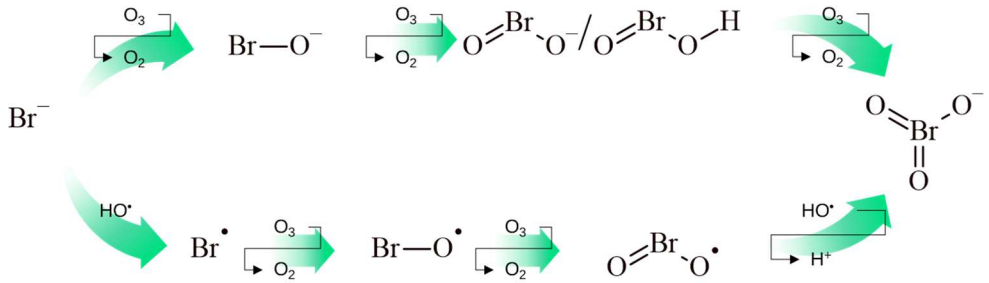

Figure 1. The formation of bromate during ozonation of wastewaters containing Br^- ions.

Unlike chlorination, the ozonation is sufficient to fragment and oxidize DOM and other into aldehydes and ketones. Then these DBPs containing aldehydes with different chain length including formaldehyde, *n*-pentanal, *n*-undecanal and *n*-tridecanal [57] are oxidized or biodegraded into CO_2 and water. On the other hand, the ozonation may lead to the formation of bromate (BrO_3^-), which are known as genotoxic and carcinogenic to living organisms [58]. As a DBP of high concern, the content of BrO_3^- ions in treated waters is controlled and the maximum allowed concentration by USEPA is 10 µg/L [58,59]. These BrO_3^- are the product of oxidation of bromide (Br^-), the concentration of which in natural waters is low and BrO_3^- is formed considerably at Br^- level in the range of 50-100 µg/L [60]. The concentration of Br^- in water can be increased naturally due to special geological formations or may have anthropogenic origin – coal mining and chemical synthesis [61].

As shown in Fig. 1, the transformation of Br^- to BrO_3^- is comprised of the subsequent oxidation steps that proceed through the formation of hypobromide (BrO^-) ion [61]. It's worth to mention that during ozonation both molecular O_3 and $HO^\bullet$ radicals oxidize Br^- and the concentration of BrO_3^- increases with the increase of the contact time, which is commonly required for inactivation of some pathogens, such as *C. parvum oocysts* [60]. To decrease the concentration of BrO_3^- below 10 µg/L in treated water, several strategies, which can be applied before and after ozonation, have been established [58]. The mitigation of BrO_3^- formation can be achieved by removing Br^- using electrochemical methods before ozonation. In addition, the preliminary reduction of dissolved organic carbon (DOC) can lower the formation of BrO_3^- by decreasing the time of treatment and exposure to O_3. During the process of ozonation, NH_3 can be added to react with HBrO and eliminate the key intermediate of BrO_3^- formation [58,62]. The reaction proceeds rapidly yielding NH_2Br, which is further oxidized to release NO_3^- and Br^-. Another approach for minimizing BrO_3^- formation is lowering pH, which shift the equilibrium

HBrO/BrO^- to the neutral form thereby preventing the oxidation of BrO^- by O_3 [63]. Higher stability of O_3 at lower pH results in lower generation of $HO^•$ radicals capable to oxidize both HBrO and BrO^-. Although the pH depression method can ensure the decrease of BrO_3^- formation by 50-60%, the widespread application in practice is limited due to the high consumption of chemicals. The level of BrO^- can also be minimized after ozonation *via* post-treatment BrO_3^- removal techniques, such as adsorption on granular activated carbon [63], biofiltration, UV light irradiation [63], reverse osmosis [64] and nanofiltration [65]. Thus, the application of reverse osmosis decreased the concentration of BrO_3^- in ground water after ozonation from 190.5 µg/L to 7.4 µg/L resulting in BrO_3^- removal of 96.1% [64]. Nanofiltration membranes with negatively charged surface also demonstrated high effectiveness in BrO_3^- removal rejecting 28.3% and 48.1% of Br^- and BrO_3^-, respectively [65]. Low-pressure mercury UV lamps, which are commonly used for disinfection purposes can be used for BrO_3^- removal as hypobromous acid (HBrO) is converted into Br^- under UV irradiation. However, the dose of UV light to reduce the concentration of BrO_3^- from 50 µg/L to 10 µg/L exceeds 1000 mJ/cm^2 [63], while the effective inactivation of *C. parvum oocysts* requires only 10-25 mJ/cm^2 [66]. Despite these methods effectively mitigate BrO_3^- to the level of regulatory requirements, their application in wastewater treatment might be expensive.

1.4.3. Coagulation and flocculation

Coagulation is an important physico-chemical process applied in wastewater treatment to remove suspended particles. The principle of coagulation is the destabilization of the colloidal system comprised of negatively charged suspended particles [67]. The effect is induced using coagulants mainly based on aluminum and iron salts, which are rapidly hydrolyzed upon addition to form oppositely charged species. Aluminum coagulants include aluminium sulfate, sodium aluminate, polyaluminum chloride, while iron-based coagulants are ferric sulfate, ferrous sulfate and ferric chloride [68,69]. The abundant application of these coagulants is due to their availability, low-cost and ability to form multi-charged polynuclear complexes [68]. The interaction of these cationic species with suspended particles reduces the static repulsion in the colloidal system thereby enabling aggregation. In the case of high coagulant dosage, the target suspended particles can be enmeshed in the amorphous precipitates of metal hydroxide, and such mechanism is known as “sweep flocculation” [70]. Nevertheless, the aggregates from coagulation further undergo flocculation, during which greater

settleable aggregates or “flocs” are formed. The flocculation is carried out under continuous mixing and polymers with higher molecular weight can be added to facilitate the process by binding the destabilized particles together. As a result, stable and stronger flocs of a greater size are formed, which can be further removed by flotation of filtration. Preliminary designed for the turbidity reduction, coagulation and flocculation are currently the essential steps in pretreatment of industrial effluents and tertiary stages of municipal wastewater treatment. Moreover, coagulation-flocculation demonstrated certain effectiveness in microplastic removal and water disinfection. Thus, 15 mM aluminum-based salts ($AlCl_3 \times 6H_2O$) exhibited 36.89% of polyethylene particles with a diameter of <0.5 mm through coagulation-flocculation mechanism at pH 7 [71]. The inactivation of pathogens can be achieved by inducing the precipitation of *Escherichia coli* cells in the presence of synthetic flocculants, such as polyethylene imine, polydiethylaminoethylmethacrylate [72]. Recent studies on coagulation-flocculation methods focus on minimizing of sludge formation, which require the implementation of proper disposal procedures. For instance, paramagnetic nanocomposites which can be easily separated were found effective and reusable for the removal of heavy metals [73]. Besides, various natural coagulants, such as chitosan [74], rice starch [75] and *Moringa oleifera* seed [76] were studied for wastewater treatment as safe and economically viable alternatives to chemical and synthetic coagulants.

1.4.4. Neutralization

The discharge of untreated wastewater into the environment is detrimental to aquatic ecosystem due to the presence of hazardous pollutants and highly acidic or alkaline pH. Therefore, the pH neutralization is a fundamental process integrated in wastewater treatment. The purpose of the process is to adjust the pH of the treated wastewater within acceptable circumneutral values (i.e., pH 6-9) before discharge [77]. It is worth to mention, that pH neutralization is not only used before discharge to protect aquatic organisms, but also it is used to protect equipment and piping from corrosion. The process pH neutralization is also employed as a preliminary treatment step prior to biological processes. The process is based on acid-base reactions producing neutral salts. Specifically, alkaline agents, such as metal hydroxides, carbonates and ammonia are added to neutralize acidic wastewaters, whereas acids and CO_2 are employed for basic wastewaters [78,79]. In industry, the pH neutralization is conducted using agents,

which are selected considering cost, buffering capacity and regulatory requirements as main criteria. Thus, the pH neutralization is often proceeded using commercial chemicals and waste from other production sites. In particular, basic wastewater from textile production was effectively neutralized by adding hydrochloric acid (HCl) [79]. On the other hand, calcium oxide (CaO)-containing waste from pulp and paper industry was used to adjust the acidic pH of wastewater from steel manufacturer [80]. Similarly, waste limestone from marble industry [78] as well as cement kiln dust from cement manufacture [81] were reported as effective and cheap agents for neutralization of acidic wastewaters. Despite the simple theoretical concept, the design of pH neutralization is related with process optimization that deal with the effect of operating parameters, including mixing and loading dosage as well as the analysis of competing side reactions, pH monitoring and control. The latter represents the key problem associated with the acid-base neutralization due to inherent non-linear behavior of pH dynamics affecting reaction kinetics and causes time delay and flow rate fluctuations [77,82]. In the light of these, various real-time pH monitoring, controlling systems and predicting models constitute the object of recent studies.

1.4.5. Chemical precipitation

The process of precipitation is a principal unit of wastewater treatment that remove soluble inorganic ions and nutrients. Based on precipitation followed by sedimentation or filtration, the mechanism of chemical precipitation resembles that of coagulation-flocculation. Nonetheless the precipitation converts the dissolved ions into insoluble precipitates by adding specific precipitating agents (e.g., sodium bicarbonate ($Na(HCO_3)_2$), lime ($Ca(OH)_2$), sodium sulfide (Na_2S)) and increasing pH using NaOH [83]. For instance, increasing the concentration of soda ash ($Na_2CO_3 \times 10H_2O$) from 10 mg/L to 400 mg/L over 90% of Zn (II) and Cu (II) was removed from a cable manufacture wastewater [84]. Both heavy metals were isolated in the form of amorphous hydroxides with large particle size, while the volume of the resulting sludge was lower. Although the precipitation of hydroxides is highly effective and simple in operation, the economic feasibility can be inadequate as large volume sludges with low density require further disposal. In contrast, the sludge formed during the precipitation using metal sulfides exhibits better settling properties, thickening and dewatering characteristics [83,85]. The precipitation using sulfides can be performed at broader pH and the solubility of the obtained metal sulfide in water is lower than that of the corresponding

hydroxides. The reaction of sulfides with metal ions proceeds with higher rate constants through complex mechanism, which is different for individual metal [85,86]. The process is sensitive to the dosage of the precipitating agent and may form colloidal precipitates which are difficult to separate. Moreover, the precipitation of sulfides is often associated with the emission of toxic hydrogen sulfide (H_2S) fumes [83]. Recently, synthetic precipitating agents, such as 2,4,6-trimercaptotriazine, a trisodium salt nonahydrate (TMT-55) [87], disodium N,N-bis-(dithiocarboxy)piperazine (Na_2BDP) [88,89], 1,3-benzenediamidoethanethiol ($BDETH_2$) [90] are evaluated for the binding and precipitation of heavy metals from wastewaters. Acting as chelating ligands, these agents bind monovalent and divalent metal ions (e.g., Ag^+, Cd^{2+}, Cu^{2+}, Hg^{2+}, Ni^{2+}, Pb^{2+}) into complexes that undergo precipitation. Chemical precipitation is also used for the removal of phosphorous from municipal and pharmaceutical wastewaters, which can be further recovered and used as a mineral fertilizer [91]. For this, soluble salts of iron, aluminum, magnesium and calcium are used to react with phosphorous yielding insoluble orthophosphates of the corresponding metals [92]. This is a widely practiced method that ensures high removal efficiency when treating high phosphorous wastewaters.

1.5. Advanced chemical processes

Tertiary technologies, such as reverse osmosis, adsorption on activated carbon, ultrafiltration, are commonly implemented in modern wastewater treatment plants. Their application is intended to remove the remaining pollutants from water to meet the regulatory requirements. However, the effectiveness of these methods decreases considerably when dealing with persistent organic pollutants (POPs). These contaminants possess high chemical stability as well as resistance to biological methods and accumulation in living organisms posing risk to environment and human health. Therefore, advanced chemical processes, namely, advanced oxidation processes (AOPs) and advanced reduction processes (ARPs) were developed to effectively degrade chemically stable and non-biodegradable pollutants. Owing to their oxidation capacity, AOPs are able to induce the complete mineralization of organic pollutants, including POPs into CO_2 and water. Alternatively, AOPs can also transform organic pollutants into less hazardous compounds, which respond to biodegradation. On the other hand, recently emerging ARPs were shown as promising tool to degrade halogen-containing organic pollutants, that avoid formation of toxic intermediates.

Generally, AOPs are defined as water treatment processes operating at room temperature and normal pressure that utilize in-situ generated $HO^{\bullet}$ radicals with oxidation potential of 2.8 V_{NHE} [93]. These radicals are highly reactive and non-selectively attack a variety of water pollutants at extremely high reaction rate leading to the complete degradation of the pollutant at sufficient concentration. Primarily started with the formation of $HO^{\bullet}$ radicals *via* the decomposition of H_2O_2 in the presence of Fe^{2+} ions and further named as Fenton's reagent in 1894, the list of AOPs is continuously expanded. Being a subject of interest of applied and fundamental studies, AOPs, nowadays, constitute a broad class of efficient water treatment methods that involve chemical, photo- and electrochemical reactions to yield $HO^{\bullet}$ radicals. Hence, the modification of Fenton's process aimed to improve its effectiveness resulted in the development of photo-Fenton, electro-photo-Fenton and other Fenton-like processes [94,95]. Frequently studied O_3-based AOPs include peroxone, catalytic ozonation using transition metal ions and metal oxides. In UV-based AOPs, the radical species can be formed due to the photolysis of O_3, H_2O_2 and photocatalysis on the surface of photocatalysts such as titanium dioxide (TiO_2). Catalyzed ozonation as well as photocatalysis on TiO_2 can also be categorized as catalytic AOPs, which involve homogeneous (e.g., Fenton's process) and heterogeneous processes utilizing solid catalysts. Newly developed processes using electrochemical reactions, plasma discharge, electron beam and radical precursor/promoter can be categorized as other. There are many classifications, but AOPs can be classified also by the type of dominating radical species. The most studied AOPs are based on formation of $HO^{\bullet}$ radicals. Since, it was found that other reactive oxygen species (ROSs), such as sulfate radicals ($SO_4^{\bullet-}$) and singlet oxygen ($^1O_2$) offer longer life-time, selectivity and tolerance to water constituents, various peroxides other than H_2O_2 or O_3 were tested for AOPs. This gave a rise to non-traditional AOPs, particularly, sulfate radical-based AOPs (SR-AOPs), which utilize persulfate and peroxymonosulfate salts. Varying radical precursor can subsequently lead to the formation of radical species with low reduction potential thereby changing the degradation pathway of the pollutant. In such a scenario, the degradation of the pollutant proceeds through the reduction by hydrated electrons ($e_{aq.}^-$), hydrogen radicals ($H^{\bullet}$), sulfur dioxide radicals ($SO_2^{\bullet-}$) and sulfite radicals ($SO_3^{\bullet-}$). These processes are known as ARPs and utilize the radical precursors, such as iodide (I^-), ferrocynide ($[Fe(CN)_6)]^{4-}$, dithionite ($S_2O_4^{2-}$) and sulfite anion (SO_3^{2-}). In the light of water pollution associated with occurrence of persistent per- and polyfluoroalkyl substances (PFAS) and other halogen-

containing organic pollutants, ARPs have received increased attention as a possible method sufficient to cleave carbon-halogen bond.

1.5.1. Ozone-based AOPs

Aside from microbial disinfection, O_3 is used in drinking water treatment to oxidize inorganic ions (Fe^{2+}, NO_2^-, HS^-) and to control odor, taste and color. The application of O_3 in wastewater treatment is mainly connected with the degradation of organic matter and recalcitrant organic compounds. For instance, as a part of a wastewater reclamation process, tertiary treatment methods, such as nanofiltration and reverse osmosis effectively separate ionic salts and micropollutants through size exclusion or electrostatic interactions. The separated streams (retentates) contain recalcitrant organic compounds in high concentration and require proper disposal before discharge. For this purpose, O_3 is supplied to the concentrate to oxidize and degrade the organic components. For example, such micropollutants, such as 2-hydroxybiphenyl, sulfamethoxazole, diclofenac, ketorolac and acetaminophen were effectively removed during the ozonation of the retentates from ultrafiltration and nanofiltration of a secondary municipal wastewater [96]. The content of micropollutants was decreased below the detection limit at low O_3 dosage (<0.5 mgO_3/mgDOC) as their reaction rate constant with O_3 exceeded 1×10^5 M^{-1} s^{-1}. In the case of metoprolol, isoproturon with rate constants of ~2 × 10^3 M^{-1} s^{-1} and caffeine with 650 M^{-1} s^{-1} at pH 7 were degraded in lower extend and required higher O_3 dosage. Furthermore, the degradation efficiency of atrazine contained in ultrafiltration retentate was only 42% indicating the resistance to ozonation. Similarly, the treatment of atenolol during the disposal of a retentate from reverse osmosis required 1.38 mgO_3/mgTOC of O_3 dosage [97], which can be attributed to the low reactivity of atenolol with molecular O_3 (i.e., <10^3 M^{-1} s^{-1}). The above observations suggest that the ozonation of retentates can be highly effective towards the micropollutants depending on the reactivity with molecular O_3. Thus, organic pollutants with electron-rich moieties and functional groups can be easily targeted and degraded at low O_3 dose. Despite high degradation efficiency of organic pollutants, the direct oxidation by O_3 is insufficient to achieve their complete mineralization. The treatment of reverse osmosis retentate with sole ozonation resulted in 33% of chemical oxygen demand (COD) reduction after 20 min of contact time [98]. The values of COD reduction were then increased to 48% and 54% for the combined O_3/H_2O_2 and O_3/H_2O_2/UV, respectively. These results demonstrate the increase of the oxidation capacity in the combined processes,

which is attributed to the formation of reactive species of higher oxidation potential than O_3. In the combined processes O_3 undergoes decomposition yielding $HO^{\bullet}$ radicals causing indirect oxidation of the present organic pollutants. In such a scenario, ozonation is considered as AOP, which is extensively modified and tested for the degradation of a variety of pollutants. The dissolved O_3 is unstable and decomposes to form $HO^{\bullet}$ radicals within seconds or hours depending on water constituents and pH (Eqs. 1.7, 1.8) [99]. The decomposition of O_3 can be accelerated by increasing pH, combining with other oxidants, energy input, and catalysts. While slowly reacting with H_2O_2, O_3 can rapidly react with HO_2^- ions derived from H_2O_2 disassociation as shown in Eq. 1.9, 1.10. The resulting $HO_2^{\bullet}$ and $O_3^{\bullet-}$ radicals participate in radical chain reactions (Eqs. 1.3, 1.5, 1.6) to form $HO^{\bullet}$ radicals. This process is commonly termed as peroxone [99,100].

$$O_3^{\bullet-} \rightarrow O^{\bullet-} + O_2 \qquad 1.7$$

$$O^{\bullet-} + H_2O \rightarrow HO^- + HO^{\bullet} \qquad 1.8$$

$$H_2O_2 \leftrightarrow HO_2^- + H^+ \qquad 1.9$$

$$O_3 + HO_2^- \rightarrow HO_2^{\bullet} + O_3^{\bullet-} \qquad 1.10$$

The direct oxidation by the molecular O_3 proceeds through electrophilic addition involving steps of electron transfer, ozone insertion, formation and subsequent decomposition of ozonides [101,102]. The indirect oxidation of organic pollutants by $HO^{\bullet}$ radicals is non-selective and exhibits significantly faster reaction kinetics. While the direct reaction of O_3 with organic compounds containing electron-rich functional groups proceeds in the range of 10^6-10^8 $M^{-1}s^{-1}$, the molecular O_3 responses slowly to saturated compounds with the rate of 10^{-3} $M^{-1}s^{-1}$ [96,99]. Compared to this, the indirect oxidation of saturated organic compounds and inorganic ions by $HO^{\bullet}$ radicals takes place within 10^8-10^{10} $M^{-1}s^{-1}$ [97,99]. The high effectiveness of O_3-based AOPs was demonstrated for the treatment of wastewaters from various industrial sectors, including dairy factory [103], hospital [104], petrochemical [105], tannery [106] and textile [107] wastewaters. These observations also confirmed the advantageous application of the indirect radical oxidation over direct oxidation. Thus, the application of 60 mg/L O_3 for the removal of organic matter from refinery wastewater received after biological process unit resulted in TOC removal below 20% after 60 min [108]. The TOC removal was then increased to 95% upon the combination of O_3 with UV light (55 W). Similarly, peroxone, O_3/UV and the combined O_3/H_2O_2/UV demonstrated higher

effectiveness in removal of trace organic compounds from a secondary wastewater effluent than sole ozonation [109]. Owing to the generation of $HO^{\bullet}$ radicals, ozone-based AOPs effectively degraded bisphenol A, carbamazepine and 17α-ethinylestradiol within 2 min. Besides, the degradation efficiency of atrazine and alachlor obtained during sole ozonation were only 8% and 20% resulting in degradation rate constants of 13 × 10^{-4} min^{-1} and 35 × 10^{-4} min^{-1}, respectively. These observations highlighted the detrimental effect of O_3 selectivity as the reaction rate constants of O_3 with atrazine and alachlor are less than 10 $M^{-1}s^{-1}$. The degradation rate constants of atrazine and alachlor were then correspondingly increased to 98 × 10^{-4} min^{-1} and 473×10^{-4} min^{-1} in the combined O_3/H_2O_2/UV due to the effective O_3 decomposition and exposure to the reactive $HO^{\bullet}$ radicals. In this study, the degradation of pollutants in O_3-based AOPs was characterized with a 30 s lag-phase as the effluent constituents (e.g., NH_4^+, NO_3^-, NO_2^- ions) competed for the consumption of oxidizing species. In the case of the treatment of hospital wastewater, O_3/H_2O_2/UV utilizing a medium pressure mercury lamp of 1000 W effectively inactivated the colonies of *Escherichia coli*, *Enterobacter aerogenes* and *Pseudomonas aeruginosa* [110]. The process degraded 73% of organic compounds in 20 min resulting in COD reduction from 145 mg/L to 20 mg/L. Noteworthy, the GC-MS analysis performed after the treatment revealed the formation of the transformation products with high toxicity. Moreover, the effectiveness of O_3/H_2O_2/UV towards eicosane, hexadecane, and octadecane was negligible due to their strong hydrophobicity and chemical inertness. These findings highlight the O_3 dosage and the generation rate of $HO^{\bullet}$ radicals as crucial factors determining the effectiveness of the process and the quality of the treated effluent. Considering that the inherent low solubility of O_3 in water, the competing secondary reactions of matrix components and the formation of hazardous intermediates in the case of the incomplete degradation of pollutants, O_3-based AOPs require intensive production of O_3 on-site. Therefore, O_3-based AOPs are considered economically infeasible due to high electric power demand and commonly applied in integration with other wastewater treatment technologies, such as aeration, coagulation and flocculation.

1.5.2. Sulfate radical-based AOPs

The level of discharge of organic pollutants posing inherent toxicity and persistence towards biodegradation introduced into the environment is increasing continuously and constitute a multidisciplinary challenge. In response to this, enormous efforts

have been made resulting in various innovative solutions with potential application in water purification. Being extensively studied, AOPs, such as H_2O_2/UV, O_3/H_2O_2, Fenton's process were proved to effectively degrade water pollutants, including POPs. These AOPs are based on the generation and utilization of highly reactive and non-selective $HO^{\bullet}$ radicals with oxidation potential of 1.8-2.7 V vs. normal hydrogen electrode (NHE). Owing to the powerful oxidation capacity of $HO^{\bullet}$ radicals, AOPs were demonstrated to effectively remove COD, TOC as well as to degrade target pollutants in wastewaters. As the spectrum of AOPs is broadening regularly depending on the oxidants and the excitation method, SR-AOPs represent a trending alternative to traditional AOPs. The advantageous application of SR-AOPs in water treatment is primarily attributed to the intrinsic features of sulfate anion ($SO_4^{\bullet-}$) radicals: high oxidation potential ranging from 2.5 to 3.1 vs. NHE, wide operational pH, longer half-life period achieving 30-40 μs (while $HO^{\bullet}$ radicals live approx. 20 ns), selective interaction with electron-rich moieties (e.g., unsaturated bonds, aromatic ring) through single electron transfer (SET). Consequently, $SO_4^{\bullet-}$ radicals can diffuse and effectively contact with the target contaminant with the second-order rate constant ranging from 10^5 to 10^9 $M^{-1}s^{-1}$. SR-AOPs involve two main processes – persulfate (PS) and peroxymonosulfate (PMS), which are activated to produce $SO_4^{\bullet-}$ radicals. Although both PS and PMS are moderate oxidants (2.01 V and 1.82 V, respectively) with high solubility in water at 20 ºC, the direct oxidation of pollutants proceeds slowly. The oxidation rate is increased significantly with activation, which is realized by the cleavage of peroxy (-O-O-) bond as illustrated in Eqs. 1.11, 1.12 The structure of PS ($S_2O_8^{2-}$) exhibits symmetrical arrangement where the peroxy bond is characterized with the length of 1.497 Å and energy of 140 kJ mol^{-1}. In contrary, the peroxy bond in asymmetrical PMS (HSO_5^-) is shorter (1.453 Å) and the energy required for bond disassociation is in the range of 140-213.3 kJ mol^{-1}. In general, the methods of activation in both cases include chemical (e.g., alkaline, quinone) and physical approaches (e.g., UV light, cavitation, gamma irradiation, electrolysis, pyrolysis). However, the activation kinetics, the predominant radical species, as well as the underlying mechanism governing the generation of radical species and degradation of the pollutants may differ. The homogeneous activation of PS and PMS in the presence of transition metals such as Ag^+, Mn^{2+}, Fe^{2+}, Ce^{3+}, Ni^{2+}, Co^{2+} resembles the mechanism of Fenton's process [111]. Among the studied metal ions, Ag^+ showed the highest activation capacity towards PS resulting in 85% degradation efficiency of 2,4-dichlorophenol in 240 min at pH 3, while it was only 8% in the case of PMS [112]. On the contrary, Co^{2+} and Ru^{3+} ions were found highly effective in PMS activation

leading to the complete degradation of the pollutant within 1 min. The coupling of Co^{2+} and Ru^{3+} ions with PMS and H_2O_2 showed negligible efficiency. Nevertheless, such methods are often associated with the following challenges: poor recovery of metal ions, secondary pollution caused by the accumulation of metal ions in effluents and strict pH maintenance to avoid precipitation. In the light of this, the heterogenous activation of PS and PMS using metal oxides, carbonaceous materials and natural minerals (e.g., magnetite, siderite) can be preferred. Along with high activation capacity, the application of heterogenous catalysts is considered environmentally compatible due to greater chemical stability, reusability and convenient separation. For instance, CuO showed the significant activity in promoting PS activation, while it was less appreciable using Fe_2O_3, MnO_2, ZnO, TiO_2, MoO_3 and CeO_2 [113]. It was proposed that the degradation of the pollutant proceeded through the nonradical route facilitated by the interaction of positively charged CuO and PS in the presence of the pollutant. In the case of PMS/CuO, the degradation of the pollutant was mainly contributed by $SO_4^{\bullet-}$ radicals [114]. In addition to metal oxides, various carbon-based materials, such as graphene oxide, nanotubes, fullerene were investigated to activate PS and PMS. Specifically, reduced graphene oxide (rGO) demonstrated the highest PMS activation ability compared to activated carbon, graphene oxide and multiwalled carbon nanotube [115]. Additionally, the oxidative degradation of phenol attained in 180 min was higher by 46.5% in PMS/rGO compared to PMS/Co_3O_4. On the other hand, single-walled nanotubes, rGO and mesoporous carbon were superior in PS activation than fullerene, nanodiamonds and graphitic carbon nitride [116]. The effectiveness of PMS/rGO tested towards the degradation of phenol exceeded that of metal oxides (e.g., MnO_2, Co_3O_4, CuO, Fe_2O_3) and comparable to zero valent iron (ZVI). Based on the observed findings, the excellent catalytic performance of the carbocatalysts was attributed to the intrinsic features including defective site and surface carbonyl groups. The mechanistic insights obtained from electron paramagnetic resonance (EPR) spectra suggested carbocatalysts as mediators of electron transfer. In order to stimulate the electronic transporting properties, various modified carbon-based materials were prepared by doping with electron donating elements and compounds. Hence, rGO doped with Co_3O_4 exhibited remarkable synergistic effect in PMS activation through the electron transfer mechanism [117]. The graphene sheets prevented the aggregation of Co_3O_4 nanoparticles providing a uniform dispersion of active sites, and high surface area along with specific electronic structure facilitated the electron migration from Co_3O_4 to PMS. Recent advances in modification of rGO for the activation of PS/PMS

include incorporation of heteroatoms [118], deposition of metal nanoparticles [119] and conjugation with other two-dimensional (2D) materials [120]. Despite the number of modification strategies and dopants is continuously growing, the large-scale implementation of PS/PMS processes activated by the novel modified materials in water treatment remains limited. A key factor limiting the practical application is the high cost of production of these materials which increases the overall treatment cost. Therefore, the development of low-cost carbon-based material that are abundant and effective for the activation of PS and PMS is in high demand. In this context, SR-AOPs in combination with non-toxic and reusable carbon material represent a promising, economically viable alternative to conventional water treatment technologies.

$$S_2O_8^{2-} \xrightarrow{energy\ input} 2SO_4^{\bullet -} \quad 1.11$$

$$HSO_5^- \xrightarrow{energy\ input} SO_4^{\bullet -} + HO^{\bullet} \quad 1.12$$

1.5.3. Sulfite-induced ARPs

Reductive processes in wastewater treatment are common in removing of hazardous inorganic ions and halogenated organic contaminants. For this purpose, metals in lower valence state, such as ZVI [121], iron (II) oxides [122] are traditionally used reductants capable to donor electrons for the decomposition of As (V), nitroaromatics and halogenated alkenes. Additionally, the reductive degradation can be conducted through catalytic hydrogenation [123] and electrolysis [124]. Nowadays the studies on the reductive processes for potential application in wastewater treatment are the topic of high interest. The trend is grounded on the growing concern associated with the detection of halogenated organic pollutants, such as pharmaceutically active substances, solvents, PFAS in aquatic environments [125,126]. These contaminants are widely incorporated in daily life, industries and agriculture, and in the absence of proper disposal management, their widespread occurrence in the environment was only a matter of time. The persistence of these pollutants is attributed to the highly stable C-Halogen bond. For instance, the binding energy of C-F bond is reported as 530 kJ/mol, while it is 410 kJ/mol for C-C bond [127]. Containing electron-withdrawing halogen atom, these molecules possess distorted electron density and the polarized structure is highly soluble in water. The attempts on the oxidative degradation of the halogen-containing contaminants were conducted using traditional and sulfate radical-based AOPs with certain success. The ozonation at

alkaline pH degraded of 85% and 100% of perfluorooctanoic acid and perfluorooctane sulfonate, respectively, in 240 min [128]. These results were attained at O_3 dosage of 8.7 g/h and pH 11, and the further improved during peroxone process at O_3/H_2O_2 molar ratio of 20%. The application of photocatalytic ozonation O_3/TiO_2/UV achieved the degradation efficiency of 99.1% towards perfluorooctanoic acid in 240 min [127]. In this case, the effective degradation of the persistent contaminant was performed using O_3 dosage of 0.025 g/h and TiO_2 dosage of 0.2 g/L. On the other hand, the defluorination rate was 44.3% after 240 min indicating that the cleavage of C-F bond by the photo-generated $HO^{\bullet}$ radicals was challenging. Fenton-like processes, catalytic ozonation and SR-AOPs were demonstrated effective for the treatment of halogen-containing contaminants, such as chlorinated compounds. Owing to the oxidative transformations induced by $HO^{\bullet}$ and $SO_4^{\bullet-}$radicals, the pollutants undergo fragmentation to yield short-chain molecules or complete mineralization into CO_2 and water. Nevertheless, the radical-mediated reactions involve multiple steps and intermediates, which may pose a higher toxicity risk than the parent pollutant. For instance, the acute toxicity displayed by 4-chlorophenol and hydroquinone - common transformation products of clofibric acid (CLA) oxidation, is greater than that of the parent molecule [129,130]. Consequently, the treatment of halogen-containing contaminant by AOPs can be associated with the concern regarding environmental sustainability in the case of incomplete degradation. In contrast to traditional reductants and AOPs, ARPs induce the reductive degradation employing powerful reductive species, such as e_{aq}^- and $H^{\bullet}$ radicals with reduction potential of -2.9 V and -2.3 V vs. NHE, respectively [131]. These species effectively attack the pollutants targeting the highly oxidized sites and electron-deficient positions caused by the presence of a halogen atom. For instance, e_{aq}^--mediated ARP of KI/UV effectively degraded perfluorooctanoic acid with a rate constant of 7.3×10^{-3} min^{-1}, providing a defluorination rate of 98.8% after 14 h [132]. In the light of this, ARPs are considered as cost-effective, technically simple and adaptive technology sufficient to transform halogen-containing persistent organic pollutants into biodegradable, less-toxic compounds.

$$SO_3^{2-} \xrightarrow{h\nu} SO_3^{\bullet-} + e_{aq.}^- \quad 1.13$$

$$HSO_3^- \xrightarrow{h\nu} SO_3^{\bullet-} + H^{\bullet} \quad 1.14$$

$$e_{aq.}^- + HSO_3^- \rightarrow SO_3^{2-} + H^{\bullet} \quad 1.15$$

$$SO_3^{\bullet-} + SO_3^{\bullet-} \rightarrow S_2O_6^{2-} \quad 1.16$$

$$SO_3^{\bullet-} + SO_3^{\bullet-} + H_2O \rightarrow SO_4^{2-} + HSO_3^- + H^+ \quad 1.17$$

$$e_{aq.}^- + O_2 \rightarrow O_2^{\bullet-} \quad 1.18$$

As a typical ARP, sulfite/UV is principled on the generation of both e_{aq}^- and $H^\bullet$ radicals to induce the photo-reduction of present organic pollutants. In this approach, the reductive species are generated through the excitation of sulfite (SO_3^{2-}) and bisulfite (HSO_3^-) anions under UV light irradiation as shown in Eqs. 1.13, 1.14 [126,133]. Sulfite anion radicals ($SO_3^{\bullet-}$) generated in both cases exhibit oxidation potential of and act either as a moderate oxidizing or reducing agent. However, the contribution of $SO_3^{\bullet-}$ radicals on the degradation of persistent organic pollutants is negligible. Instead, $SO_3^{\bullet-}$ radicals preferably undergo recombination leading to the formation of other sulfur species, such as dithionate ($S_2O_6^{2-}$) and SO_4^{2-} anions as illustrated in Eqs. 1.16, 1.17 [126,131]. Hence, the degradation of halogenated pollutants in SO_3^{2-}/UV is conducted by e_{aq}^- and $H^\bullet$ radicals, which effectively cleave C-Halogen bonds. Except photoionization, e_{aq}^- and $H^\bullet$ radicals in SO_3^{2-}/UV are additionally produced as a result of radical recombination reactions. The SO_3^{2-}/UV demonstrated high degradation efficiency towards chlorinated hydrocarbons [133], perchlorate [134] and BrO_3^- [135]. Owing to the increased UV absorptivity of BrO_3^- and SO_3^{2-} at 222 nm, greater generation rate of e_{aq}^- species as well as the direct photolysis of BrO_3^- were observed [135]. Based on the results, it was suggested that e_{aq}^- species instantaneously attacked BrO_3^- to abstract oxygen with a rate constant of 3×10^9 $M^{-1}s^{-1}$. Consequently, BrO_3^- was sequentially reduced into bromite (BrO_2^-), hypobromide (BrO^-) and bromide (Br^-) ion, releasing SO_4^{2-} ions and water. Coupled with vacuum UV light (185 nm), SO_3^{2-}/UV degraded 64% of perfluorooctane sulfonate in 360 min resulting in 58.9% of defluorination due to the increased generation of e_{aq}^- species [136]. In addition, the degradation of perfluorooctanoic acid was decreased below detection limit after 24 h treatment by SO_3^{2-}/UV at pH 12 resulting in 98% of defluorination [137]. Although the degradation efficiency of perfluorooctanoic acid was significantly inhibited in the presence of carbonate (CO_3^{2-}), nitrate (NO_3^-) ions and humic acids, SO_3^{2-}/UV maintained the effectiveness at extreme salinity conditions. This indicated the high potential of SO_3^{2-}/UV wastewater treatment aimed for PFAS destruction. However, SO_3^{2-}/UV at the current stage of development is significantly limited due to the scavenging of the reactive species. In particular, e_{aq}^- species can be rapidly

consumed by DO with a rate constant of 1.9×10^{10} M^{-1} s^{-1} as illustrated in Eq. 1.18 [126]. Furthermore, other secondary sulfur species and radicals may also act as scavengers of e_{aq}^- species competing with the pollutant. The production of reductive species in SO_3^{2-}/UV is insufficient for the effective degradation of the pollutants and demands high electric power input and precursor loadings. Therefore, current studies are focused on enhancing the performance of SO_3^{2-}/UV based on various strategies. For example, additional external oxidizing/reducing agents as well as UV light sources can be employed to facilitate the generation and availability of e_{aq}^- species. Nevertheless, the modified SO_3^{2-}/UV processes operate at anaerobic conditions and require the deoxygenation step, which is economically infeasible in large-scale wastewater treatment practice.

1.5.4. Key parameters affecting advanced chemical processes

1.5.4.1. Effect of oxidant/reductant dosage

In advanced chemical processes, the amount of the radical precursor is a crucial parameter determining the generation of radical species, and thus, the effectiveness of the process in removing water contaminants. Specifically, this parameter is often associated with advanced chemical processes in homogenous systems containing dissolved radical precursors (e.g., H_2O_2, O_3, PMS) which undergo activation to produce radicals. While the concentration of reactive radicals is directly connected to the effectiveness of the developed process, the dosage of the precursor is also related to its economic feasibility. In particular, high O_3 concentrations in O_3-assisted AOPs require large electric power thereby increasing the operational cost of the process. In addition, the carrier gas containing O_3 is supplied with consideration of the mass transfer of O_3 from gaseous phase to liquid phase. The mass transfer of O_3 is limited at high concentrations and can be facilitated by the decomposition of the dissolved O_3 in the saturated liquid phase. Considering the mass transfer limits, decomposition rate, activation method and the characteristics of the target contaminants, the dosage of the influent O_3 required the effective degradation efficiency may differ from one to another AOP. Therefore, the determination of the optimal O_3 dosage in O_3-assisted AOPs is necessary.

As the composition of wastewaters is complex and contain various organic and inorganic substances that may react with $HO^{\bullet}$ radicals. Considering this, the degradation of target recalcitrant contaminants during the wastewater treatment in O_3-assisted AOPs require higher O_3 dosage. The treatment of a secondary effluent

spiked with 42 pharmaceuticals showed that the degradation of 80% of the active pharmaceutical ingredients (APIs) by 90% required the O_3 dosage of 1.4 g per 1 g DOC [138]. APIs containing electron-withdrawing groups, such as flutamide, fluconazole, ketoprofen and beclomethasone were less reactive to electrophilic attacks by O_3 and required 2.4 g/DOC. Similarly, ozone dosages of 0.5 g/DOC and 4.7 g/DOC were sufficient to attain 90% removal of sulfadiazine and diatrizoic acid from hospital wastewater [139]. Along with the structural persistence to O_3 attacks, the demand on the increased O_3 dosage can be also arise from the effect of wastewater matrix composition. For instance, the application of 1 mg/L O_3 resulted in complete degradation of phenacetin in ground water, while 0.9 µM of the residual concentration was still detected in municipal wastewater [140]. Thus, the application of 5 mg/L of O_3 was recommended to ensure the complete removal of pharmaceuticals, including metoprolol, naproxen, amoxicillin and phenacetin.

In lab-scale studies investigating the effectiveness of O_3-assisted AOPs towards model recalcitrant water contaminants, the dosage of the applied O_3 is lower and selected based on the amount of the model pollutant. Hence, the O_3 dosage in the range of 0.1 mg/L to 1.0 mg/L was evaluated to determine the optimal dosage for the ozonation of 200 µg/L of bisphenol A in 500 mL batch reactor [141]. Similarly, the range between 0.37 g/h and 4.37 g/h was tested for the degradation of 100 mg/L benzalkonium chloride in O_3/UV [142]. According to the findings, the increase of O_3 dosage demonstrate a noticeable enhancement of the degradation efficiency up to optimal concentration (i.e., 2.37 g/h). The enhancement of the degradation efficiency was diminished upon further increase of O_3 dosage to 3.37 g/h and 4.37 g/h. This is commonly attributed to the scavenging of radical species due to the reaction of $HO^{\bullet}$ radicals with excessive O_3 and radical recombination reactions [143]:

$$O_3 + HO^{\bullet} \rightarrow HO_2^{\bullet} + O_2 \qquad 1.19$$

$$HO^{\bullet} + HO_2^{\bullet} \rightarrow H_2O + O_2 \qquad 1.20$$

$$HO^{\bullet} + HO^{\bullet} \rightarrow H_2O_2 \qquad 1.21$$

These interactions decrease the fraction of radical species available for the reaction with pollutants. The above observations highlight the significant impact of O_3 concentration in O_3-assisted AOPs and the optimization of O_3 dosage is an effective tool to obtain the maximize the potential of the developed process at lowest electrical power input.

As an emerging alternative to traditional AOPs, SR-AOPs are intensively studied for the removal of recalcitrant contaminants from various types of wastewaters. With an aim to exploit the advantageous features of $SO_4^{\bullet-}$ radicals, such as higher oxidation capacity, wide operation pH and simplicity in operation, PS and PMS have been studied extensively. Thus, PS activated under UV light was evaluated for the degradation of 200 mg/L humic acid from the laboratory simulated wastewater resulting in 76.17% of TOC removal [144]. Such removal efficiency was attained at PS concentration of 25 mmol/L and recommended for potential application in deep treatment of landfill leachate. The effectiveness of SR-AOPs in the treatment of raw municipal landfill leachate was confirmed through thermally-activated PS, which simultaneously removed COD and ammonia [145]. In this study, the utilization of $SO_4^{\bullet-}$ radicals derived from relatively low PS dosage decreased COD concentration from 1096 mg/L to 214 mg/L at pH 8.2, while the NH_3 content was reduced from 540 mg/L to 72 mg/L. During the process, NH_3 was converted into NO_3^- ions, excessive content of which require further denitrification. Moreover, it was proposed that the increased PS dosage at basic conditions led to the recombination $SO_4^{\bullet-}$ radicals into $HO^\bullet$ radicals, which facilitated the NH_3/NO_3^- conversion. High PS dosage was also found detrimental due to the pH drop below 4 which add pH recovery step before discharge. In the case of PMS, the treatment of semi-aerobic aged refuse biofilters effluent arising from treating landfill leachate using PMS/UV resulted in 37.39% COD removal, whereas PMS/H_2O_2/UV and H_2O_2/UV declined COD by 30.51% and 28.59%, respectively [146]. These resulted indicated the superior oxidation capacity of $SO_4^{\bullet-}$ radicals over $HO^\bullet$ radicals for the degradation of refractory organic compounds (e.g., fulvic and humic-like substances). The photo-activated PMS was proven effective in treating refractory pollutants contained in incineration leachate removing 70.6% of COD at optimal PMS dosage of 10 g/L, pH 8.96 within 60 min [147]. The increase of PMS dosage to 15 g/L increased the COD removal negligibly and 0.59 g/L of residual PMS was detected after the treatment. Taking into account that the residual PMS at optimal concentration was 0.39 g/L, it was suggested that excess PMS was consumed throughout the process participating in reactions with $SO_4^{\bullet-}$ and $HO^\bullet$ radicals (Eqs. 1.22-1.25). The detrimental effect of these transformations is the formation of the radical species with lower oxidation potential (e.g., peroxysulfate and hydroperoxyl radicals), which is reflected in the decrease of the degradation efficiency. For instance, the inhibitory effect high PMS dosage was observed upon the increase of PMS concentration from 1.5 mM to 2.0 mM during the degradation of benzotriazole in PMS/O_3/US. Moreover, a slight decrease in the degradation

efficiency of Orange II was observed during the US-assisted heterogeneous activation of PMS by Fe-CO-SBA catalyst. The decolorization of the pollutant was increased from 77.4% to 95.5% with the increase of PMS concentration from 1.6 mM to 3.2 mM. Subsequent increase of PMS dosage to 4.0 mM decreased the degradation efficiency by 2.1% declining the rate from 0.0246 min^{-1} to 0.0216 min^{-1}.

$$HSO_5^- + SO_4^{\bullet -} \rightarrow SO_5^{\bullet -} + HSO_4^- \quad 1.22$$

$$HSO_5^- + SO_4^{\bullet -} + H_2O \rightarrow 2SO_4^{2-} + HO_2^{\bullet} + 2H^+ \quad 1.23$$

$$HSO_5^- + HO^{\bullet} \rightarrow SO_5^{\bullet -} + H_2O \quad 1.24$$

$$HSO_5^- + HO^{\bullet} \rightarrow SO_4^{2-} + HO_2^{\bullet} + H^+ \quad 1.25$$

The excess dosage of PS can also lead to the undesirable consumption of $SO_4^{\bullet -}$ radicals. The depletion of $SO_4^{\bullet -}$ and $HO^{\bullet}$ radicals by PS proceeds with the rate constants of 6.3×10^5 $M^{-1}s^{-1}$ and 1.4×10^7 $M^{-1}s^{-1}$, respectively, and produce $S_2O_8^{\bullet -}$ radicals, which undergo decomposition during hydrolyzation as shown in Eqs. 1.26-1.28 [148]. This radical inactivation mechanism was suggested to occur with the increase of PS concentration from 1 mM to 10 mM in PS/V_2O_3 [148]. This decreased the degradation rate constant of 2,4,4′-trichlorobiphenyl from 0.0117 min^{-1} to 0.0078 min^{-1}. Bimolecular recombination of $SO_4^{\bullet -}$ radicals (Eq. 1.29) with a rate constant of 1.6-8.1 × 10^8 $M^{-1}s^{-1}$ is additionally recognized as a detrimental impact of high PS dosage [144].

$$S_2O_8^{2-} + SO_4^{\bullet -} \rightarrow S_2O_8^{\bullet -} + SO_4^{2-} \quad 1.26$$

$$S_2O_8^{2-} + HO^{\bullet} \rightarrow S_2O_8^{\bullet -} + HO^- \quad 1.27$$

$$\frac{3}{2}S_2O_8^{\bullet -} + H_2O \rightarrow 2SO_4^{2-} + \frac{3}{4}O_2 + 3H^+ \quad 1.28$$

$$SO_4^{\bullet -} + SO_4^{\bullet -} \rightarrow S_2O_8^{2-} \quad 1.29$$

Studies on photo-activation of sulfite for ARPs for performed in a manner of AOPs investigating the effect of key operation parameters, including the dosage of the reductant. Similar to AOPs, it was found that the concentration of the applied SO_3^{2-} significantly affect the effectiveness of the ARP, by determining the formation and stability of the reductive species. At optimal concentration level, SO_3^{2-}/UV produces sufficient amount of $e_{aq.}^-$ and $H^{\bullet}$ radicals, thereby enabling the reductive

degradation of pollutants. For instance, different SO_3^{2-} dosage in the range of 0.1 mM to 1.6 mM in SO_3^{2-}/UV for the degradation of carbamazepine showed the gradual increase of the degradation efficiency from 24.5% to 99.6% in 20 min. These results suggested that at lower SO_3^{2-} dosage, the formation of the reductive species was limited, while the increased SO_3^{2-} dosage promoted their production. Similarly, the degradation of N-nitrosodimethylamine by SO_3^{2-}/UV was increased from 35.39% to 67.73% within 5 min as SO_3^{2-} dosage was increased from 0.5 mM to 1.0 mM [149]. The rate constants of BrO_3^- degradation in SO_3^{2-}/UV were 0.026 min^{-1}, 0.033 min^{-1} and 0.056 min^{-1} for SO_3^{2-} concentration of 6.4 mg/L, 12.8 mg/L and 25.6 mg/L, respectively [135]. Assuming that the BrO_3^- can be degraded either through the direct UV photolysis or radical-induced reduction, the favorable impact of high SO_3^{2-} dosage was due to the promotion of radical-induced reduction. In the case of the dominant contribution of the direct photolysis, the increase of SO_3^{2-} ions having higher UV absorbance could decrease the effectiveness of SO_3^{2-}/UV process. Conversely, the increase of SO_3^{2-} dosage was related to radical scavenging reactions causing the decline in degradation efficiency as was discussed for PS/PMS-based AOPs. Hence, the treatment of BrO_3^- solution under SO_3^{2-}/VUV revealed three stages based on the correlation between the rate constant of BrO_3^- degradation and SO_3^{2-} dosage [150]. In the stage I, where the SO_3^{2-} dosage was 0.25-5.0 mM, the rate constant remained constant as $HO^{\bullet}$ from UV photolysis of water consumed the reductive species. At SO_3^{2-} dosage in the range of 5.0-1.0 mM (stage II), the linear increase of rate constant was observed, whereas the increase of the rate constant was lower at 1.0-5.0 mM SO_3^{2-} (stage III). The decline in the growth of the rate constant was attributed to consumption of $e_{aq.}^-$ by $SO_3^{\bullet-}$ radicals as followed [135]:

$$SO_3^{\bullet-} + e_{aq.}^- \rightarrow SO_3^{2-} \qquad 1.30$$

1.5.4.2. Effect of solution pH

The effectiveness of O_3-assisted AOPs is strongly dependent on solution pH as this parameter determine the mechanism of O_3 reaction with pollutants. The oxidation of pollutants can proceed through the electrophilic attacks of molecular O_3 or non-selectively by $HO^{\bullet}$ radicals. At acidic pH, O_3 which is relatively stable and the degradation of organic pollutants is mainly contributed by the direct interaction. In such a scenario, organic compounds with electron-rich functional groups, such as activated aromatic rings and double bonds are degraded preferably as the oxidation by molecular O_3 is selective. As a result, the generation of $HO^{\bullet}$ radicals

in O_3-assisted AOPs operating at acidic pH is suppressed and the degradation efficiency is limited. At neutral pH, both direct and indirect routes are involved in the oxidative degradation of pollutants. At circumneutral conditions, O_3 is partially converted into $HO^{\bullet}$ radicals and the co-existence of both oxidative species can ensure the degradation of a variety of pollutants. For instance, the degradation of complex organic substances containing diverse types of functional groups and bonds can be effectively induced through the simultaneous action of both direct and indirect oxidation in O_3-assisted AOPs at near-neutral pH. Nevertheless, O_3-assisted AOPs exhibit the highest effectiveness at basic pH. At pH > 8, O_3 is unstable and readily decomposed to form $HO^{\bullet}$ radicals as HO^- ions initiate radical chain reactions. Owing to the accelerated generation of $HO^{\bullet}$ radicals, the ozonation at basic pH is considered as individual AOP, the effectiveness of which was proven towards industrial effluents [151]. For instance, the ozonation by applying 2.37 g/h O_3 dosage degraded 18.6% of benzalkonium chloride at pH 5.0 in 20 min, while the degradation efficiency of 98.2% was achieved at pH 11.0 [142]. The increase of pH from 5.0 to 11.0 similarly increased the degradation efficiency of the pollutant under the combined O_3/UV process. Additionally, the degradation efficiency of bisphenol a was enhanced from 22% to 45% after 20 min of peroxone treatment upon the increase of initial pH from 3 to 11 [141]. Although alkaline pH is favorable for O_3-assisted AOPs, the effectiveness of these processes can be diminished by naturally-occurring carbonate/bicarbonate (CO_3^{2-}/HCO_3^-) ions. The dissolution of atmospheric CO_2 and minerals are main the sources of carbonates in natural water matrix and CO_3^{2-}/HCO_3^- ions act as scavengers of $HO^{\bullet}$ radicals producing carbonate anion radicals ($CO_3^{\bullet-}$) [152]. The formed radicals exhibit lower oxidation capacity than $HO^{\bullet}$ radicals, and such conversion declines the effectiveness of O_3-assisted AOPs.

In contrast to O_3-assisted AOPs, PS/PMS processes exhibit higher effectiveness within a broader range of pH. As an important operating parameter, the solution pH affects the generation of radical species and determines the distribution of $SO_4^{\bullet-}$ and $HO^{\bullet}$ radicals. Under acidic conditions, the activation of both PS and PMS leads to the predominant generation $SO_4^{\bullet-}$ radicals, which attack the target compounds *via* single electron transfer. At pH > 7, $SO_4^{\bullet-}$ radicals are relatively stable, while PMS and PS exist in protonated forms, i.e., HSO_5^- and $HS_2O_8^-$ monoanions [153,154]. The composition of the reactive species at neutral conditions consists of both $SO_4^{\bullet-}$ and $HO^{\bullet}$ radicals. The presence of both radicals is also supported by the interconversion according to Eq. 1.31 [153,155].

$$SO_4^{\bullet-} + H_2O \rightarrow HO^{\bullet} + SO_4^{2-} + H^+ \quad 1.31$$

$$SO_4^{\bullet-} + HO^- \rightarrow HO^{\bullet} + SO_4^{2-} \quad 1.32$$

$$S_2O_8^{2-} + 2H_2O \rightarrow SO_4^{\bullet-} + O_2^{\bullet-} + SO_4^{2-} + 4H^+ \quad 1.33$$

In basic solutions, the interconversion of $SO_4^{\bullet-}$ and $HO^{\bullet}$ radicals is accelerated due to the presence of HO^- ions (Eq. 1.32). In this, $SO_4^{\bullet-}$ radicals react with HO^- ions to yield $HO^{\bullet}$ radicals, which play a major role in degradation of water pollutants in both PS/PMS processes. Although $HO^{\bullet}$ radicals exhibit higher oxidation potential, the interconversion of radicals at basic conditions can lower the degradation efficiency of PS/PMS processes. For instance, the degradation rate of atenolol was dropped drastically with the increase of pH from optimal 9 to 11 [155]. Such decline in degradation efficiency was explained by the non-selectivity and short half-life of $HO^{\bullet}$ radicals. Alternatively, PS-activated by iron-containing water treatment residuals demonstrated the highest degradation efficiency of sulfamethoxazole at pH 3.5 [156]. With increase of initial pH from 3.5 to 10.1, the degradation efficiency was declined from 83% to 40% after 60 min. Along with the complexation of active metal sites, bimolecular recombination of $SO_4^{\bullet-}$ radicals prevailing the rate of $SO_4^{\bullet-}$/$HO^{\bullet}$ interconversion was indicated among the negative impact of alkaline pH. On the other hand, highly alkaline conditions are able to activate PS as shown in Eq. 1.33 [157,158]. The alkali activation is performed by bases, such as NaOH, KOH and produces $SO_4^{\bullet-}$ superoxide anion ($O_2^{\bullet-}$) radicals. Taken together, the above observations underscore the solution pH as a parameter that can tune the effectiveness of PS/PMS processes towards the target pollutant. Hence, unsaturated substances can be selectively degraded by $SO_4^{\bullet-}$ radicals at acidic pH, while the dominance of $HO^{\bullet}$ radicals at higher pH values can non-selectively oxidize persistent pollutants.

The degradation performance of SO_3^{2-}/UV is pH-dependent, as the distribution of S(IV) species in the form of sulfurous acid (H_2SO_3), bisulfite (HSO_3^-) and SO_3^{2-} ions is directly controlled by solution pH [159]. At acidic pH, S(IV) species exist in the protonated HSO_3^- form, while SO_3^{2-} are the dominant form at higher pH. While HSO_3^- and SO_3^{2-} ions exhibit absorbance at different wavelength, the absorbance of UV light by HSO_3^- ions in range of 225-300 nm is lower than that of SO_3^{2-} ions [160]. Specifically, the molar absorptivity of SO_3^{2-} ions at 222 nm at pH 3 is reported as 90 $M^{-1}cm^{-1}$, while it was found as 1460 $M^{-1}cm^{-1}$ at pH 11 [159]. Consequently, the lowered utilization of UV light at acidic pH decreases the photo-ionization of

SO_3^{2-} resulting in lowered generation of reactive species. For instance, the degradation efficiency of perfluorooctane sulfonate in SO_3^{2-}/UV was 2.8% at pH 3 after 90 min, whereas it was 23.3% and 30.7% at pH 9 and 12, respectively [136]. The detrimental effect of acidic pH on SO_3^{2-}/UV is also ascribed to the rapid scavenging of $e_{aq.}^-$ by H^+ with a rate constant of 2.3×10^{10} $M^{-1}s^{-1}$ (Eq. 1.34**)** [137,161]. In contrast, the HO^- ions present at basic pH are reported to promote the generation of $e_{aq.}^-$ according to Eq. 1.35 [161]. The favorable impact of HO^- ions on SO_3^{2-}/UV was confirmed by the increase of defluorination of perfluorooctanoic acid from 36% to 57% within 30 min upon the increase of solution pH from 9 to 12 [137]. On the other hand, the degradation rate constant of diclofenac in SO_3^{2-}/UV was decreased from 0.2294 min^{-1} to 0.1303 min^{-1} with the increase of pH from 6 to 9 [162]. In this study, the acidic conditions were suggested favorable as $H^{\bullet}$ radicals derived from the activation of HSO_3^- ions were responsible for the degradation of diclofenac. Similar tendency was observed during the reductive degradation of vinyl chloride by SO_3^{2-}/UV [163]. In this case, the degradation rate constant of vinyl chloride gradually grew from 0.001 min^{-1} to 0.042 min^{-1} with the increase of pH from 5 to 9. At highly alkaline conditions of pH 11, the degradation rate constant was dropped to 0.016 min^{-1} and explained by the importance of competing scavenging reactions consuming $e_{aq.}^-$.

$$e_{aq.}^- + H^+ \rightarrow H^{\bullet} \quad 1.34$$

$$H^{\bullet} + HO^- \rightarrow e_{aq.}^- + H_2O \quad 1.35$$

To conclude, the solution pH serves as a control parameter in SO_3^{2-}/UV determining the generation and speciation of reductive species. The solution pH in SO_3^{2-}/UV requires careful optimization considering the scavenging reactions and target pollutant in order to maximize the degradation performance.

1.5.4.3. Effect of water constituents

The composition of real-case wastewaters as well as natural water bodies is complex and contains a variety of organic and inorganic substances, including naturally-occurring inorganic ions. In order to assess the applicability of advanced chemical processes in practice, the effect of water constituent on the degradation efficiency of the target pollutant is investigated along with other critical process parameters. Since the presence of inorganic anions is ubiquitous in natural waters, the effect of chloride (Cl^-), CO_3^{2-}, sulfate (SO_4^{2-}), and nitrate (NO_3^-) anions on the effectiveness of the process is commonly evaluated. In general, the effect of co-

existing anions is considered as detrimental to the overall performance of advanced chemical processes due to the interaction with reactive species thereby competing with the target compound. In this, the scavenging effect is typically attributed to the formation of the secondary radical species that exhibit lower reactivity towards the target pollutant. In the case of O_3-assisted AOPs, the occurrence of CO_3^{2-} anions may pose a significant inhibition impact as the primary $HO^{\bullet}$ radicals highly reactive with CO_3^{2-} and HCO_3^- anions. The reaction of CO_3^{2-} and HCO_3^- ions with $HO^{\bullet}$ radicals proceeds rapidly with a rate constant of 3.9×10^8 $M^{-1}s^{-1}$ and 1.6×10^6 $M^{-1}s^{-1}$, respectively, producing $CO_3^{\bullet-}$ radicals with oxidation potential of 1.59 eV as shown in Eqs. 1.36-1.38 [152,164]. Consequently, with the conversion of $HO^{\bullet}$ into $CO_3^{\bullet-}$ radicals, the oxidation capacity of O_3-assisted AOPs decreases. For instance, the presence of 2 mM and 10 mM CO_3^{2-} anions decreased the degradation rate constant of benzalkonium chloride in O_3/UV from 0.306 min^{-1} to 0.281 min^{-1} and 0.236 min^{-1}, respectively, after 25 min [142]. On the other hand, $CO_3^{\bullet-}$ radicals exhibit longer life-time and selectively attack electron-rich functional groups (e.g., $-NH_2$, -OH) through electron transfer mechanism [152]. Moreover, the elevation of pH induced by CO_3^{2-}/HCO_3^- equilibrium can promote the decomposition of O_3 into $HO^{\bullet}$ radicals. In particular, the COD removal efficiency of phenol solution was 50% after 30 min sole ozonation, and was increased to 60% and 65% upon addition of 250 mg/L and 500 mg/L [165]. The ozonation in the absence of anion at pH adjusted similar to the buffering effect of CO_3^{2-}/HCO_3^- conversion (~9.5-12.5), resulted in 70% COD reduction, confirming the favorable effect of HO^- ions. Compared to CO_3^{2-} ions, the reaction of Cl^- ions with $HO^{\bullet}$ radicals generates $Cl^{\bullet}$ radicals with relatively high oxidation potential of 2.4 eV as depicted in Eqs. 1.39, 1.40 [164]. The reaction occurs spontaneously with the rate constant of 4.3×10^9 $M^{-1}s^{-1}$ and represent an initiation step of radical transformations to yield $Cl_2^{\bullet-}$ radicals (2.0 eV) according to Eq. 1.41. Owing to the predominant contribution of $Cl^{\bullet}$ radicals, a slight improvement in degradation efficiency of O_3-assisted AOPs is commonly observed. While at higher Cl^- ion dosages, less reactive $Cl_2^{\bullet-}$ radicals are the major secondary reactive species and the effectiveness of O_3-assisted AOPs is suppressed. For instance, the degradation rate constant of benzalkonium chloride in O_3/UV was primarily increased from 0.306 min^{-1} to 0.319 min^{-1} upon addition of 2 mM of Cl^- ions [142]. Further increase of Cl^- ions to 10 mM decreased the rate constant to 0.286 min^{-1}. Although the degradation efficiency is affected slightly in the presence of Cl^- ions, the transformation products require careful investigation due to the possible formation of toxic halogenated substances. In the presence of SO_4^{2-} ions, $HO^{\bullet}$ radicals can be converted into $SO_4^{\bullet-}$ radicals (Eq. 1.42)

with negligible change in oxidation potential and prolonged life-time. Considering the selectivity of $SO_4^{\bullet-}$ radicals to electron-rich moieties, $HO^{\bullet}/SO_4^{\bullet-}$ recombination can be beneficial in removal of certain pollutants. However, the addition of SO_4^{2-} ions at higher dosage inhibits the effectiveness of AOPs utilizing $HO^{\bullet}$ radicals, which is explained based on Nernst Equation [166] (Eq. 1.43).

$$CO_3^{2-} + HO^{\bullet} \rightarrow CO_3^{\bullet-} + HO^{-} \quad 1.36$$

$$HCO_3^{-} + HO^{\bullet} \rightarrow HCO_3^{\bullet} + HO^{-} \quad 1.37$$

$$HCO_3^{\bullet} \leftrightarrow CO_3^{\bullet-} + H^{+} \quad 1.38$$

$$Cl^{-} + HO^{\bullet} \rightarrow HClO^{\bullet-} \quad 1.39$$

$$HClO^{\bullet-} + H^{+} \rightarrow Cl^{\bullet} + H_2O \quad 1.40$$

$$Cl^{\bullet} + Cl^{-} \rightarrow Cl_2^{\bullet-} \quad 1.41$$

$$SO_4^{2-} + HO^{\bullet} \rightarrow SO_4^{\bullet-} + HO^{-} \quad 1.42$$

$$E_{(SO_4^{\bullet-}/SO_4^{2-})} = E^0_{(SO_4^{\bullet-}/SO_4^{2-})} + \frac{RT}{zF} ln \frac{[SO_4^{\bullet-}]}{[SO_4^{2-}]} \quad 1.43$$

, where $E_{(SO4\bullet-/SO42-)}$ and $E^0_{(SO4\bullet-/SO42-)}$ represent half-reaction reduction potential and the standard half-reaction reduction potential, R – universal gas constant, T – temperature, z is the number of electrons transferred in the half-reaction, and F is the Faraday constant.

According to Nernst Equation, the oxidation potential of $SO_4^{\bullet-}$ radicals is decreased at high concentration of SO_4^{2-} ions. Except traditional AOPs, the similar effect SO_4^{2-} ions was observed also for SR-AOPs. Thus, with the increase of concentration of SO_4^{2-} ions from 1 mM to 10 mM $E_{(SO4\bullet-/SO42-)}$ was reduced by 0.0582 V and 0.3408 V with the further increase to 100 mM [167]. This explained the inhibited degradation of trichloroethylene over Fe(II)-activated PS. The reactivity of $SO_4^{\bullet-}$ radicals with CO_3^{2-} anions is comparable to that of $HO^{\bullet}$ radicals as shown in Eqs. 1.44-1.46. More specifically, the presence of CO_3^{2-}/HCO_3^{-} ions converts $SO_4^{\bullet-}$ radicals into $CO_3^{\bullet-}$ radicals with lower oxidation potential thereby reducing the degradation of recalcitrant pollutants. Hence, the addition of 5 mM of CO_3^{2-} decreased the degradation efficiency of O_3/PMS process towards atrazine, nitrobenzene by 27% and 40% [168]. The degradation efficiency of aniline after 60 min treatment in PS/Fe(II) was decreased from 66.36% to 17.32% with increase in concentration of CO_3^{2-} anions from 1 mM to 10 mM [169]. Since $SO_4^{\bullet-}$ radicals are

converted into $HO^{\bullet}$ radicals at basic pH, the scavenging effect CO_3^{2-} ions was attributed to the reaction of $HO^{\bullet}$ radicals with CO_3^{2-} anions. The negligible effect of co-exiting anions, including CO_3^{2-} ions is commonly observed in PS/PMS processes that proceed through nonradical mechanism. For instance, the degradation efficiency of sulfadiazine in PS process activated by N-doped biochar was barely affected by the presence of 20 mM CO_3^{2-} anions [170]. In this case, the mechanism of sulfadiazine degradation involved electron transfer excluding the formation of radical species, hence, the scavenging by CO_3^{2-} ions was insignificant. The interaction of $SO_4^{\bullet-}$ radicals with halide ions (e.g., Cl^-, Br^-) resembles that of with $HO^{\bullet}$ radicals (Eqs. 1.47, 1.48). However, along with the formation of less reactive corresponding radicals, these halide ions can be transformed into toxic and carcinogenic chlorates (ClO_3^-) and bromates (BrO_3^-) based on Eqs. 1.49-1.51 [171]. These by-products are derived from the reaction of HOCl and HBrO with $SO_4^{\bullet-}$ radicals and the strategies of their control include pH adjustment and quenching halide radicals by CO_3^{2-}/HCO_3^- ions. In AOPs and SR-AOPs, the effect of NO_3^- anions is associated with possible formation of nitrate ($NO_3^{\bullet}$) radicals that exhibit slightly lower oxidation potential of 2.3-2.5 V [166]. The reaction between $SO_4^{\bullet-}$ radicals and NO_3^- anions proceeds slowly with a rate constant of 2.1×10^0 $M^{-1}s^{-1}$, while it is not reported for $HO^{\bullet}$ radicals [172]. The slow response explains the negligible effect of NO_3^- anions in the concentration range of 1-50 mM on the degradation of Orange II in PMS process activated by cobalt phosphide nanoparticles [173]. Similarly, no considerable impact of NO_3^- anions in the range of 10-500 mM was observed during the degradation of benzene, toluene, ethylbenzene and xylenes using thermally-activated PS [174]. Again, the presence of NO_3^- anions can improve the performance of UV-assisted processes by contributing to the formation of $HO^{\bullet}$ radicals according to Eq. 1.52 [166,175].

$$CO_3^{2-} + SO_4^{\bullet-} \rightarrow CO_3^{\bullet-} + SO_4^{2-} \quad 1.44$$

$$HCO_3^- + SO_4^{\bullet-} \rightarrow HCO_3^{\bullet} + SO_4^{2-} \quad 1.45$$

$$HCO_3^{\bullet} \leftrightarrow CO_3^{\bullet-} + H^+ \quad 1.46$$

$$Cl^- + SO_4^{\bullet-} \rightarrow Cl^{\bullet} + SO_4^{2-} \quad 1.47$$

$$Cl^{\bullet} + Cl^- \rightarrow Cl_2^{\bullet-} \quad 1.48$$

$$Cl_2^{\bullet-} + Cl^{\bullet} \rightarrow Cl_2 + Cl^- \quad 1.49$$

$$Cl_2 + H_2O \rightarrow HClO + H^+ + Cl^- \quad 1.50$$

$$HClO + SO_4^{\bullet -} \rightarrow \cdots \rightarrow ClO_3^- + SO_4^{2-} \quad 1.51$$

$$NO_3^- + H_2O \xrightarrow{h\nu} NO_2^{\bullet} + HO^{\bullet} + HO^- \quad 1.52$$

In contrast to AOPs, the presence of NO_3^- anions demonstrate high inhibitory effect on ARPs. Co-existing NO_3^- anions instantaneously react with $e_{aq.}^-$ at a rate constant estimated as 9.7×10^9 $M^{-1}s^{-1}$ [176]. Owing to this, NO_3^- anions are employed as a specific scavenger to evaluate the contribution of $e_{aq.}^-$ in ARPs. For this, the quenching with NO_3^- ions are conducted in parallel with nitrite ions (NO_2^-), which effectively scavenge both $e_{aq.}^-$ and $H^{\bullet}$ radicals with a rate constant of 4.1×10^9 $M^{-1}s^{-1}$ and 7.1×10^8 $M^{-1}s^{-1}$, respectively [176]. The reaction of $e_{aq.}^-$ with CO_3^{2-} anions proceeds slowly with a rate constant of 3.9×10^5 $M^{-1}s^{-1}$ [177], and, therefore, the inhibitory effect caused by the presence of CO_3^{2-} anions is less pronounced. For example, the presence of 10 mM CO_3^{2-} anions could inhibit the degradation efficiency of atrazine in $SO_3^{2-}/I^-/UV$ only by 2% after 60 min of treatment [176]. Similarly, the inhibitory effect of ~5% on BrO_3^- degradation was observed upon the addition of 1-4 mM HCO_3^- ions in SO_3^{2-}/UV [178]. The negligible inhibition was attributed to the greater reaction rate constant of $e_{aq.}^-$ and $H^{\bullet}$ radicals with BrO_3^- (10^7-10^8 $M^{-1}s^{-1}$) as compared to that of with HCO_3^- ions (10^4-10^5 $M^{-1}s^{-1}$). In contrast, the complete degradation of 4-chloro-2-methylphenoxyacetic acid in SO_3^{2-}/UV attained within 25 min was reduced to 77% due to the scavenging effect of HCO_3^- ions on $e_{aq.}^-$ [179]. The interference of Cl^- and SO_4^{2-} ions on SO_3^{2-}-based ARPs exhibits a negligible inhibitory effect due to lower reactivity to both $e_{aq.}^-$ and $H^{\bullet}$ radicals (<10^5-10^6 $M^{-1}s^{-1}$). Hence, the photo-reduction of atrazine in $SO_3^{2-}/I^-/UV$ was inhibited by 3% in presence of SO_4^{2-} ions, while it remained unchanged after adding 10 mM of Cl^- ions [176]. Additionally, 10 mM Cl^- ions had no effect on the photo-reductive removal of As (III) and As (IV) in $SO_3^{2-}/I^-/UV$ [177]. The complete degradation 4-chloro-2-methylphenoxyacetic acid in SO_3^{2-}/UV achieved in the absence of co-existing anions was depleted to 94.13% and 90% in the presence of SO_4^{2-} and Cl^- ions, respectively [179]. Nonetheless, these observations imply that SO_3^{2-}-based ARPs are less sensitive to the presence of common inorganic anions (excluding NO_3^-/NO_2^- ions), and considering matrix composition, SO_3^{2-}-based photo-reduction can be applied for the remediation of water contaminated with halogen-containing persistent pollutants.

1.6. From claws to laser beams – a brief survey on cavitation

The phenomenon of cavitation appears widely in nature, specifically amongst the living organisms of the aquatic environment. Cavitation-related processes limit the speed of dolphins at 15 ms^{-1} and induce damages on the body of mackerels and tuna [180]. On the other hand, the species, such as pistol shrimps (*alpheidae*) and mantis shrimps (*odontodactylidae*) evolved to exploit the effect of cavitation [181,182]. For instance, pistol shrimps or snapping shrimps actively use the invisible force of cavitation to hunt and protect. Owing to the special shape of claws, pistol shrimps create water jets of high velocity, which cause pressure drop followed by a local vaporization of water, i.e., forming cavitation bubbles. Nevertheless, for many people cavitation is commonly associated with marine technology, particularly, with a negative effect on hydraulic machinery. In 1894, the British engineers encountered an unexpected issue during the test of the torpedo-boat destroyer “Daring”. The ship could only achieve 24 knots, while the declared speed was 27 knots [183]. Throughout the solving of the problem, it was found that the engine power was partially consumed in the formation of water vapor bubbles causing the reduced propeller performance. In addition, the implosion of the bubbles was accompanied with high pressure and temperature that damage the propeller blades. To explain this phenomenon, the term cavitation meaning “hollow” in Latin (*cavus*) was introduced by Barnaby and Parsons who quoted Froude in 1895 [184].

Nowadays, cavitation represents a complex process involving the formation of cavitation bubbles due to the rapid transition from liquid to the gaseous state resulting from pressure drop. The dynamic process of cavitation includes the initial formation of cavitation nuclei as liquid enters a low-pressure region. Then bubbles undergo isothermal expansion growing to a critical size prior to the adiabatic collapse in the case of successful compression cycle [185]. The collapse of cavitation bubbles occurs in a short time interval and create local regions of high pressure and temperature (i.e., 9869 atm, 4726.8 ºC), so-called “hot-spots” [185,186]. Such extreme conditions are often compared to the conditions on the surface of the sun. Unlike boiling induced by high temperature and vacuum, the effect of cavitation is localized within the collapsing bubble rather than applied to the whole volume of the liquid.

Depending on the conditions and method, cavitation can be classified as acoustic, hydrodynamic, optic and particle. In acoustic cavitation (AC), the liquid is subjected to excitation by ultrasonic irradiation and cavitation bubbles are generated as a

result of pressure variations and vibration of the surroundings caused by sound waves [186]. Cavitation bubbles can also be generated by forcing a liquid flow to pass through a mechanical constriction of specific geometrical configuration as in hydrodynamic cavitation (HC) [185,186]. When the liquid passes through the constriction, the local static pressure drops below the vapor pressure of the liquid leading to the formation of cavitation bubbles. This pressure drop occurs due to the increased velocity of the liquid passing through the decreased flow area as follows from Bernoulli's principle (Eq. 1.53) [187]. With the recovery of the static pressure at the downstream of the constriction, cavitation bubbles undergo violent collapse releasing a large magnitude of energy. In the case of optical cavitation, short laser pulses of high intensity induce a plasma which causes a rapid vaporization of water producing cavitation bubbles [188]. Similarly, particle cavitation can occur as a beam of elementary particles, e.g., protons, neutrons rupture the liquid [189]. In practice, both optical and particle cavitation are induced by energy-intensive lasers and, therefore, their large-scale application is hindered due to high operational cost. The sources of AC and HC require less energy input, while the design of reactors is simple and scalable. Hence, AC and HC are amongst the most investigated cavitation approaches, which found application in water treatment [190,191], chemical synthesis [192–194], biotechnology [195], medicine [196,197], pharmaceuticals [198], food [199,200] and petroleum industry [201].

$$\frac{V^2}{2g} + \frac{p}{\rho g} + h = const \qquad 1.53$$

, where V – flow velocity, p – pressure, ρ – fluid density, g – gravitational acceleration, h – height.

The employment in various applications is due to the advantageous effects of cavitation, i.e., physical and chemical. The formation of shock waves, microjets and high shear stress in water represent the physical (mechanical) effect of cavitation, which are resulted from the adiabatic compression and collapse of bubbles. The chemical effect of cavitation is directly connected to the localized high temperature and pressure in "hot-spots", where enormous chemical transformations can take place. Specifically, such conditions may initiate the pyrolytic disassociation of water molecules resulting in the formation of radical species, such as $HO^{\bullet}$ radicals. The aforementioned features provide cavitation technologies with facilitated mass transfer and moderate oxidation capacity. Thus, AC and HC were extensively utilized in water treatment for physico-chemical

removal of organic pollutants and inactivation of microorganisms. For instance, AC and HC demonstrated effective inactivation of microalgae [202], baker's yest cells [203], *escherichia coli* [204], *microcystis aeruginosa* [205] through cell disruption. The effectiveness of AC induced by ultrasonic irradiation was observed towards the degradation of organic pollutants, such as *p*-nitrophenol [206], 1,2-dichloroethane [190], carbon tetrachloride [207], hexachloroethane [208], polypropylene [209], rhodamine B [210], trichloroethylene and chlorobenzene [211]. On the other hand, the sole application of HC exhibited high removal efficiency of chitosan [212], alachlor [213], pharmaceutical micropollutants [214], organic solvents [215], carbon tetrachloride and chloroform [216]. Nevertheless, the effectiveness of AC and HC is insufficient to conduct an effective degradation of POPs due to the limited generation of reactive radical species, e.g., $HO^{\bullet}$ radicals. To solve the issue, the cavitation techniques were coupled with AOPs giving a rise to the trend of the hybrid cavitation-based AOPs as illustrated in Fig. 2. Along with high degradation efficiency of POPs, the hybrid methods exhibited lower consumption of chemicals and electric power resulting in the reduced treatment time and cost.

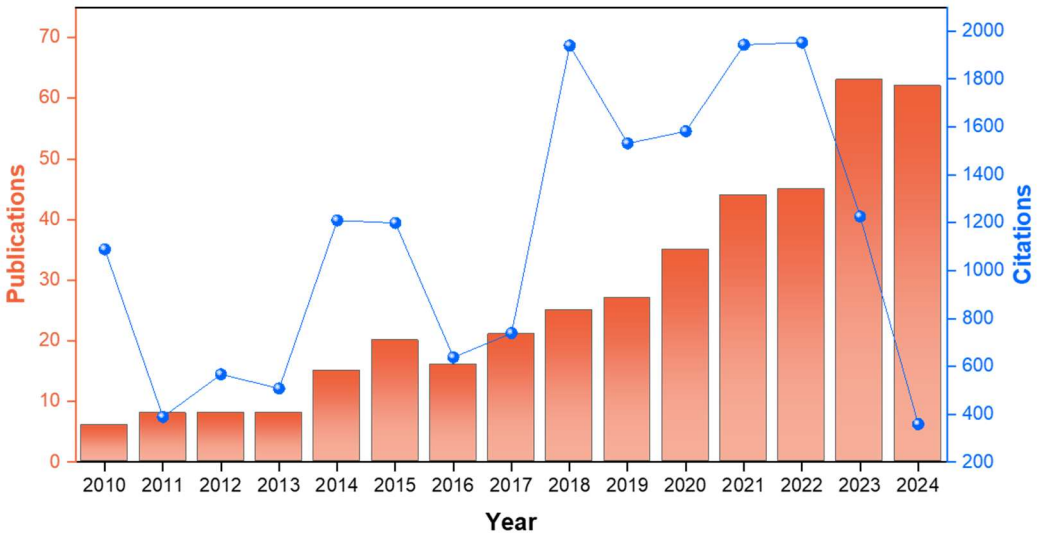

Figure 2. Number of documents reporting cavitation-based AOPs published within the past 15 years (according to Scopus database available on 20.11.2025).

The effect of cavitation is determined by the intensity of cavitation events as well as collapse pressure of cavities and, thereby, is affected by various physico-chemical factors, including the energy input, geometry of the cavitating device, vapor pressure of the treated liquid, temperature, presence of DO or suspended particles. Similarly, the effective utilization of AOPs implies the optimization of pH, time of treatment, concentration of reactants including catalysts to achieve the

highest rate of generation of radical species. In the case of the hybrid process, the mechanism relying behind the generation of radicals and degradation of organic pollutants can be altered due to the interaction of both processes. Consequently, the mechanism proposed for the generation of radical species and degradation of pollutants in cavitation-based AOPs is an object of intense discussion.

Considering the abovementioned, this work attempts to provide mechanistic insights in cavitation-based AOPs, i.e., AC/HC combined with sulfate anion radical-based AOPs (SR-AOPs) and ozone (O_3) evaluating their effectiveness towards POPs. The obtained results were discussed and interpretated to clarify mechanism of radicals' production and degradation of pollutants. Based on this, various modification routes were tested to improve the effectiveness of cavitation-based AOPs. A set of experiments measuring the effect of environmentally relevant factors, such as solution pH, dosage of radical pre cursors, presence of co-existing ions was conducted.

1.6.1. The role of cavitation in hybrid methods for water and wastewater treatment

As a unit in water and wastewater treatment schemes, cavitation is commonly employed for homogenization and fragmentation of the waste. While the force emitted during bubble collapse ensures the cell damage of pathogenic microorganisms, the radical species generated in "hot-spots" provide the oxidation of organic pollutants. These features make cavitation a versatile and effective tool with variety of valuable applications. In this regard, the implosion of cavitation bubble is a driving force responsible for initiation of key chemical transformations, including the depletion of water molecules and pyrolysis of organic pollutants. Although cavitation is defined as formation, growth and subsequent collapse bubbles, the whole process appears to be more complex involving multiple steps. In particular, cavitation nuclei are formed due to the sharp decrease in pressure below the vapor pressure of the liquid. This stage requires energy input, e.g., ultrasonic waves to induce AC and fluid flow acceleration for HC. In the case of AC, the presence of DO and suspended particles is important as they can act as centers of nucleation. Along with pressure variations, cavitation bubbles undergo multiple cycles of rarefication and compression, during which they expand. Once cavitation bubbles achieve a critical size, they become unstable and collapse rapidly creating localized "hot spots", shockwaves and liquid microjets. The intensity of cavitation as well as its chemical effect are dependent on bubble size,

collapse time, internal collapse pressure. Being induced by US waves with a frequency range of 20 kHz to 1 MHz [189], AC can be characterized using parameters, such as power and amplitude of the applied US as well as sound intensity. In general, US power and amplitude are proportional to the intensity of sound wave, which is related to pressure amplitude through Eq. 1.54 [189,217]:

$$I = \frac{P_a^2}{2pc} \qquad 1.54$$

, where I – power of sound intensity (W/m^2), P_a is the maximum pressure amplitude (Pa), ρ-density of the liquid (kg/m^3) and c – sound speed in liquid (m/s).

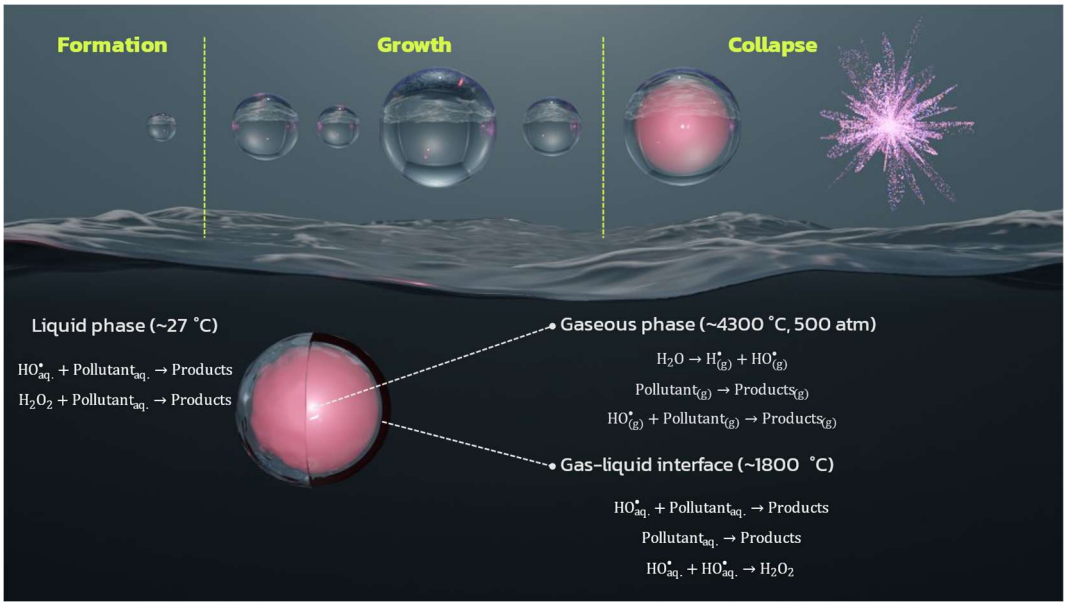

Figure 3. Simplified scheme showing the formation, growth and collapse of cavitation bubbles and different reaction zones (illustration prepared by the author).

In HC, the inlet pressure of a treated liquid before the cavitating device is amongst parameters significantly affecting the intensity of cavitational events along with geometry of cavitating device, flow velocity of liquid and temperature. To describe the cavitation and its effectiveness, cavitation number (C_v), a non-dimensional parameter connecting flow conditions and cavitation intensity was introduced and can be determined as follows [185,186]:

$$Cv = \frac{p_2 - p_V}{\frac{1}{2}u_0^2 p} \qquad 1.55$$

, where, p_2 – the downstream pressure (Pa), p_V – vapor pressure of the liquid (Pa), u_0 is the linear velocity at the throat of the cavitating device (m/s), and ρ – density of the liquid (kg/m^3).

As shown in Fig. 3, there are 3 phases, where chemical transformations take place during the cavitation: gaseous, gas-liquid interface and bulk liquid [186,218]. The extreme conditions within the cavity interior are driving force for generation of radicals *via* the depletion of water vapor, nitrogen and oxygen from air. In addition, organic pollutants are readily decomposed into CO_2 and water in gaseous phase. The pyrolytic decomposition is commonly associated with the degradation of hydrophobic compounds, e.g., VOCs as they tend to diffuse inside the cavity interior. At the interfacial region, the degradation of the pollutants is caused by the attack of radical species. Moreover, the radical species may migrate further to the bulk liquid and react with pollutants of higher solubility. Upon combination with AOPs, the generation of radical species proceeds through a variety of transformation, including radical chain reactions. In such a scenario, a radical precursor of a particular AOP is disassociated (i.e., activated) inside the cavitation bubble or at the interfacial region to yield radicals species. Unlike water, the radical precursors, especially peroxides, exhibit lower bond energy resulting in higher generation rate of radicals. Additionally, the substantial number of radical species can also be produced *via* the radical-water, radical-precursor interaction. The promoted generation of radicals provide hybrid cavitation-based AOPs/ARPs with an increased degradation rate constant (*k*) of pollutants compared to sole utilization of cavitation. Therefore, the observed *k* value of a pollutant obtained in hybrid process is typically higher than the sum of *k* values of the sole processes (e.g., cavitation, AOPs, ARPs). Such findings indicate a synergistic effect between the coupled techniques, which is expressed in synergistic index (ξ) calculated according to Eq. 1.56. It is worth to note, that if ξ=1 or <1, the effect is considered cumulative or antagonistic, respectively.

$$\xi = \frac{k_{cavitation/AOPs/ARPs}}{k_{cavitation} + k_{AOPs/ARPs}} \qquad 1.56$$

Combining AC with AOPs represents a promising strategy on large-scale utilization of sono-chemical transformations in water and wastewater treatment. Thus, the effective application of the hybrid AC/AOPs could significantly reduce treatment time and energy consumption offering an effective conversion of POPs into less-harmful biodegradable substances or their complete mineralization. Throughout the years of extensive studies, the effect of AC was employed in couple with hydrogen peroxide (H_2O_2), ozone (O_3), Fenton's process, photocatalysis, PS and PMS to degrade various water pollutants [219–221]. The effectiveness of AC/AOPs was also demonstrated in the treatment of wastewater derived from cellulose fiber

manufacturing [222], textile [223] and pharmaceutical industry [224]. For instance, the combination of AC and H_2O_2 reduced 40% of COD from bitumen production effluent in 360 min giving ξ 1.79 [225]. Similarly, the hybrid AC/Fenton' process exhibited ξ of 2.42 reducing 85.29% of COD from coke oven plant effluent within 120 min [226], while ξ of 4.78 was attained using AC/O_3 as 99.8% of ciprofloxacin was degraded in 90 min from batik industry wastewater [227]. The synergistic effect in the hybrid AC/AOPs processes is commonly attributed to the intensified production of the radical species as cavitation effectively activates the oxidizing agents (i.e., precursors). The intensified yield of $HO^{\bullet}$ radicals in AC/H_2O_2 was achieved by the continuous addition of H_2O_2 at optimal dosage that inhibited the radical recombination reactions. In AC/Fenton's process, the production of $HO^{\bullet}$ radicals was improved due to the disassociation of $[Fe\text{-}OOH]^{2+}$ complex that ensured the regeneration of Fe^{2+} ions, while the thermal disassociation of O_3 was the main source of radical species in AC/O_3. As compared to AC, the amplification of HC-based AOPs for large-scale water treatment purposes possesses higher potential due to higher energy efficiency and simplicity in design [228,229]. The synergistic effect in the combined HC/AOPs was reported for the treatment of model contaminant solutions in laboratory scale as well as for the real wastewaters in pilot scale reactors. For instance, over 90% of COD was reduced in 10 min under HC/Fenton's process during the treatment of 500 L of cellulosic fiber industry effluent [230]. The semi-pilot scale treatment of 4 L real industrial effluent containing phenolic derivatives using HC/H_2O_2 reduced COD by 40.3% in 120 min resulting in ξ of 2.75. Similarly, the combined operation of HC and photolysis (TiO_2/UV) decolorized 82.13% of 5 L ternary dye wastewater in 120 min giving ξ of 2.11 [231]. According to the studies on HC-assisted processes for water treatment, it was found that the application of HC significantly increases the biodegradability index of the treated wastewater [232,233]. Therefore, the pre-treatment of wastewaters by combined HC/AOPs before biological treatment were suggested as sustainable, economically feasible approach to ensure high biodegradation and elimination of the bio-refractory constituents. Despite the variety of configurations and designs offering high treatment capacity and reasonable energy consumption, the full-scale industrial implementation of HC-assisted processes is hindered. This issue is assumed to arise from the satisfactory efficiency HC/AOPs towards real wastewaters due to the suboptimal design HC reactors, unclear process routing and conditions [233]. The model of HC reactors with potential of industrial amplification is being expanded based on experimental and computational studies

taking into account the parameters affecting the intensity of cavitation (e.g., pressure, temperature, turbulence fluctuations) [234,235].

Water pollution caused by the occurrence of heavy metal ions and microplastics is addressed by chemical precipitation and coagulation-flocculation methods at certain level. These tertiary methods are evolving to demonstrate higher effectiveness. On the other hand, the issue of water pollution by persistent organic compounds, such VOCs and pharmaceuticals, is a growing challenge posing a great toxicity risk on living organisms. In regards with this, the implementation of advanced chemical processes as a tertiary treatment method in WWTPs represents a vital topic.

1.7. Summary of literature review

The integrated sequence of physical, biological and chemical methods involved in WWTPs effectively accomplishes the removal of suspended solids, organic matter, nutrients and pathogenic microorganisms. The mechanical separation techniques provide high TSS removal, while biological treatment methods are capable to recover nutrients, such as phosphorous and nitrogen. The secondary wastewaters containing heavy metal ions and pathogens can be effectively treated by chemical methods, such as coagulation-flocculation and chlorination prior to discharge. However, the listed methods are not designed to effectively treat POPs, among which pharmaceuticals, VOCs and PFAS represent a challenge of high concern. Initially regulating 12 POPs from three categories (i.e., pesticides, industrial chemicals, by-products) upon its adoption, the list of chemicals targeted by the Stockholm convention is continuously expanded. Recently, the stricter standards for wastewater treatment and discharge were adopted by the European Union in a revision of the Urban Wastewater Treatment Directive, on late 2024. According to the updated document, WWTPs were obliged to perform higher extend of nutrient removal and abatement of micropollutants, including pharmaceuticals, cosmetics and PFAS. These regulatory efforts reflect an urgent demand to protect public health and aquatic environment ensuring safe rivers and lakes.

In the light of this, advanced chemical processes, namely, advanced oxidation and reduction processes exploiting high reactivity of radical species are among the most promising strategies. Nevertheless, the generation of radicals requires energy input and, therefore, AOPs as well as ARPs are energy-intensive. This is the major factor hindering their large-scale implementation as a tertiary or (or quaternary) method in conventional WWTPs. In this context, the phenomenon of

cavitation emerges an overseen technology which found application in limited sectors of industry. Represented mainly by acoustic and hydrodynamic types, cavitation reactors are characterized with simplicity in design and maintenance and can operate in continuous flow mode. More importantly, the adiabatic collapse of cavitation bubbles can provide energy sufficient for activation or intensification of radical-mediated processes. Hence, the development and evaluation of the combined cavitation-based AOPs/ARPs for potential application as a tertiary stage method for the degradation of POPs is of high interest.

2. Research aims and objectives

In this thesis, the combined application of AC and HC with O_3-based AOPs and SR-AOPs (i.e., PS/PMS) was studied and examined for the treatment of model solutions of organic pollutants. The combined application of HC and SR-AOPs, i.e., PS and PMS was evaluated towards the degradation of BTEX. In the case of AC, the activation of PS and PMS was induced in the presence of asphaltenes and the developed processes were tested for BTEX degradation. The effectiveness of the hybrid process of AC and ozonation was tested on BTEX and performed in dual-frequency ultrasound reactors. The combination of HC and O_3-based AOPs was conducted in the presence of SPC, which served as a carrier of H_2O_2. The HC-based modified peroxone process was examined for the degradation of recalcitrant and highly toxic 1,4-dioxane. In addition, the effect of HC on photo-reductive capacity of sulfite/UV ARP was studied for the degradation of CLA. The obtained results were discussed based on experimental findings observed on cavitation-based AOPs and recent progress on ARPs. In order to systematically investigate the developed hybrid processes, the following objectives were defined:

1. Assess the effectiveness of sole and combined processes for the degradation of selected water pollutants and determine the role of cavitation in the developed processes.
2. Evaluate the effect of operating parameters, such as oxidant/reductant concentration (r_{rox}/r_{red}), solution pH on the degradation efficiency of pollutants and interpret the results;
3. Examine the effect of common inorganic ions on the degradation efficiency of the developed processes;
4. Verify the presence of radical species *via* quenching method selecting specific scavenging agents. Elucidate the predominant radical species responsible for the degradation of the pollutant. Identify the transformations products using GC-MS and propose the reaction mechanism to describe the degradation pathway;
5. Evaluate the potential of HC in ARPs, based on studies on combined HC/SO_3^{2-}/UV and verify the reductive pathway of CLA degradation using DFT calculations.

3. Materials and methods

3.1. Chemicals

Benzene (99.7%), sodium azide (pure p.a., 99.0%), sodium carbonate (anhydrous, pure p.a., 99.8%), sodium sulfate (anhydrous, pure p.a., 99%), sodium sulfite (anhydrous, pure p.a., 96.0%) and sulfuric acid (pure p.a., 95%) were purchased from Chempur (Poland). 1,4-dioxane (reagent grade, p.a., 99%), toluene (pure), ethylbenzene (99%), *ortho*-xylene (≥98%), sodium hydroxide (pure p.a., 98.8%), sodium nitrate (pure), potassium iodide (pure p.a.), potassium dihydrogen phosphate (pure p.a.), sodium thiosulfate pentahydrate (ACS pure p.a.), methanol (pure, 95%), sodium peroxydisulfate, oxone® (triple potassium salt, $2KHSO_5 \times KHSO_4 \times K_2SO_4$), sodium chloride (pure p.a.), hydrogen peroxide (pure p.a., 30%), 2-propanol (pure p.a.), acetone, dichloromethane, chloroform, as well as benzyl alcohol, benzoic acid, benzaldehyde, ortho-cresol used for preparation of 50 ppm (w/w) standard solutions were obtained from POCH (Poland). Clofibric acid (2-(4-chlorophenoxy)-2-methylpropanoic acid, pure p.a., 98%) and sodium nitrite were purchased from Chemat (Poland). Ortho-phosphoric acid (EMSURE®, 85%) and *n*-heptane (EMPLURA®) were obtained from Merck KGaA (Germany), while 1,4-benzoquinone (99%) was obtained from Acros Organics (Belgium). Sodium percarbonate (avail. H_2O_2 20-30%), tert-butyl alcohol, cyclohexanone and phenol were purchased from Sigma-Aldrich (Germany). Acetonitrile (HPLC gradient grade, ≥99.9%) was purchased from Fisher Chemicals (UK) and humic acids (sodium salts, 97%) was supplied by Angene (China). Argon was provided by Air-Liquide (Poland). A fraction of asphaltenes was isolated from bitumen 20/30 SDA supplied by Lotos Group (Gdańsk, Poland). The extraction of BTEXs from asphaltenes was conducted using *n*-pentane (ARG) purchased from Sigma-Aldrich (USA). All solutions were prepared in ultrapure quality water (18.2 MΩ*cm at 25 ºC) produced by a Millipore® system (Direct-Q UV-R model).

3.2. Experimental procedures

Procedure 1. Experimental procedure for the HC-SR-AOPs. Degradation experiments involving HC were carried out in a close-circuit system (Fig. 4A). As shown in Fig. 4B, the installation of the system was comprised of a tank equipped with a mixer, temperature sensor and a cooling system. The feed tank was connected to the cavitating device through main line and by-pass line. The model

solution was circulated using sequential pumping system (MS 801-4, 1360 min^{-1}, TECHTOP® MOTOR, Shanghai, China) and flowrate was monitored with electromagnetic flowmeter (MPP 600 by MAGFLO®). In this installation, Venturi tube made of brass was used as a cavitating device and the geometrical dimensions are presented in Fig. 4C.

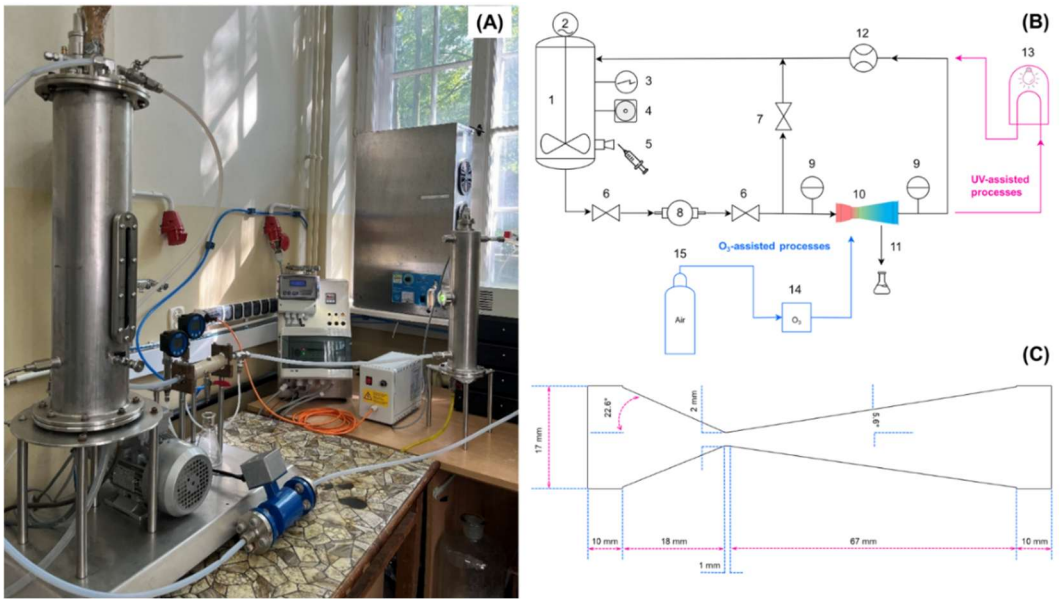

Figure 4. Photograph of HC installation (A), schematic representation of HC installation: 1-tank, 2-mixer, 3-temperature sensor, 4-cooling water circle, 5-injection port, 6-main flow valves, 7-by-pass line valve, 8-vane pump, 9-digital manometers, 10-Venturi tube, 11-sampling point, 12-flowmeter, 13-UV-chamber, 14-ozone generator, 15-dry compressed air (B), Venturi tube dimensions (C).

Digital manometers (Suku, Germany) at inlet and outlet positions of Venturi tube were mounted to measure pressure. The model solution in the volume of 5 L containing 50 ppm BTEX was treated for 360 min at 20±2 ºC. The aqueous solutions of PS and PMS were injected through the injection port with septum (Thermogreen® LB-2 Septa, Merck Supelco) located on the feed tank to attain the required molar ratio to the pollutant. The units of the installation were connected using pipes made of polytetrafluoroethylene (PTFE) and stainless-steel joints. The samples of 20 mL were collected before the starting the process and at 30 min, 60 min, 120 min, 180 min and 240 min from the sampling point located in the outlet of Venturi tube. The degradation experiments were performed in duplicates to give reproducibility within 5% and the error bars represent the data range.

Procedure 2. Experimental procedure for the AC-SR-AOPs. In the combined action of AC and SR-AOPs, the activation of PS and PMS was conducted in ultrasonic

bath (Sonorex RK 156 BH, Bandelin Electronic, Germany) operating at 35 kHz and max power output of 860 W. The bath was connected with a refrigerated bath (Chrompack RTE-110B, Neslab Instruments, USA) to maintain the reaction temperature at 25±2 ºC. The model solution containing 40 ppm of BTEX was prepared in 700 mL of deionized water, which was stirred at 1500 rpm using a magnetic stirrer (Chemland, Poland) at room temperature (approx. 25 ºC) for 60 min. In a typical experiment, a glass flask containing 700 mL of BTEX solution was placed inside the ultrasonic bath and the solution of PS/PMS was introduced with a flowrate of 1.4 mL/min. This was carried out using HPLC pump, the outlet capillary of which was placed in the bottom of the flask. The concertation of PS/PMS solution varied depending on the molar ratio of the oxidant to pollutant, while studies involving catalyst were conducted in the presence of 0.5 g/L asphaltenes. The treatment was performed for 360 min, where samples of 20 mL were taken before the treatment and every 15 min. The degradation experiments were repeated at least two times, yielding reproducibility within 5%. Error bars represent the corresponding data rangerior to extraction, the samples containing asphaltenes were filtered through hydrophilic 0.45 μm PTFE membrane.

Procedure 3. Experimental procedure for the AC-O_3-AOPs. The ozonation experiments under AC were performed in self-designed sono-reactors manufactured by Beijing Yongda Ultrasonic CO., LTD (China). The sono-reactors had similar arrangement of US generators and geometrical dimensions (280 mm×130 mm) as depicted in Fig. 5A. Owing to the transducers mounted on the wall and a sonotrode connected to the removable cover, the sono-reactors were able to produce ultrasonic irradiation of a different frequency. In a low-frequency sono-reactor, transducers and sonotrode were able to produce ultrasonic waves with frequency of 40 kHz and 120 kHz, respectively. The transducers and sonotrode in high-frequency sono-reactor operated at frequencies of 80 kHz and 200 kHz, respectively. Besides, the sono-reactors were provided with temperature sensor, mixer and cooling system. For ozonation experiments, 3.8 L of model solution containing 50 ppm of BTEX (i.e., 50 mg/kg of each component) was placed in the sono-reactor and treated for 60 min at a constant temperature maintained at 20±2 ºC. The O_3 was supplied from Tytan 32 ozone generator (Erem) using a dry air. The flowrate of the dry air was set to 0.5 L/min and the produced O_3-containing gas stream was introduced using a porous frit placed in the bottom of the reactor for better distribution (Fig. 5B). The temperature was controlled using tap water circulating through stainless steel coil placed inside the sono-reactors. To prevent the evaporation of BTEX from the reaction system, a glass condenser was

connected to the ozone outlet. The condenser was filled with methanol circulating from a thermostat HAAKE DC30 K^{20} (Thermo Scientific, Germany) with temperature set to -5 ºC. Samples of 20 mL were collected prior to the treatment and every 10 min. The experiments were performed in duplicates with <5% variation and the error bars represent the data range.

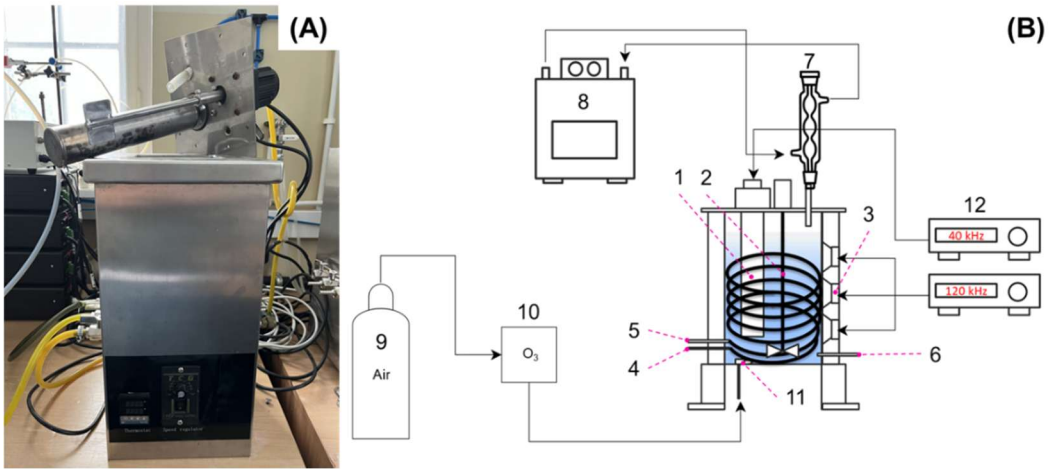

Figure 5. Photograph of DFUS reactor (A); schematic representation of the experimental set-up: 1-sonotrode, 2-mixer, 3-transducers, 4-cooling water inlet, 5-cooling water outlet, 6- sampling point, 7-condenser, 8-thermostat, 9-dry compressed air, 10-ozone generator, 11-ozone dispenser (frit), 12-US generators (B).

Procedure 4. Experimental procedure for the HC-O_3-AOPs. To perform the degradation of 1,4-dioxane in HC/SPC/O_3, the installation described in Procedure 1 was connected with Tytan 32 ozone generator (Erem). For this, the outlet line from ozone generator was connected to the gas injection port located at inlet of Venturi tube, through which a compressed dry air carrying O_3 was purged. Such gas supply allowed to deliver O_3 directly to the cavitational events ensuring high decomposition and generation rate of radical species. The solution of sodium percarbonate at certain concentration was injected through the injection port on the feed tank. Degradation experiments were conducted using 5 L of 100 ppm solution of 1,4-dioxane for 120 min at 20±2 ºC. The samples of 20 mL were collected before the starting the process and at 15 min, 30 min, 45 min, 60 min and 120 min from the sampling point located in the outlet of Venturi tube. The degradation experiments were conducted in duplicates ensuring reproducibility within 5% and the error bars denote the range between the measurements.

Procedure 5. Experimental procedure for the HC-ARPs. The degradation of CLA in HC/SO_3^{2-}/UV was performed in the HC installation described in Procedure 1 with additional unit - UV chamber connected to the outlet of Venturi tube. In this study,

the UV chamber with operating volume of 3 L was equipped with a UV mercury lamp (UVQ 250Z, 250 W, UV-Technik, Germany). The model solution containing 100 ppm of CLA was prepared in 8 L of ultra-pure water was circulated within the sealed installation at non-cavitating conditions for 15 min to ensure that units and pipes are filled with the solution. For the experiments at anaerobic conditions, the preliminary circulation was accompanied with purging Ar was for 15 min to remove DO. The units were connected using pipes made of polytetrafluoroethylene (PTFE) and stainless-steel joints. The treatment of CLA solution was conducted for 90 min at 20±2.5 ^{o} and the samples of 20 mL were collected before the starting the process and at 15 min, 30 min, 45 min, 60 min, 75 min and 90 min from the sampling point located in the outlet of Venturi tube. The degradation experiments were performed in duplicates to give the reproducibility within 5% and the error bars represents the data range.

3.3. Analytical procedures

Preparation of BTEX samples. The samples of BTEX were prepared for GC-FID analysis using dispersive liquid-liquid microextraction (DLLME). For this, 10 mL of the sample was placed in a round-bottomed glass vial and 10 µL of internal standard solution containing 10 mg/mL of 4-chlorophenol was injected. Then 0.9 mL of mixture of dichloromethane and acetone at molar ratio of 50:40 (v/v) and serving as extraction and dispersive solvents, respectively, were added. The resulting solution was shaken for 1 min and centrifugated at 4000 rpm for 8 min (EBA 8S, Hettich, Germany) for separation. The obtained organic phase was extracted using a micropipette and transferred to 300 µL micro inserts placed inside of 2 mL vials, which were then placed into GC-FID autosampler for analysis.

Preparation of 1,4-dioxane samples. The samples of 1,4-dioxane were prepared for GC-FID analysis following the DLLME protocol of BTEX using a different internal standard. In this case, the internal standard solution of 10 µL containing 10 mg/mL of cyclohexanone was injected into 10 mL sample of 1,4-dioxane. Cyclohexanone was selected as internal standard due to comparable physico-chemical properties with the analyte, while it was not present in the primary and post-processed samples. The following steps were the same as described for BTEX.

Extraction of BTEX from asphaltenes. Asphaltenes are traditionally isolated by precipitation in saturated hydrocarbons, e.g., *n*-pentane, *n*-heptane. In this study, the preparation method of the asphaltenes involved Soxhlet extraction step using

n-heptane, which assured the absence of leaching components. This was confirmed by the lack of UV-vis absorbance (300-800 nm) in DR5000 (HACH Lange) spectrophotometer of extraction solutions from second stage treatment by methanol and water (in respect to pure solvents) after Soxhlet extraction step. In these studies, the extraction of BTEX adsorbed on asphaltenes was conducted using *n*-pentane as an extraction solvent. Prior to extraction, recovery studies were performed and confirmed BTEXs are effectively desorbed form the asphaltenes using *n*-pentane. To measure the amount of adsorbed BTEX, the used asphaltenes were isolated from the reaction solution by vacuum filtration using hydrophilic PTFE membranes with pore size of 0.45 µm, and the separated particles were placed in a round-bottomed glass flask. The adsorbed BTEXs were extracted from asphaltenes by adding 5 mL *n*-heptane and shaking. Then 250 µL of *n*-heptane was transferred to 2 mL vials for GC-FID analysis.

GC-FID analysis of BTEX. The quantitative analysis of BTEX was performed in Clarus 500 (PerkinElmer, USA) gas chromatograph equipped with flame ionization detector (GC-FID). Column: the separation of analytes was achieved using a capillary column (60 m×0.32 mm ID, 1.8 µm DB624, Agilent, USA). Method: a 2 µL of extract obtained from DLLME was injected in splitless injection mode, oven temperature program was set follows: 50 °C (5 min) ramped at 10 °C/min to 275 °C (20 min). The volumetric flowrate of nitrogen employed as a carrier gas was 5 mL/min. The temperature values of the injection port and detector were 300 °C and 275 °C, respectively. The flowrate of hydrogen in FID was 40 mL/min, while air flow in FID was 430 mL/min.

GC-FID analysis of 1,4-dioxane. The quantitative analysis of 1,4-dioxane concentration was performed in Clarus 500 (PerkinElmer, USA) gas chromatograph equipped with flame ionization detector (GC-FID). Column: the separation of analytes was achieved using a capillary column (60 m×0.32 mm ID, 1.8 µm DB624, Agilent, USA). Method: the injection volume was 2 µL (splitless mode), while the oven temperature program was as set follows: 50 °C (5 min) ramped at 10 °C/min to 275 °C (5 min). The volumetric flowrate of nitrogen employed as a carrier gas was 5 mL/min. The temperature values of injection port and detector were 300 °C and 275 °C, respectively. The flowrate of hydrogen in FID was 40 mL/min, air flow was supplied at 450 mL/min.

UHPLC analysis of CLA. The concentration of CLA in collected samples was monitored in ultra-high performance liquid chromatography (UHPLC) Nexera XS system (Shimadzu, Japan). The system was equipped with UV diode array detector SPD-M40 (Shimadzu, Japan) for measurements at 230 nm. Additionally,

autosampler (SIL-40 XS, Shimadzu, Japan) was used for injection of 20 µL samples. The mobile phase was composed of a phosphate buffer solution (1 L Milli-Q water, 1.36 g KH_2PO_4 and 0.5 mL 85% H_3PO_4, pH 3) mixed with acetonitrile at 50:50 ratio (v/v) and flowrate was 1.0 mL/min flowrate. Column: the chromatographic separation of analytes was performed on a Zorbax C-18 reversed-phase column (4.6×150 mm, 3.5 µm) from Agilent Technologies.

HPLC-UV-DAD analysis of intermediates from HC/SR-AOPs. Qualitative analyses using Merck-Hitachi (Germany) HPLC system consisting of a four-channel low pressure gradient system, model 7455 diode array detector (DAD), model 1037A refractive index detector, L-6200 pump, thermostat, Rheodyne Rh7161 (USA) injector with a 20 µL sample loop and HSM software was used for identification of degradation intermediates. Column: a Zorbax C-18 reversed-phase column (4.6x150 mm, 3.5 µm) from Agilent Technologies. Mobile phase: acetonitrile/water mixture at 20:80 ratio (v/v) with flowrate at 1 mL/min. The identification of degradation products was carried out by comparing the obtained UV-VIS spectra and retention time values with those of standard solutions containing 50 ppm of the analyte.

GC-MS analysis of intermediates. Qualitative analyses using GCMSQP2010SE (Shimadzu, Japan) gas chromatograph coupled to a mass spectrometer (GC-MS) were performed to explore the degradation intermediates of BTEX, 1,4-dioxane and CLA. Column: the chromatographic separation of analytes was performed on a capillary column (100 m×0.2 mm ID, 0.1 µm DHA, Restek, USA). Method: the temperature in transfer line and injection port were 310 °C and 300 °C, respectively. The temperature of GC oven was 40 °C (5 min, isothermal mode) and ramped at 5 °C/min to 220 °C. The temperature at the MS ionization source (EI 70 eV) was 200 °C. A flow of hydrogen was used as a carrier gas at a flowrate of 1 mL/min and supplied from PGX500 hydrogen generator (PerkinElmer, USA). The analysis of BTEX and 1,4-dioxane intermediates was acquired in the full scan mode with m/z ranging from 34 to 220, while it was 34-350 m/z for the intermediates of CLA degradation. The intermediates were identified based on similarity test with mass spectral library available in The National Institute of Standards and Technology (NIST) dataset.

Iodometric titration. The dose of the applied O_3 was determined using iodometric titration method. For this, O_3 was supplied from Tytan 32 ozone generator (Erem, Poland) to two gas washing connected in sequence. Both bottles were filled with 500 mL of 2% (w/w) potassium iodide (KI) solution of with pH 3 adjusted by adding 2 M H_2SO_4 solution. Using compressed air as the carrier gas, O_3 was sparged to

KI solution through sintered glass disc located in the bottom of the bottles. The supply of O_3 was removed upon the color change in the second bottle and the solution of KI was titrated by adding 0.001 M solution of $Na_2S_2O_3$ in the in presence of 5% (w/v) starch used as an indicator. Thus, the dose of O_3 applied for the degradation of BTEX in dual-frequency sono-reactors was found as 2.1 g/h. In the case of 1,4-degradation in HC/SPC/O_3, the doses of O_3 0.23 g/h, 0.40 g/h, 0.74 g/h, 0.86 g/h and 0.94 g/h were obtained for the corresponding carrier gas flowrates of 0.5 L/min, 1.0 L/min, 1.5 L/min, 2.0 L/min and 2.5 L/min.

Mineralization studies. The mineralization rate of a pollutant in the developed processes was determined by measuring total organic carbon (TOC), which was determined by TOC-LCSH instrument (Shimadzu, Japan).

Experimental design. The effect of pH and SO_3^{2-} concentration on CLA degradation in HC/SO_3^{2-}/UV were discussed using a mathematical model developed *via* central composite design (CCD) and response surface methodology (RSM) and in Minitab Statistical Software 22 (Minitab Inc., USA). The experimental parameters, such as the dosage of SO_3^{2-} (related as molar ratio of reductant to pollutant, r_{red}), pH and treatment time were set as independent variables and denoted as X_1, X_2 and X_3, respectively, while the degradation efficiency of CLA was considered as response (Y). The list of factors with coded levels (-1, 0, +1) is summarized in Table 1.

Table 1. Coded independent variables with experimental ranges and levels.

Variables	Factor	Ranges and levels				
	X_i	-α	-1	0	1	+α
r_{red}	X_1	0.31	0.5	3.25	5	6.19
pH	X_2	2.3	4	6.5	9	10.7
Treatment time, min	X_3	9.55	30	60	90	110.45

Based on the preliminary experiments and literature, the ranges of X_1, X_2 and X_3 were 0.5-5, 4-9, 30-90 min, respectively. The total number of experiments was 20, including 6 center points, 6 replicate runs at the center point and 8 factor points. The CCD results were analyzed and used to fit the following second-order polynomial equation:

$$Y = \beta_0 + \sum_{i=1}^{k} \beta_i X_i + \sum_{i=1}^{k} \beta_{ii} X_i^2 + \sum_{i=1}^{k} \sum_{j=1}^{k} \beta_{ij} X_i X_j + \varepsilon \qquad 3.1$$

, where Y represents response, X_i and X_j – the coded independent variables, while β_0, β_i, β_{ii}, β_{ij} denote intercept, linear, quadratic and interaction terms, ε – random error.

The suitability of the model to predict the CLA degradation was assessed by Analysis of Variance (ANOVA) and the resulting quadratic model was determined as:

$$R(\%) = 14.88 + 5.370X_1 + 7.405X_2 + 1.2761X_3 - 0.3121X_1X_1 - 0.4766X_2X_2 - 0.006690X_3X_3 - 0.1649X_1X_2 - 0.02342X_1X_3 - 0.00878X_2X_3 \quad 3.2$$

, where R is the degradation efficiency of CLA (%), X_1, X_2, and X_3 represent r_{red}, pH, and treatment time (min), respectively.

From ANOVA results presented in Table 2, the F-value of 231.01 indicates that the second-order polynomial model is highly significant. The corresponding P-value is <0.0001, which further indicates a reliable model with high confidence level. The value of "lack-of-fit" found as 21.18 implies that the residual error caused by noise is statistically insignificant. The close values of correlation coefficient R^2=99.52% with adjusted R^2=99.09% and predicted R^2=96.46% confirm that the model provides a reasonable prediction and reproducibility.

Table 2. ANOVA results for the response surface quadratic model.

Source of variations	DF	Adjusted mean square	F-value	P-value
Regression model	9	231.10	231.01	0.000
Linear	3	484.98	484.80	0.000
Square	3	201.73	201.66	0.000
Interaction	3	6.57	6.57	0.010
Error	10	1	-	-
Lack-of-fit	5	1.91	21.18	0.002
Pure error	5	0.09	-	-
R^2=99.52, $R^2_{adj.}$=99.09, $R^2_{pred.}$=96.46				

Computational methods. The density functional theory (DFT) calculations of CLA and sulfite ion were performed by using Gaussian 09 package (Gaussian, Inc., USA). The geometry optimization as well as the calculation of the highest occupied molecular orbital (HOMO) and the lowest unoccupied molecular orbital (LUMO) were performed at the B3LYP/6-31G (d, p). The theoretical vertical detachment energy (VDE) was estimated based on the energy difference between sulfite monoanion and dianion (Eq. 3.3). For this, single-point energies were calculated for the optimized geometry of sulfite in the dianion and monoanion forms considering the solvent effect of water.

$$\mathrm{VDE} = \mathrm{E}_{\mathrm{monoanion}} - \mathrm{E}_{\mathrm{dianion}} \quad 3.3$$

As a concept, condensed Fukui function is a powerful tool that can predict active sites susceptible for electrophilic, nucleophilic and radical attacks. In the case of HC/SO_3^{2-}/UV, it was important to indicate the active sites in CLA molecule which would be vulnerable for nucleophilic attack by the reductive species. Therefore, Fukui indices f, f^0 and f^+ for electrophilic, radical and nucleophilic attacks, respectively, were calculated on the basis of natural population analysis (NPA) as shown in Eqs. 3.4-3.6.

$$f_A^+ = q_N^A - q_{N+1}^A \quad 3.4$$

$$f_A^- = q_{N-1}^A - q_N^A \quad 3.5$$

$$f_A^0 = (q_{N-1}^A - q_{N+1}^A)/2 \quad 3.6$$

, where q^A is the NPA charge of atom A in CLA molecule at a corresponding N, N+1, N-1 state.

4. Results and discussion

Focusing on the development and assessment of novel cavitation-based advanced chemical processes, this thesis presents the results obtained during the study of five distinct processes. The discussion of each process is provided in a separate section as illustrated in Fig. 6. According to the scheme, both AC and HC were coupled with SR-AOPs and ozonation resulting in 4 cavitation-based AOPs, while the ARP was combined with HC as the fifth process. Among them, the effectiveness of 3 processes, namely HC/SR-AOPs, AC/SR-AOPs and AC/O_3, was evaluated through the degradation of BTEX in water. In contrast, HC coupled with a modified peroxone (HC/O_3) and HC/ARP were tested for the degradation of 1,4-dioxane and CLA, respectively. Accordingly, each section discusses a cavitation-based process derived from a research paper, to which I made a major contribution by designing the study, performing the experiments and preparing the manuscript.

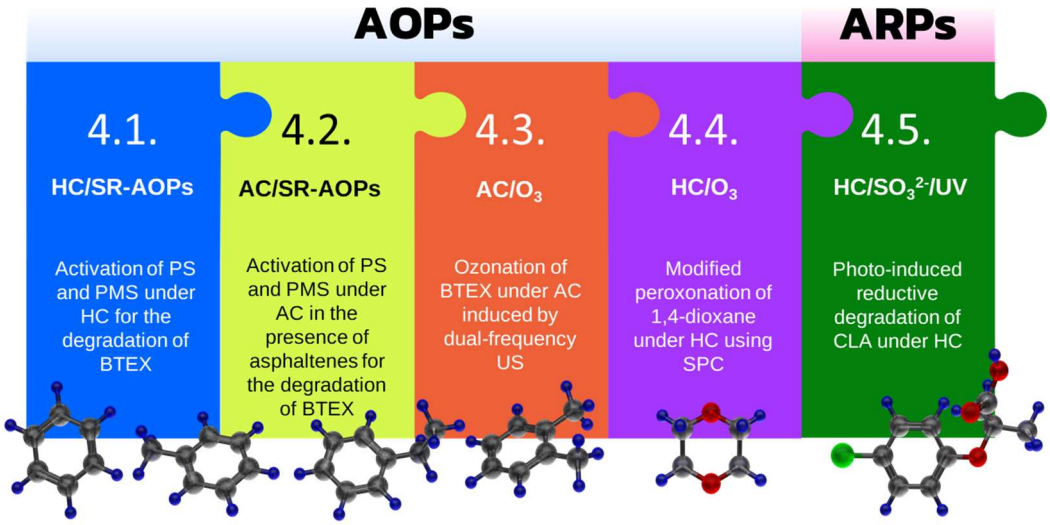

Figure 6. Schematic representation of discussion section.

In section 4.1., HC induced by Venturi tube was coupled with SR-AOPs to explore the applicability of HC in activation PS and PMS. The effectiveness of the developed HC/PS and HC/PMS processes was evaluated towards the degradation of BTEX by monitoring the concentration in the treated samples. This study included the degradation of BTEX in sole HC, HC/PS and HC/PMS at various molar ratio (r_{ox}). After selecting the optimal r_{ox}, HC/PS and HC/PMS were tested for the degradation of BTEX in the presence of inorganic anions and radical scavengers to determine the reactive species. Then the model solutions containing the components of BTEX individually were treated HC/PS and HC/PMS and the

samples were analyzed by HPLC-UV-DAD to identify the intermediates, based on which the degradation pathway was proposed. The outcomes of this study were published in the following paper: *Combination of hydrodynamic cavitation and SR-AOPs for simultaneous degradation of BTEX in water*. **Fedorov, K**., Sun, X., Boczkaj, G., 2020. Chem. Eng. J.

The results demonstrating the capacity of AC in the activation of PS and PMS were discussed in section 4.2. For this, the degradation of BTEX was performed under AC induced by US irradiation in the presence of PS and PMS at various r_{ox}. Then the degradation efficiency of BTEX in US/PS and US/PMS were tested upon addition of asphaltenes. The studies on US/PS/ASPH and US/PMS/ASPH included radical quenching experiments and reusability test of asphaltenes. The results of this study were summarized in paper: *Ultrasound-assisted heterogeneous activation of persulfate and peroxymonosulfate by asphaltenes for the degradation of BTEX in water*. **Fedorov, K.**, Plata-Gryl, M., Khan, J.A., Boczkaj, G., 2020. J. Hazard. Mater. 397, 122804.

Then AC generated in dual-frequency US reactors was combined with ozonation and tested for the degradation of BTEX. As presented in section 4.3., AC was induced in sono-reactors generating low-frequency dual US operating at 40 kHz and 120 kHz (LFDUS), and high-frequency dual US (HFDUS) with 80 kHz, 200 kHz. The degradation of BTEX was performed in various single- and dual-frequency US as well as in O_3-assisted hybrid processes to determine the synergistic effect in LFDUS/O_3 and HFDUS/O_3. The studies investigated the effect of pH, radical scavengers and inorganic anions on the degradation efficiency of BTEX in LFDUS/O_3 and HFDUS/O_3. The degradation pathway of BTEX was proposed based on the reaction intermediates identified by GC-MS analysis of the samples from the treatment of model solutions individually spiked by BTEX components. These findings were presented in paper *High-performance activation of ozone by sonocavitation for BTEX degradation in water*. **Fedorov, K**., Kong, L., Wang, C., Boczkaj, G., 2024. J. Environ. Manage. 363, 121343.

The hybrid process of HC and ozonation is presented in section 4.4. The discussed process represents a modified version of peroxone (i.e., H_2O_2/O_3) combined with HC and utilizes stable and safe alternative of H_2O_2 - sodium percarbonate (SPC). In this study, the effectiveness of the developed HC/SPC/O_3 process was evaluated towards the degradation of persistent and highly toxic 1,4-dioxane. The synergistic effect was investigated by conducting the degradation of 1,4-dioxane in

sole and hybrid processes. Besides, the study explored the effect of various parameters such as cavitation number (C_v), r_{ox} and pH on the degradation of the pollutant. Then the degradation efficiency of HC/SPC/O_3 was evaluated in the presence of scavengers and common water constituents. The degradation pathway of 1,4-dioxane was proposed based on the intermediates identified using GC-MS. Based on these results the following paper was prepared and published: *Activated sodium percarbonate-ozone (SPC/O_3) hybrid hydrodynamic cavitation system for advanced oxidation processes (AOPs) of 1,4-dioxane in water*. **Fedorov, K**., Rayaroth, M.P., Shah, N.S., Boczkaj, G., 2023. Chem. Eng. J. 456, 141027.

The section 4.5. presents the results obtained while attempting to develop a hybrid process based on cavitation and ARP. In this study, HC was coupled with SO_3^{2-}/UV and tested for the degradation of CLA. Synergistic effect was investigated by the degradation experiments of CLA in sole and hybrid processes, while the effect of C_v, r_{red}, pH and water constituents were also studied. In addition, the quenching experiments using specific scavengers of reductive species were performed. The reductive pathway of CLA degradation was proposed based on the intermediates identified by GC-MS analysis and supported by theoretical DFT calculations. The outcomes of this study were included in research paper titled Boosting the radical-induced reductive degradation of clofibric acid in water: *Synergistic effect of SO_3^{2-}/UV and hydrodynamic cavitation (HC)*. **Fedorov, K**., Wang, C., Shah, N.S., Boczkaj, G., 2025.. J. Environ. Manage. 391, 126506.

4.1. PS/PMS activation under HC for the degradation of BTEX

4.1.1. BTEX degradation under sole HC

The degradation of pollutants under cavitation is accomplished by thermal decomposition inside the collapsing bubbles and oxidation by $HO^{\bullet}$ radicals derived from water disassociation (Eq. 4.1). In order to evaluate the effect of cavitation, BTEX degradation was conducted by sole HC at a cavitation number (C_v) 0.27, at operating inlet pressure of 8 bar. In this study, the value of C_v was set to 0.27 according to the optimization of C_v from 0.14 to 1.2 for the degradation Brilliant Blue Cresyl dye in the same installation [236].

$$H_2O \xrightarrow{cavitation} HO^{\bullet} + H^{\bullet} \quad 4.1$$

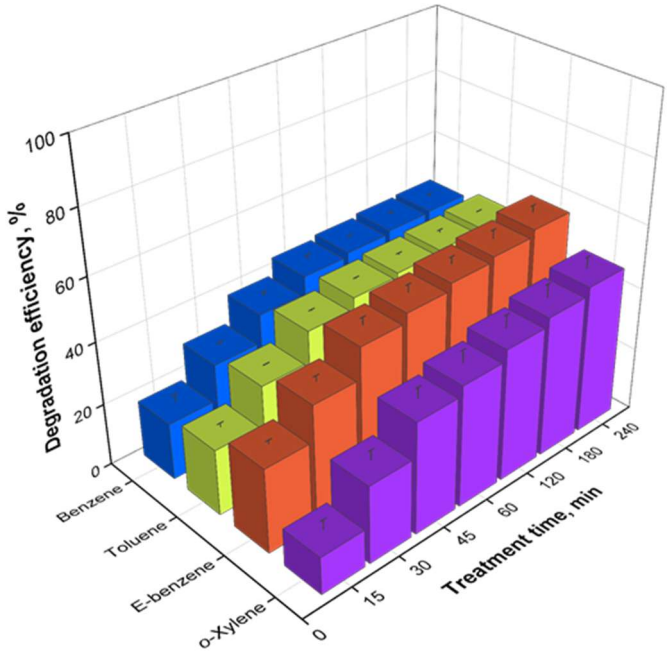

Figure 7. Degradation efficiency of BTEX by sole HC; $[BTEX]_0$ 50 mg/L, C_v 0.27, pH~6.5, 20±2.5 °C.

As shown in Fig. 7, 43.9%, 46.2%, 50.8%, and 38.7% of benzene, toluene, ethylbenzene and *o*-xylene, respectively, were degraded within 60 min. Then the degradation efficiency of BTEX were correspondingly increased to 46%, 49%, 56%, and 47% after 240 min. This finding indicates that up to 50% of BTEXs can be degraded under intensified cavitational events (e.g., greater number, intense collapse of cavities). Nevertheless, the sole application of HC was insufficient to attain the complete degradation of BTEX due to the limited number of generated

$HO^{\bullet}$ radicals. In contrast to Braeutigam et al., no accumulation of benzene as a product of ethylbenzene or *o*-xylene degradation was observed as the components of BTEX under HC were degraded at relatively similar extent and the degradation efficiency of benzene was not inhibited [237].

4.1.2. Effect of PS/PMS dosage on BTEX degradation

As relatively strong oxidant with oxidation potential of 1.96 V, PS is widely used in various sectors of chemical industry. In water treatment, the application of PS is commonly associated with the formation of $SO_4^{\bullet-}$ radicals, which are considered as alternative to $HO^{\bullet}$ radicals. Although $SO_4^{\bullet-}$ radicals exhibit longer lifetime and high oxidation potential of 2.6 V, the formation of $SO_4^{\bullet-}$ radicals from PS require the cleavage of the O-O bond – i.e., activation (Eq. 1.11). Among the widely studied catalysts (e.g., transition metals, carbon-based materials, quinones) and physical methods (UV-light, heat), HC represent an emerging activation approach with high potential for a large-scale application. Hence, to explore the capability of HC in PS activation, the degradation of BTEX under HC was performed with addition of PS. For this, the degradation of BTEX was conducted in HC/PS at molar ratio (r_{ox}) of PS to BTEX of 1, 5, 10, whereas pH was unadjusted (~6.5) and temperature was maintained at 20±2.5 °C to ensure the environmental relevance.

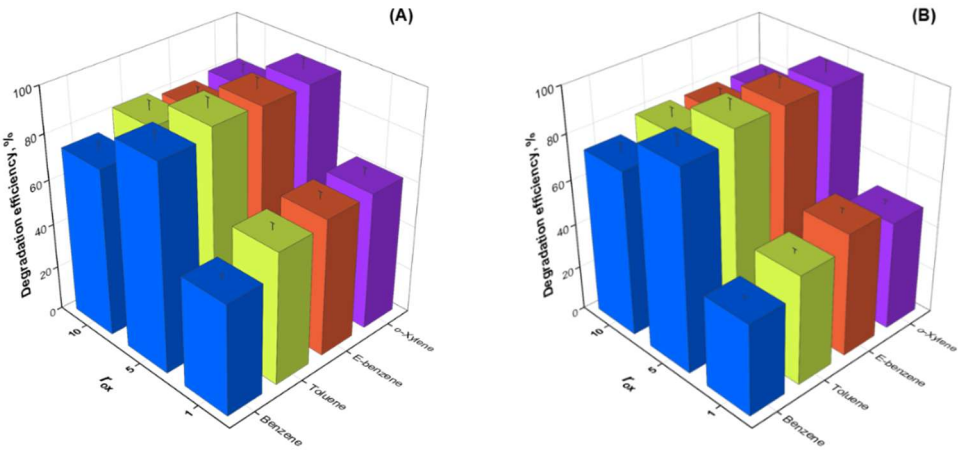

Figure 8. Degradation efficiency of BTEX by HC/PS (A), HC/PMS (B) at different r_{ox}; $[BTEX]_0$ 50 mg/L, C_v 0.27, pH~6.5, 20±2.5 °C.

Based on Fig. 8A, at lower concentration of PS (r_{ox} 1), the degradation efficiency of BTEX was the lowest due to the insufficient amount of the generated $SO_4^{\bullet-}$ radicals. The degradation efficiency of benzene, toluene, ethylbenzene and *o*-xylene was then increased by 29%, 34%, 24% and 35%, respectively, at HC/PS r_{ox} 5 as compared to sole HC. This implies the effective activation of PS ensuring high

number of $SO_4^{\bullet-}$ radicals available to react with BTEX. However, with further increasing of PS dosage to r_{ox} 10, the degradation efficiency of BTEX was declined, suggesting the occurrence of competing self-quenching reactions. Specifically, $SO_4^{\bullet-}$ radicals undergo recombination or scavenging by residual PS through Eqs. 1.26, 1.29. These findings highlight the important balance between the enhanced radical production and scavenging reactions by optimizing PS dosage.

Commonly supplied in the triple salt Oxone®, PMS is a moderate oxidant exhibiting oxidation potential of 1.86 V. The oxidation by PMS proceeds slowly under ambient conditions and can be significantly enhanced by the formation of $SO_4^{\bullet-}$ radicals. Similar to PS, the conversion of PMS into $SO_4^{\bullet-}$ radicals, i.e., activation requires the application of a catalyst, oxidants or energy input (Eq. 1.12). Despite the asymmetric structure, the bond disassociation energy of PMS is higher than that of PS due to the shorter peroxy bond. In particular, the bond in PMS has 1.46 Å length and disassociation energy of 377 kJ/mol, while the bond in PS with 1.497 Å length requires 140 kJ/mol. Nevertheless, several studies demonstrated that the effectiveness of PMS-based AOPs can prevail over PS in wastewater treatment with complex matrices containing. In order to explore the applicability of HC for PMS, the degradation of BTEX in water was conducted at various PMS molar ratios (r_{ox} 1, 5, 10) and C_v 0.27. As shown in Fig. 8B, the degradation efficiency of BTEX at r_{ox} 1 was increased negligibly compared to the effect of sole HC. Then with the increase of PMS dosage at r_{ox} 5, the degradation efficiency of benzene, toluene, ethylbenzene and *o*-xylene reached 90.85%, 94.50%, 94.36% and 93.07%, respectively, after 240 min. At r_{rox} 10 the degradation efficiency of HC/PMS was declined due to the scavenging reactions that convert $SO_4^{\bullet-}$ radicals into less reactive $SO_5^{\bullet-}$ and $HO_2^{\bullet}$ radicals (Eqs. 22, 23). The kinetics of BTEX degradation in both HC/PS and HC/PMS at r_{ox} 5 were investigated and can be fitted to the pseudo-first-order kinetics model (Eq. 4.2). The reaction rate constants of BTEX degradation (*k*) were determined by plotting $\ln(C_0/C_t)$ versus treatment time as depicted in Fig. 9.

$$ln\frac{C_0}{C_t} = kt \qquad 4.2$$

, where C_0 is the initial concentration (mg/L) of the pollutant, C_t – residual concentration (mg/L), t – treatment time (min) and *k* denotes the kinetic pseudo-first-order rate constant (min^{-1}).

The obtained rate constants listed in Table 3 showed that the degradation of BTEX proceeded faster in HC/PS as compared to HC/PMS at r_{rox} 5. This can be attributed to the lower disassociation energy of the peroxy bond in PS, which undergo heterolytic cleavage under HC.

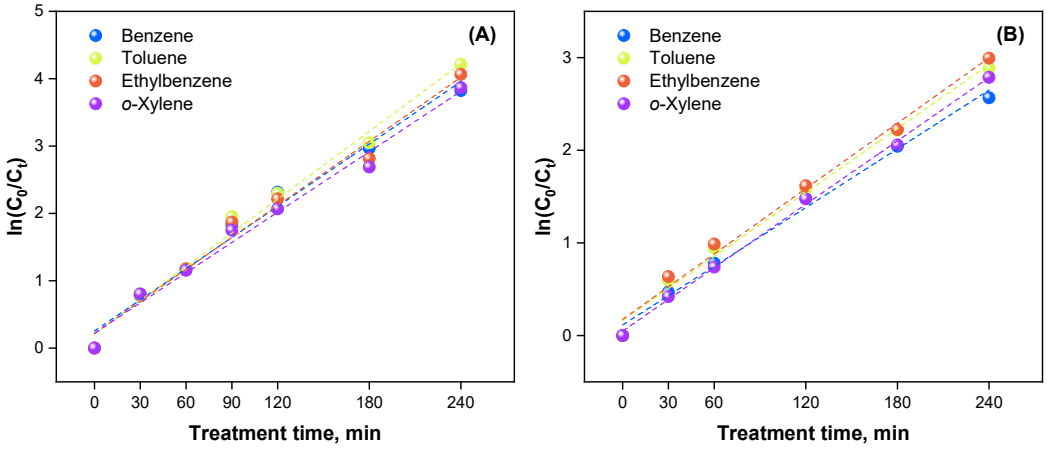

Figure 9. Pseudo-first-order kinetic plots of BTEX degradation by HC/PS (A), HC/PMS (B); $[BTEX]_0$ 50 mg/L, C_v 0.27, r_{rox} 5, pH~6.5, 20±2.5 °C.

Table 3. Degradation rate constants of BTEX in HC/PS and HC/PMS at r_{ox} 5.

Process	***k*, min^{-1}**			
	Benzene	Toluene	Ethylbenzene	*o*-Xylene
HC/PS	0.0159	0.0168	0.0158	0.0149
HC/PMS	0.0106	0.0115	0.0118	0.0114

4.1.3. Identification of dominant radical species

As it was mentioned above, the multiple types of radical species, such as $SO_4^{\bullet-}$, $HO^{\bullet}$, $O_2^{\bullet-}$ radicals (Eqs. 1.29-1.31) can be generated during PS/PMS activation and contribute to BTEX degradation. To identify the primary reactive species responsible for BTEX degradation in HC/PS and HC/PMS, radical quenching experiments were performed. The impact of both $SO_4^{\bullet-}$ and $HO^{\bullet}$ radicals was evaluated by adding methanol (MeOH) that correspondingly react with these radicals at a rate constant of 3.2×10^6 M^{-1} s^{-1} and 9.7×10^8 M^{-1} s^{-1} [172,238]. While MeOH with α-hydrogen was selected to quench both $SO_4^{\bullet-}$ and $HO^{\bullet}$ radicals, *tert*-butyl alcohol (TBA) was used to distinguish the contribution of $SO_4^{\bullet-}$ radicals. This was based on the greater reactivity of TBA with $HO^{\bullet}$ radicals (6.0×10^8 M^{-1} s^{-1}), while the rate constant with $SO_4^{\bullet-}$ radicals is 4.0×10^5 M^{-1} s^{-1} [172,238]. In addition,

para-benzoquinone (*p*-BQ) with a rate constant of 0.9-1 × 10^9 M^{-1} s^{-1} was employed to verify the presence of $O_2^{\bullet-}$ radicals [172,239].

From Fig. 10A, it can be seen that the addition of MeOH reduced the degradation efficiency of benzene, toluene, ethylbenzene and *o*-xylene from 91.5 %, 95.5 %, 94.6 %, 94.9 % to 55.8 %, 64.1 %, 66.9 %, and 63.6 %, respectively, in 240 min. The presence of TBA in HC/PS, resulted in the corresponding degradation efficiency of 75.3%, 80.8%, 80.4% and 77.7% in 240 min. Based on these, it can be proposed that both $SO_4^{\bullet-}$ and $HO^{\bullet}$ radicals present and accounted the oxidation of BTEX in HC/PS at r_{rox} 5. In the case of HC/PMS (Fig. 10B), the degradation efficiency of benzene, toluene, ethylbenzene and *o*-xylene was decreased from 90.85%, 94.50%, 94.36%, 93.07% to 36.94%, 42.20%, 47.49%, and 40.46%, respectively, after 240 min.

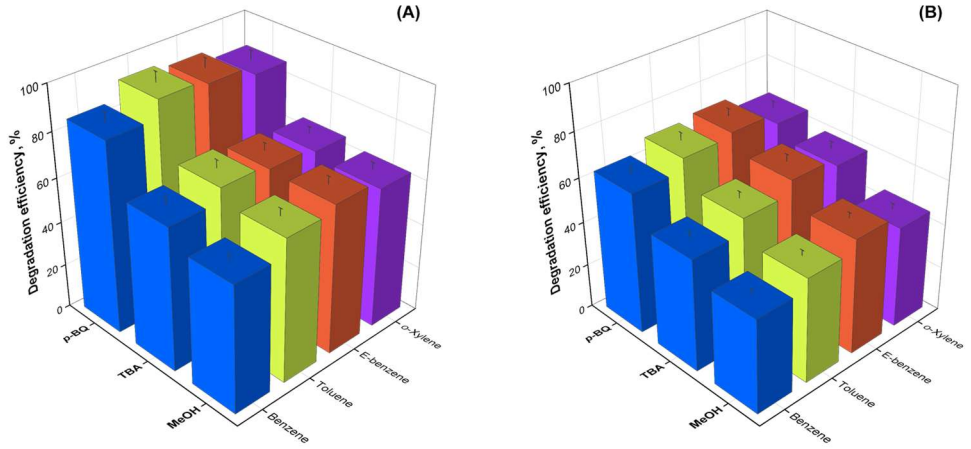

Figure 10. Degradation efficiency of BTEX by HC/PS (A), HC/PMS (B) in the presence of scavengers; $[BTEX]_0$ 50 mg/L, C_v 0.27, r_{rox} 5, [PS]:[PMS]:[Scavenger] 1:1:100, pH~6.5, 20±2.5 °C.

The inhibitory effect caused by quenching of $HO^{\bullet}$ radicals using TBA caused the decline of the corresponding degradation efficiencies to 50.58%, 54.54%, 57.65% and 53.29% in 240 min. These findings suggested the higher contribution of $SO_4^{\bullet-}$ and $HO^{\bullet}$ radicals to BTEX oxidation and the impact $HO^{\bullet}$ radicals in HC/PMS at r_{rox} 5 was higher than in HC/PS. In addition, the degradation efficiency of benzene, toluene, ethylbenzene and *o*-xylene were inhibited to 50.58%, 54.54%, 57.65% and 53.29%, respectively, in 240 min upon addition of *p*-BQ to HC/PMS at r_{rox} 5. On the other hand, the presence of *p*-BQ in HC/PS correspondingly suppressed the BTEX components by 5.8%, 2.1%, 3.2% and 7.4% in 240 min, indicating the negligible contribution of $O_2^{\bullet-}$ radicals. In contrast, the noticeable inhibitory effect observed in HC/PMS verified the presence of $O_2^{\bullet-}$ radicals, which can be generated due to the self-decomposition of PMS (Eqs. 4.3, 4.4) [240]. Overall, it can be

concluded that both $SO_4^{\bullet-}$ and $HO^{\bullet}$ radicals were the primary reactive species in HC/PS and HC/PMS. The secondary $O_2^{\bullet-}$ radicals additionally contributed to the degradation of BTEX in HC/PMS.

$$HSO_5^- \rightarrow SO_5^{2-} + H^+ \quad 4.3$$

$$SO_5^{2-} + H_2O \rightarrow SO_4^{2-} + O_2^{\bullet-} + 2H^+ \quad 4.4$$

4.1.4. Effect of water constituents on BTEX degradation

Natural water bodies contain various substances, including inorganic anions that may affect the performance of SR-AOPs. Hence, to evaluate the applicability of HC/PS and HC/PMS in complex water matrices, the degradation of BTEX was conducted in the presence of co-existing ions, such Cl^-, SO_4^{2-} and CO_3^{2-} anions. As shown in Fig. 11B, the degradation efficiency of benzene, toluene, ethylbenzene and *o*-xylene after 240 min treatment in HC/PS was decreased to 17%, 43.79%, 46.89% and 58.92%, respectively, in the presence of Cl^- anions. The addition of Cl^- anions in HC/PMS inhibited the degradation efficiency of benzene from 90.85% to 36.31%, while toluene, ethylbenzene and *o*-xylene were degraded to 94.50%, 90.93% and 98,57%, respectively, in 240 min (Fig. 12B). The contrasting effect of Cl^- anions on HC/PS and HC/PMS can be explained by chemical transformations resulting in different products. Generally, both $SO_4^{\bullet-}$ and $HO^{\bullet}$ radicals rapidly react with Cl^- anions at rate constants of 3-4.3 x 10^9 M^{-1} s^{-1} and 1.3-6.6 x 10^8 M^{-1} s^{-1}, respectively, to yield $Cl^{\bullet}$ and $Cl_2^{\bullet-}$ radicals. The obtained radicals are highly selective to electron-rich compounds and this can explain higher degradation efficiency of BTEX components with electron-donating substituents. In addition, $Cl^{\bullet}$ radicals can partially react with water to produce weaker $H_2ClO^{\bullet}$ radicals at pH ≥ 5 as illustrated in Eq. 4.5. While $Cl^{\bullet}$ and $Cl_2^{\bullet-}$ radicals are also generated in HC/PMS, Cl^- anions can directly interact with PMS producing HOCl and Cl_2 (Eqs. 4.6, 4.7).

$$Cl^- + H_2O \rightarrow H_2ClO^{\bullet} \quad 4.5$$

$$Cl^- + HSO_5^- \rightarrow HOCl + SO_4^{2-} \quad 4.6$$

$$2Cl^- + HSO_5^- + H^+ \rightarrow Cl_2 + SO_4^{2-} + H_2O \quad 4.7$$

The formed $Cl^{\bullet}$ and $Cl_2^{\bullet-}$ radicals as well HOCl and Cl_2 attack BTEX thereby promoting the oxidation capacity of HC/PMS. The treatment of BTEX under HC in the presence Cl^- anions without PS and PMS degraded 47.04%, 50.73%, 56.50% and 50.33% of benzene, toluene, ethylbenzene and *o*-xylene, respectively, in 240

min. The observed efficiency was comparable to that of sole HC, confirming that $Cl^{\bullet}$ and $Cl_2^{\bullet-}$ radicals were derived from the reaction of Cl^- anions with $SO_4^{\bullet-}$ and $HO^{\bullet}$ radicals.

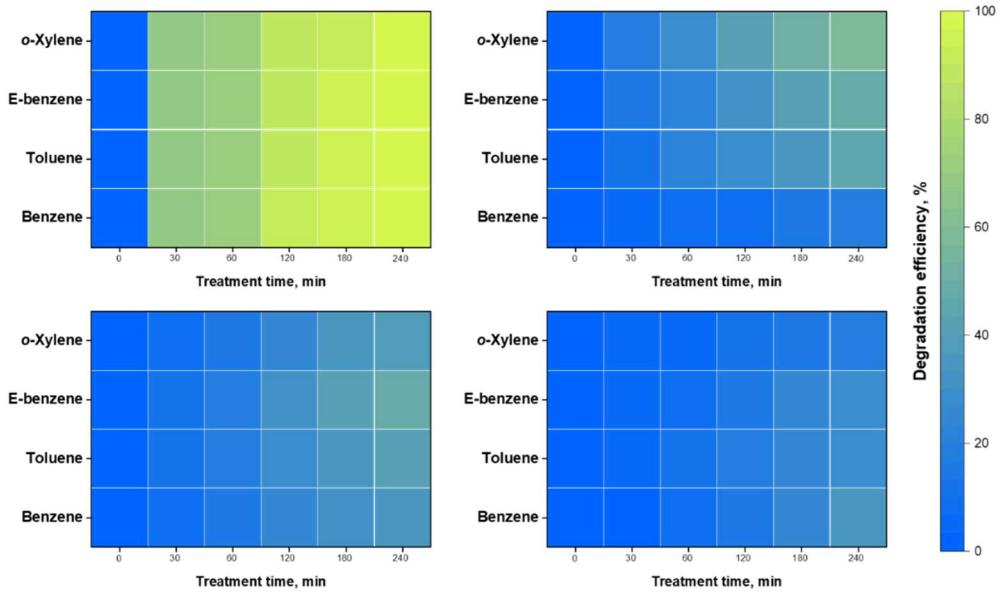

Figure 11. Degradation efficiency of BTEX by HC/PS (A), in the presence of Cl^- (B) SO_4^{2-} (C), CO_3^{2-} ions (D); $[BTEX]_0$ 50 mg/L, C_v 0.27, r_{rox} 5, [PS]:[Anion] 1:10, pH~6.5, 20±2.5 °C.

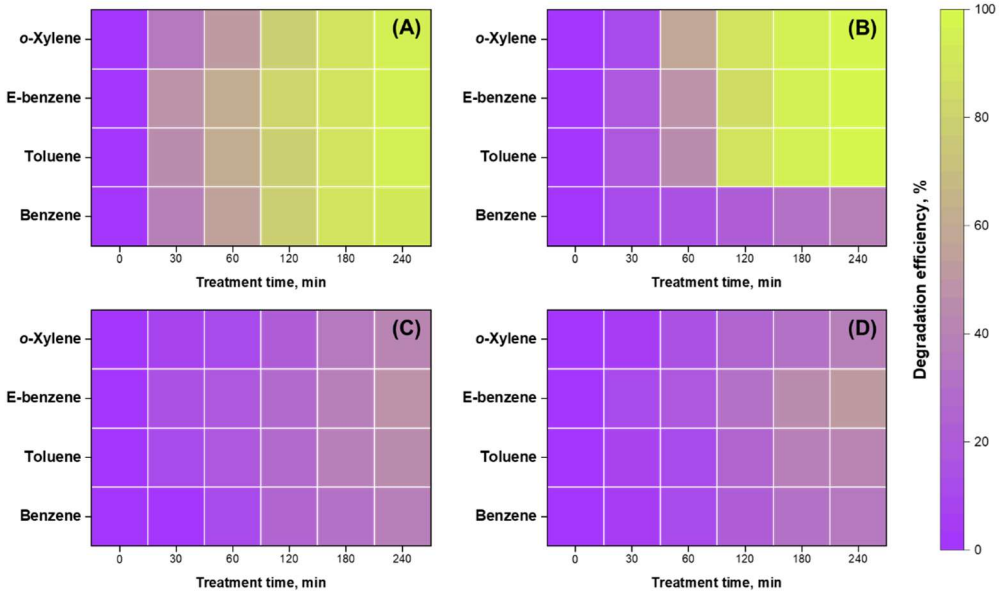

Figure 12. Degradation efficiency of BTEX by HC/PMS (A), in the presence of Cl^- (B) SO_4^{2-} (C), CO_3^{2-} ions (D); $[BTEX]_0$ 50 mg/L, C_v 0.27, r_{rox} 5, [PMS]:[Anion] 1:10, pH~6.5, 20±2.5 °C.

According to Fig. 11D and Fig. 12D, the addition of CO_3^{2-} anions in HC/PS and HC/PMS consistently inhibited the degradation of BTEX. Hence, the degradation efficiency of benzene, toluene, ethylbenzene and *o*-xylene in HC/PS were decreased from 91.50%, 95.50%, 94.64%, 94.94% to 33.99%, 29.63%, 28.91% and 18.34%, respectively, after 240 min. In HC/PMS, the degradation efficiency of benzene, toluene, ethylbenzene and *o*-xylene were decreased to 36.09%, 42,85%, 50.13% and 39.39%, respectively, in the presence of CO_3^{2-} anions.

The observed inhibitory effect can be attributed to the scavenging effect of CO_3^{2-} /HCO_3^- anions, which react with $SO_4^{\bullet-}$, $HO^\bullet$ and $O_2^{\bullet-}$ radicals to produce less reactive $CO_3^{\bullet-}$/$HCO_3^\bullet$ radicals. The addition of SO_4^{2-} anions suppressed the degradation of BTEX in both processes (Fig. 11C, Fig. 12C), but in lower extent than CO_3^{2-} anions. Specifically, 35.56%, 41.21%, 47.10% and 39.83% of benzene, toluene, ethylbenzene and *o*-xylene, respectively, were degraded by HC/PS after 240 min in the presence of SO_4^{2-} anions. The degradation efficiency of BTEX in HC/PMS was correspondingly retarded to 39.66%, 43.84%, 47.77%, 41.96% in 240 min. As can be predicted by Nernst equation (Eq. 1.43), the excess of SO_4^{2-} anions reduced the redox potential of SO_4^{2-}/$SO_4^{\bullet-}$ cycle, thereby lowering the oxidation capacity of HC/PS and HC/PMS. To summarize, the inhibitory effect of the studied anions on BTEX degradation in both processes followed the order: $CO_3^{2-} > SO_4^{2-} > Cl^-$. These results demonstrated that inorganic anions present in natural water matrices can affect the effectiveness of HC-based SR-AOPs by altering radical speciation. Therefore, the composition of the wastewater should be carefully analyzed and adjusted prior to treatment.

4.1.5. The proposed degradation pathway of BTEX in HC/PS and HC/PMS

The degradation of organic pollutants is a complex process involving oxidative transformations that lead to the formation of multiple intermediates. While the identification of the intermediates and by-products helps to assess the toxicity risk, it can also be used to propose the degradation pathway of the pollutant in the developed process. In this study, the samples were analyzed by HPLC-UV-DAD and based on the identified intermediates, the degradation pathway of BTEX in HC/PS and HC/PMS were proposed. To maximize the peaks intensity of the intermediates, the model solutions containing 800 ppm of benzene, 450 ppm of toluene, 300 ppm of ethylbenzene and 250 ppm of *o*-xylene were prepared and treated individually under HC/PS and HC/PMS at r_{rox} 5 for 240 min. At such elevated initial concentration for degradation experiment, HPLC-UV-DAD analysis

revealed six dominant aromatic intermediates: catechol, benzyl alcohol, phenol, benzoic acid, benzaldehyde and *para*-cresol. Additional unaccounted peaks were attributed to low-molecular aliphatic compounds (e.g., acetic, formic acid).

In both HC/PS and HC/PMS, catechol was found as major intermediate of benzene degradation, while benzyl alcohol was detected as common intermediate of toluene, ethylbenzene and *o*-xylene samples. Benzaldehyde was present in the degradation products of toluene and *o*-xylene, benzoic acid appeared only among the degradation intermediates of ethylbenzene. Phenol was detected for both ethylbenzene and *o*-xylene sample, and *o*-cresol was associated with *o*-xylene degradation.

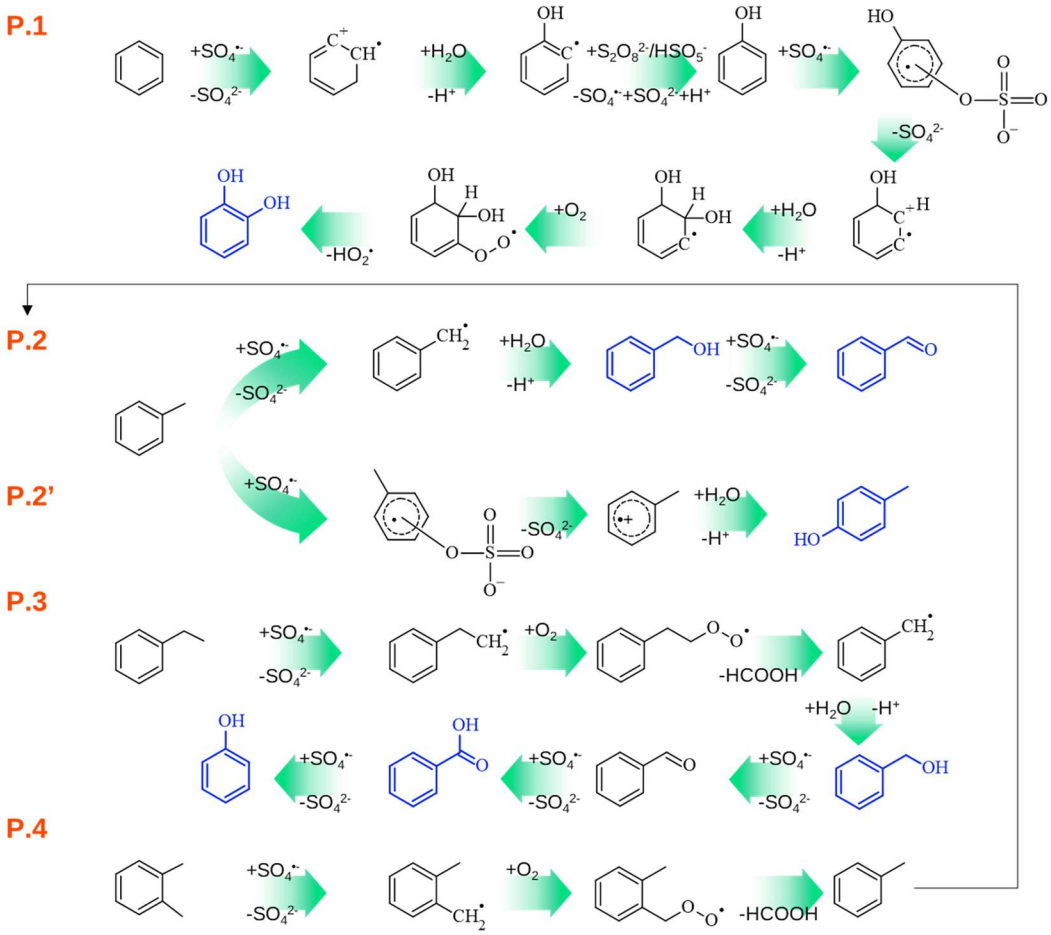

Figure 13. The possible degradation pathways of BTEX components in HC/PS and HC-PMS based on the intermediates identified using HPLC-UV-DAD.

As presented in Fig. 13, the degradation of benzene (P.1) was initiated by the attack of $SO_4^{\bullet-}$ radicals to yield carbon-centered hydroxy-cyclohexadienyl radical, which undergo hydroxylation into phenol and catechol. In the case of the substituted derivatives of benzene, the primary step of H-abstraction occurred from methyl- and ethyl- groups. In particular, the H-abstraction from methyl group was

preferrable in toluene (P.2) as C-H bond disassociation energy in methyl group (3.7 eV) was lower than in aromatic ring (4.4 eV). Then the radical intermediate formed after H-abstraction is subjected to hydroxylation to yield benzyl alcohol, which is further oxidized to benzaldehyde. Alternatively, $SO_4^{\bullet-}$ radicals can be directly attracted by the aromatic system of toluene (P.2') resulting in the formation of *p*-cresol. The H-abstraction from the alkyl chain of ethylbenzene (P.3) led to the formation of radical intermediate, which proceeded through dealkylation in the presence of DO based on the detection of benzyl alcohol. The formation of benzyl alcohol and phenol during the degradation of *o*-xylene (P.4) suggests the dealkylation of one methyl group facilitated by DO after H-abstraction. These steps convert *o*-xylene into toluene, which repeat the previously described pathway.

The mineralization studies of 50 ppm BTEX solution showed that TOC values were decreased below the detection limit (< 1.0 mg/L) after 240 min treatment in HC/PS and HC/PMS at r_{rox} 5. Considering this, it can be suggested that continuous oxidation by $SO_4^{\bullet-}$/$HO^{\bullet}$ radicals led to ring opening reactions of the detected aromatic intermediates, fragmentation into short-chain carboxylic acid and mineralization.

To sum up, the effect of HC induced by Venturi tube at C_v 0.27 activated PS and PMS and effectively degraded BTEX. Both HC/PS and HC/PMS demonstrated the highest oxidation capacity at oxidant/pollutant molar ratio (r_{ox}) of 5, at pH 6.5 and 25±2 °C, attaining >90% of BTEX degradation within 240 min. Based on quenching experiments, the occurrence of $SO_4^{\bullet-}$ and $HO^{\bullet}$ radicals was verified in both processes, while the contribution of secondary $O_2^{\bullet-}$ radicals was also observed in HC/PMS. The presence of inorganic anions decreased the degradation efficiency of BTEX in HC/PS and HC/PMS and the inhibitory effect was as follows: CO_3^{2-} > SO_4^{2-} > Cl^-. In the case of HC/PMS, the presence of Cl^- ions increased the degradation efficiency of TEX due to the formation of reactive chlorine species. The oxidative degradation of BTEX by radical species was initiated by single-electron transfer, H-abstraction followed by hydroxylation and dealkylation.

4.2. PS/PMS activation under AC in the presence of asphaltenes for BTEX degradation

4.2.1. BTEX degradation under US/PS and US/PMS

The US irradiation in AOPs is commonly utilized as a source of HO• radicals in aqueous media, which contribute to the degradation of pollutants. These HO• radicals are generated through the thermal disassociation of water induced by AC according to Eq. 4.1. Such effect of AC is conditioned by the violent collapse of cavitation bubbles that creates high temperature and pressure. Owing to this effect, AC can be employed for the activation of PS and PMS in a similar manner as thermal activation. Till date, the capacity of the energy emitted during AC to activate PS/PMS was extensively evaluated. The effectiveness of the US-activated PS/PMS were studied and tested for the degradation of various organic pollutants in wastewater. Along with high degradation efficiency, the studies revealed the complex reaction pathways and the generation of various reactive species, such as $SO_4^{\bullet-}$, $SO_5^{\bullet-}$, $O_2^{\bullet-}$ radicals and $^1O_2$. In this study, PS/PMS at molar ratio (r_{rox}), 1, 5 and 10 was added into BTEX model solution and treated under US to explore the effect of PS/PMS dosage.

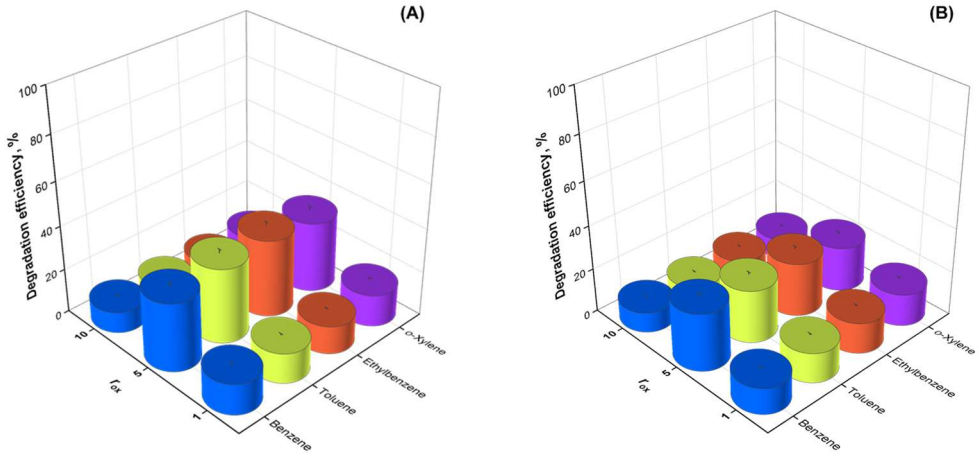

Figure 14. Degradation efficiency of BTEX by US/PS (A), US/PMS (B) at different r_{ox}; $[BTEX]_0$ 40 mg/L, pH~5, US 35 kHz, 860 W, 25±2 °C, 360 min.

Based on Fig. 14 showing the effect of PS/PMS dosage on BTEX degradation, the degradation efficiency of BTEX was increased with the increase of r_{rox} from 1 to 5. Then the effectiveness of both US/PS and US/PMS was declined at r_{rox} 10. As shown in Fig. 14A, the highest extend of BTEX degradation in US/PS was observed at r_{rox} 5, in which 31% of benzene was degraded in 360 min. Compared to this, the degradation efficiency of benzene in US/PS r_{rox} 1 and r_{rox} 10 were 14%

and 10% after 360 min, respectively. Similarly, US/PMS at r_{rox} 5 degraded 26% of benzene in 360 min (Fig. 14B), while the corresponding degradation efficiencies of 11% and 9% were obtained at r_{rox} 1 and 10. The enhanced BTEX degradation in US/PS and US/PMS at r_{rox} 5 indicates the accelerated generation of $SO_4^{\bullet-}$ radicals - the primary oxidizing species in sono-activated PS and PMS. At r_{rox} 1 the degradation of BTEX was lower due to the limited production of $SO_4^{\bullet-}$ radicals, whereas the excessive PS and PMS added at r_{rox} 10 decreased the number of available $SO_4^{\bullet-}$ radicals. This scavenging effect can be attributed to the reaction of residual precursors (i.e., PS, PMS) with $SO_4^{\bullet-}$ radicals resulting in radical species of lower oxidation potential (Eqs. 1.22, 1.23 and 1.26).

4.2.2. BTEX degradation in US/PS and US/PMS in the presence of asphaltenes

As presented in literature, the activation of PS/PMS can be achieved by using carbon-based catalysts, such as activated carbon, graphite, graphene oxide, nanodiamonds and carbon nanotubes [241,242]. The activation using such materials proceeds through electron donation from electron-rich surface functional groups, incorporated metal active sites and sp^2-hybridized carbon lattice. Nonetheless, the mechanism of PS/PMS activation using such materials requires further investigation, whereas the fabrication of nanocomposite doped with metal ions is economically infeasible. In the light of this, asphaltenes represent a promising alternative to carbonaceous composites in large-scale utilization. Asphaltenes can be characterized as a polycyclic aromatic macromolecule composed of fused aromatic rings containing alkyl chains and polar functional groups, such as carboxyl, hydroxyl and amines. Besides, the structure of asphaltenes also contain heteroatoms (O, S, N) and trace metals (Ni, V), which can participate in redox reactions as well as electron transfer through sp^2 carbon network.

To explore the catalytic activity of asphaltenes in US/PS and US/PMS, the experiment on BTEX degradation were performed under different processes at r_{rox} 5 and the concentration of asphaltenes of 0.5 g/L (selected during preliminary studies). As shown in Fig. 15AB, the sole application of US degraded 9.5%, 11.1%, 10.7% and 7.1% of benzene, toluene, ethylbenzene and *o*-xylene after 360 min, respectively, implying to the limited generation of radical species. Upon combination of US with PS and PMS, the degradation efficiency of BTEX was increased considerably, which can be attributed the generation of $SO_4^{\bullet-}$ radicals

from sono-activated PS/PMS. Thus, the degradation efficiency of benzene, toluene, ethylbenzene and *o*-xylene were found as 31.2%, 34.3%, 35.5%, and 32.2%, respectively, within 360 min treatment by US/PS as depicted in Fig. 15A. Likewise, the corresponding degradation efficiency values of 26.4%, 24.2%, 24.5% and 20.4% were obtained in US/PMS (Fig. 15B). The degradation efficiency of BTEX was further increased with the introduction of asphaltenes in US/PS and US/PMS. As a result, the degradation efficiency of US/PS towards benzene, toluene, ethylbenzene and *o*-xylene was found as 78%, 94%, 98% and 98%, respectively, in the presence of asphaltenes within 360 min. In the case of US/PMS/ASPH, these pollutants were correspondingly degraded to 76%, 91%, 97%, 97% after 360 min.

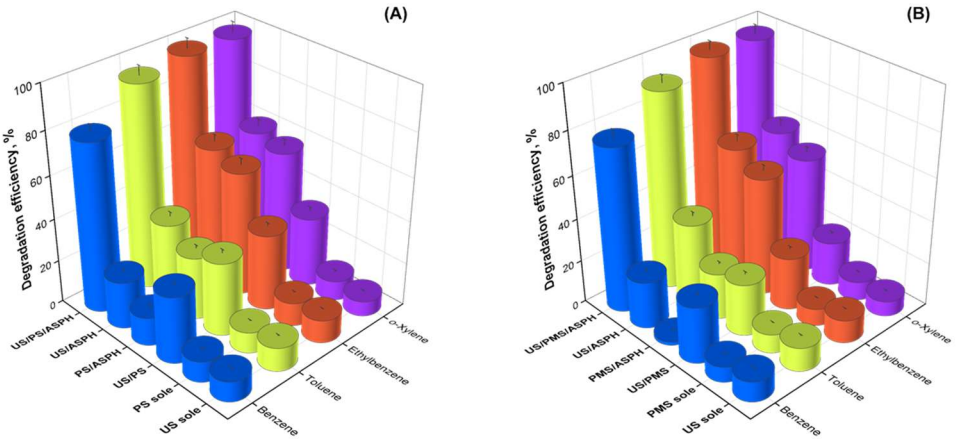

Figure 15. Degradation efficiency of BTEX in sole and different PS- (A) and PMS-activated (B) processes; $[BTEX]_0$ 40 mg/L, r_{ox} 5, [ASPH] 0.5 g/L, pH~5, US 35 kHz, 860 W, 25±2 °C, 360 min.

Considering that the adsorption on the surface of asphaltenes may account the enhanced BTEX removal from water, the spent asphaltenes after the process were separated by filtration and washed with *n*-pentane to extract BTEX. Effectiveness of *n*-pentane in desorption of BTEXs from the asphaltenes surface was confirmed during a dedicated series of experiments with standard BTEX solutions. The amount of ethylbenzene and *o*-xylene in asphaltenes from US/PS/ASPH was less than 1%, while 3% and 2% of ethylbenzene and *o*-xylene were detected in the asphaltenes separated from US/PMS/ASPH. Based on this, it can be proposed that the degradation of BTEX in both US/PS/ASPH and US/PMS/ASPH was due to oxidation.

The synergistic indices estimated by BTEX degradation rate constants were 4.07 and 4.12 for US/PS/ASPH and US/PMS/ASPH, respectively. The synergistic effect observed for BTEX degradation in US/PS/ASPH and US/PMS/ASPH can be

ascribed to the dual role of asphaltenes. Hence, the solid particles of asphaltenes dispersed in the volume of the treated liquid served as additional cavitation nuclei and, thus, intensified the cavitational events. In this, BTEXs are readily adsorbed on the surface of asphaltenes due to high affinity and undergo pyrolytic decomposition inside the gaseous phase. In such a scenario, the factor limiting the mass transfer of BTEXs from liquid to gaseous phase is reduced. Owing to these factors, US/ASPH degraded 21%, 37%, 62%, 60% of benzene, toluene, ethylbenzene and *o*-xylene in 360 min. Secondly, asphaltenes may encounter PS/PMS in the gas-liquid interfacial phase to induce activation by electron transfer from electron-rich functional groups and heteroatoms along the carbon network. These findings highlight the important role of asphaltenes as adsorbent and catalyst for the degradation of BTEX in the combined US/PS/ASPH and US/PMS/ASPH processes.

4.2.3. Identification of dominant radical species

Although the removal of water pollutants in SR-AOPs is generally accomplished by means of $SO_4^{\bullet-}$ radicals, $HO^{\bullet}$ and $O_2^{\bullet-}$ radicals can contribute to the overall oxidation capacity at certain extend. These radicals can be generated as a result of radical recombination or side reactions of radical precursors. In order to elucidate the role of $SO_4^{\bullet-}$, $HO^{\bullet}$ and $O_2^{\bullet-}$ radicals, the degradation of BTEX in US/PS/ASPH and US/PMS/ASPH was conducted in the presence of specific radical scavengers. For this, the contribution of both $SO_4^{\bullet-}$ and $HO^{\bullet}$ radicals on BTEX degradation was assessed by addition of MeOH, while TBA was used to distinguish the relative impact of $SO_4^{\bullet-}$ radicals. The role of $O_2^{\bullet-}$ radicals US/PS/ASPH and US/PMS/ASPH was evaluated by applying *p*-BQ.

As shown in Fig. 16A, the degradation efficiency of benzene, toluene, ethylbenzene and *o*-xylene were drastically inhibited from 78.7%, 94%, 98.2%, 97.7% to 19.8%, 35.9%, 54.9% and 54.7%, respectively, in the presence of MeOH. The observed strong inhibition suggested that both $SO_4^{\bullet-}$ and $HO^{\bullet}$ radicals were involved in BTEX degradation by US/PS/ASPH. In contrast, the degradation efficiency of BTEXs after 360 min were correspondingly suppressed to 31.9%, 44.9%, 62.7% and 59.8% upon the addition of TBA in US/PS/ASPH. Since, the inhibitory effect caused by the selective quench $HO^{\bullet}$ radicals by TBA was comparable to that of observed in the presence of MeOH, it can be proposed that $SO_4^{\bullet-}$ radicals were the predominant radical species responsible for BTEX degradation in US/PS/ASPH. The addition of *p*-BQ in US/PS/ASPH showed a

marginal inhibitory effect on BTEX degradation implying that the generation of $O_2^{\bullet-}$ radicals was negligible. For instance, the degradation efficiency of toluene was inhibited by 11.8% after 360 min in the presence of *p*-BQ. In the case of US/PMS/ASPH, quenching experiment showed similar trend as in US/PS/ASPH.

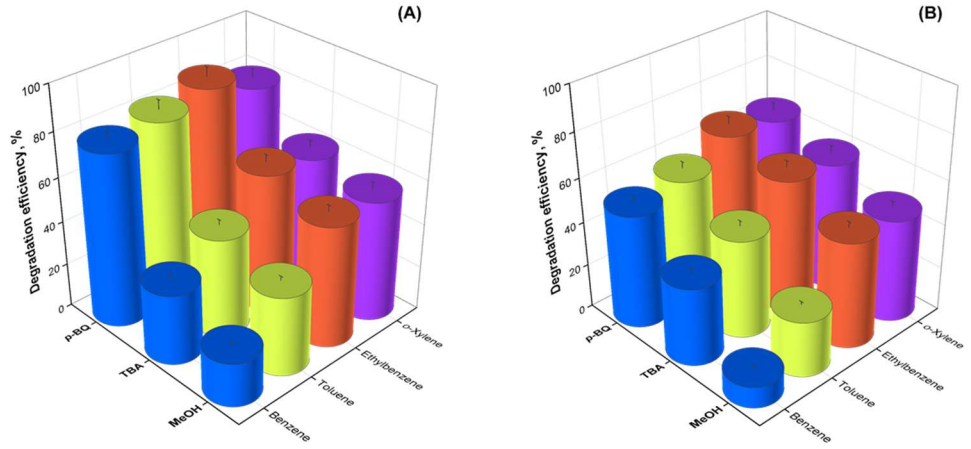

Figure 16. Degradation efficiency of BTEX in US/PS/ASPH (A) and US/PMS/ASPH (B) in the presence of scavengers; $[BTEX]_0$ 40 mg/L, r_{ox} 5, [ASPH] 0.5 g/L, pH~5, US 35 kHz, 860 W, 25±2 °C, 360 min.

According to Fig. 16B, the degradation efficiency of benzene, toluene, ethylbenzene and toluene in the presence of MeOH was significantly inhibited from 76%, 91%, 97%, 97% to 9%, 25%, 48% and 46%, respectively, in 360 min. The observed results demonstrated the occurrence of both $SO_4^{\bullet-}$ and $HO^{\bullet}$ radicals in US/PMS/ASPH, which actively participated in BTEX oxidation. The effectiveness of US/PMS/ASPH towards BTEX degradation was correspondingly suppressed to 35.3%, 44.6%, 60.4% and 57.5% in 360 min in the presence of TBA. Considering the observed inhibitory effect of TBA, it can be stated the $SO_4^{\bullet-}$ radicals played the dominant role. In contrast to US/PS/ASPH, the inhibitory effect on BTEX degradation caused by the addition *p*-BQ was more pronounced. The formation of $O_2^{\bullet-}$ radicals was reported for the activation of PMS by carbon-based composites, such as Mn-doped g-C_3N_4 and Pd/g-C_3N_4 *via* electron transfer between transition metal sites and DO [243,244]. While this mechanism is also valid for asphaltene containing naturally present trace amount of transition metals, $O_2^{\bullet-}$ radicals can also be generated through the self-decomposition of PMS according to Eqs. 4.3, 4.4.
To conclude, the quenching experiments demonstrated that both US/PS/ASPH and US/PMS/ASPH generated multiple types of radical species. The degradation of BTEXs in both processes was primarily induced by $SO_4^{\bullet-}$ radicals, while $HO^{\bullet}$ radicals were the secondary oxidant. Despite the minor contribution, $O_2^{\bullet-}$ radicals

were present in both processes and their effect on BTEX degradation was more obvious in US/PMS/ASPH.

4.2.4. Reusability of asphaltenes for the activation of PS/PMS

In order to assess the practical applicability of asphaltenes in SR-AOPs, the reusability of asphaltenes in US/PS/ASPH and US/PMS/ASPH was tested for three consecutive cycles of BTEX degradation. Asphaltenes were separated after each cycle using vacuum filtration using hydrophilic PTFE membranes with pore size of 0.45 µm, washed with deionized water and reused.

As shown in Fig. 17A, the degradation efficiency of benzene, toluene, ethylbenzene and *o*-xylene were 42.3%, 55.8%, 65.6% and 62.4%, respectively, after 360 min treatment in US/PS/ASPH at the second cycle. This demonstrated the decline in the degradation efficiency by approx. 30% at the second cycle and further loss in activity during the third cycle. In US/PMS/ASPH (Fig. 17B), the performance of asphaltenes was at the comparable level. As reported for other carbon-based composites, the loss in activity observed for asphaltenes can be attributed to the surface fouling due to the adsorption of aromatic intermediates on π-conjugated network of asphaltenes. In addition, metal active sites can be irreversibly consumed by donating an electron to PS as illustrated in Eq. 4.8. In the case of PMS, the metal active sites can be recovered through the formation of $SO_5^{\bullet-}$ radicals as shown in Eqs. 4.9, 4.10. This can explain higher catalytic activity of asphaltenes observed at the third cycles in US/PMS/ASPH compared to US/PS/ASPH.

The key advantage of asphaltenes over complex carbon-based composites relies on their origin and disposal. As a component of bitumen, asphaltenes are produced in large-scale as a by-product of so-called bitumen-blowing and residual oil solvent extraction (ROSE) processes. Hence, asphaltenes are readily available and can be blended with bitumen at certain dosage as a disposal strategy. Since, the application of asphaltenes under US can cause the release of polycyclic aromatic hydrocarbons (PAHs), the blank experiments were performed by sonicating asphaltenes in aqueous solution containing PS/PMS at r_{rox} 5 in 360 min. The treated solution was filtered and tested by UV-vis spectrophotometer in the range of 300-800 nm. According to the obtained UV-vis spectra, no noticeable change in the absorbance of the filtrates from the blank experiments compared to the control solutions containing PS/PMS was found. This suggested that the leakage of PAHs

from asphaltenes was negligible confirming the effectiveness of the preparation method, which includes purification by Soxhlet extraction with *n*-heptane.

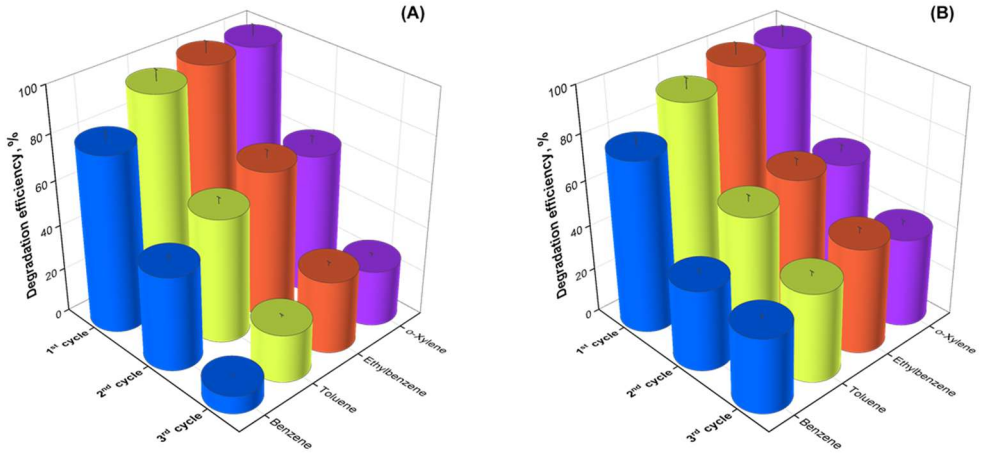

Figure 17. Reusability of asphaltenes in three sequential runs of BTEX degradation in US/PS/ASPH (A) and US/PMS/ASPH (B); $[BTEX]_0$ 40 mg/L, r_{ox} 5, [ASPH] 0.5 g/L, pH~5, US 35 kHz, 860 W, 25±2 °C, 360 min.

$$S_2O_8^{2-} + Me^{n+} \rightarrow Me^{(n+1)+} + SO_4^{\bullet-} + SO_4^{2-} \quad 4.8$$

$$HSO_5^- + Me^{n+} \rightarrow Me^{(n+1)+} + SO_4^{\bullet-} + HO^- \quad 4.9$$

$$HSO_5^- + Me^{(n+1)+} \rightarrow Me^{n+} + SO_5^{\bullet-} + H^+ \quad 4.10$$

As conclusion, the sole effect of AC generated under US irradiation was insufficient to effectively activate PS/PMS and resulted in the limited degradation of BTEX after 360 min. The activation of both PS and PMS was greatly enhanced upon the addition of asphaltenes at the dosage of 0.5 g/L. At oxidant/pollutant molar ratio (r_{ox}) of 5, at pH 5 and 25±2 °C, the highest degradation efficiency of BTEX was observed for both processes in 360 min. The synergistic effect observed in AC/PS/ASPH and AC/PMS/ASPH was attributed to the crucial role of asphaltenes, which served as nucleation centers of cavitation bubbles and adsorbed BTEX facilitating their contact with collapsing cavitation bubbles. The degradation of BTEX in AC/PS/ASPH and AC/PMS/ASPH was mainly contributed by $SO_4^{\bullet-}$ and $HO^{\bullet}$ radicals, while $O_2^{\bullet-}$ radicals played a minor role in AC/PMS/ASPH according to quenching experiments.

4.3. Ozonation of BTEX under AC induced by dual-frequency US

4.3.1. BTEX degradation under different US modes

These studies were performed in the low-frequency sono-reactor operated at 40-120 kHz and the high-frequency sono-reactor equipped with transducers and sonotrode irradiating US waves with 80-200 kHz. These sono-reactors were correspondingly marked as LFDUS and HFDUS. Before testing the combined effect of AC induced by LFDUS and HFDUS and ozonation, the effect of single and dual-frequency US on BTEX degradation was evaluated. For this, 3.8 L of model BTEX solution was treated for 60 min by US at a single-frequency (i.e., 40 kHz, 80 kHz, 120 kHz, 200 kHz) and dual-frequency mode (40-120 kHz and 80-200 kHz).

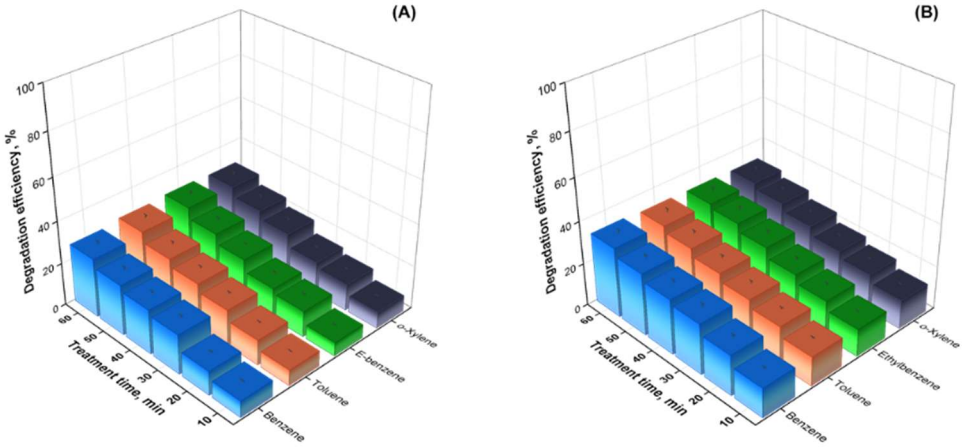

Figure 18. Degradation efficiency of BTEX in LFDUS (A), HFDUS (B); $[BTEX]_0$: 50 ppm (v/v), pH 6.5, 20±2.5 °C, US: 600 W, 40/120 kHz, 80/200 kHz for LFDUS and HFDUS, respectively.

As shown in Fig. 18A, the treatment in LFDUS sono-reactor operating at 40-120 kHz degraded 27.64%, 29.08%, 29.85% and 29.39% of benzene, toluene, ethylbenzene and *o*-xylene, while the corresponding values obtained in HFDUS were 32.92%, 32.06%, 31.76% and 31.50% (Fig. 18B). In the absence of external additives (e.g., oxidants, radical precursors) the degradation of contaminants under US is accomplished by the effect of AC. The degradation can occur directly through the pyrolytic decomposition due to the localized extreme conditions inside the cavitation bubbles. Moreover, these conditions are sufficient to cause the dissociation of water yielding reactive radicals, which can non-selectively attack the contaminant. The radicals generated in gaseous and gas-liquid phases can be transferred into the bulk liquid to react with pollutants or produce secondary radical

species (i.e., $HO_2^{\bullet}$ radicals) in the presence of the DO (Eq. 4.11). Nevertheless, the generation of ROSs *via* water sonolysis is limited and in the absence of scavengers these radicals are recombined. In this case, hydrophobic BTEX molecules tend to diffuse into gaseous phase of bubble interior, where undergo thermal decomposition or oxidative degradation by radical species. The obtained results suggest that the intensity of cavitational events as well as the yield of ROSs was slightly higher in HFDUS – which is in agreement with the conclusions reported in the literature. However, the value of ξ (Eq. 1.56) for LFDUS and HFDUS calculated based on the effect of single-frequency US were found as 1.13 and 0.94, respectively.

$$HO^{\bullet} + O_2 \rightarrow HO_2^{\bullet} \qquad 4.11$$

4.3.2. BTEX degradation under US/O_3

Next experiments on BTEX degradation were performed over the combined processes involving O_3. First of all, the ozonation of BTEX was performed using single frequency US (SFUS) at different frequency and compared to sole ozonation (Fig. 19A) to clarify the effect of AC. Then, the effect of cavitation induced by SFUS was compared to DFUS.

As illustrated in Fig. 19B, SFUS/O_3 at 40 kHz degraded 43.49%, 43.22%, 41.58% and 32.26% of benzene, toluene, ethylbenzene and *o*-xylene after 60 min, respectively. With the increase of frequency to 200 kHz, the degradation efficiency of BTEX by SFUS/O_3 were correspondingly increased to 64.64%, 64.78%, 67.45% and 57.21%. Compared to the combined SFUS/O_3, sole ozonation attained the degradation efficiency of BTEXs in the range of 26.81%-40.71%. These findings demonstrated the limited interaction of molecular O_3 with BTEX due to low reactivity and hindered gas-liquid mass transfer. On the other hand, the application of US provided microcirculation and turbulence in the aqueous solution thereby decreasing the mass transfer resistance. More importantly, the effect of AC induced by SFUS initiated the decomposition of O_3 as depicted in Eqs. 4.12, 4.13 [102]. The generated $HO^{\bullet}$ radicals exhibit higher reactivity compared to O_3 resulting in higher degradation efficiency of BTEX.

$$O_3 \xrightarrow{cavitation} O^{\bullet} + O_2 \qquad 4.12$$

$$O^{\bullet} + H_2O \xrightarrow{cavitation} 2HO^{\bullet} \qquad 4.13$$

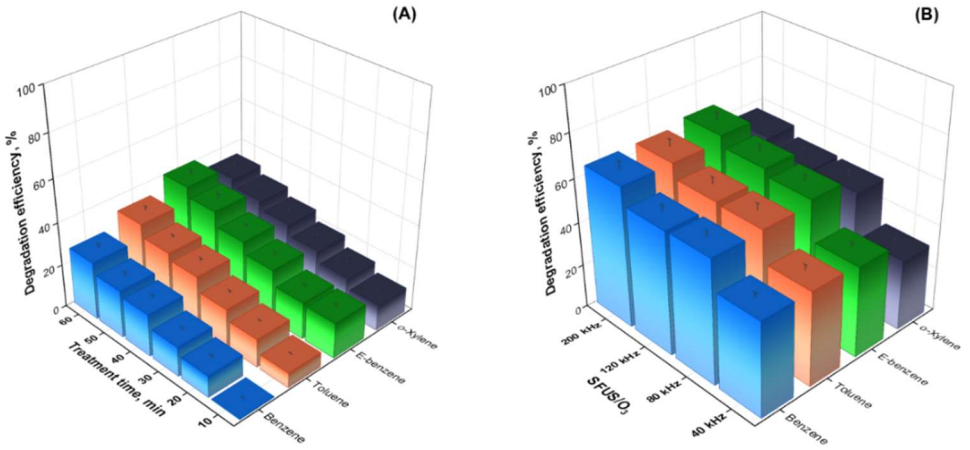

Figure 19. Degradation efficiency of BTEX in sole O_3 (A) and SFUS/O_3 operating at different frequency; $[BTEX]_0$: 50 ppm (v/v), pH 6.5, O_3 flowrate: 0.5 L/min, US: 600 W, 20±2.5 °C.

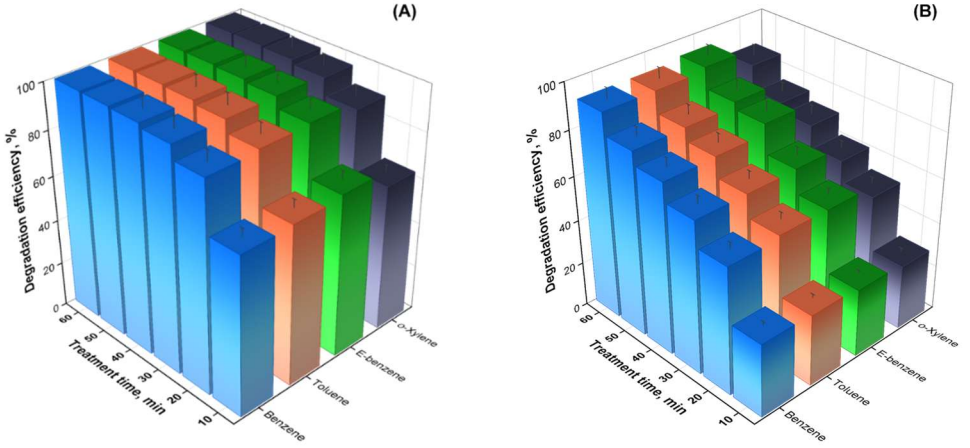

Figure 20. Degradation efficiency of BTEX in LFDUS/O_3 (A), HFDUS/O_3 (B); $[BTEX]_0$: 50 ppm (v/v), O_3 flowrate: 0.5 L/min, pH 6.5, US: 600 W, 40/120 kHz, 80/200 kHz for LFDUS and HFDUS, respectively, 20±2.5 °C.

Upon the dual-frequency sonication, the effectiveness of ozonation towards BTEX was increased significantly as compared to SFUS/O_3. Thus, the simultaneous operation of 40-120 kHz US in LFDUS/O_3 resulted in BTEX degradation efficiency of 99.37%-99.69% within 40 min (Fig. 20A). The peaks of BTEX were note detected in the samples collected at 50 min and 60 min. In the case of HFDUS/O_3, the degradation efficiency of BTEX was in the range of 86.09%-91.76% after 60 min of treatment (Fig. 20B). The enhancement effect of DFUS can be attributed to the complex bubble dynamics caused by the disruption of the steady-state oscillation. Hence, the unstable oscillation accelerated the collapse of cavitation bubbles. Unlike cavitation in SFUS, the cavitation bubbles generated in DFUS at the same power are characterized with higher maximum radius and collapse

pressure. Additionally, DFUS causes higher disturbance of the reaction solution, higher energy dissipation and greater cavitational yield. As a result, the decomposition of O_3 along with the formation of $HO^{\bullet}$ radicals are increased in both LFDUS/O_3 and HFDUS/O_3 giving ξ of 7.86 and 2.9, respectively.

Table 4. Degradation rate constants of BTEX in O_3-assisted processes.

Process	***k*, min^{-1}**			
	Benzene	Toluene	E-benzene	*o*-Xylene
Sole O_3	0.0055	0.0067	0.0081	0.0067
SFUS/O_3 40 kHz	0.0094	0.0093	0.0089	0.0070
SFUS/O_3 80 kHz	0.0144	0.0144	0.0151	0.0119
SFUS/O_3 120 kHz	0.0143	0.0152	0.0172	0.0131
SFUS/O_3 200 kHz	0.0179	0.0182	0.0200	0.0141
LFDUS/O_3	0.1431	0.1419	0.1387	0.1282
HFDUS/O_3	0.0384	0.0385	0.0425	0.0304

4.3.3. Effect of pH on BTEX degradation in DFUS/O_3

As well known, the effectiveness of O_3-based AOPs is significantly affected by solution pH. Depending on pH, the oxidation of water pollutants proceeds either through direct electrophilic attacks by molecular O_3 or indirectly by ROSs from O_3 decomposition. In order to examine the effect of solution pH, the degradation of BTEX in LFDUS/O_3 and HFDUS/O_3 was conducted at acidic and basic conditions. As depicted in Fig. 21, the degradation efficiency of BTEX in both LFDUS/O_3 and HFDUS/O_3 were declined considerably at pH 3. In particular, the degradation efficiency of benzene, toluene, ethylbenzene and *o*-xylene was decreased by 67.81%, 69.61%, 76.53% and 80.60%, respectively, in LFDUS/O_3 in 40 min (Fig. 21A).

In the case of HFDUS/O_3, the corresponding decline was found as 63.54%, 60.81%, 60.76% and 53.70% after 60 min as shown in Fig. 21B. As O_3 is stable at acidic pH, the oxidation of BTEX occurs through the direct interaction with molecular O_3, which is selective and slow. Therefore, the dominance of the direct pathway at pH 3 suppressed the effectiveness of both LFDUS/O_3 and HFDUS/O_3. In contrast to acidic conditions, the increase of pH to 11 affected the degradation efficiency of BTEX negligibly. After 60 min of treatment, 98.76%, 99.22%, 98.81% and 96.71% of benzene, toluene, ethylbenzene and *o*-xylene were degraded, respectively, in LFDUS/O_3, whereas the corresponding values were found as

90.20%, 89.80%, 88.24% and 80.28% for HFDUS/O_3. Although the indirect oxidation pathway by $HO^{\bullet}$ radicals is major route of BTEX degradation at basic conditions, the effectiveness of LFDUS/O_3 and HFDUS/O_3 was not improved significantly. This can be attributed to the lower amount of $HO^{\bullet}$ radicals available for BTEX degradation in gas phase as the reaction of O_3 and HO^- took place in bulk liquid. Additionally, the accelerated generation $HO^{\bullet}$ radicals is associated to the scavenging through Eq. 1.19. Based on these findings, the pH 6.5 was selected as optimal for further experiments.

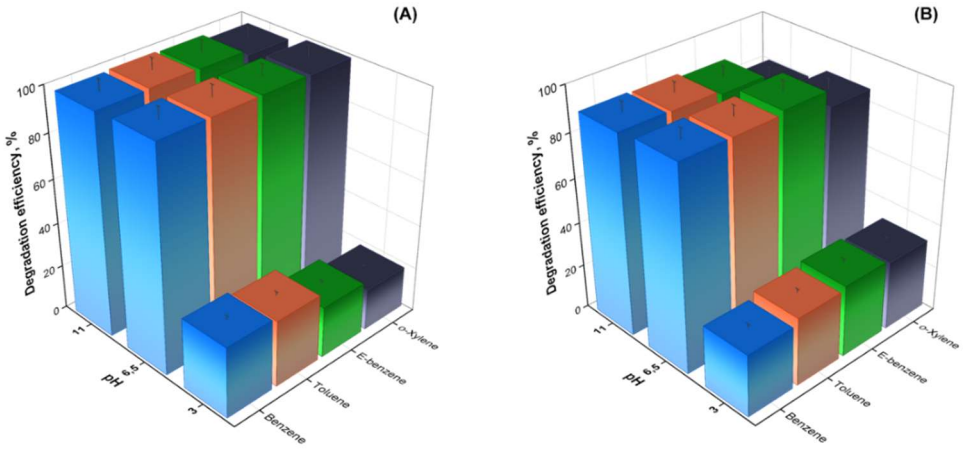

Figure 21. Degradation efficiency of BTEX in LFDUS/O_3 (A), HFDUS/O_3 (B) at different pH; $[BTEX]_0$: 50 ppm (v/v), O_3 flowrate: 0.5 L/min, US: 600 W, 40/120 kHz, 80/200 kHz for LFDUS and HFDUS, respectively, 20±2.5 °C.

4.3.4. Identification of dominant radical species

Besides $HO^{\bullet}$ radicals, $O_2^{\bullet-}$ radicals and $^1O_2$ can be generated in O_3-based AOPs as secondary ROSs and contribute to the degradation of pollutants. These secondary $O_2^{\bullet-}$ radicals are the products of the competing route of O_3 decomposition, which occurs slowly (70 $M^{-1}s^{-1}$) at acidic and neutral conditions (Eq. 4.14) [245]. Additionally, $^1O_2$ can be generated from the reaction with $HO^{\bullet}$, $HO_2^{\bullet}$ and $O_2^{\bullet-}$ radicals (Eqs. 4.15-4.17) [246]. To clarify the contribution of each ROS, the BTEX degradation in LFDUS/O_3 and HFDUS/O_3 were conducted in the presence of specific radical scavengers. Hence, the contribution of $HO^{\bullet}$ radicals was assessed in the presence of MeOH as it rapidly reacts with $HO^{\bullet}$ radicals. Owing to high reactivity, *p*-BQ was selected as a scavenger of $O_2^{\bullet-}$ radicals, while the $^1O_2$ were quenched sodium azide (NaN_3) reacting at ~10^9 $M^{-1}s^{-1}$ [247].

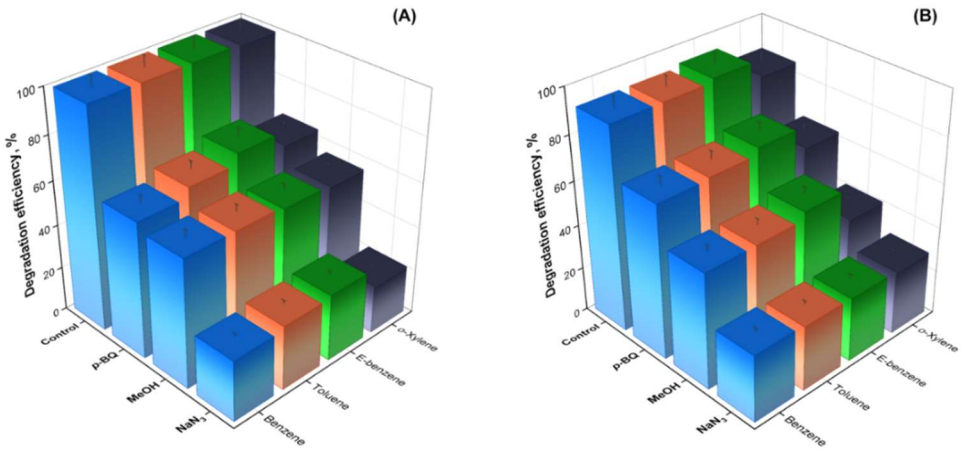

Figure 22. Degradation efficiency of BTEX in LFDUS/O_3 (A), HFDUS/O_3 (B) in the presence of scavengers; $[BTEX]_0$: 50 ppm (v/v), [PS]:[PMS]:[Scavenger] 1:1:100, O_3 flowrate: 0.5 L/min, pH 6.5, US: 600 W, 40/120 kHz, 80/200 kHz for LFDUS and HFDUS, respectively, 20±2.5 °C.

$$O_3 + HO^- \rightarrow O_2^{\bullet -} + HO_2^{\bullet} \quad 4.14$$

$$O_2^{\bullet -} + HO^{\bullet} \rightarrow \quad {}^1O_2 + HO^- \quad 4.15$$

$$O_2^{\bullet -} + HO_2^{\bullet} + H^+ \rightarrow \quad {}^1O_2 + H_2O_2 \quad 4.16$$

$$O_2^{\bullet -} + O_2^{\bullet -} + 2H^+ \rightarrow \quad {}^1O_2 + H_2O_2 \quad 4.17$$

As illustrated in Fig. 22A, the degradation efficiency of BTEXs in LFDUS/O_3 was decreased from 99.37%-99.69% to 42.3%-45.7 % in 40 min, indicating the considerable impact of $HO^{\bullet}$ radicals. Similarly, 57.4%-64% of BTEXs were degraded by HFDUS/O_3 in the presence of MeOH (Fig. 22B). To specify, the contribution as well as the generation of $HO^{\bullet}$ radicals was higher in LFDUS/O_3 as the degradation rate constants of BTEX were hampered by ~90%, whereas in it was ~68% in HFDUS/O_3. Upon the addition of *p*-BQ in LFDUS/O_3, the degradation efficiency of benzene, toluene, ethylbenzene and *o*-xylene were found as to 61.50%, 65.88%, 70.49%, and 64.42%, respectively, in 60 min. The corresponding values of BTEX degradation efficiency in HFDUS/O_3 were 69.34%, 70.11%, 73.05% and 63.36%. Although these implied a noticeable contribution of $O_2^{\bullet -}$ radicals, *p*-BQ can partially react with $HO^{\bullet}$ radicals with 6.6×10^9 $M^{-1}s^{-1}$. Hence, while the occurrence of $O_2^{\bullet -}$ radicals was confirmed, their contribution on BTEX degradation was lower than that of $HO^{\bullet}$ radicals. The addition of NaN_3 in LFDUS/O_3 decreased the degradation efficiency of BTEX in lower extend resulting in 78.6%-83.9% after 40 min. The inhibitory effect of NaN_3 was more pronounced in HFDUS/O_3 and 57.4%-64% of BTEXs were degraded in 60 min. Taking into

account the reactivity of NaN_3 with $HO^{\bullet}$ radicals (1.2×10^{10} $M^{-1}s^{-1}$) and O_3 (2.5×10^6 $M^{-1}s^{-1}$), it can be assumed that the contribution of $^1O_2$ was negligible. Based on these findings, it can be proposed that $HO^{\bullet}$ radicals were the primary species responsible for BTEX degradation in LFDUS/O_3 and HFDUS/O_3 and $O_2^{\bullet-}$ as well as $^1O_2$ played a minor role.

4.3.5. Effect of water constituents on BTEX degradation

In order to investigate the effect of co-existing inorganic anions, the degradation of BTEX was in LFDUS/O_3 and HFDUS/O_3 was performed in the presence of Cl^-, CO_3^{2-} and SO_4^{2-} anions. From Fig. 23B, it can be seen that the presence Cl^- ions had negligible effect on LFDUS/O_3 inhibiting the degradation efficiency of BTEX by 4.35%-10.1% within 40 min.

On the other hand, the degradation efficiency of HFDUS/O_3 towards BTEX after 60 min was decreased by 22.89%-24.95%. The inhibitory effect of Cl^- ions is commonly attributed to the conversion of $HO^{\bullet}$ radicals into $Cl^{\bullet}$ and $Cl_2^{\bullet-}$ radicals with lower oxidation potential. Nevertheless, the effect of these transformations observed in LFDUS/O_3 was insignificant. Therefore, the decrease in degradation efficiency of BTEX in HFDUS/O_3 (Fig. 24B) can be attributed to competitive consumption of O_3 by Cl^- ions. As demonstrated through quenching experiments, the contribution of $O_2^{\bullet-}$ radicals and $^1O_2$ in BTEX degradation was noticeable in HFDUS/O_3. Thus, the decreased BTEX degradation can be attributed to the competing reactions of $O_2^{\bullet-}$ radicals and $^1O_2$ with Cl^- anions. In the case of CO_3^{2-} anions, the degradation efficiency of BTEX was declined in both LFDUS/O_3 and HFDUS/O_3 processes. After 40 min, the degradation of BTEX was inhibited by 4.9%-11.4% in LFDUS/O_3 and by 13.4-15.1% in HFDUS/O_3 in 60 min.

Typically, inhibitory effect of CO_3^{2-} anions is related to the formation of less reactive and selective $CO_3^{\bullet-}$ anion radicals. However, the inhibitory effect of CO_3^{2-} anions on LFDUS/O_3 and HFDUS/O_3 was less pronounced as the elevated pH due to CO_3^{2-}/HCO_3^- promoted O_3 decomposition. Likewise, the degradation efficiency of BTEX in LFDUS/O_3 and HFDUS/O_3 was decreased in the presence of SO_4^{2-} anions. The degradation efficiency of LFDUS/O_3 was inhibited by 43.1%-48.7%, while it was 40.7%-43.04% for HFDUS/O_3. These observations can be ascribed to conversion of highly reactive and non-selective $HO^{\bullet}$ radicals into $SO_4^{\bullet-}$ anion radicals, which possess relatively lower oxidation potential and exhibit selectivity towards electron-rich moieties.

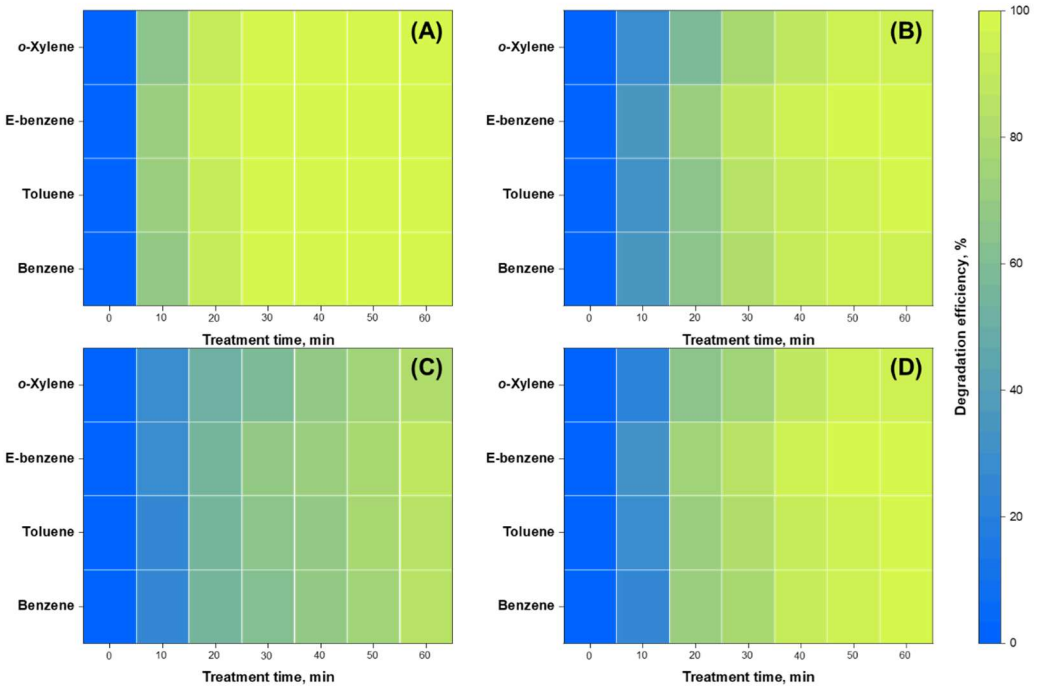

Figure 23. Degradation efficiency of BTEX in LFDUS/ O_3 (A), in the presence of Cl^- (B) SO_4^{2-} (C) and CO_3^{2-} (D); $[BTEX]_0$: 50 ppm (v/v), $[O_3]$:[Anion]: 1:10, O_3 flowrate: 0.5 L/min, pH_0 6.5, US: 600 W, 40/120 kHz, 20±2.5 °C.

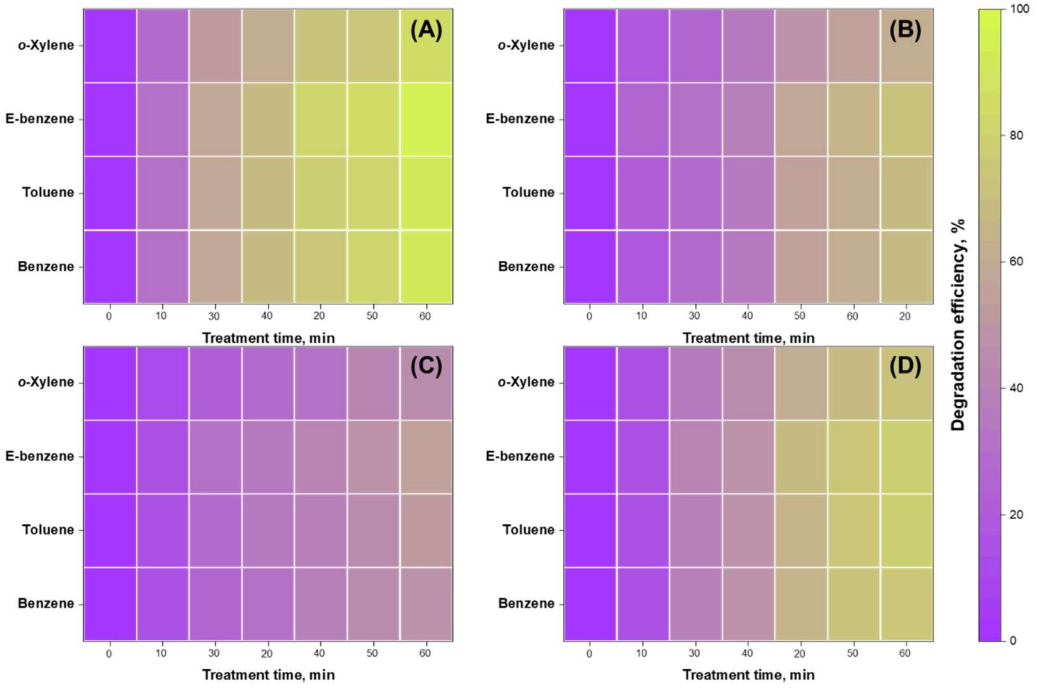

Figure 24. Degradation efficiency of BTEX in HFDUS/O_3 (A), in the presence of Cl^- (B) SO_4^{2-} (C) and CO_3^{2-} (D); $[BTEX]_0$: 50 ppm (v/v), $[O_3]$:[Anion]: 1:10, O_3 flowrate: 0.5 L/min, pH_0 6.5, US: 600 W, 80/200 kHz, 20±2.5 °C.

4.3.6. The proposed degradation pathway of BTEX

In the studies of AOPs, the identification of reaction intermediates is essential to elucidate the mechanism of chemical transformations and assessing potential toxicity risk. In order to identify the reaction intermediates of BTEX degradation in LFDUS/O_3 and HFDUS/O_3, the samples were analyzed by GC-MS. The intermediates were detected in SCAN mode and identified through peak similarity test. Based on the identified intermediates, a possible degradation pathway was proposed for each component of BTEX. For the accurate detection and enhanced signal of the intermediates, model solutions individually containing 800 ppm, 450 ppm, 300 ppm and 250 ppm of benzene, toluene, ethylbenzene and *o*-xylene, respectively, were prepared and treated in LFDUS/O_3 and HFDUS/O_3.

As shown in Fig. 25, phenol, hydroquinone and *p*-benzoquinone were the products of benzene degradation. Based on the detected intermediates it can be proposed that $HO^{\bullet}$ radicals attacked benzene through H-abstraction to yield a cation radical. The cation radical then reacted with water introducing a hydroxyl group and forming phenol (m/z 94). Then phenol underwent another radical propagation and hydroxylation steps to yield hydroquinone (m/z 110) and *p*-benzoquinone (m/z 108). In the case of toluene, ethylbenzene and o-xylene, the H-abstraction occurred from alkyl groups, as these groups have lower C-H bond disassociation energy than in those in the aromatic ring. For toluene, H-abstraction from methyl group by $HO^{\bullet}$ radicals was the initial step and formed benzyl radical. The benzyl radical underwent hydroxylation in water and subsequently oxidized by ROSs resulting in benzyl alcohol (m/z 108) and benzaldehyde (m/z 106). These intermediates were also detected among the by-products of ethylbenzene degradation suggesting that the dealkylation of the ethyl group via elimination of formic acid. After that, the resulting radical adduct repeated the degradation steps similar to toluene. Alternatively, the detection of 1-phenylethanol (m/z 122) and acetophenone (m/z 120) indicates that the non-selective attacks of $HO^{\bullet}$ radicals led H-abstraction from β-carbon of ethylbenzene. The initial H-abstraction in *o*-xylene was from one of the methyl groups and the formation of *o*-methylbenzyl alcohol (m/z 122) and *o*-tolualdehyde (m/z 120) suggests the consecutive hydroxylation and oxidation of the methyl group. None of these intermediates were detected in final samples confirming the complete degradation of BTEX in LFDUS/O_3 and HFDUS/O_3.

The effect of AC induced by US generators operating at two different frequencies greatly enhanced the effectiveness of ozonation towards BTEX. Compared to SFUS (US/O_3 at 40 kHz, 80 kHz, 120 kHz, 200 kHz), the ozonation under DFUS

resulted in higher degradation efficiency of BTEX due to the higher intensity of cavitational events.

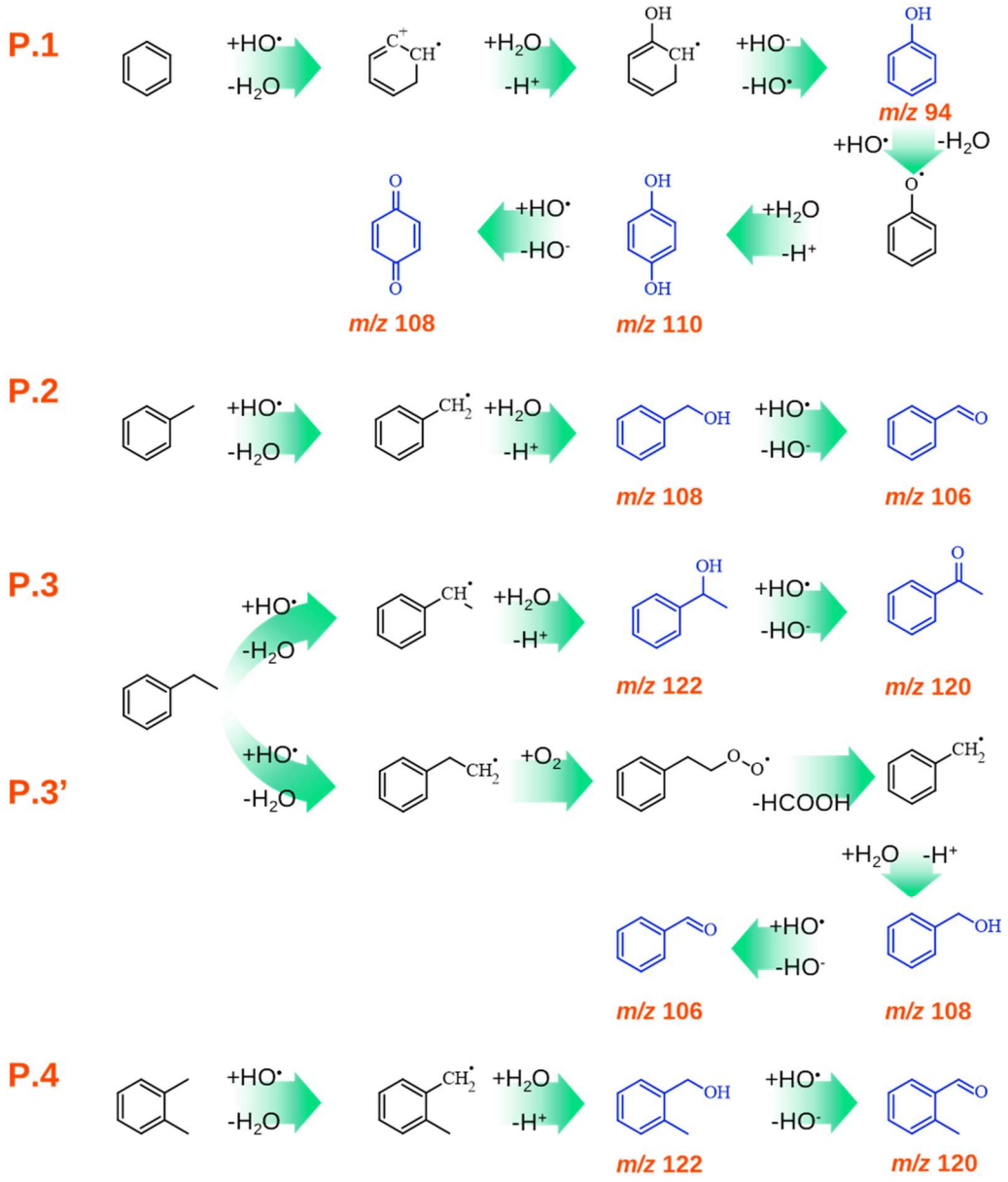

Figure 25. The possible degradation pathways of BTEX components in LFDUS/O_3 and HFDUS/O_3 based on the intermediates identified using GC-MS.

Owing to the combined operation of 40 kHz transducers and 120 kHz sonotrodes, LFDUS/O_3 achieved the complete degradation of BTEX in 40 min at pH 6.5, r_{ox} 6.25, 20±2.5 °C. The complete degradation of BTEX in HFDUS/O_3 with 80 kHz-200 kHz was attained after 60 min at identical conditions. The findings highlighted the crucial role of US frequency on cavitation parameters, such collapse pressure, which is directly connected to sono-chemical generation of radical species. Based on the quenching experiments, $HO^{\bullet}$ radicals were found as predominant reactive species responsible for BTEX degradation. The inhibitory effect of inorganic anions

followed the order SO_4^{2-} > Cl^- > CO_3^{2-} for both LFDUS/O_3 and HFDUS/O_3. The oxidative degradation of BTEX by radical species was initiated by H-abstraction by $HO^{\bullet}$ radicals followed by hydroxylation and dealkylation.

4.3.7. The comparison of cavitation-based AOPs for BTEX degradation

The hybrid cavitation-based AOPs (i.e., AC/SR-AOPs, HC/SR-AOPs and AC/AOPs) demonstrated high effectiveness for the degradation of BTEX in water. The processes exhibited high oxidation performance at relatively low r_{ox} values and near-neutral pH. Specifically, PS and PMS showed the highest BTEX degradation extend at r_{ox} 5 under both HC and AC, while the r_{ox} value of O_3 was 6.25 in AC/O_3. In addition, the hybrid processes operated at environmentally relevant conditions, i.e., without pH adjustment, at room temperature. These features grant the hybrid processes with high potential in practice. Nevertheless, AOPs are commonly known for high demand in electric energy for devices, e.g., UV lamp, pumps, heaters, US generators, which is commonly reflected in high treatment cost. Hence, the comparison of the hybrid processes can be performed based on the treatment cost taking into account the degradation rate constant of BTEX, electrical and oxidants consumption. From this perspective, AC/PS/ASPH and AC/PMS/ASPH attaining the highest degradation efficiency after 360 min of US irradiation are the least economically attractive among the developed processes. Moreover, the utilization of asphaltenes requires additional step of purification after treatment. In contrast, HC/PS, HC/PMS, LFDUS/O_3 and HFDUS/O_3 were able to degrade BTEX in shorter treatment time without a catalyst. The total treatment cost of these processes was estimated using electric energy per order (E_{EO}) from Eq. 4.18 and 4.19 [248]. This parameter allows to estimate the electric energy required to reduce the concentration of a pollutant by one order of magnitude (i.e., 90% degradation) in 1 m^3 contaminated liquid. In Poland, the wholesale electricity price for industrial customers was 105.88 EUR/MWh (i.e., 0.106 EUR/kWh) on July 2025 [249].

$$E_{EO} = \frac{P_{el} * t * 100}{V * 60 * log\,(\frac{C_0}{C_t})} \qquad 4.18$$

, where P_{el} denotes an electric power (kW), t is treatment time (min), V is the volume (L) of the treated solution, C_0 and C_t are initial and final concentration of the pollutant (mg/L).

Considering Eq. 4.2, the Eq. 4.18 can be expressed as follows:

$$E_{EO} = \frac{38.4 * P_{el}}{V * k} \qquad 4.19$$

The treatment cost of HC/PS and HC/PMS also included the cost of oxidants required for the treatment 1 m^3 BTEX-contaminated water i.e., 2.24 kg and 2.82 kg of PS and PMS (Oxone®), respectively [250]. The average price of PS and Oxone® in wholesale market taken as 1.5 EUR/kg and 2.5 EUR/kg, respectively. As listed in Table 5, LFDUS/O_3 exhibited the lowest electric energy demand and, thereby, the lowest total treatment cost of 7.62 EUR.

Table 5. The E_{EO} (kWh/m^3/order) values of the cavitation-based AOPs for BTEX degradation.

Process	**E_{EO}, (kWh/m^3/order)**				**Avg.**	**Energy cost, EUR**	**Oxidant, kg**	**Oxidant cost, EUR**	**Total cost, EUR**
	B	T	E	X					
HC/PS	77,28	73,14	77,77	82,47	77,67	8,23	2,24	3,36	11,59
HC/PMS	115,92	106,85	104,14	107,79	108,68	11,52	2,82	7,05	18,57
LDFUS/O_3	69,20	69,79	71,40	77,25	71,91	7,62	0	0	7,62
HDFUS/O_3	257,89	257,22	233,02	325,76	268,47	28,46	0	0	28,46

The results indicated LFDUS/O_3 as the most energy-effective, while the BTEX ozonation in HFDUS/O_3 was the most energy intensive. The cost of treatment in HC/PS was estimated as 11.59 EUR, in which 3.36 EUR is the cost of the oxidant. In real case scenario, the treatment in HC/PS would be more favorable due to the simplicity in operation and maintenance. On the other hand, LFDUS/O_3 may require additional indirect expenses related to the maintenance of the sono-reactor and O_3 generator, which is connected to the system of dry-air supply. In the light of this, HC/PS with a total treatment cost of 11.6 EUR can be preferred due to the installation simplicity and potentially lower maintenance requirements.

4.4. Ozonation of 1,4-dioxane under HC in the presence of SPC

So far, the effectiveness of the developed processes (i.e., HC/SR-AOPs, AC/SR-AOPs/ASPH, AC/O_3) has been evaluated for the degradation of BTEX. The studies indicated that the degradation of BTEX in the hybrid process involves the diffusion of hydrophobic molecules into the cavity interior. Considering this, the study on the degradation of a hydrophilic and persistent pollutant in the cavitation-based AOP represented a particular research interest. Therefore, 1,4-diethylene oxide or 1,4-dioxane with a cyclic structure with high water solubility and notable resistance to biodegradation, was selected for further degradation experiments. Classified as potentially carcinogenic by USEPA, 1,4-dioxane has been reported to occur in various water bodies, including municipal water supply and groundwater. As a result of extensive investigations on 1,4-dioxane degradation, AOPs were found as effective and green methods. For instance, traditional peroxone was reported highly effective towards 1,4-degradation. However, H_2O_2 is chemically unstable, can be dangerous during transportation as it is explosive at higher concentrations and may corrode the metallic parts of equipment. On the other hand, sodium percarbonate (SPC) is emerging as a safe and stable alternative to H_2O_2, which can be potentially used in peroxone process. Hence, the modified peroxone using SPC was performed under HC and the developed process was evaluated for the degradation of 1,4-dioxane.

4.4.1. 1,4-dioxane degradation under sole HC

In order to select the optimal C_v, the degradation of 1,4-dioxane was conducted varying the C_v from 0.02 to 0.92. According to Fig. 26A, the degradation efficiency of 1,4-dioxane after 120 min was found as 11.63%, 16.04%, 17.03%, 15.76% and 15.51% for C_v 0.92, 0.47, 0.27, 0.18 and 0.02, respectively. Correspondingly, the degradation rate constant of 1,4-dioxane rose from 1.03×10^{-3} min^{-1} to 1.43×10^{-3} min^{-1} as C_v was decreased from 0.92 to 0.27 (Fig. 26B). With further increased of inlet pressure and decrease of C_v to 0.18 and 0.02, the rate constant of 1,4-dioxane was declined to 1.41×10^{-3} min^{-1} and 1.4×10^{-3} min^{-1}, respectively. These observations indicate that the increase of a liquid velocity and, thus, decreasing C_v resulted in higher cavitation intensity promoting the pollutant degradation. However, the degradation of 1,4-dioxane lowered with further decrease of C_v to 0.18 and 0.02, which can be attributed to “supercavitation” or choked cavitation.

The phenomenon of “supercavitation” occurs when C_v is near 0 and vaporous cavity clouds with reduced the collapse pressure are formed as a result of bubble coalescence. Thereby “supercavitation” strongly reduces the intensity of cavitation. Considering the obtained results, C_v of 0.27 was selected as the optimal operating conditions for subsequent experiments.

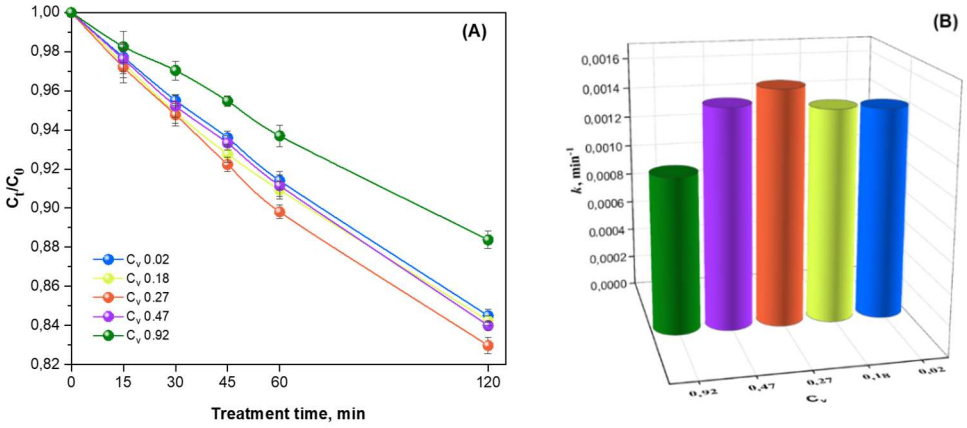

Figure 26. Degradation efficiency of 1,4-dioxane under sole HC at various C_v (A) and the corresponding degradation rate constants (B); $[1,4\text{-dioxane}]_0$ 100 ppm, pH ~5, 20±2 °C.

4.4.2. Effect of SPC dosage on 1,4-dioxane degradation

Since SPC containing H_2O_2 serves as a radical precursor in HC/SPC/O_3, the dosage of SPC plays an important role on the degradation of 1,4-dioxane. In order to determine the optimal SPC dosage, the experiment of 1,4-degradation in HC/SPC were conducted varying the molar ratio of SPC to 1,4-dioxane (r_{rox}) ranging from 1-10.

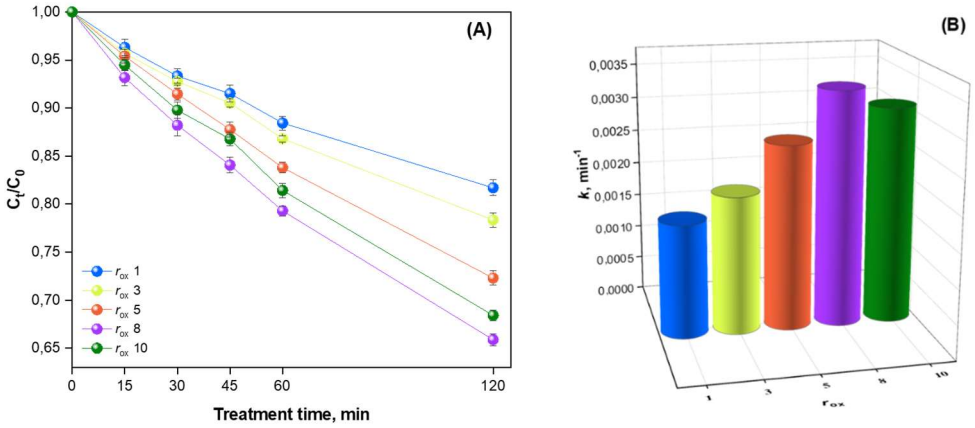

Figure 27. Degradation efficiency of 1,4-dioxane in HC/SPC at various SPC dosage (r_{ox}) (A) and the corresponding degradation rate constants (B); $[1,4\text{-dioxane}]_0$ 100 ppm, C_v 0.27, pH ~5, 20±2 °C.

As shown in Fig. 27A, the degradation efficiency of 1,4-dioxane was increased with the increase of r_{rox} from 1 to 8, while it was lowered at r_{rox} 10. In particular, 18.34%, 22.11%, 27.52% and 37.15% of 1,4-dioxane was degraded at r_{rox} 1, 3, 5 and 8 at pH 5 in 120 min. The increasing trend was reflected in the increase of degradation rate constants from 1.55×10^{-3} min^{-1} to 3.42×10^{-3} min^{-1} as illustrated in Fig. 27B. Then the degradation efficiency observed after 120 min at r_{rox} 10 was declined to 31.94% resulting in the rate constant of 3.14×10^{-3} min^{-1}. The observed decline in efficiency at higher SPC concentration can be attributed to the scavenging reactions that consume $HO^{\bullet}$ radicals. Similar to H_2O_2-assisted AOPs, $HO^{\bullet}$ radicals in HC/SPC were consumed by side reactions with H_2O_2, DO and radical recombination reactions. These reactions predominantly yield radical species that exhibit lower oxidation potential. Based on the obtained results, r_{rox} 8 was identified as the optimal SPC dosage for remaining experiments.

4.4.3. Effect of O_3 dosage on 1,4-dioxane degradation

To explore the effect of O_3 dosage, the degradation of 1,4-dioxane was performed in HC/SPC/O_3 at C_v of 0.27, r_{rox} 8 varying the O_3 feed dosage from 0.23 g/h to 0.94 g/h. As presented in Fig. 28A, employing the O_3 dosage of 0.23 g/h, 0.40 g/h, 0.74 g/h and 0.86 g/h, 39.65%, 59.55%, 90.35% and 99.34% of 1,4-dioxane was degraded in 120 min, respectively. The increasing trend of degradation efficiency upon the increase of O_3 dosage from 0.23 g/h to 0.86 g/h reflected in the increase of rate constant of 1,4-degradation from 4.11×10^{-3} min^{-1} to 4.04×10^{-2} min^{-1}. The degradation rate constant observed in HC/SPC/O_3 at 0.86 g/h was significantly greater compared to the rate constant of 3.74×10^{-3} min^{-1} obtained in HC/SPC. This can be attributed to the interaction between O_3 and H_2O_2 from SPC, resulting in mutual decomposition generating $HO^{\bullet}$ radicals. Besides, the mass transfer of the supplied O_3 into liquid phase is facilitated by the elevated pressure in inlet of Venturi tube and the turbulence caused by cavitation. These factors facilitate the contact of O_3 and H_2O_2 in HC/SPC/O_3, ensuring effective utilization of both oxidants. For instance, the outlet concentration of O_3 in HC/SPC/O_3 was 0.135 g/h, while it was 0.384 g/h in SPC/O_3 in the absence of cavitation. Owing to the effective utilization of O_3, 99.34% of 1,4-dioxane was degraded in HC/SPC/O_3, while SPC/O_3 degraded 56.02% in 120 min with a rate constant of 6.60×10^{-3} min^{-1}. On the other hand, the degradation efficiency of 1,4-dioxane was declined from 99.34% to 97.12% with the increase of O_3 dosage from 0.86 g/h to 0.94 g/h. This was accompanied with a decrease in degradation rate constants from 4.04×10^{-2}

min^{-1} to 2.82 × 10^{-2} min^{-1}. The scavenging effect caused by the excess of O_3 can be ascribed to the reaction of dissolved O_3 with $HO^{\bullet}$ radicals that compete with the reaction of 1,4-dioxane with $HO^{\bullet}$ radicals.

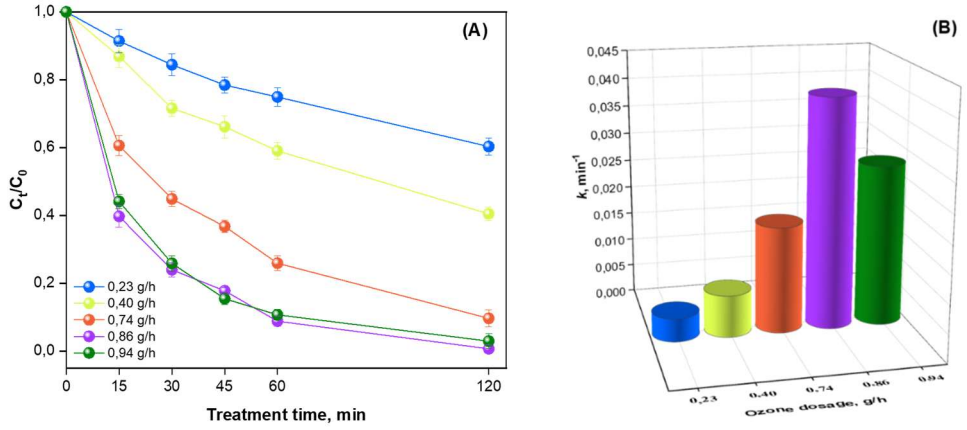

Figure 28. Degradation efficiency of 1,4-dioxane in HC/SPC/O_3 at various O_3 dosage (A) and the corresponding degradation rate constants (B); $[1,4\text{-dioxane}]_0$ 100 ppm, C_v 0.27, r_{ox} 8, pH ~5, 20±2 °C.

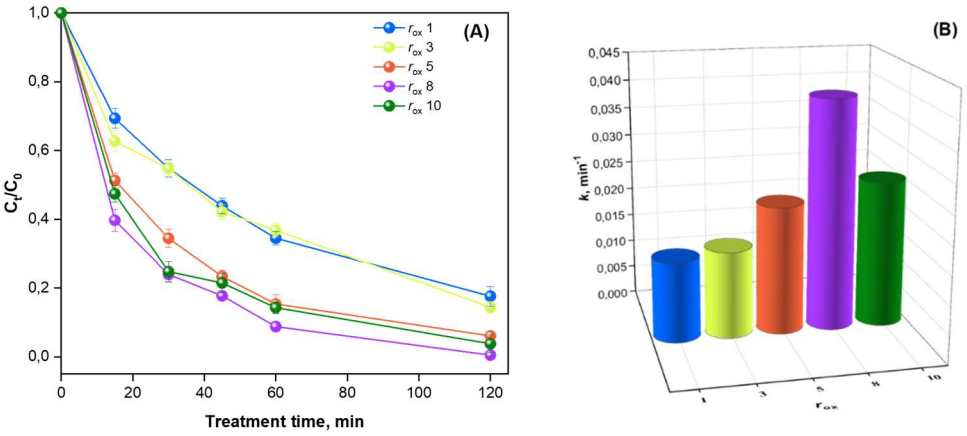

Figure 29. Degradation efficiency of 1,4-dioxane in HC/SPC/O_3 at various SPC dosage (r_{ox}) and fixed O_3 dosage (A) and the corresponding degradation rate constants (B); $[1,4\text{-dioxane}]_0$ 100 ppm, C_v 0.27, $[O_3]$ 0.86 g/L, pH ~5, 20±2 °C.

To further assess the effect of O_3 dosage, the degradation of 1,4-dioxane was carried out at O_3 dosage fixed as 0.86 g/h and varying the SPC dosage at r_{rox} in the range of 1-10. As shown in Fig. 29A, the degradation efficiency of 1,4-dioxane observed in HC/SPC at r_{rox} 1, 3, 5, 8 and 10 were improved by 64.02%, 63.47%, 66.37%, 62.15% and 64.24%, respectively, in the presence of O_3. Although, the improvement in degradation efficiency was the highest at r_{rox} 5, the degradation rate constant of 1,4-dioxane at r_{rox} 1, 3, 5, 8 and 10 was improved by 1.236 × 10^{-2} min^{-1}, 1.324 × 10^{-2} min^{-1}, 1.973 × 10^{-2} min^{-1}, 3.699 × 10^{-2} min^{-1} and 2.249 × 10^{-2} min^{-}

[1], respectively (Fig. 29B). These findings highlight that the dosage of both SPC and O_3 as well as their ratio are key factors determining the oxidative capacity of HC/SPC/O_3 towards 1,4-dioxane.

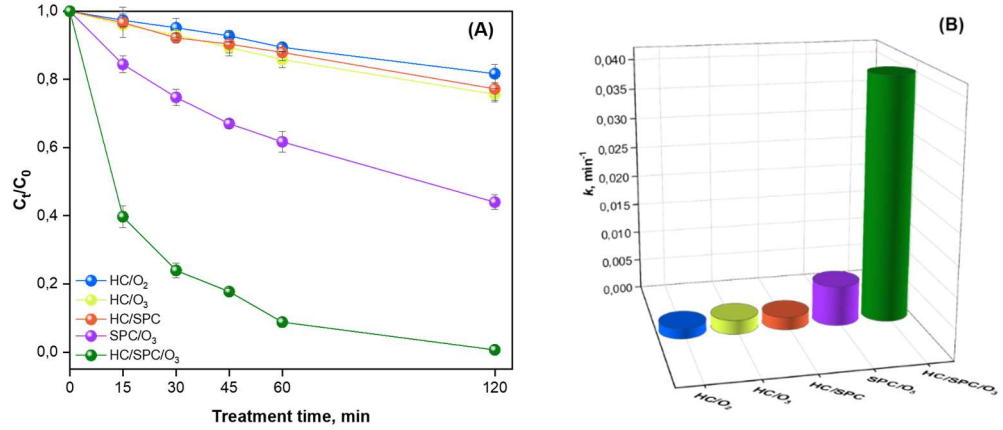

Figure 30. Degradation efficiency of 1,4-dioxane in various processes (A) and the corresponding degradation rate constants (B); $[1,4\text{-dioxane}]_0$: 100 ppm, C_v 0.27, r_{ox} 8, $[O_3]$ 0.86 g/L, pH ~5, T 20±2 °C.

To determine the synergistic effect in the combined HC/SPC/O_3, the effectiveness of HC/O_2, HC/O_3, HC/SPC and SPC/O_3 towards 1,4-dioxane was evaluated. As depicted in Fig. 30A, the treatment of 1,4-dioxane in HC with O_2 purging for 120 min resulted 18.29% of degradation efficiency exceeding that of HC alone. In this case, the improvement is attributed to the gas stream injected to the upstream of the Venturi tube that increased the number of nuclei available for cavitation bubble growth. In the combined HC/SPC and HC/O_3, 22.76% and 24.34% of 1,4-dioxane was correspondingly degraded within 120 min, which exceeded the effectiveness of sole HC and HC/O_2 due the intensified generation of $HO^{\bullet}$ radicals from O_3 and H_2O_2 decomposition. When SPC was combined with O_3, the degradation of 1,4-dioxane was 56.02% after 120 min. In SPC/O_3, the generation of radical species primarily proceeds through well-known peroxone process (Eqs. 1.9, 1.10). Additionally, the presence of SPC can also initiate the decomposition of O_3 and H_2O_2. Thus, both oxidants undergo decomposition at basic conditions to yield HO_2^- ions that can be converted into $HO^{\bullet}$ radicals *via* a series of radical chain reactions. As integrated with HC, SPC/O_3 achieved 99.34% of 1,4-dioxane degradation in 120 min. Taking into account the observed finding and recent progress in cavitation-based AOPs, the synergistic effect in the combined HC/SPC/O_3 can be due to the following factors: i) extreme conditions in “hot-spots” facilitated the bond cleavage in radical precursors, initiating chain radical reactions; ii) owing to the continuous circulation and shock waved produced by cavitation, the mass transfer

and utilization of O_3 were enhanced; iii) the effect of cavitation provided the continuous generation of radical species and promoted the radical-driven degradation of 1,4-dioxane. As a result, the ξ value of HC/SPC/O_3 was found as 4.32, indicating a remarkable synergy compared to the cumulative effect of the individual process (i.e., HC, SPC/O_3, HC/SPC, HC/O_3).

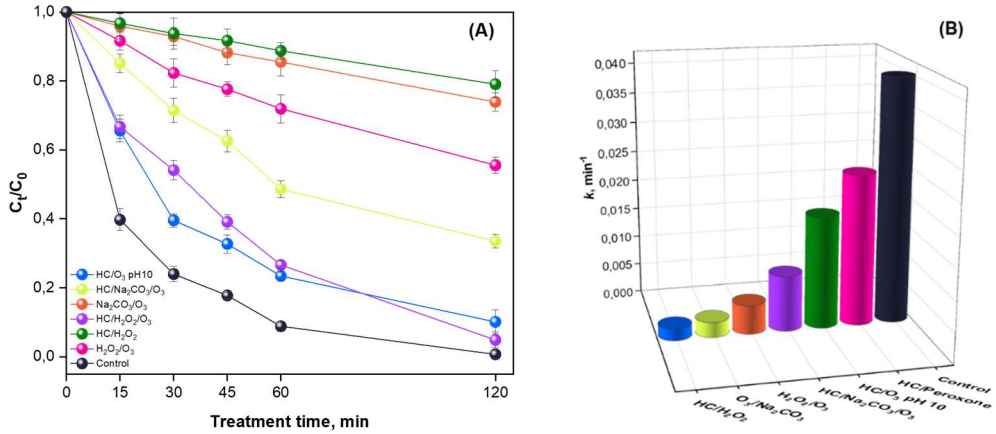

Figure 31. Degradation efficiency of 1,4-dioxane in various O_3-assisted processes (A) and the corresponding degradation rate constants (B); $[1,4\text{-dioxane}]_0$ 100 ppm, C_v 0.27, r_{ox} 8, [SPC]=[Na_2CO_3]=[H_2O_2], [O_3] 0.86 g/L, pH ~5, 20±2 °C.

To elucidate the role of SPC in HC/SPC/O_3, a series of comparative experiments involving sodium carbonate (Na_2CO_3) to replace SPC were conducted. As demonstrated in Fig. 31A, the degradation efficiency of 1,4-dioxane was 26.11% and 66.50% in Na_2CO_3/O_3 and HC/Na_2CO_3/O_3 after 120 min, respectively. While, this highlights the contribution of HC to O_3 decomposition, the replacement of SPC with Na_2CO_3 was detrimental. Specifically, the degradation efficiency of 1,4-dioxane in HC/Na_2CO_3/O_3 was lower by 32.84% compared to HC/SPC/O_3, while Na_2CO_3/O_3 was less effective than SPC/O_3 by 29.91%. When H_2O_2 was added in HC/O_3 instead of SPC, 70.82% of 1,4-dioxane was degraded in 120 min. Likewise, HC/O_3 with pH adjusted at 10 resulted in 65.55% of 1,4-dioxane degradation. This obtained result of HC/O_3 at pH 10 was higher than that of HC/O_3 at pH ~6.5 by 41.21%, demonstrating the significant contribution of $HO^{\bullet}$ radicals derived from O_3 decomposition at basic conditions. However, both HC/Na_2CO_3/O_3 and HC/O_3 at pH 10 were less effective compared to HC/SPC/O_3. This can be due to the formation of the secondary $HCO_3^{\bullet}$ and $CO_3^{\bullet-}$ radicals participating in degradation of 1,4-dioxane. The extent of this contribution is provided by exploring the effect of specific radical scavengers.

4.4.4. Effect of pH on 1,4-dioxane degradation in HC/SPC/O_3

As in typical O_3-based AOPs, the solution pH plays a critical role in generation of radical species thereby affecting the overall effectiveness of HC/SPC/O_3. Besides, the solution pH affects the oxidation potential of the generated radicals, interaction of SPC and O_3 as well as the speciation of the pollutant and oxidants in the treated liquid. In order to investigate the effect of pH, the degradation of 1,4-dioxane in HC/SPC/O_3 was conducted by varying the initial pH (pH_0) in the range 3-12.

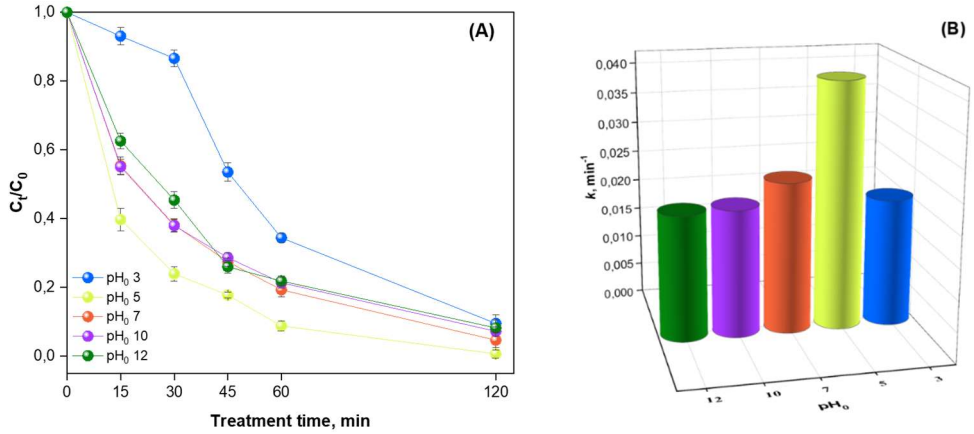

Figure 32. Degradation efficiency of 1,4-dioxane in HC/SPC/O_3 at various pH_0 (A) and the corresponding degradation rate constants (B); $[1,4\text{-dioxane}]_0$ 100 ppm, C_v 0.27, r_{ox} 8, $[O_3]$ 0.86 g/L, 20±2 °C.

According to Fig. 32A, HC/SPC/O_3 showed the highest effectiveness at pH_0 5 (unadjusted), while pH_0 3, 7, 10 and 12 had suppressive effect. For instance, the degradation efficiency of 1,4-dioxane was decreased to 90.49% in 120 min when pH_0 was decreased to 3. Since, O_3 is more stable and the degradation of pollutants proceed *via* the direct oxidation at acidic conditions, the degradation efficiency of 1,4-dioxane was hindered and the rate constant was 2.09×10^{-2} min^{-1} (Fig. 32B**)**. The rate constant was then increased to 4.04×10^{-2} min^{-1} degrading 99.34% of 1,4-dioxane in 120 min at pH_0 5. Nevertheless, with further increase of pH_0 to 10 and 12, the degradation efficiency of HC/SPC/O_3 was declined to 92.76% and 91.78%, indicating the occurrence of scavenging reactions consuming $HO^{\bullet}$ radicals. For instance, the excess of HO_2^- ions generated from Eqs. 4.20, 4.21, may serve as a scavenger of $HO^{\bullet}$ radicals to form less-reactive secondary radicals as shown in Eq. 4.22. On the other hand, pH_0 adjusted at 3 was gradually increased upon the addition of SPC due to the presence of CO_3^{2-} ions, which accelerated the base-induced decomposition of O_3 into $HO^{\bullet}$ radicals thereby effectively degrading 1,4-

dioxane. Hence, the increase of pH_0 3 to 6 after 45 min in HC/SPC/O_3 reflected in the substantial increase of the degradation efficiency from 6.92% to 46.47%.

$$O_3 + HO^- \rightarrow HO_2^- + O_2 \quad (4.20)$$

$$H_2O_2 \leftrightarrow HO_2^- + H^+ \quad (4.21)$$

$$HO_2^- + HO^\bullet \rightarrow HO_2^{\bullet -} + HO^- \quad (4.22)$$

4.4.5. Identification of dominant radical species

In addition to $HO^\bullet$ radicals, the degradation of 1,4-dioxane in HC/SPC/O_3 can be contributed by $O_2^{\bullet -}$ and $CO_3^{\bullet -}$ radicals. In order to elucidate the role of each reactive radical, the degradation of 1.4-dioxane was conducted by adding a specific radical scavenger. As reported, isopropyl alcohol (IPA) easily reacts with $HO^\bullet$ radicals with a rate constant of 3.9×10^9 M^{-1} s^{-1}, while the reactions with $O_2^{\bullet -}$ and $CO_3^{\bullet -}$ radicals proceeds slowly at rate constants of 1.0×10^6 M^{-1} s^{-1} and 4.0×10^4 M^{-1} s^{-1}, respectively. Moreover, IPA reacts with $HO^\bullet$ radicals more rapidly than 1,4-dioxane, H_2O_2 and CO_3^{2-} anions, which react with $HO^\bullet$ radicals at a rate constant of 2.8×10^9 M^{-1} s^{-1}, 2.7×10^7 M^{-1} s^{-1} and 3.9×10^8 M^{-1} s^{-1}, respectively.

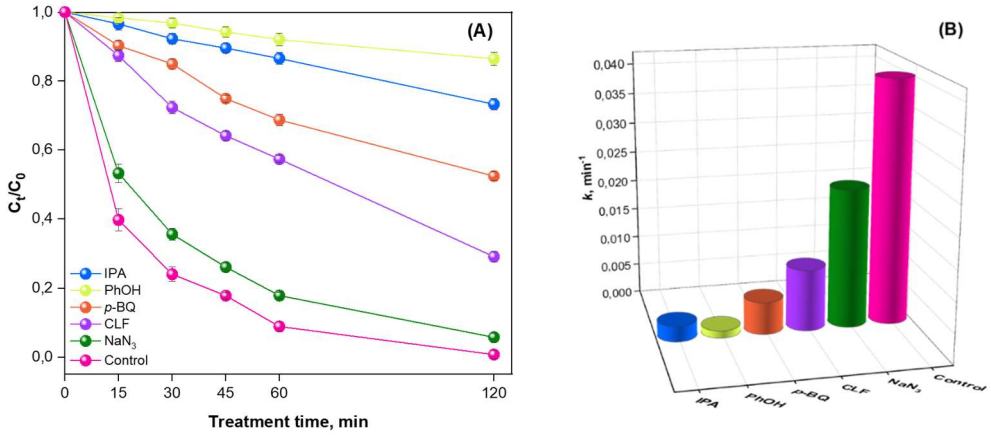

Figure 33. Degradation efficiency of 1,4-dioxane in HC/SPC/O_3 in the presence of scavengers (A) and the corresponding degradation rate constants (B); [1,4-dioxane]$_0$ 100 ppm, C_v 0.27, r_{ox} 8, [O_3] 0.86 g/L, [SPC]:[Scavenger] 1:10, 20±2 °C.

Thus, in the presence of IPA:SPC at a molar ratio of 10:1, the degradation efficiency of 1,4-dioxane was decreased from 99.34% to 26.71% after 120 min as shown in Fig. 33A. The corresponding degradation rate constant was dropped to 2.58×10^{-3} min^{-1} (Fig. 33B). This revealed the dominant role of $HO^\bullet$ radicals in the degradation of 1,4-dioxane. To evaluate the contribution of $O_2^{\bullet -}$ radicals, phenol

(PhOH) that react with $HO^{\bullet}$ and $CO_3^{\bullet-}$ radicals at 6×10^8 M^{-1} s^{-1} and 1.2×10^9 M^{-1} s^{-1}, respectively, was added in HC/SPC/O_3. In this case, the degradation efficiency of 1,4-dioxane was inhibited to 13.52% in 120 min, indicating the moderate contribution of $CO_3^{\bullet-}$ radicals and the occurrence $O_2^{\bullet-}$ radicals.

In addition, the presence of *p*-BQ and chloroform (CLF) that quenches $O_2^{\bullet-}$ radicals with a rate constant of 3.9×10^{10} M^{-1} s^{-1}, inhibited the degradation of 1,4-dioxane by 52.99% and 29.21% after 120 min. Taking into account that hydrophobic CLF mainly quench $O_2^{\bullet-}$ radicals in the gaseous phase of cavitation bubbles, it can be proposed that the generation $O_2^{\bullet-}$ radicals took place in bulk liquid. While these observations supported the noticeable contribution of $O_2^{\bullet-}$ radicals, it is worth to mention that both *p*-BQ and CLF can also react with $HO^{\bullet}$ radicals. In HC/SPC/O_3, $O_2^{\bullet-}$ radicals can be transformed through the Eqs. 4.23, 4.24 and form $^1O_2$. The impact of $^1O_2$ was examined by the addition of NaN_3. Based on Fig. 33A, the degradation efficiency of 1,4-dioxane in the presence of NaN_3 was reduced by 5.03% suggesting the negligible contribution of $^1O_2$. The results from scavenging experiments suggested $HO^{\bullet}$ radicals as the main reactive species responsible for the degradation of 1,4-dioxane in HC/SPC/O_3. In this, $CO_3^{\bullet-}$ radicals also contributed to the degradation efficiency, while the impact of $O_2^{\bullet-}$ radicals was negligible.

$$O_2^{\bullet-} + HO^{\bullet} \rightarrow \quad {}^1O_2 + HO^- \qquad 4.23$$

$$O_2^{\bullet-} + HO_2^{\bullet} + H^+ \rightarrow \quad {}^1O_2 + H_2O_2 \qquad 4.24$$

4.4.6. Effect of water constituents on 1,4-dioxane degradation

The inorganic anions, such as Cl^-, NO_3^- and SO_4^{2-} are commonly present natural waters and may affect the effectiveness of HC/SPC/O_3 by scavenging $HO^{\bullet}$ radicals. To explore the effect of these anions, the degradation of 1,4-dioxane was conducted in the presence of Cl^-, NO_3^- and SO_4^{2-} ions at molar ratio to SPC at 10:1. According to the results displayed in Fig. 34A, the addition of Cl^- had negligible effect on HC/SPC/O_3 decreasing the degradation efficiency from 99.34% to 95.74% after 120 min. Similar to the inhibitory effect observed during BTEX degradation in LFDUS/O_3 and HFDUS/O_3, the effect of Cl^- ions can be attributed to the reaction with O_3 form hypochlorous acid. In contrast to LFDUS/O_3 and HFDUS/O_3 the co-existing SO_4^{2-} anions resulted in lower inhibitory effect, reducing the degradation efficiency of 1,4-dioxane by 12.28% within 120 min. Moreover, the

decline in degradation efficiency was found as 7.51% in the presence of NO_3^- anions.

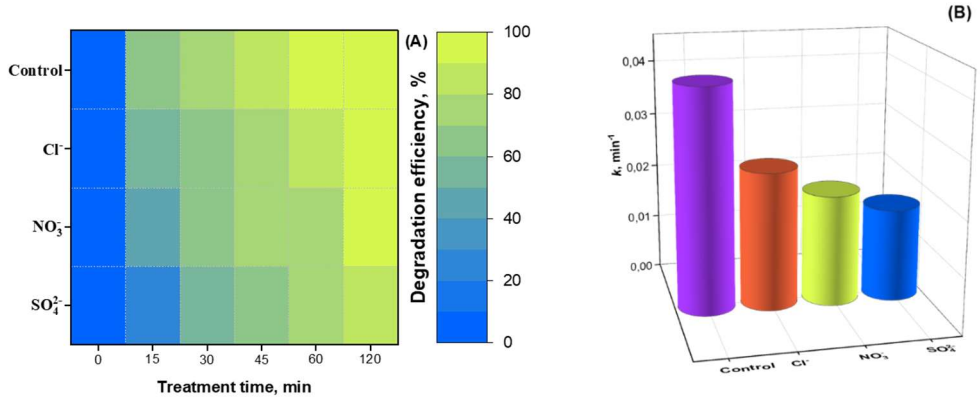

Figure 34. The effect of water constituents on degradation efficiency of 1,4-dioxane (A) and the corresponding degradation rate constants (B); $[1,4\text{-dioxane}]_0$ 100 ppm, C_v 0.27, r_{ox} 8, $[O_3]$ 0.86 g/L, [SPC]:[Anion] 1:10, 20±2 °C.

The degradation rate constants of 1,4-dioxane in HC/SPC/O_3 upon addition of Cl^-, SO_4^{2-} and NO_3^- ions were 2.50×10^{-2} min^{-1}, 1.68×10^{-2} min^{-1} and 2.01×10^{-2} min^{-1}, respectively (Fig. 34B). Consistently, the inhibitory effect of the studied anions followed the order: SO_4^{2-}>NO_3^-> Cl^-.

4.4.7. The proposed degradation pathway of 1,4-dioxane

The structural transformations of 1,4-dioxane induced by the non-selective oxidation by highly reactive $HO^•$ radicals along with electrophilic attacks by $CO_3^{•-}$ radicals may lead to the formation of a variety of compounds. Since the incomplete degradation of organic pollutants can cause secondary pollution due to the formation of hazardous substances often posing higher toxicity than the parent contaminant. To elucidate the degradation pathway, the model solution containing 1000 ppm 1,4-dioxane was treated in HC/SPC/O_3 for 120 min at optimal operating conditions and the collected samples were analyzed in GC-MS to identify the degradation intermediates. Based on the GC-MS results, ethylene glycol diformate (EGDF) was identified as the principal intermediate and, the proposed degradation pathway of 1,4-dioxane is illustrated in Fig. 35.

The initial step of the oxidative transformation included H-abstraction by $HO^•$ radicals transforming 1,4-dioxane into 1,4-dioxanyl radical. In the presence of DO, 1,4-dioxanyl radical forms a peroxyl radical, which is further converted into α-oxyl radical - a widely recognized intermediate of 1,4-dioxane degradation in AOPs. The aromaticity is further disrupted as α-oxyl radical undergoes ring-opening through

ΔC-C splitting at α-carbon. The resulting radical adduct reacts with oxygen, undergo dimerization and subsequent fragmentation to yield EGDF. Continuously generated radical species in HC/SPC/O_3 decompose EGDF forming low-molecular intermediates (e.g., glycolic, formic acids), which are further mineralized. TOC measurements confirmed the near-complete mineralization of 50 ppm 1,4-dioxane in HC/SPC/O_3 in 120 min at optimal conditions, which was found as approx. 95%. The developed HC/SPC/O_3 process effectively degraded 1,4-dioxane and highlighted the advantageous application of SPC in peroxone over H_2O_2. The study revealed that the synergistic effect occurred under HC allowed HC/SPC/O_3 to attain nearly a complete degradation of 1,4-dioxane in 120 min at pH_0 5, 20±2 ºC. The effect of cavitation in HC/SPC/O_3 facilitated the gas-liquid mass transfer of O_3 and participated in decomposition of O_3 to yield HO• radicals. The presence of CO_3^{2-} ions derived from SPC dissolution contributed to the synergistic effect by elevating the pH_0 from 5 to 8, thereby increasing the decomposition rate of O_3 into HO• radicals. Moreover, the utilization of SPC was attributed to the formation of $CO_3^{\bullet-}$ radicals which were found as secondary reactive species, while HO• radicals were the primary species responsible for the degradation of 1,4-dioxane in HC/SPC/O_3. The inhibitory effect of the co-existing anions on the degradation efficiency of HC/SPC/O_3 followed the order: SO_4^{2-}>NO_3^->Cl^-. The detection of EGDF as the main degradation intermediate by GC-MS suggested the radical route of degradation that includes H-abstraction, dimerization and ΔC-C splitting.

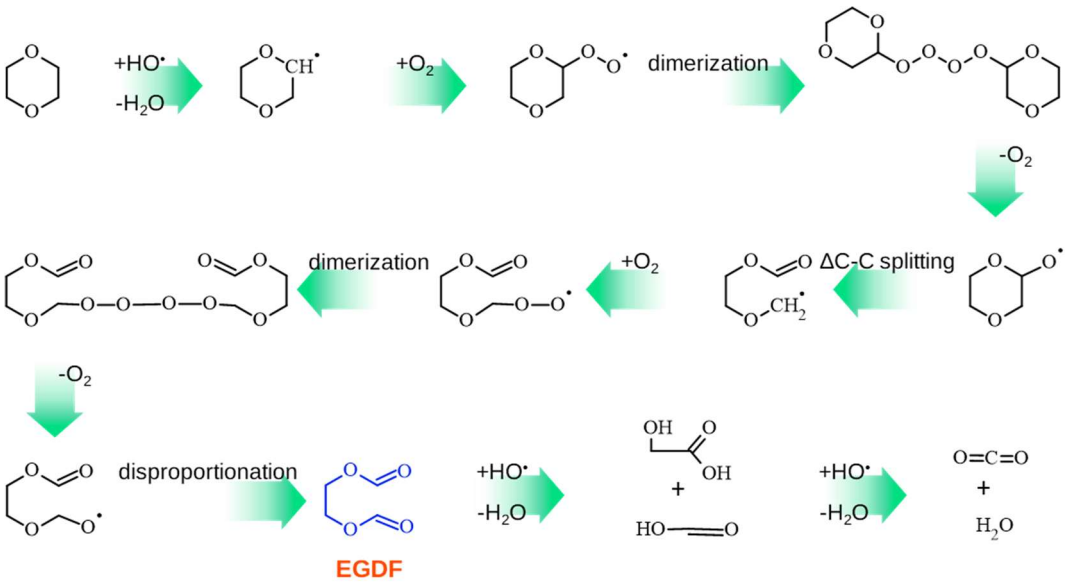

Figure 35. The possible degradation pathway of 1,4-dioxane in HC/SPC/O_3 based on the intermediates identified using GC-MS.

4.5. Photo-reduction of clofibric acid (CLA) in the SO_3^{2-}/UV under HC

As a response to the growing number of reports on the detection of halogen-containing organic pollutants in aquatic environment, ARPs have emerged as safe and promising methods in water treatment. The increasing interest of scientific community on ARPs was also reasoned due to noticeable persistence of these compounds (e.g., PFAS) to the conventional water treatment methods. When subjected to AOPs, these halogen-containing organic pollutants can be transformed into more recalcitrant and toxic compounds (e.g., BrO_3^-, ClO_3^- ions). In the light of this, ARPs utilizing reductive species ($e_{aq.}^-$, $H^\bullet$ radicals) can offer the reductive degradation of the pollutants potentially avoiding the risk of secondary pollution. Accordingly, further studies were focused on the development of hybrid processes based on HC and ARPs, the effectiveness of which was evaluated towards the degradation of a chlorinated pollutant - CLA. Followed by the literature survey, for this thesis several HC/ARPs were initially tested to degrade CLA. For instance, the preliminary studies included the degradation of CLA by the hybrid HC/I^-/UV, HC/DTN, HC/PS/SO_3^{2-}, HC/I^-/Co^{2+} and HC/SO_3^{2-}/Co^{2+} processes. However, the degradation efficiency observed in the hybrid process was lower than the cumulative effect of sole processes, resulting in $\xi \leq 1$. In contrast, HC/SO_3^{2-}/UV process exhibited markedly degradation efficiency suggesting that the photo-reductive degradation CLA by SO_3^{2-}/UV can be enhanced under HC conditions. Hence, the hybrid HC/SO_3^{2-}/UV process was studied for CLA degradation and the effect of C_v, SO_3^{2-} dosage, pH and co-existing anions was investigated. The presence of reductive species was verified using quenching experiments, while the reductive pathway of CLA degradation was proposed based on the identified intermediates by GC-MS supported by DFT calculations.

4.5.1. CLA degradation under sole HC

The integration of the cavitation phenomenon with emerging ARPs remains unexplored and requires special attention. This study represents the first attempt on the combination of HC with SO_3^{2-}/UV ARP for the reductive degradation of CLA – a chlorinated persistent contaminant was not yet studied.

Before studying the hybrid HC/SO_3^{2-}/UV, the effect of C_v on the degradation of CLA in HC/SO_3^{2-} at r_{red} 3.25 was initially examined. For this, the degradation experiments were carried out in HC/SO_3^{2-} varying C_v from 0.16 to 0.82. As shown

in Fig. 36A, HC/SO_3^{2-} at C_v 0.82, 0.51, 0.27, 0.2 degraded 24.73%, 26.33%, 30.84% and 30.53% of CLA, respectively, in 90 min. The corresponding rate constants of CLA degradation were found as 2.70 × 10^{-3} min^{-1}, 3.08 × 10^{-3} min^{-1}, 4.03 × 10^{-3} min^{-1} and 4.28 × 10^{-3} min^{-1} (Fig. 36B).

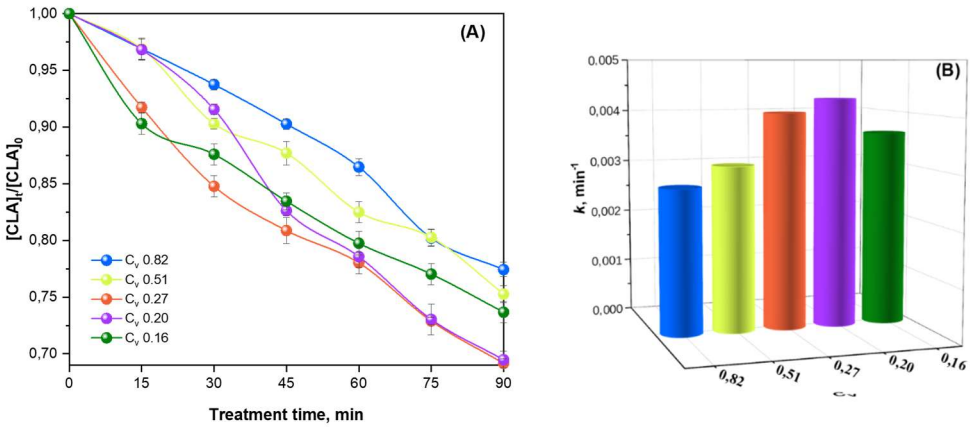

Figure 36. The effect of C_v on degradation efficiency of CLA (A) and the corresponding degradation rate constants (B); $[CLA]_0$ 100 mg/L, pH~6.5, 20±2 °C.

The obtained results indicated that decrease of C_v from 0.82 to 0.2 and, thereby, increasing the operating inlet pressure to 8 bar, enhanced the cavitational events reflecting in higher degradation efficiency of CLA. With the decrease of C_v 0.16 (inlet pressure: 9 bar), the degradation efficiency of CLA was found as 22.57% in 90 min. This indicated the occurrence of conditions close to "supercavitation" as C_v nearly reached 0. As it was described in HC/SPC/O_3, "supercavitation" causes the drop of collapse pressure due to the coalescence of cavitation bubbles thereby diminishing the intensity of cavitation. Based on these results, C_v 0.2 was used as the optimal operating parameter for the remaining experiments.

4.5.2. Synergistic effect in HC/SO_3^{2-}/UV

Next, HC was combined with SO_3^{2-}/UV at r_{red} 3.25 and C_v 0.2. To assess the synergistic effect in the combined HC/SO_3^{2-}/UV, the degradation of CLA was performed in different processes, such as HC, UV, HC/SO_3^{2-}, UV/SO_3^{2-} and HC/UV. As shown in Fig. 37A, the application of sole HC degraded 12.66% of CLA in 90 min, while the degradation efficiency was increased to 30.53% in HC/SO_3^{2-}. Considering the negligible CLA degradation (approx. 7%) observed in sole SO_3^{2-} after 90 min (Fig. 37A), these findings highlight the high persistence of CLA and reveal the limited activation of SO_3^{2-} by sole HC. In contrast, sole UV irradiation degraded 67.68% of CLA in 30 min demonstrating considerable effect of photo-induced oxidation of CLA. Furthermore, the degradation efficiency of CLA was

increased to 77.90% within 30 min upon the simultaneous application of SO_3^{2-} and UV photolysis. Owing to the formation of $SO_3^{\bullet-}$ radicals in SO_3^{2-}/UV, the rate constant of CLA degradation was increased from 3.66 × 10^{-2} min^{-1} to 4.56 × 10^{-2} min^{-1} as compared to sole UV as illustrated in Fig. 37B. The combined HC/SO_3^{2-}/UV attained the degradation efficiency of 91.21% within 30 min and 99.68% in 90 min of treatment with a rate constant of 6.67 × 10^{-2} min^{-1}. The developed HC/SO_3^{2-}/UV exhibited higher degradation efficiency than AOPs, e.g., catalytic ozonation on MnO_x/SBA-15 and Fenton-like process using FeOOH, which required longer treatment time to achieve comparable degradation extend [251,252]. Besides, HC/SO_3^{2-}/UV exceeded the rate constants of PS/UV and Cl/UV which were of 1.76 × 10^{-2} min^{-1} and 1.56 × 10^{-2} min^{-1}, respectively [253]. The ξ value of 1.42 determined from Eq. 1.56 revealed that the HC/SO_3^{2-}/UV exceeded the additive effect of individual processes, confirming synergism of the combined process.

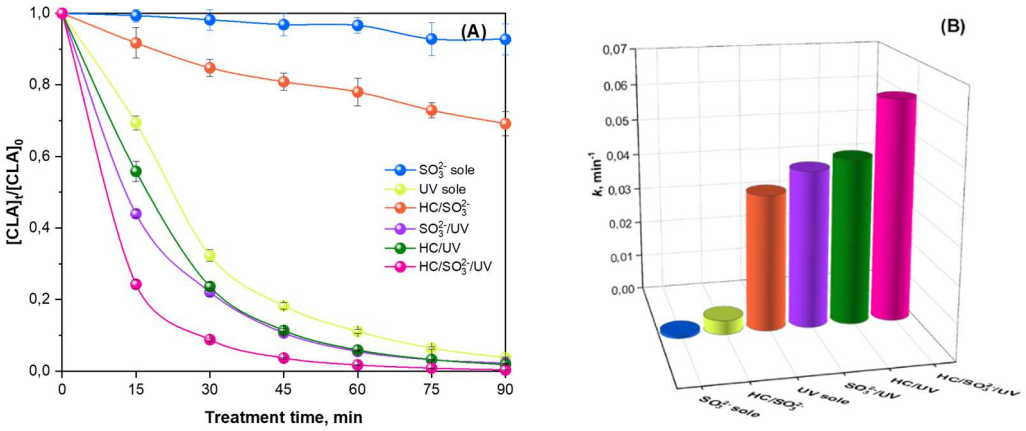

Figure 37. Degradation efficiency of CLA (A) and the corresponding degradation rate constants (B); $[CLA]_0$ 100 mg/L, C_v 0.2, r_{red} 3.25, pH~6.5, 20±2 °C.

The capacity of HC and UV in activation of SO_3^{2-} in the combined HC/SO_3^{2-}/UV was further verified. Thus, the degradation of CLA in HC/SO_3^{2-} and SO_3^{2-}/UV proceeded with a rate constant of 2.77 × 10^{-3} min^{-1} and 4.56 × 10^{-2} min^{-1}, indicating the prevailing contribution of the photolytic activation of SO_3^{2-} ions. This suggests that the energy of UV photons was capable to overcome the vertical detachment energy (VDE) which was determined as 2.69 eV according to Eq. 3.3:

$$\mathrm{VDE} = \mathrm{E_{monoanion}} - \mathrm{E_{dianion}} = (-623{,}9025268) - (-624{,}0016509) = \quad (4.25)$$

$$= 0{,}0991\ \mathrm{Hartree} = 2{,}69\ \mathrm{eV}$$

The extreme conditions of high pressure and temperature as well as sonoluminescence created by cavitation were insufficient to activate SO_3^{2-}.

Nonetheless, HC/UV and SO_3^{2-}/UV showed high efficiency degrading 98.21% and 97.80% of CLA, respectively, in 90 min. From these results, it can be suggested that the effect of HC contributed to the generation of radical species. Hence, HC facilitated the generation of radical species along with radical-substrate interaction by reducing the mass transfer resistance in HC/SO_3^{2-}/UV.

Because e_{aq}^- instantaneously reacts with oxygen forming $O_2^{\bullet-}$ radicals, the effectiveness of SO_3^{2-}/UV can be inhibited in the presence of DO. In parallel, $SO_3^{\bullet-}$ radicals can react with DO and the subsequent oxidative $SO_5^{\bullet-}$ and $SO_4^{\bullet-}$ radicals can emerge as shown in Eqs. 4.26-4.28. In such a scenario, the degradation of CLA would proceed through the oxidation induced by the secondary $SO_5^{\bullet-}$ and $SO_4^{\bullet-}$ radicals rather than the reduction by e_{aq}^-. To explore the role of DO on HC/SO_3^{2-}/UV, the degradation of CLA was performed at anaerobic conditions, which were achieved by purging Ar at 1 L/min through the model solution circulated at non-cavitating conditions (C_v>1) for 15 min.

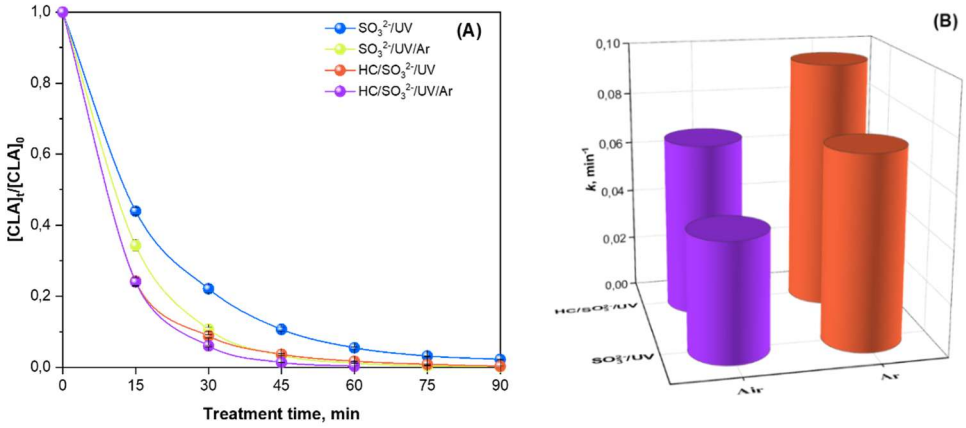

Figure 38. The effect of Ar purging on degradation efficiency of CLA (A) and the corresponding degradation rate constants (B) in SO_3^{2-}/UV and HC/SO_3^{2-}/UV; $[CLA]_0$ 100 mg/L, C_v 0.2, r_{red} 3.25, pH~6.5, 20±2 °C.

From Fig. 38A, the degradation efficiency of CLA in SO_3^{2-}/UV in the presence of DO was 94.51% of CLA after 60 min. At deoxygenated conditions, the degradation efficiency of CLA in SO_3^{2-}/UV reached 98.87%. In the case of HC/SO_3^{2-}/UV, the degradation efficiency CLA observed in the presence of O_2 and Ar were found as 98.31% and 99.69% after 60 min, respectively. As compared to air-saturated experiments, the rate constants of CLA degradation in SO_3^{2-}/UV and HC/SO_3^{2-}/UV were enhanced by 2.79 × 10^{-2} min^{-1} and 2.88 × 10^{-2} min^{-1}, respectively (Fig. 38B). These results indicated that the presence of DO partially consumes the reductive species through Eqs. 4.26, 4.27 The effect of HC improved the utilization of SO_3^{2-} by 28.6% ensuring high yield of radical species in the presence of DO. Considering

this, it can be stated that the activation of SO_3^{2-} was promoted under cavitation conditions resulting in faster and efficient degradation of CLA. By maintaining high yield of primary reductive species in the presence of DO, the application of HC eliminates the deoxygenation step, thereby improving the economic feasibility HC/SO_3^{2-}/UV.

$$e_{aq.}^{-} + O_2 \rightarrow O_2^{\bullet -} \qquad 1.9 \times 10^{10}\ M^{-1}s^{-1} \qquad 4.26$$

$$SO_3^{\bullet -} + O_2 \rightarrow SO_5^{\bullet -} \qquad 1.2 \times 10^{9}\ M^{-1}s^{-1} \qquad 4.27$$

$$SO_5^{\bullet -} + SO_3^{\bullet -} \rightarrow SO_4^{\bullet -} + SO_4^{\bullet -} \qquad 4.28$$

4.5.3. Effect of pH and SO_3^{2-} dosage on CLA degradation in HC/SO_3^{2-}/UV

In this study, the effect of pH and r_{red} on CLA degradation in HC/SO_3^{2-}/UV were investigated using CCD and the obtained results were analyzed by RSM. Table 6 shows the experimental matrix and corresponding predicted and observed degradation efficiency of CLA. Using Minitab Statistical Software 22, two-dimensional contour plots were generated to visualize the interaction between the studied variables, while maintaining the third parameter at central level (Fig. 39). As shown in Fig. 39A**,** the increase of r_{red} from 0.31 to 6.19 subsequently increased the degradation efficiency of CLA observed in 60 min from 93.91% to 98.28%, respectively. This suggested that the number of radical species for CLA degradation was increased with the increase of SO_3^{2-} concentration.

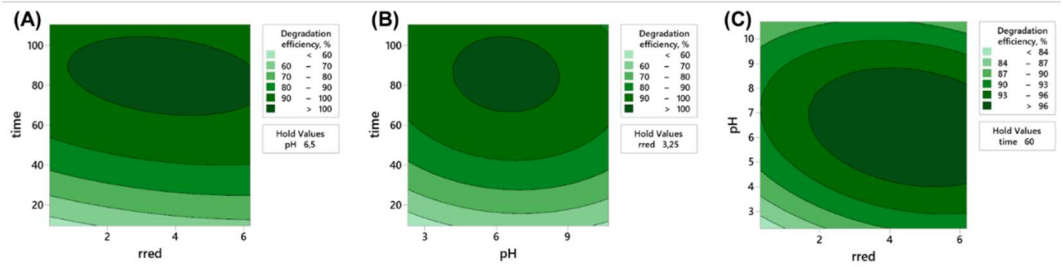

Figure 39. 2-D contour plots showing the effects of r_{red}-time (A), pH-time (B) and r_{red}-pH (C) on CLA degradation in HC/SO_3^{2-}/UV; $[CLA]_0$ 100 mg/L, C_v 0.2, 20±2 °C.

Typically, the effectiveness of conventional SO_3^{2-}/UV process is lower at higher SO_3^{2-} dosage due to the radical recombination reactions scavenging the radicals. However, such scavenging effect was not observed in HC/SO_3^{2-}/UV suggesting that the effect of cavitation mitigated the radical recombination reactions as cavitation-induced microturbulence and localized high temperature and pressure provided effective utilization of SO_3^{2-} and contact between CLA and radical species.

Similarly, prolonging the treatment time from 10 min to 110 min in HC/SO_3^{2-}/UV resulted in 63.75% and 99.78% of CLA degradation. This increase can be attributed to the progressive accumulation of radical species and noticeable contribution of UV photolysis of CLA throughout the process. The effectiveness of SO_3^{2-}/UV is highly pH-dependent as the form of S(IV) species (e.g., H_2SO_3, HSO_3^- and SO_3^{2-}) and associated reaction kinetics are affected by solution pH.

Table 6. Three test variables CCD matrix along with observed and predicted CLA degradation efficiency.

#	Run	r_{red}	pH	Treatment time, min	CLA degradation efficiency, %	
					Experimental	Predicted
1	5	1,5	4	30	72,89	73,50
2	18	5	4	30	80,71	80,42
3	14	1,5	9	30	76,74	77,42
4	11	5	9	30	80,50	81,46
5	2	1,5	4	90	96,94	97,68
6	17	5	4	90	98,67	99,69
7	4	1,5	9	90	96,99	98,97
8	8	5	9	90	97,00	98,09
9	3	0,31	6,5	60	93,91	93,07
10	13	6,19	6,5	60	98,28	98,16
11	1	3,25	2,30	60	89,47	89,03
12	10	3,25	10,70	60	91,27	90,99
13	6	3,25	6,5	9,55	63,75	64,13
14	9	3,25	6,5	110,45	99,78	98,45
15	20	3,25	6,5	60	97,73	98,32
16	16	3,25	6,5	60	97,96	98,32
17	15	3,25	6,5	60	97,81	98,32
18	19	3,25	6,5	60	97,77	98,32
19	12	3,25	6,5	60	98,46	98,32
20	7	3,25	6,5	60	98,27	98,32

In Fig. 39B, the degradation efficiency of CLA in HC/SO_3^{2-}/UV at pH 2.3 was found as 89.47% after 60 min. With the increase of pH to 6.5, the degradation efficiency was increased to 98.46% and declined to 91.27% as pH was further raised to 10.7. At acidic conditions, HSO_3^- predominates over deprotonated SO_3^{2-}, which exhibit

higher UV absorption than HSO_3^-. Hence, the increase of pH from 2.3 to 6.5 increased the UV absorption and facilitated the generation of radical species in HC/SO_3^{2-}/UV. On the other hand, the increase of pH level from 6.5 to 10.5 decreased the effectiveness of HC/SO_3^{2-}/UV reflecting in the corresponding degradation rate constants of 6.67×10^{-2} min^{-2} and 4.03×10^{-2} min^{-2}. Considering that the molar absorptivity of SO_3^{2-} at 254 nm increases from 15.2 M^{-1} cm^{-1}, to 18.2 M^{-1} cm^{-1} with the increase of pH from 7.5 to 10.9, the inhibition at pH 10.5 can indicate the occurrence of side reactions that deplete the number of reactive species. The RSM analysis confirmed the strong dependance of CLA degradation on both pH and r_{red}.

The optimal parameter values predicted by the model for HC/SO_3^{2-}/UV were r_{red} 5.68, pH 7.6 and treatment time of 75.6 min, to degrade 99.99% of CLA. According to the model, the degradation efficiency can be enhanced by 0.3% and the treatment time reduced by 14 min with almost twofold increase of r_{red} at elevated pH. While these values are statistically optimal, their practical applicability is hindered due to the increased chemical demand for the additional reductant and pH adjustment. The predicted optimal values confirm the experimentally observed trend that the increase in SO_3^{2-} r_{red} increases the degradation efficiency of CLA in HC/SO_3^{2-}/UV.

4.5.4. Identification of dominant radical species

The photo-excitation of SO_3^{2-} under UV can results in generation of the reductive reactive species ($e_{aq.}^-$, $H^\bullet$ radicals) as well as oxidizing $SO_3^{\bullet-}$, $SO_4^{\bullet-}$ and $HO^\bullet$ radicals according to Eqs. 1.13, 1.14, 1.31, 4.28. While $SO_3^{\bullet-}$ radicals are relatively weak oxidants (0.63 V_{NHE}, pH 7) slowly reacting with unsaturated compounds at higher pH [172], $SO_4^{\bullet-}$ and $HO^\bullet$ radicals are powerful oxidants capable of initiating the oxidative degradation of CLA in HC/SO_3^{2-}/UV. In order to elucidate the respective role of these species in CLA degradation, quenching experiments were conducted using specific radical scavengers at a molar ratio of SO_3^{2-} to scavenger of 1:10. The role of oxidizing radicals was evaluated by IPA, which effectively quench both $SO_4^{\bullet-}$ and $HO^\bullet$ radicals. The individual contribution of the oxidizing radical was assessed by addition of TBA, which spontaneously quench $HO^\bullet$ radicals, while the reaction with $e_{aq.}^-$ and $H^\bullet$ radicals proceeds slowly with a rate constant of 4.0×10^5 $M^{-1}s^{-1}$ and 1.7×10^5 $M^{-1}s^{-1}$, respectively [238,254]. In the case of the reductive species, sodium nitrite (NO_2^-) highly reactive to $e_{aq.}^-$ (4.1×10^9 $M^{-1}s^{-1}$) and $H^\bullet$ radicals (7.1×10^8 $M^{-1}s^{-1}$) was selected to examine their impact on CLA degradation

[238,255]. Owing to the distinct reactivity with $e_{aq.}^-$ and H• radicals with a rate constant of 9.7 × 10^9 $M^{-1}s^{-1}$ and 1.4 × 10^6 $M^{-1}s^{-1}$, respectively, sodium nitrate (NO_3^-) was added to reveal the contribution of $e_{aq.}^-$ [238,255]. As illustrated in Fig. 40A, a negligible inhibitory effect was observed in upon addition of IPA and TBA in HC/SO_3^{2-}/UV. Specifically, the degradation efficiency of CLA was declined from 99.68% to 99.42% and 99.37% after 90 min in the presence of IPA and TBA, respectively. These findings indicated the oxidizing $SO_4^{\bullet-}$ and HO• radicals were not involved in CLA degradation. In contrast, the presence of TBA and IPA in SO_3^{2-}/UV slightly increased the degradation rate constant of CLA from 4.56 × 10^{-2} min^{-1} to 4.99 × 10^{-2} min^{-1} and 5.06 × 10^{-2} min^{-1}, respectively. As $SO_3^{\bullet-}$ and $SO_5^{\bullet-}$ radicals slowly react with TBA and IPA (<10^3 $M^{-1}s^{-1}$), the enhanced CLA degradation can be attributed to the organic radicals generated under UV light. The degradation efficiency of CLA in HC/SO_3^{2-}/UV and SO_3^{2-}/UV was inhibited significantly with addition of NO_2^- implying to predominant role of reductive species. After 30 min, the degradation efficiency of CLA in HC/SO_3^{2-}/UV was decreased from 91.21% to 77.90%, and the rate constant was declined by 3.22 × 10^{-2} min^{-1} (Fig. 40B).

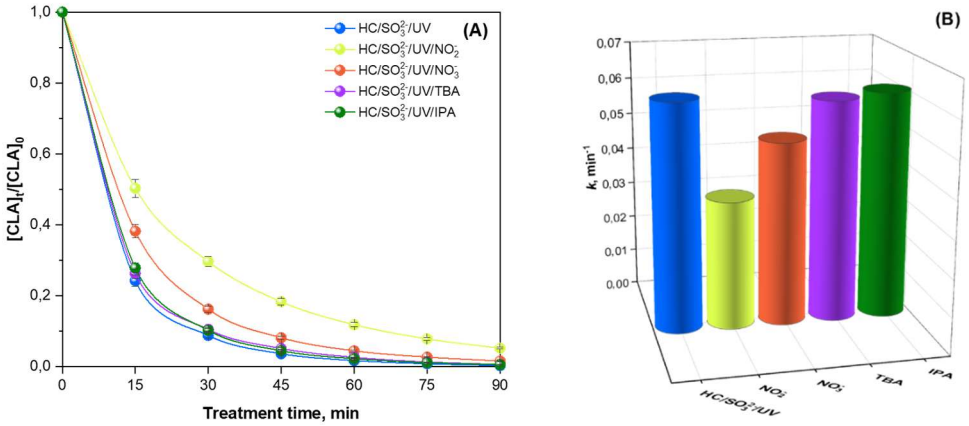

Figure 40. The effect of radical scavengers on degradation efficiency of CLA in HC/SO_3^{2-}/UV (A) and the corresponding degradation rate constants (B); $[CLA]_0$ 100 mg/L, C_v 0.2, r_{red} 3.25, pH~6.5, 20±2 °C, [Scavenger]:[SO_3^{2-}] 10:1.

For SO_3^{2-}/UV, CLA degradation efficiency was inhibited from 77.90% to 64.73% in 30 min causing the reduction of CLA degradation rate constant by 1.48 × 10^{-2} min^{-1} (Fig. 41). The quenching of $e_{aq.}^-$ by adding NO_3^- demonstrated a minor inhibitory effect in both HC/SO_3^{2-}/UV and SO_3^{2-}/UV processes. Thus, it can be proposed that H• radicals were the major reactive species responsible for the reductive degradation of CLA. The stronger inhibitory effect of NO_2^- in HC/SO_3^{2-}/UV emphasizes that the effect of cavitation promoted the generation of reductive species.

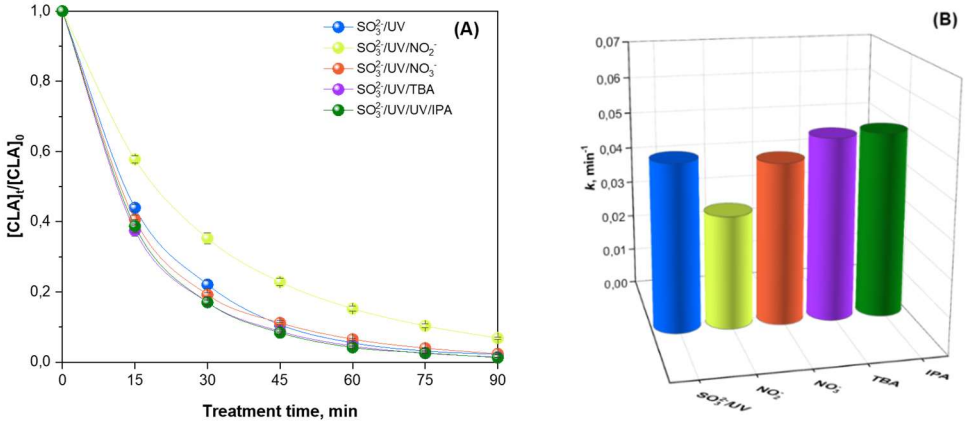

Figure 41. The effect of radical scavengers on degradation efficiency of CLA in SO_3^{2-}/UV (A) and the corresponding degradation rate constants (B); $[CLA]_0$ 100 mg/L, r_{red} 3.25, pH~6.5, 20±2 °C, [Scavenger]:[SO_3^{2-}] 10:1.

4.5.5. Effect of water constituents on CLA degradation

Inorganic ions as well as DO and natural organic matter (NOM) can affect effectiveness of the developed process by reacting with the generated radicals. To explore the effect of common water constituents on HC/SO_3^{2-}/UV, the degradation of CLA was carried out in the presence of Cl^-, SO_4^{2-}, CO_3^{2-} anions and humic acids (HA). Each anion was introduced separately in the form of sodium salt at molar ratio to SO_3^{2-} of 10:1, while the concentration of HA was taken as 125 mg/L. From Fig. 42A, the presence of SO_4^{2-} ions had a negligible effect on HC/SO_3^{2-}/UV, slightly decreasing the degradation rate constant of CLA from 6.67× 10^{-2} min^{-1} to 6.62 × 10^{-2} min^{-1} after 90 min (Fig. 42B). This shows that SO_4^{2-} ions didn't interfere in the generation of reductive species, which is supported by the relatively low reaction rate constant of SO_4^{2-} ions with $e_{aq.}^-$ reported to be 1 × 10^6 $M^{-1}s^{-1}$.

Similarly, a minor inhibitory effect was observed upon the addition of Cl^- anions, which declined the degradation rate constant of CLA to 5.74 × 10^{-2} min^{-1}. The insignificant suppression can be attributed to the low reactivity of Cl^- ions with e_{aq}^- (< 10^6 $M^{-1}s^{-1}$) and H• radicals (< 10^5 $M^{-1}s^{-1}$) [238]. Unlike SO_4^{2-} and Cl^- ions, the inhibitory effect caused by the presence of CO_3^{2-} anions was more pronounced decreasing the degradation efficiency of CLA in HC/SO_3^{2-}/UV to 97.15% in 90 min with a rate constant of 2.53 × 10^{-2} min^{-1}.

Taking into account that CO_3^{2-} anions react with e_{aq}^- slowly at a rate constant of 3.9 × 10^5 $M^{-1}s^{-1}$, the suppressed CLA degradation can be attributed to the elimination of H^+ from the system, which is needed for conversion of e_{aq}^- to H• according to Eq.

4.29. In this, the presence of CO_3^{2-} anions elevates the solution pH through CO_3^{2-} /HCO_3^- cycle, thereby consuming H^+ and hindering the generation of $H^\bullet$ radicals.

$$e_{aq.}^- + H^+ \rightarrow H^\bullet \qquad 4.29$$

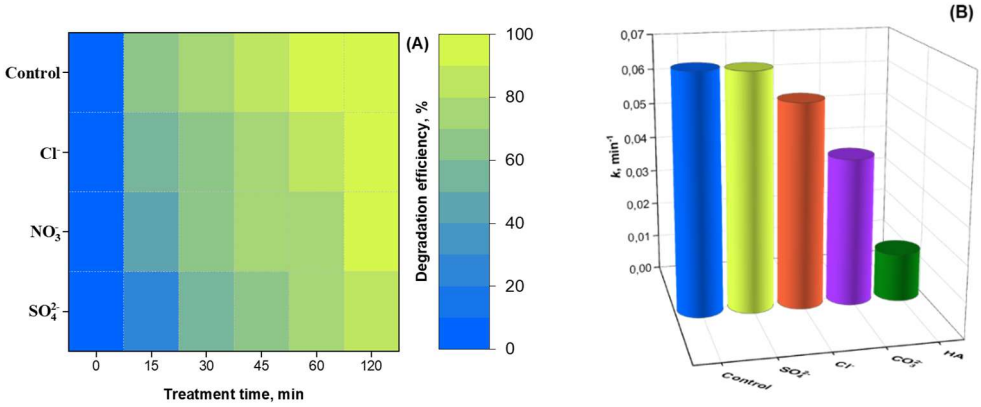

Figure 42. The effect of water constituents on degradation efficiency of CLA (A) and the corresponding degradation rate constants (B); $[CLA]_0$ 100 mg/L, C_v 0.2, r_{red} 3.25, pH~6.5, 20±2 °C, [Anion]:[SO_3^{2-}] 10:1, [HA] 125 mg/L.

As noticed from Fig. 42, the presence of HA significantly impeded the effectiveness of HC/SO_3^{2-}/UV retarding the degradation efficiency of CLA from 99.68% to 71.33% in 90 min. In this, the degradation rate constant of CLA in HC/SO_3^{2-}/UV was 1.34 × 10^{-2} min^{-1}, whereas it was found as 3.66 × 10^{-2} min^{-1} in the case of sole UV. These observations indicate the photo-induced activation of SO_3^{2-} as well as direct UV photolysis were hindered. This can be attributed to the role of HA competing for UV light absorbance, thereby suppressing UV light penetration and generation of reactive species.

4.5.6. The proposed degradation pathway of CLA

In order to elucidate the reductive transformations of CLA in HC/SO_3^{2-}/UV, the reaction intermediates were analyzed by GC-MS. The degradation mechanism was proposed based on the intermediates detected in GC-MS and supported by DFT calculations, such as natural population analysis (NPA) charge distribution and Fukui function. To enable the effective and accurate detection of intermediates, the initial concentration of CLA was increased to 1000 ppm and treated under the optimal operating conditions. The collected CLA samples were prepared for GC-MS analysis *via* DLLME. The reductive species, such as $e_{aq.}^-$ and $H^\bullet$ radicals possess nucleophilic properties selectively targeting electron-deficient sites of a pollutants.

As presented in Fig. 43B, the highest occupied molecular orbital (HOMO) and the lowest unoccupied molecular orbital (LUMO) energy levels of CLA were found as -6.49 eV and -0.487 eV, respectively. This indicates that CLA was predisposed to electrophilic attacks, and a broad gap implies to the electronic delocalization due to the hybridization of lone electron pairs from oxygen atom of isopropoxy group with π-orbitals of the benzene ring. It can be seen from Fig. 43B, HOMO was located over the benzene ring and isopropoxy group, while LUMO is mainly concentrated on ortho- and meta- positions of the ring. Based on Fukui indices (Fig. 43C), the atoms C5-C8 with higher nucleophilic attack indices (f^+) were the active sites vulnerable for the attacks by $e_{aq.}^-$ and H• radicals. Considering this and the identified degradation intermediates, three distinct pathways were proposed and illustrated in Fig. 44.

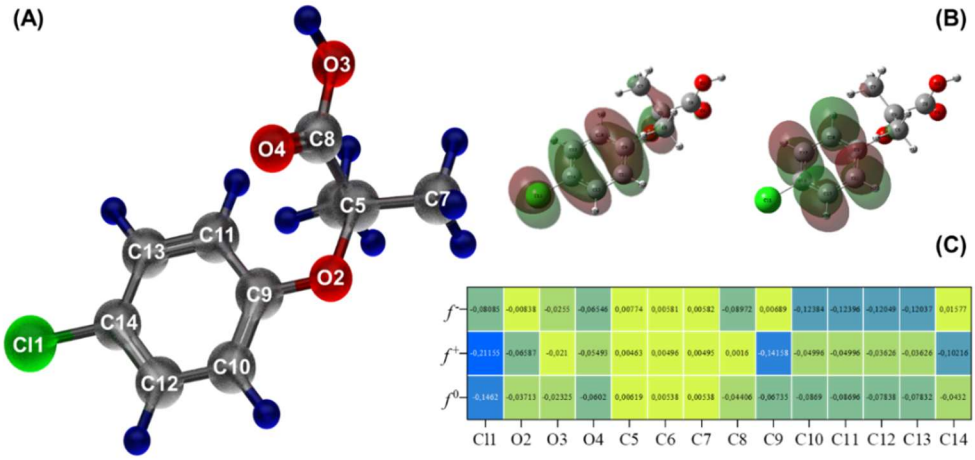

Figure 43. The optimized structure (A), HOMO and LUMO (B) and Fukui indices (C) of CLA calculated at the B3LYP/6-31G (d, p) level of theory.

Pathway 1. The nucleophilic attack of $e_{aq.}^-$ and H• radicals on C8 in carbonyl group transformed CLA into 1-(tert-butoxy)-4-chlorobenzene, which underwent intramolecular cyclization to yield 2,2-dimethyl-2,3-dihydrobenzofuran. Continuous attacks of $e_{aq.}^-$ and H• radicals led to the dearomatization and converted 2,2-dimethyl-2,3-dihydrobenzofuran into 2-(2-methyl-2-propenyl)-2-cyclohexen-1-one (*m/z* 150).

Pathway 2. Alternatively, C5 atom can be the initial target of nucleophilic attacks. In this case, 4-chloro-1-isopropoxy benzene is produced as the main intermediate and produces 5-chloro-2-methyl-2,3-dihydrobenzofuran (*m/z* 186) after cyclization. The detection of 3-methylbutanal (*m/z* 86) as the degradation product indicates the depletion of the aromatic ring in 5-chloro-2-methyl-2,3-dihydrobenzofuran through

the formation of 4-chloro-2-propyl-2-cyclohexen-1-one radical and 4-chloro-2-isopropyl-2-cyclohexen-1-one intermediates.

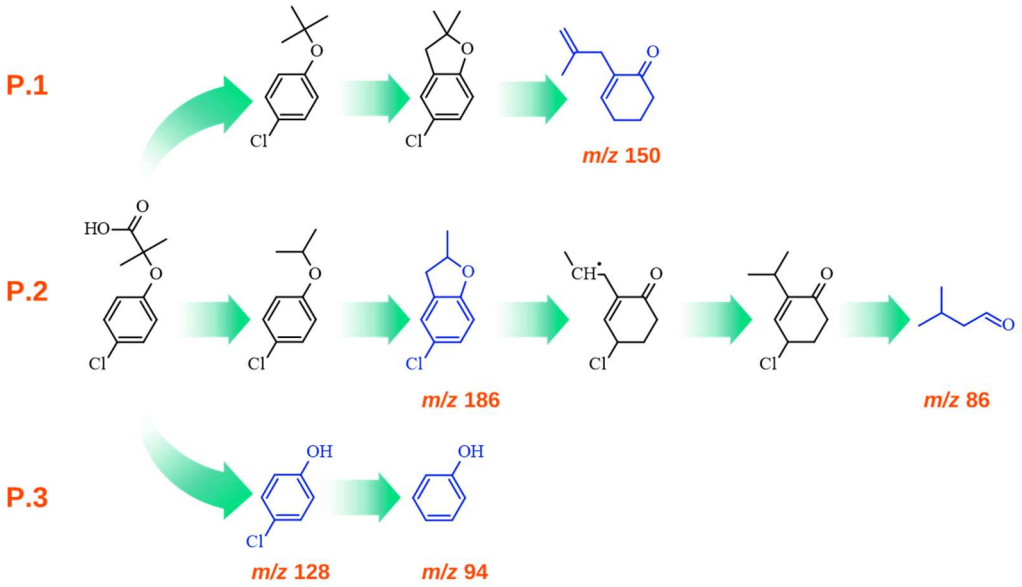

Figure 44. Three possible degradation pathways of CLA in HC/SO_3^{2-}/UV on the basis of five intermediates identified using GC-MS.

Pathway 3. Chlorophenol and phenol are the common oxidation intermediate in AOPs and value of electrophilic attack index (f^+) of 0.01577 supports this. However, the radical quenching experiments revealed the negligible contribution of $SO_4^{\bullet-}$ and $HO^{\bullet}$ radicals on CLA degradation in HC/SO_3^{2-}/UV. Therefore, the detection of chlorophenol (*m/z* 128) was attributed to the nucleophilic attack on C5 resulting in the cleavage of C5-O2 bond. The chlorophenol underwent dechlorination through nucleophilic substitution to yield phenol *(m/z* 94).

Owing to the synergistic effect between the coupled techniques, the developed HC/SO_3^{2-}/UV exhibited high effectiveness for CLA degradation in water at r_{red} 3.25, pH 6.5, 20±2 ºC. According to the quenching experiments, $H^{\bullet}$ radicals were the main reactive species generated in HC/SO_3^{2-}/UV, while the contribution of oxidizing radicals on CLA degradation was negligible. Although HC was not involved in SO_3^{2-} activation, the effect of cavitation promoted the generation of $H^{\bullet}$ radicals in HC/SO_3^{2-}/UV by reducing the detrimental effect of scavenging reactions. In contrast to cavitation-based AOPs, the effectiveness of HC/SO_3^{2-}/UV was affected by co-existing anions in lower extend following the order: CO_3^{2-}>Cl^->SO_4^{2-}. Based on the identified intermediates, three distinct degradation pathways of CLA were proposed. The photo-reductive degradation of CLA in HC/SO_3^{2-}/UV included nucleophilic addition, cyclization and further fragmentation of the intermediation into low-molecular compounds.

5. Conclusions and perspectives

As a result of the extensive multidisciplinary research, the scope of cavitation application is currently expanded to several industrial sectors, including wastewater treatment. The efforts are made on the development of hybrid treatment methods integrating the distinct characteristics of cavitation techniques and advanced chemical processes. In this study, AC and HC combined with SR-AOPs, O_3-based AOPs and ARPs were developed. The hybrid processes were attested treating the model solutions of organic pollutants of high concern. Based on the observed findings the following conclusions can be proposed:

1. Both AC and HC demonstrated promising potential in the combined application with SR-AOPs, effectively activating PS and PMS. As the activation of PS/PMS under sole US was negligible, asphaltenes were used as a catalyst to facilitate the activation. As a result, the developed US/PS/ASPH and US/PMS/ASPH effectively degraded BTEX in the presence of 0.5 g/L asphaltenes at r_{ox} 5, pH 5 in 360 min. In both cases, the particles of asphaltenes played a crucial role and directly contributed to the synergistic mechanism of BTEX degradation. Specifically, asphaltenes served as additional nuclei for cavitation bubbles, adsorbent for BTEX and catalyst activating PS/PMS. Asphaltenes are widely available as a heaviest component of crude oil and can be modified to obtain catalysts for PS/PMS activation with enhanced activity and stability. The activation of PS and PMS assisted by HC proceeded through the direct disassociation of the peroxy bond in the absence of a catalyst. At r_{ox} 5, pH 5, HC/PS and HC/PMS were capable to degrade >90% of BTEX within 240 min. The presence of common anions was detrimental for both HC/PS and HC/PMS due to the scavenging of radicals, except Cl^- ions, which were converted into reactive chlorine radicals in HC/PMS. The activation of PS/PMS under the condition of AC and HC led to the formation of $SO_4^{\bullet-}$ and $HO^\bullet$ radicals, which were the predominant species responsible for BTEX degradation. The degradation of BTEX in HC/SR-AOPs was initiated by H-abstraction and included multipole steps of hydroxylation and dealkylation. As compared to US/PS/ASPH and US/PMS/ASPH, HC/PS and HC/PMS are more attractive for large-scale implementation due to the simple design and economic feasibility derived from a relatively low electric energy demand.

2. As a part of traditional AOPs utilizing $HO^{\bullet}$ radicals, O_3-based AOPs are studied in higher extend than SR-AOPs and partially applied in practice. Considering this, the combination of ozonation with cavitation was implemented with several modifications and tested towards different water pollutants. Hence, the ozonation of BTEX was conducted under AC induced by sonotrode and transducers of different US frequency. In this, the hybrid process of LFDUS/O_3 operating at 40-120 kHz, r_{ox} 6.25, pH 6.5 achieved the complete degradation of BTEX in 40 min resulting in ξ 7.86. On the other hand, it took 60 min to achieve a comparable BTEX degradation with ξ 2.9 in HFDUS/O_3 utilizing 80-200 kHz at the same process parameters. The observed synergistic effect in LFDUS/O_3 was attributed to the intensified generation of cavitation bubbles with high collapse pressure, which ensured high decomposition rate of O_3. The combination of HC with modified peroxone process based on the ozonation in the presence of SPC was studied and evaluated for the degradation of 1,4-dioxane. At optimal parameters, i.e., C_v 0.27, SPC r_{ox} 8, O_3 dosage of 0.86 g/L and pH 5, 99.34% of 1,4-dioxane was degraded in 120 min giving ξ of 4.32. In this study, the synergistic effect was ascribed to the effective conversion of O_3 into $HO^{\bullet}$ radicals through the localized thermal effect and pressure of cavitation in HC/SPC/O_3. In both processes representing AC and HC combined with O_3-assisted AOPs, $HO^{\bullet}$ radicals were the main reactive species and the effect of inorganic anions was detrimental due to the higher reactivity of $HO^{\bullet}$ radicals. The degradation pathway of BTEX included H-abstraction, hydroxylation and dealkylation, while the degradation of 1,4-dioxane involved dimerization, ΔC-C splitting and disproportionation. The E_{EO} of HC/SPC/O_3 estimated to degrade 90% of 1,4-dioxane in 1 m^3 was 102.65 kWh $m^{-3}order^{-1}$, while LFDUS/O_3 required 71.91 kWh $m^{-3}order^{-1}$ for the treatment of 1 m^3 water containing BTEX. When compared from economical perspective, LFDUS/O_3 seems a favorable option as HC/SPC/O_3 requires higher electric energy supply and expenses for SPC. However, it is important to mention that 1,4-dioxane exhibit higher persistent as water pollutant compared to BTEX. Under the conditions of HC at C_v 0.27, 43.9%, 46.2%, 50.8%, and 38.7% of benzene, toluene, ethylbenzene and *o*-xylene, respectively, were degraded in 60 min, while only 17.03% of 1,4-dioxane was degraded in 120 min.
3. While studying the cavitation-based ARPs it was found that the photo-reductive capacity of SO_3^{2-}/UV towards CLA was increased upon

combination with HC. Owing to the effect of cavitation in HC/SO_3^{2-}/UV increased the generation of primary H$^{\bullet}$ radicals which caused the degradation of CLA. Specifically, 99.68% of CLA was degraded at C_v 0.2, r_{red} 3.25, pH 6.5 in 90 min ensuring ξ of 1.42. The enhanced degradation of CLA was attained in the presence of DO as the effect of cavitation reduced the scavenging effect of DO by 28.6%. Although, the effect of cavitation was insufficient to induce the direct activation of SO_3^{2-} ions, the high turbulence, shear mixing along with localized extreme conditions generated by HC facilitated the transformations of SO_3^{2-} ions to yield H$^{\bullet}$ radicals under UV light. In addition, the hybrid HC/SO_3^{2-}/UV process demonstrated high tolerance to water matrix components effectively degrading CLA in the presence of inorganic anions (i.e., Cl^-, SO_4^{2-}, CO_3^{2-}). The effectiveness of HC/SO_3^{2-}/UV was noticeably suppressed upon the addition of 125 mg/L HA, as the penetration of UV light into the volume of liquid was limited. The GC-MS analysis of degradation intermediates and DFT-based Fukui function calculations confirmed the reductive pathway of CLA degradation initiated on electron-deficient sites. Hence, the coupled cavitation-based ARPs display a valid advantage representing a new alternative to AOPs for the treatment of wastewaters containing halogenoorganic substances.

In the light of environmental challenges related with the occurrence of persistent organic pollutants, advanced chemical processes are widely recognized as highly effective technologies. Along with the wide number of tertiary wastewater treatment methods potentially degrading organic pollutants at acceptable level, advanced chemical processes accomplish the complete degradation of most organic pollutants within a short treatment time. Further steps in the development of advanced chemical processes would involve the overcoming of inherent disadvantages, such as high operating cost due to high energy and chemical consumption. In this context, the economic feasibility in the hybrid processes can be significantly improved owing to the synergistic effect and the efforts can be made to test the large-scale applications. In this regard, the combined application of HC with AOPs in continuous flow reactors could be suitable for the integration in conventional wastewater treatment scheme. For example, HC/SPC/O_3 can be implemented for the degradation of persistent organic pollutants and inactivation of microorganisms as a part of a tertiary treatment stage. Decontamination using hybrid cavitation-based ARPs is less understood and further studies revealing the mechanism of generation of reductive species and degradation pathway of

pollutants are required. Considering the enhanced generation of reductive species and observed high tolerance to co-existing anions, the degradation of PFAS/PFOS also known as “forever chemicals” in various wastewater matrices by cavitation-based ARPs represents a particular interest. In addition, the cavitation-based ARPs can be considered as a post-treatment option following ozonation to reduce the content of BrO_3^-/ClO_3^- below the maximum allowed concentration. Future research directions in cavitation-based ARPs may explore the utilization of alternative source of energy that are economically feasible and environmentally sustainable, such as solar light.

6. List of scientific achievements

Authored journal publications

- **K. Fedorov**, M. Plata-Gryl, J. Ali Khan, G. Boczkaj, Ultrasound-assisted heterogeneous activation of persulfate and peroxymonosulfate by asphaltenes for the degradation of BTEX in water, Journal of Hazardous Materials, 397, 2020, 122804, IF 10.58, DOI: https://doi.org/10.1016/j.jhazmat.2020.122804.
- **K. Fedorov**, X. Sun, G. Boczkaj, Combination of hydrodynamic cavitation and SR-AOPs for simultaneous degradation of BTEX in water, Chemical Engineering Journal, 417, 2021, 128081, IF 16.74, DOI: https://doi.org/10.1016/j.cej.2020.128081.
- **K. Fedorov**, K. Dinesh, X. Sun, R. D. C. Soltani, Z. Wang, S. Sonawane, G. Boczkaj, Synergistic effects of hybrid advanced oxidation processes (AOPs) based on hydrodynamic cavitation phenomenon – A review, Chemical Engineering Journal, 432, 2022, 134191, IF 15.1, DOI: https://doi.org/10.1016/j.cej.2021.134191.
- **K. Fedorov**, M. P. Rayaroth, N. S. Shah, G. Boczkaj, Activated sodium percarbonate-ozone (SPC/O_3) hybrid hydrodynamic cavitation system for advanced oxidation processes (AOPs) of 1,4-dioxane in water, Chemical Engineering Journal, 456, 2023, 141027, IF 13.3, DOI: https://doi.org/10.1016/j.cej.2022.141027.
- **K. Fedorov**, L. Kong, C. Wang, G. Boczkaj, High-performance activation of ozone by sonocavitation for BTEX degradation in water, Journal of Environmental Management, 363, 2024, 121343, IF 8.4, DOI: https://doi.org/10.1016/j.jenvman.2024.121343.
- **K. Fedorov**, C. Wang, N. S. Shah, G. Boczkaj, Boosting the radical-induced reductive degradation of clofibric acid in water: Synergistic effect of SO_3^{2-}/UV and hydrodynamic cavitation (HC), Journal of Environmental Management, 391, 2025, 126506, IF 8.4, DOI: https://doi.org/10.1016/j.jenvman.2025.126506.

Co-authored journal publications

- M. Gągol, E. Cako, **K. Fedorov**, R. D. C. Soltani, A. Przyjazny, G. Boczkaj, Hydrodynamic cavitation based advanced oxidation processes: Studies on specific effects of inorganic acids on the degradation effectiveness of organic pollutants, Journal of Molecular Liquids, 307, 2020, 113002, IF 6.6, DOI: https://doi.org/10.1016/j.molliq.2020.113002.
- S. Sonawane, **K. Fedorov**, M. P. Rayaroth, G. Boczkaj, Degradation of 1,4-dioxane by sono-activated persulfates for water and wastewater treatment applications, Water Resources and Industry, 28, 2022, 100183, IF 5.1. DOI: https://doi.org/10.1016/j.wri.2022.100183.
- S. Sonawane, M. P Rayaroth, V. K Landge, **K. Fedorov**, G. Boczkaj, Thermally activated persulfate-based Advanced Oxidation Processes — recent progress and challenges in mineralization of persistent organic chemicals: a review, Current Opinion in Chemical Engineering, 37, 2022, 100839, IF 6.6, DOI: https://doi.org/10.1016/j.coche.2022.100839.
- P. V. Nidheesh, G. Boczkaj, S. O. Ganiyu, A. A. Oladipo, **K. Fedorov**, R. Xiao, D. D. Dionysiou, Generation, properties, and applications of singlet oxygen for wastewater treatment: a review. Environmental Chemistry Letters, 23, 2024, 195–240, IF 20.4, DOI: https://doi.org/10.1007/s10311-024-01798-0.
- Z. Honarmandrad, **K. Fedorov**, G. Boczkaj, Hydrodynamic cavitation based advanced reduction process (ARP) for degradation of 2-nitrophenol in aqueous environment, Water Research, 286, 2025, 124250, IF 12.4. DOI: https://doi.org/10.1016/j.watres.2025.124250.

Book chapters

- **K. Fedorov**, E. Cako, K. Dinesh, R. D. C. Soltani, Z. Wang, J. A. Khan, G. Boczkaj, Cavitation-Based Processes for Water and Wastewater Treatment. In: Cost-efficient Wastewater Treatment Technologies. The Handbook of Environmental Chemistry, 118, 2022, Springer, Cham., DOI: https://doi.org/10.1007/698_2022_866.
- **K. Fedorov**, M. P. Rayaroth, X. Sun, R. D. C. Soltani, S. Sonawane, N. S. Shah, V. Srivastava, Z. Wang, G. Boczkaj, Sonochemical Based Processes for Treatment of Water and Wastewater in Sonochemistry Source of Clean

Energy, chapter 7, 2024, CRC Press, DOI: https://doi.org/10.1201/9781003267713.

- M. P Rayaroth, **K. Fedorov**, G. Boczkaj, Y. Patil, S. H. Sonawane, Chapter 5 - Hydrodynamic cavitation in wastewater treatment in Advanced Technologies in Wastewater Treatment, Elsevier, 115-145, 2025, DOI: https://doi.org/10.1016/B978-0-443-26500-6.00005-5.

Conferences

- **K. Fedorov** (presenter), G. Boczkaj, Combination of hydrodynamic cavitation with advanced oxidation processes: activation of persulfate and percarbonate, 11th IWA International Symposium on Waste Management Problems in Agro-Industry, Gdansk, Poland, 26-28.10.2022.
- **K. Fedorov** (presenter), G. Boczkaj, Synergistic effect in hybrid cavitation-based advanced chemical processes for degradation of water pollutants, 18th International Conference on Environmental Science and Technology, Athens, Greece, 30.08.- 02.09.2023.

7. References

[1] J.P. Kushwaha, A review on sugar industry wastewater: sources, treatment technologies, and reuse, Desalin. Water Treat. 53 (2015) 309–318. doi:10.1080/19443994.2013.838526.

[2] L. Mishra, K.K. Paul, S. Jena, Coke wastewater treatment methods: Mini review, J. Indian Chem. Soc. 98 (2021) 100133. doi:10.1016/J.JICS.2021.100133.

[3] M. Ljunggren, Micro screening in wastewater treatment-an overview, Vatten. 62 (2006) 171.

[4] N.R. Esfahani, M.N. Mobarekeh, M. Hoodaji, Effect of Grit Chamber Configuration on Particle Removal: Using Response Surface Method, J. Membr. Sep. Technol. 7 (2018) 12–16. doi:10.6000/1929-6037.2018.07.02.

[5] A. Tamayol, B. Firoozabadi, M. A. Ashjari, Hydrodynamics of Secondary Settling Tanks and Increasing Their Performance Using Baffles, J. Environ. Eng. 136 (2010) 32–39. doi:10.1061/(ASCE)EE.1943-7870.0000126.

[6] S.F. Ahmed, M. Mofijur, S. Nuzhat, A.T. Chowdhury, N. Rafa, M.A. Uddin, A. Inayat, T.M.I. Mahlia, H.C. Ong, W.Y. Chia, P.L. Show, Recent developments in physical, biological, chemical, and hybrid treatment techniques for removing emerging contaminants from wastewater, J. Hazard. Mater. 416 (2021) 125912. doi:10.1016/J.JHAZMAT.2021.125912.

[7] M. Hanafy, H.I. and Nabih, Treatment of Oily Wastewater Using Dissolved Air Flotation Technique, Energy Sources, Part A Recover. Util. Environ. Eff. 29 (2007) 143–159. doi:10.1080/009083190948711.

[8] L. Yu, M. Han, F. He, A review of treating oily wastewater, Arab. J. Chem. 10 (2017) S1913–S1922. doi:10.1016/J.ARABJC.2013.07.020.

[9] R.T. Rodrigues, J. Rubio, DAF–dissolved air flotation: Potential applications in the mining and mineral processing industry, Int. J. Miner. Process. 82 (2007) 1–13. doi:10.1016/J.MINPRO.2006.07.019.

[10] S. Kato, Y. Kansha, Comprehensive review of industrial wastewater treatment techniques, Environ. Sci. Pollut. Res. 31 (2024) 51064–51097. doi:10.1007/s11356-024-34584-0.

[11] M. Boroski, A.C. Rodrigues, J.C. Garcia, A.P. Gerola, J. Nozaki, N. Hioka, The effect of operational parameters on electrocoagulation–flotation process followed by photocatalysis applied to the decontamination of water effluents from cellulose

and paper factories, J. Hazard. Mater. 160 (2008) 135–141. doi:10.1016/J.JHAZMAT.2008.02.094.

[12] G.Z. Kyzas, K.A. Matis, Flotation in Water and Wastewater Treatment, Processes. 6 (2018) 116. doi:10.3390/pr6080116.

[13] S.M. Roy, J. P, R. Machavaram, C.M. Pareek, B.C. Mal, Diversified aeration facilities for effective aquaculture systems—a comprehensive review, Aquac. Int. 29 (2021) 1181–1217. doi:10.1007/s10499-021-00685-7.

[14] S.M. Roy, M. Tanveer, R. Machavaram, Applications of gravity aeration system in aquaculture—a systematic review, Aquac. Int. 30 (2022) 1593–1621. doi:10.1007/s10499-022-00851-5.

[15] G. Skouteris, G. Rodriguez-Garcia, S.F. Reinecke, U. Hampel, The use of pure oxygen for aeration in aerobic wastewater treatment: A review of its potential and limitations, Bioresour. Technol. 312 (2020) 123595. doi:10.1016/J.BIORTECH.2020.123595.

[16] N.T. Nguyen, T.S. Vo, P.L. Tran-Nguyen, M.N. Nguyen, V.H. Pham, R. Matsuhashi, K. Kim, T.T.B.C. Vo, A comprehensive review of aeration and wastewater treatment, Aquaculture. 591 (2024) 741113. doi:10.1016/J.AQUACULTURE.2024.741113.

[17] Y. Chen, H. Zhang, Y. Yin, F. Zeng, Z. Cui, Smart energy savings for aeration control in wastewater treatment, Energy Reports. 8 (2022) 1711–1721. doi:10.1016/J.EGYR.2022.02.038.

[18] E. Pérez-Botella, S. Valencia, F. Rey, Zeolites in Adsorption Processes: State of the Art and Future Prospects, Chem. Rev. 122 (2022) 17647–17695. doi:10.1021/acs.chemrev.2c00140.

[19] S. Wang, Y. Peng, Natural zeolites as effective adsorbents in water and wastewater treatment, Chem. Eng. J. 156 (2010) 11–24. doi:10.1016/J.CEJ.2009.10.029.

[20] D. Caputo, F. Pepe, Experiments and data processing of ion exchange equilibria involving Italian natural zeolites: a review, Microporous Mesoporous Mater. 105 (2007) 222–231. doi:10.1016/J.MICROMESO.2007.04.024.

[21] S.T. Bosso, J. Enzweiler, Evaluation of heavy metal removal from aqueous solution onto scolecite, Water Res. 36 (2002) 4795–4800. doi:10.1016/S0043-1354(02)00208-7.

[22] P. Huttenloch, K.E. Roehl, K. Czurda, Sorption of Nonpolar Aromatic Contaminants by Chlorosilane Surface Modified Natural Minerals, Environ. Sci. Technol. 35 (2001) 4260–4264. doi:10.1021/es010131f.

[23] D. Karadag, E. Akgul, S. Tok, F. Erturk, M.A. Kaya, M. Turan, Basic and Reactive Dye

Removal Using Natural and Modified Zeolites, J. Chem. Eng. Data. 52 (2007) 2436–2441. doi:10.1021/je7003726.

[24] S. Capasso, E. Coppola, P. Iovino, S. Salvestrini, C. Colella, Sorption of humic acids on zeolitic tuffs, Microporous Mesoporous Mater. 105 (2007) 324–328. doi:10.1016/J.MICROMESO.2007.04.017.

[25] S. Wang, T. Terdkiatburana, M.O. Tadé, Adsorption of Cu(II), Pb(II) and humic acid on natural zeolite tuff in single and binary systems, Sep. Purif. Technol. 62 (2008) 64–70. doi:10.1016/J.SEPPUR.2008.01.004.

[26] S.I. Alhassan, L. Huang, Y. He, L. Yan, B. Wu, H. Wang, Fluoride removal from water using alumina and aluminum-based composites: A comprehensive review of progress, Crit. Rev. Environ. Sci. Technol. 51 (2021) 2051–2085. doi:10.1080/10643389.2020.1769441.

[27] S. Ghorai, K.K. Pant, Investigations on the column performance of fluoride adsorption by activated alumina in a fixed-bed, Chem. Eng. J. 98 (2004) 165–173. doi:10.1016/J.CEJ.2003.07.003.

[28] Z. Hashmi, A.S. Jatoi, S. Nadeem, A. Anjum, S.M. Imam, H. Jangda, Comparative analysis of conventional to biomass-derived adsorbent for wastewater treatment: a review, Biomass Convers. Biorefinery. 14 (2024) 45–76. doi:10.1007/s13399-022-02443-y.

[29] Z.A. Kassam, L. Yerushalmi, S.R. Guiot, A Market Study on the Anaerobic Wastewater Treatment Systems, Water. Air. Soil Pollut. 143 (2003) 179–192. doi:10.1023/A:1022807416773.

[30] C.L. Hansen, D.Y. Cheong, Agricultural Waste Management in Food Processing, Handb. Farm Dairy Food Mach. (2007) 609–661. doi:10.1016/B978-081551538-8.50022-4.

[31] A.J. Ward, P.J. Hobbs, P.J. Holliman, D.L. Jones, Optimisation of the anaerobic digestion of agricultural resources, Bioresour. Technol. 99 (2008) 7928–7940. doi:10.1016/J.BIORTECH.2008.02.044.

[32] G. F. Parkin, W. F. Owen, Fundamentals of Anaerobic Digestion of Wastewater Sludges, J. Environ. Eng. 112 (1986) 867–920. doi:10.1061/(ASCE)0733-9372(1986)112:5(867).

[33] K. Xiao, G. Abbt-Braun, H. Horn, Changes in the characteristics of dissolved organic matter during sludge treatment: A critical review, Water Res. 187 (2020) 116441. doi:10.1016/J.WATRES.2020.116441.

[34] W.S. Adney, C.J. Rivard, M. Shiang, M.E. Himmel, Anaerobic digestion of

lignocellulosic biomass and wastes, Appl. Biochem. Biotechnol. 30 (1991) 165–183. doi:10.1007/BF02921684.

[35] S. Ray, C. Kuppam, S. Pandit, P. Kumar, Biogas Upgrading by Hydrogenotrophic Methanogens: An Overview, Waste and Biomass Valorization. 14 (2023) 537–552. doi:10.1007/s12649-022-01888-6.

[36] M. Świątek, A. Lewicki, D. Szymanowska, P. Kubiak, The effect of introduction of chicken manure on the biodiversity and performance of an anaerobic digester, Electron. J. Biotechnol. 37 (2019) 25–33. doi:10.1016/J.EJBT.2018.11.002.

[37] R.F. V Novaes, Microbiology of Anaerobic Digestion, Water Sci. Technol. 18 (1986) 1–14. doi:10.2166/wst.1986.0159.

[38] B. Wintsche, N. Jehmlich, D. Popp, H. Harms, S. Kleinsteuber, Metabolic Adaptation of Methanogens in Anaerobic Digesters Upon Trace Element Limitation, Front. Microbiol. Volume 9- (2018). https://www.frontiersin.org/journals/microbiology/articles/10.3389/fmicb.2018.00405.

[39] P.L. McCarty, D.P. Smith, Anaerobic wastewater treatment, Environ. Sci. Technol. 20 (1986) 1200–1206. doi: 10.1021/es00154a002.

[40] F. Ehlinger, J.M. Audic, D. Verrier, G.M. Faup, The Influence of the Carbon Source on Microbiological Clogging in an Anaerobic Filter, Water Sci. Technol. 19 (1987) 261–273. doi:10.2166/wst.1987.0207.

[41] Y.X. Sun, Q.Y. Wu, H.Y. Hu, J. Tian, Effects of operating conditions on THMs and HAAs formation during wastewater chlorination, J. Hazard. Mater. 168 (2009) 1290–1295. doi:10.1016/J.JHAZMAT.2009.03.013.

[42] L. Snowden-Swan, J. Piatt, A. Lesperance, Disinfection Technologies for potable water and wastewater treatment: alternatives to chlorine gas, Pacific Northwest Natl. Lab. (PNNL). Prep. US Army Forces Command Air Qual. Div. United State. (1998).

[43] W.A. Rutala, D.J. Weber, Uses of inorganic hypochlorite (bleach) in health-care facilities, Clin. Microbiol. Rev. 10 (1997) 597–610. doi:10.1128/cmr.10.4.597.

[44] W.S. da Cruz Nizer, V. Inkovskiy, J. Overhage, Surviving Reactive Chlorine Stress: Responses of Gram-Negative Bacteria to Hypochlorous Acid, Microorganisms. 8 (2020). doi:10.3390/microorganisms8081220.

[45] S. FUKUZAKI, Mechanisms of Actions of Sodium Hypochlorite in Cleaning and Disinfection Processes, Biocontrol Sci. 11 (2006) 147–157. doi:10.4265/bio.11.147.

[46] Q. Lin, J.Y.C. Lim, K. Xue, P.Y.M. Yew, C. Owh, P.L. Chee, X.J. Loh, Sanitizing agents for

virus inactivation and disinfection, VIEW. 1 (2020) e16. doi:https://doi.org/10.1002/viw2.16.

[47] V. Lazarova, P. Savoye, M.L. Janex, E.R. Blatchley, M. Pommepuy, Advanced wastewater disinfection technologies: State of the art and perspectives, Water Sci. Technol. 40 (1999) 203–213. doi:10.1016/S0273-1223(99)00502-8.

[48] N. Dhanda, S. Kumar, Water disinfection and disinfection by products, Environ. Monit. Assess. 197 (2025) 461. doi:10.1007/s10661-025-13915-9.

[49] X. Zhang, Y. Liu, Potential toxicity and implication of halogenated byproducts generated in MBR online-cleaning with hypochlorite, J. Chem. Technol. Biotechnol. 95 (2020) 20–26. doi:https://doi.org/10.1002/jctb.6199.

[50] J. Han, X. Zhang, J. Jiang, W. Li, How Much of the Total Organic Halogen and Developmental Toxicity of Chlorinated Drinking Water Might Be Attributed to Aromatic Halogenated DBPs?, Environ. Sci. Technol. 55 (2021) 5906–5916. doi:10.1021/acs.est.0c08565.

[51] S.D. Richardson, C. Postigo, Drinking Water Disinfection By-products BT - Emerging Organic Contaminants and Human Health, in: D. Barceló (Ed.), Springer Berlin Heidelberg, Berlin, Heidelberg, 2012: pp. 93–137. doi:10.1007/698_2011_125.

[52] B.L. Loeb, C.M. Thompson, J. Drago, H. Takahara, S. Baig, Worldwide Ozone Capacity for Treatment of Drinking Water and Wastewater: A Review, Ozone Sci. Eng. 34 (2012) 64–77. doi:10.1080/01919512.2012.640251.

[53] A.M.-A. Simpson, W.A. Mitch, Chlorine and ozone disinfection and disinfection byproducts in postharvest food processing facilities: A review, Crit. Rev. Environ. Sci. Technol. 52 (2022) 1825–1867. doi:10.1080/10643389.2020.1862562.

[54] C. Wei, F. Zhang, Y. Hu, C. Feng, H. Wu, Ozonation in water treatment: the generation, basic properties of ozone and its practical application, 33 (2017) 49–89. doi:doi:10.1515/revce-2016-0008.

[55] J. Hoigné, Chemistry of aqueous ozone and transformation of pollutants by ozonation and advanced oxidation processes, in: Qual. Treat. Drink. Water II, Springer, 1998: pp. 83–141.

[56] Y. Wang, E.M. Rodríguez, D. Rentsch, Z. Qiang, U. von Gunten, Ozone Reactions with Olefins and Alkynes: Kinetics, Activation Energies, and Mechanisms, Environ. Sci. Technol. 59 (2025) 4733–4744. doi:10.1021/acs.est.4c07119.

[57] S.D. Richardson, A.D. Thruston, T. V Caughran, P.H. Chen, T.W. Collette, T.L. Floyd, K.M. Schenck, B.W. Lykins, G. Sun, G. Majetich, Identification of New Ozone Disinfection Byproducts in Drinking Water, Environ. Sci. Technol. 33 (1999) 3368–

3377. doi:10.1021/es981218c.

[58] C.M. Morrison, S. Hogard, R. Pearce, A. Mohan, A.N. Pisarenko, E.R. V Dickenson, U. von Gunten, E.C. Wert, Critical Review on Bromate Formation during Ozonation and Control Options for Its Minimization, Environ. Sci. Technol. 57 (2023) 18393–18409. doi:10.1021/acs.est.3c00538.

[59] S. Liang, T.I. Yun, S.W. Krasner, R.S. Yates, Evaluation of Emerging Bromate Control Strategies, Water Pract. Technol. 5 (2010) wpt2010064. doi:10.2166/wpt.2010.064.

[60] U. Von Gunten, Ozonation of drinking water: Part II. Disinfection and by-product formation in presence of bromide, iodide or chlorine, Water Res. 37 (2003) 1469–1487. doi:10.1016/S0043-1354(02)00458-X.

[61] U. von Gunten, J. Hoigne, Bromate Formation during Ozonization of Bromide-Containing Waters: Interaction of Ozone and Hydroxyl Radical Reactions, Environ. Sci. Technol. 28 (1994) 1234–1242. doi:10.1021/es00056a009.

[62] R. Hofmann, R.C. Andrews, Ammoniacal bromamines: a review of their influence on bromate formation during ozonation, Water Res. 35 (2001) 599–604. doi:10.1016/S0043-1354(00)00319-5.

[63] M. Siddiqui, G. Amy, K. Ozekin, W. Zhai, P. Westerhoff, Alternative strategies for removing bromate, J. AWWA. 86 (1994) 81–96. doi:https://doi.org/10.1002/j.1551-8833.1994.tb06263.x.

[64] S. Gyparakis, E. Diamadopoulos, Formation and Reverse Osmosis Removal of Bromate Ions during Ozonation of Groundwater in Coastal Areas, Sep. Sci. Technol. 42 (2007) 1465–1476. doi:10.1080/01496390701290011.

[65] D. Lin, H. Liang, G. Li, Factors affecting the removal of bromate and bromide in water by nanofiltration, Environ. Sci. Pollut. Res. 27 (2020) 24639–24649. doi:10.1007/s11356-019-06002-3.

[66] S.A. Craik, D. Weldon, G.R. Finch, J.R. Bolton, M. Belosevic, Inactivation of cryptosporidium parvum oocysts using medium- and low-pressure ultraviolet radiation, Water Res. 35 (2001) 1387–1398. doi:10.1016/S0043-1354(00)00399-7.

[67] T. Li, Z. Zhu, D. Wang, C. Yao, H. Tang, Characterization of floc size, strength and structure under various coagulation mechanisms, Powder Technol. 168 (2006) 104–110. doi:10.1016/J.POWTEC.2006.07.003.

[68] J. Bratby, Coagulation and Flocculation in Water and Wastewater Treatment, IWA Publishing, 2016. https://books.google.pl/books?id=PabQDAAAQBAJ.

[69] J.Q. Jiang, B. Lloyd, Progress in the development and use of ferrate(VI) salt as an

oxidant and coagulant for water and wastewater treatment, Water Res. 36 (2002) 1397–1408. doi:10.1016/S0043-1354(01)00358-X.

[70] D. Ghernaout, B. Ghernaout, Sweep flocculation as a second form of charge neutralisation—a review, Desalin. Water Treat. 44 (2012) 15–28. doi:10.1080/19443994.2012.691699.

[71] B. Ma, W. Xue, C. Hu, H. Liu, J. Qu, L. Li, Characteristics of microplastic removal via coagulation and ultrafiltration during drinking water treatment, Chem. Eng. J. 359 (2019) 159–167. doi:10.1016/J.CEJ.2018.11.155.

[72] S. Barany, A. Szepesszentgyörgyi, Flocculation of cellular suspensions by polyelectrolytes, Adv. Colloid Interface Sci. 111 (2004) 117–129. doi:10.1016/J.CIS.2004.07.003.

[73] K. Mandel, F. Hutter, C. Gellermann, G. Sextl, Reusable superparamagnetic nanocomposite particles for magnetic separation of iron hydroxide precipitates to remove and recover heavy metal ions from aqueous solutions, Sep. Purif. Technol. 109 (2013) 144–147. doi:10.1016/J.SEPPUR.2013.03.002.

[74] H. Ganjidoust, K. Tatsumi, T. Yamagishi, R.N. Gholian, Effect of synthetic and natural coagulant on lignin removal from pulp and paper wastewater, Water Sci. Technol. 35 (1997) 291–296. doi:10.1016/S0273-1223(96)00943-2.

[75] C.Y. Teh, T.Y. Wu, J.C. Juan, Optimization of agro-industrial wastewater treatment using unmodified rice starch as a natural coagulant, Ind. Crops Prod. 56 (2014) 17–26. doi:10.1016/J.INDCROP.2014.02.018.

[76] A.H. Jagaba, S.R.M. Kutty, G. Hayder, A.A.A. Latiff, N.A.A. Aziz, I. Umaru, A.A.S. Ghaleb, S. Abubakar, I.M. Lawal, M.A. Nasara, Sustainable use of natural and chemical coagulants for contaminants removal from palm oil mill effluent: A comparative analysis, Ain Shams Eng. J. 11 (2020) 951–960. doi:10.1016/J.ASEJ.2020.01.018.

[77] M. AFOLABI, O.A. ONUKOGU, T.O. IGUNMA, A.K. ADELEKE, Z.Q.S. NWOKEDIEGWU, Systematic Review of pH-Control and Dosing System Design for Acid-Base Neutralization in Industrial Effluents, (2021).

[78] D. Petruzzelli, M. Petrella, G. Boghetich, P. Calabrese, V. Petruzzelli, A. Petrella, Neutralization of Acidic Wastewater by the Use of Waste Limestone from the Marble Industry. Mechanistic Aspects and Mass Transfer Phenomena of the Acid−Base Reaction at the Liquid−Solid Interface, Ind. Eng. Chem. Res. 48 (2009) 399–405. doi:10.1021/ie8014268.

[79] M. Ramesh Kumar, R. Malathy, S. Paramasivam, I.-M. Chung, S.-H. Kim, P.

Mayakrishnan, pH neutralization of textile industry wastewater for effective recycling, Pigment Resin Technol. 51 (2021) 80–90. doi:10.1108/PRT-10-2020-0106.

[80] T. Jarnerud, A. V Karasev, P.G. Jönsson, Neutralization of Acidic Wastewater from a Steel Plant by Using CaO-Containing Waste Materials from Pulp and Paper Industries, Materials (Basel). 14 (2021). doi:10.3390/ma14102653.

[81] A. Mackie, S. Boilard, M.E. Walsh, C.B. Lake, Physicochemical characterization of cement kiln dust for potential reuse in acidic wastewater treatment, J. Hazard. Mater. 173 (2010) 283–291. doi:10.1016/J.JHAZMAT.2009.08.081.

[82] N.H.S. Abdullah, M.N. Karsiti, R. Ibrahim, A review of pH neutralization process control, in: 2012 4th Int. Conf. Intell. Adv. Syst., 2012: pp. 594–598. doi:10.1109/ICIAS.2012.6306084.

[83] I. Zinicovscaia, Conventional methods of wastewater treatment, Cyanobacteria for Bioremediation of Wastewaters. (2016) 17–25.

[84] M.C. Benalia, L. Youcef, M.G. Bouaziz, S. Achour, H. Menasra, Removal of Heavy Metals from Industrial Wastewater by Chemical Precipitation: Mechanisms and Sludge Characterization, Arab. J. Sci. Eng. 47 (2022) 5587–5599. doi:10.1007/s13369-021-05525-7.

[85] A. Pohl, Removal of Heavy Metal Ions from Water and Wastewaters by Sulfur-Containing Precipitation Agents, Water, Air, Soil Pollut. 231 (2020) 503. doi:10.1007/s11270-020-04863-w.

[86] A.E. Lewis, Review of metal sulphide precipitation, Hydrometallurgy. 104 (2010) 222–234. doi:10.1016/J.HYDROMET.2010.06.010.

[87] M.M. Matlock, K.R. Henke, D.A. Atwood, D. Robertson, Aqueous leaching properties and environmental implications of cadmium, lead and zinc Trimercaptotriazine (TMT) compounds, Water Res. 35 (2001) 3649–3655. doi:10.1016/S0043-1354(01)00091-4.

[88] F.L. Fu, Q.R. Xuan, R.M. Chen, Y. Xiong, Removal of Cu2+ and dye from wastewater using the heavy metal precipitant N,N-bis-(dithiocarboxy)piperazine, Environ. Chem. Lett. 4 (2006) 41–44. doi:10.1007/s10311-005-0032-z.

[89] F. Fu, R. Chen, Y. Xiong, Comparative investigation of N,N′-bis-(dithiocarboxy)piperazine and diethyldithiocarbamate as precipitants for Ni(II) in simulated wastewater, J. Hazard. Mater. 142 (2007) 437–442. doi:10.1016/J.JHAZMAT.2006.08.036.

[90] M.M. Matlock, B.S. Howerton, D.A. Atwood, Irreversible precipitation of mercury

and lead, J. Hazard. Mater. 84 (2001) 73–82. doi:10.1016/S0304-3894(01)00190-X.

[91] L. Egle, H. Rechberger, J. Krampe, M. Zessner, Phosphorus recovery from municipal wastewater: An integrated comparative technological, environmental and economic assessment of P recovery technologies, Sci. Total Environ. 571 (2016) 522–542. doi:10.1016/J.SCITOTENV.2016.07.019.

[92] W. Sun, G. Ma, Y. Sun, Y. Liu, N. Song, Y. Xu, H. Zheng, Effective treatment of high phosphorus pharmaceutical wastewater by chemical precipitation, Can. J. Chem. Eng. 95 (2017) 1585–1593. doi:https://doi.org/10.1002/cjce.22799.

[93] W.H. Glaze, J.-W. Kang, D.H. Chapin, The Chemistry of Water Treatment Processes Involving Ozone, Hydrogen Peroxide and Ultraviolet Radiation, Ozone Sci. Eng. 9 (1987) 335–352. doi:10.1080/01919518708552148.

[94] S. Hussain, E. Aneggi, D. Goi, Catalytic activity of metals in heterogeneous Fenton-like oxidation of wastewater contaminants: a review, Environ. Chem. Lett. 19 (2021) 2405–2424. doi:10.1007/s10311-021-01185-z.

[95] H.J.H. Fenton, LXXIII.—Oxidation of tartaric acid in presence of iron, J. Chem. Soc. Trans. 65 (1894) 899–910.

[96] J.L. Acero, F.J. Benitez, F.J. Real, F. Teva, Micropollutants removal from retentates generated in ultrafiltration and nanofiltration treatments of municipal secondary effluents by means of coagulation, oxidation, and adsorption processes, Chem. Eng. J. 289 (2016) 48–58. doi:10.1016/J.CEJ.2015.12.082.

[97] A. Justo, O. González, J. Aceña, S. Pérez, D. Barceló, C. Sans, S. Esplugas, Pharmaceuticals and organic pollution mitigation in reclamation osmosis brines by UV/H2O2 and ozone, J. Hazard. Mater. 263 (2013) 268–274. doi:10.1016/J.JHAZMAT.2013.05.030.

[98] S.M.R. Vendramel, A. Justo, O. González, C. Sans, S. Esplugas, Reverse osmosis concentrate treatment by chemical oxidation and moving bed biofilm processes, Water Sci. Technol. 68 (2013) 2421–2426. doi:10.2166/wst.2013.510.

[99] U. von Gunten, Ozonation of drinking water: Part I. Oxidation kinetics and product formation, Water Res. 37 (2003) 1467.

[100] M.M. Sein, A. Golloch, T.C. Schmidt, C. von Sonntag, No Marked Kinetic Isotope Effect in the Peroxone (H2O2/D2O2+O3) Reaction: Mechanistic Consequences, ChemPhysChem. 8 (2007) 2065–2067. doi:https://doi.org/10.1002/cphc.200700493.

[101] U. von Gunten, The basics of oxidants in water treatment. Part B: ozone reactions, Water Sci. Technol. 55 (2007) 25–29. doi:10.2166/wst.2007.382.

[102] G. Boczkaj, M. Gągol, M. Klein, A. Przyjazny, Effective method of treatment of effluents from production of bitumens under basic pH conditions using hydrodynamic cavitation aided by external oxidants, Ultrason. Sonochem. 40 (2018) 969–979. doi:10.1016/j.ultsonch.2017.08.032.

[103] Y. Kaya, Z.B. Gönder, I. Vergili, A. Ongen, Application of experimental design method for advanced treatment of dairy wastewater by ozonation, Environ. Prog. Sustain. Energy. 38 (2019) e13025. doi:https://doi.org/10.1002/ep.13025.

[104] Y. Lee, L. Kovalova, C.S. McArdell, U. von Gunten, Prediction of micropollutant elimination during ozonation of a hospital wastewater effluent, Water Res. 64 (2014) 134–148. doi:10.1016/J.WATRES.2014.06.027.

[105] Y. Huang, M. Luo, Z. Xu, D. Zhang, L. Li, Catalytic ozonation of organic contaminants in petrochemical wastewater with iron-nickel foam as catalyst, Sep. Purif. Technol. 211 (2019) 269–278. doi:10.1016/J.SEPPUR.2018.09.080.

[106] K. Sivagami, K.P. Sakthivel, I.M. Nambi, Advanced oxidation processes for the treatment of tannery wastewater, J. Environ. Chem. Eng. 6 (2018) 3656–3663. doi:10.1016/J.JECE.2017.06.004.

[107] S. Bakht Shokouhi, R. Dehghanzadeh, H. Aslani, N. Shahmahdi, Activated carbon catalyzed ozonation (ACCO) of Reactive Blue 194 azo dye in aqueous saline solution: Experimental parameters, kinetic and analysis of activated carbon properties, J. Water Process Eng. 35 (2020) 101188. doi:10.1016/J.JWPE.2020.101188.

[108] B.M. Souza, B.S. Souza, T.M. Guimarães, T.F.S. Ribeiro, A.C. Cerqueira, G.L. Sant'Anna, M. Dezotti, Removal of recalcitrant organic matter content in wastewater by means of AOPs aiming industrial water reuse, Environ. Sci. Pollut. Res. 23 (2016) 22947–22956. doi:10.1007/s11356-016-7476-5.

[109] Z. Liu, M. Chys, Y. Yang, K. Demeestere, S. Van Hulle, Oxidation of Trace Organic Contaminants (TrOCs) in Wastewater Effluent with Different Ozone-Based AOPs: Comparison of Ozone Exposure and •OH Formation, Ind. Eng. Chem. Res. 58 (2019) 8896–8902. doi:10.1021/acs.iecr.9b00293.

[110] C. Mejía-Morales, F. Hernández-Aldana, D.M. Cortés-Hernández, J.A. Rivera-Tapia, D. Castañeda-Antonio, N. Bonilla, Assessment of Biological and Persistent Organic Compounds in Hospital Wastewater After Advanced Oxidation Process UV/H2O2/O3, Water, Air, Soil Pollut. 231 (2020) 89. doi:10.1007/s11270-020-4463-8.

[111] R. Xiao, Z. Luo, Z. Wei, S. Luo, R. Spinney, W. Yang, D.D. Dionysiou, Activation of

peroxymonosulfate/persulfate by nanomaterials for sulfate radical-based advanced oxidation technologies, Curr. Opin. Chem. Eng. 19 (2018) 51–58. doi:10.1016/J.COCHE.2017.12.005.

[112] G.P. Anipsitakis, D.D. Dionysiou, Radical Generation by the Interaction of Transition Metals with Common Oxidants, Environ. Sci. Technol. 38 (2004) 3705–3712. doi:10.1021/es035121o.

[113] T. Zhang, Y. Chen, Y. Wang, J. Le Roux, Y. Yang, J.-P. Croué, Efficient Peroxydisulfate Activation Process Not Relying on Sulfate Radical Generation for Water Pollutant Degradation, Environ. Sci. Technol. 48 (2014) 5868–5875. doi:10.1021/es501218f.

[114] J. Hu, H. Dong, J. Qu, Z. Qiang, Enhanced degradation of iopamidol by peroxymonosulfate catalyzed by two pipe corrosion products (CuO and δ-MnO2), Water Res. 112 (2017) 1–8. doi:10.1016/J.WATRES.2017.01.025.

[115] H. Sun, S. Liu, G. Zhou, H.M. Ang, M.O. Tadé, S. Wang, Reduced Graphene Oxide for Catalytic Oxidation of Aqueous Organic Pollutants, ACS Appl. Mater. Interfaces. 4 (2012) 5466–5471. doi:10.1021/am301372d.

[116] X. Duan, H. Sun, J. Kang, Y. Wang, S. Indrawirawan, S. Wang, Insights into Heterogeneous Catalysis of Persulfate Activation on Dimensional-Structured Nanocarbons, ACS Catal. 5 (2015) 4629–4636. doi:10.1021/acscatal.5b00774.

[117] Y. Yao, Z. Yang, H. Sun, S. Wang, Hydrothermal Synthesis of Co3O4–Graphene for Heterogeneous Activation of Peroxymonosulfate for Decomposition of Phenol, Ind. Eng. Chem. Res. 51 (2012) 14958–14965. doi:10.1021/ie301642g.

[118] X. Duan, K. O'Donnell, H. Sun, Y. Wang, S. Wang, Sulfur and Nitrogen Co-Doped Graphene for Metal-Free Catalytic Oxidation Reactions, Small. 11 (2015) 3036–3044. doi:https://doi.org/10.1002/smll.201403715.

[119] C.M. Park, J. Heo, D. Wang, C. Su, Y. Yoon, Heterogeneous activation of persulfate by reduced graphene oxide–elemental silver/magnetite nanohybrids for the oxidative degradation of pharmaceuticals and endocrine disrupting compounds in water, Appl. Catal. B Environ. 225 (2018) 91–99. doi:10.1016/J.APCATB.2017.11.058.

[120] A. Shahzad, J. Ali, J. Ifthikar, G.G. Aregay, J. Zhu, Z. Chen, Z. Chen, Non-radical PMS activation by the nanohybrid material with periodic confinement of reduced graphene oxide (rGO) and Cu hydroxides, J. Hazard. Mater. 392 (2020) 122316. doi:10.1016/J.JHAZMAT.2020.122316.

[121] F. Sun, K.A. Osseo-Asare, Y. Chen, B.A. Dempsey, Reduction of As(V) to As(III) by commercial ZVI or As(0) with acid-treated ZVI, J. Hazard. Mater. 196 (2011) 311–

317. doi:10.1016/J.JHAZMAT.2011.09.029.

[122] F. Luan, L. Xie, J. Li, Q. Zhou, Abiotic reduction of nitroaromatic compounds by Fe(II) associated with iron oxides and humic acid, Chemosphere. 91 (2013) 1035–1041. doi:10.1016/J.CHEMOSPHERE.2013.01.070.

[123] L. Shi, X. Tan, J. Long, X. Xiong, S. Yang, P. Xue, H. Lv, X. Zhang, Direct Catalytic Hydrogenation of Simple Amides: A Highly Efficient Approach from Amides to Amines and Alcohols, Chem. – A Eur. J. 23 (2017) 546–548. doi:https://doi.org/10.1002/chem.201604904.

[124] X. Zhao, A. Li, X. Quan, S. Chen, H. Yu, S. Zhang, Efficient electrochemical reduction of nitrobenzene by nitrogen doped porous carbon, Chemosphere. 238 (2020) 124636. doi:10.1016/J.CHEMOSPHERE.2019.124636.

[125] C. Zwiener, F.H. Frimmel, Residues of Clofibric Acid, Ibuprofen and Diclofenac in the Aquatic Environment and their Elimination in Sewage Treatment and Drinking Water Production BT - Pharmaceuticals in the Environment: Sources, Fate, Effects and Risks, in: K. Kümmerer (Ed.), Springer Berlin Heidelberg, Berlin, Heidelberg, 2004: pp. 121–132. doi:10.1007/978-3-662-09259-0_9.

[126] J. Cui, P. Gao, Y. Deng, Destruction of Per- and Polyfluoroalkyl Substances (PFAS) with Advanced Reduction Processes (ARPs): A Critical Review, Environ. Sci. Technol. 54 (2020) 3752–3766. doi:10.1021/acs.est.9b05565.

[127] J. Huang, X. Wang, Z. Pan, X. Li, Y. Ling, L. Li, Efficient degradation of perfluorooctanoic acid (PFOA) by photocatalytic ozonation, Chem. Eng. J. 296 (2016) 329–334. doi:10.1016/J.CEJ.2016.03.116.

[128] A.Y.C. Lin, S.C. Panchangam, C.Y. Chang, P.K.A. Hong, H.F. Hsueh, Removal of perfluorooctanoic acid and perfluorooctane sulfonate via ozonation under alkaline condition, J. Hazard. Mater. 243 (2012) 272–277. doi:10.1016/J.JHAZMAT.2012.10.029.

[129] A. González-Suárez, P. Guerra-Blanco, T. Poznyak, J. Morales, I. Chairez, J. Dueñas-Moreno, Experimental criteria of sequential continuous ozonation and semi-continuous biodegradation for the decomposition of 4-chlorophenol, J. Environ. Chem. Eng. 11 (2023) 110571. doi:10.1016/J.JECE.2023.110571.

[130] M. Quero-Pastor, C. Garrido-Perez, A. Acevedo Merino, J.M. Quiroga Alonso, Toxicity and Degradation Study of Clofibric Acid by Treatment with Ozone in Water, Ozone Sci. Eng. 38 (2016) 425–433. doi:10.1080/01919512.2016.1203288.

[131] P. Mukherjee, K. Sathiyan, T. Zidki, M.N. Nadagouda, V.K. Sharma, Can ultraviolet-assisted advanced reduction processes effectively destroy per- and polyfluoroalkyl

substances in real water matrices?, Curr. Opin. Chem. Eng. 42 (2023) 100971. doi:10.1016/J.COCHE.2023.100971.

[132] Y. Qu, C. Zhang, F. Li, J. Chen, Q. Zhou, Photo-reductive defluorination of perfluorooctanoic acid in water, Water Res. 44 (2010) 2939–2947. doi:10.1016/J.WATRES.2010.02.019.

[133] S. Yoon, D.S. Han, X. Liu, B. Batchelor, A. Abdel-Wahab, Degradation of 1,2-dichloroethane using advanced reduction processes, J. Environ. Chem. Eng. 2 (2014) 731–737. doi:10.1016/J.JECE.2013.11.013.

[134] B.P. Vellanki, B. Batchelor, Perchlorate reduction by the sulfite/ultraviolet light advanced reduction process, J. Hazard. Mater. 262 (2013) 348–356. doi:10.1016/J.JHAZMAT.2013.08.061.

[135] V.S.V. Botlaguduru, B. Batchelor, A. Abdel-Wahab, Application of UV–sulfite advanced reduction process to bromate removal, J. Water Process Eng. 5 (2015) 76–82. doi:10.1016/J.JWPE.2015.01.001.

[136] E. Banayan Esfahani, F. Asadi Zeidabadi, M. Jafarikojour, M. Mohseni, Photo-reductive decomposition of perfluorooctane sulfonate (PFOS) and its common alternatives by UV/VUV/sulfite process: Mechanism, kinetic modeling, and water matrix effects, Sci. Total Environ. 951 (2024) 175796. doi:10.1016/J.SCITOTENV.2024.175796.

[137] Z. Ren, U. Bergmann, T. Leiviskä, Reductive degradation of perfluorooctanoic acid in complex water matrices by using the UV/sulfite process, Water Res. 205 (2021) 117676. doi:10.1016/J.WATRES.2021.117676.

[138] M.G. Antoniou, G. Hey, S. Rodríguez Vega, A. Spiliotopoulou, J. Fick, M. Tysklind, J. la Cour Jansen, H.R. Andersen, Required ozone doses for removing pharmaceuticals from wastewater effluents, Sci. Total Environ. 456–457 (2013) 42–49. doi:10.1016/J.SCITOTENV.2013.03.072.

[139] K.M.S. Hansen, A. Spiliotopoulou, R.K. Chhetri, M. Escolà Casas, K. Bester, H.R. Andersen, Ozonation for source treatment of pharmaceuticals in hospital wastewater – Ozone lifetime and required ozone dose, Chem. Eng. J. 290 (2016) 507–514. doi:10.1016/J.CEJ.2016.01.027.

[140] F. Javier Benitez, J.L. Acero, F.J. Real, G. Roldán, Ozonation of pharmaceutical compounds: Rate constants and elimination in various water matrices, Chemosphere. 77 (2009) 53–59. doi:10.1016/J.CHEMOSPHERE.2009.05.035.

[141] Z. Liu, N. Wardenier, S. Hosseinzadeh, Y. Verheust, P.-J. De Buyck, M. Chys, A. Nikiforov, C. Leys, S. Van Hulle, Degradation of bisphenol A by combining ozone

with UV and H2O2 in aqueous solutions: mechanism and optimization, Clean Technol. Environ. Policy. 20 (2018) 2109–2118. doi:10.1007/s10098-018-1595-2.

[142] X. Yu, M. Kamali, P. Van Aken, L. Appels, B. Van der Bruggen, R. Dewil, Advanced oxidation of benzalkonium chloride in aqueous media under ozone and ozone/UV systems – Degradation kinetics and toxicity evaluation, Chem. Eng. J. 413 (2021) 127431. doi:10.1016/J.CEJ.2020.127431.

[143] M.A. Oturan, J.-J. Aaron, Advanced Oxidation Processes in Water/Wastewater Treatment: Principles and Applications. A Review, Crit. Rev. Environ. Sci. Technol. 44 (2014) 2577–2641. doi:10.1080/10643389.2013.829765.

[144] L. Huang, Z. Li, G. Wang, W. Zhao, Y. Xu, D. Wang, Experimental study on advanced treatment of landfill leachate by ultraviolet catalytic persulfate, Environ. Technol. Innov. 23 (2021) 101794. doi:10.1016/J.ETI.2021.101794.

[145] C. Chen, H. Feng, Y. Deng, Re-evaluation of sulfate radical based–advanced oxidation processes (SR-AOPs) for treatment of raw municipal landfill leachate, Water Res. 153 (2019) 100–107. doi:10.1016/J.WATRES.2019.01.013.

[146] S. Guo, Q. Wang, C. Luo, J. Yao, Z. Qiu, Q. Li, Hydroxyl radical-based and sulfate radical-based photocatalytic advanced oxidation processes for treatment of refractory organic matter in semi-aerobic aged refuse biofilter effluent arising from treating landfill leachate, Chemosphere. 243 (2020) 125390. doi:10.1016/J.CHEMOSPHERE.2019.125390.

[147] F. Jiang, B. Qiu, D. Sun, Advanced degradation of refractory pollutants in incineration leachate by UV/Peroxymonosulfate, Chem. Eng. J. 349 (2018) 338–346. doi:10.1016/J.CEJ.2018.05.062.

[148] G. Fang, W. Wu, C. Liu, D.D. Dionysiou, Y. Deng, D. Zhou, Activation of persulfate with vanadium species for PCBs degradation: A mechanistic study, Appl. Catal. B Environ. 202 (2017) 1–11. doi:10.1016/J.APCATB.2016.09.006.

[149] X. Zha, S. Wang, D. Zhang, Reductive Degradation of N-Nitrosodimethylamine via UV/Sulfite Advanced Reduction Process: Efficiency, Influencing Factors and Mechanism, Water. 15 (2023). doi:10.3390/w15203670.

[150] J. Zhang, J. Li, W. Tang, X. Liu, C. Yang, J. Ma, Highly efficient reduction of bromate by vacuum UV/sulfite system, Chemosphere. 349 (2024) 140875. doi:10.1016/J.CHEMOSPHERE.2023.140875.

[151] G. Boczkaj, A. Fernandes, M. Gągol, Studies on Treatment of Bitumen Effluents by Means of Advanced Oxidation Processes (AOPs) in Basic pH Conditions BT - Frontiers in Wastewater Treatment and Modelling, in: G. Mannina (Ed.), Springer

International Publishing, Cham, 2017: pp. 331–336.

[152] M.P. Rayaroth, G. Boczkaj, O. Aubry, U.K. Aravind, C.T. Aravindakumar, Advanced Oxidation Processes for Degradation of Water Pollutants - Ambivalent Impact of Carbonate Species: A Review, Water. 15 (2023). doi:10.3390/w15081615.

[153] C. Liang, Z.S. Wang, C.J. Bruell, Influence of pH on persulfate oxidation of TCE at ambient temperatures, Chemosphere. 66 (2007) 106–113. doi:10.1016/J.CHEMOSPHERE.2006.05.026.

[154] Y.-H. Guan, J. Ma, X.-C. Li, J.-Y. Fang, L.-W. Chen, Influence of pH on the Formation of Sulfate and Hydroxyl Radicals in the UV/Peroxymonosulfate System, Environ. Sci. Technol. 45 (2011) 9308–9314. doi:10.1021/es2017363.

[155] X. Liu, T. Zhang, Y. Zhou, L. Fang, Y. Shao, Degradation of atenolol by UV/peroxymonosulfate: Kinetics, effect of operational parameters and mechanism, Chemosphere. 93 (2013) 2717–2724. doi:10.1016/J.CHEMOSPHERE.2013.08.090.

[156] C. Qi, G. Yu, J. Huang, B. Wang, Y. Wang, S. Deng, Activation of persulfate by modified drinking water treatment residuals for sulfamethoxazole degradation, Chem. Eng. J. 353 (2018) 490–498. doi:10.1016/J.CEJ.2018.07.056.

[157] O.S. Furman, A.L. Teel, R.J. Watts, Mechanism of Base Activation of Persulfate, Environ. Sci. Technol. 44 (2010) 6423–6428. doi:10.1021/es1013714.

[158] A. Derbalah, H. Sakugawa, Sulfate Radical-Based Advanced Oxidation Technology to Remove Pesticides From Water A Review of the Most Recent Technologies, Int. J. Environ. Res. 18 (2024) 11. doi:10.1007/s41742-023-00561-7.

[159] V.S.V. Botlaguduru, B. Batchelor, A. Abdel-Wahab, Application of UV–sulfite advanced reduction process to bromate removal, J. Water Process Eng. 5 (2015) 76–82. doi:10.1016/J.JWPE.2015.01.001.

[160] E. Hayon, J. Wilf, Electronic spectra, photochemistry, and autoxidation mechanism of the sulfite-bisulfite-pyrosulfite systems. SO2-, SO3-, SO4-, and SO5-radicals, J. Am. Chem. Soc. 94 (1972) 47–57.

[161] Y. Gu, T. Liu, H. Wang, H. Han, W. Dong, Hydrated electron based decomposition of perfluorooctane sulfonate (PFOS) in the VUV/sulfite system, Sci. Total Environ. 607–608 (2017) 541–548. doi:10.1016/J.SCITOTENV.2017.06.197.

[162] X. Yu, D. Cabooter, R. Dewil, Efficiency and mechanism of diclofenac degradation by sulfite/UV advanced reduction processes (ARPs), Sci. Total Environ. 688 (2019) 65–74. doi:10.1016/J.SCITOTENV.2019.06.210.

[163] X. Liu, S. Yoon, B. Batchelor, A. Abdel-Wahab, Degradation of vinyl chloride (VC) by the sulfite/UV advanced reduction process (ARP): Effects of process variables and

a kinetic model, Sci. Total Environ. 454–455 (2013) 578–583. doi:10.1016/J.SCITOTENV.2013.03.060.

[164] R. Luo, C. Wang, Y. Yao, J. Qi, J. Li, Insights into the relationship of reactive oxygen species and anions in persulfate-based advanced oxidation processes for saline organic wastewater treatment, Environ. Sci. Water Res. Technol. 8 (2022) 465–483. doi:10.1039/D1EW00731A.

[165] H. Barndõk, D. Hermosilla, L. Cortijo, C. Negro, Á. Blanco, Assessing the Effect of Inorganic Anions on TiO2-Photocatalysis and Ozone Oxidation Treatment Efficiencies, 15 (2012) 125–132. doi:doi:10.1515/jaots-2012-0114.

[166] J. Wang, S. Wang, Effect of inorganic anions on the performance of advanced oxidation processes for degradation of organic contaminants, Chem. Eng. J. 411 (2021) 128392. doi:10.1016/J.CEJ.2020.128392.

[167] X. Wu, X. Gu, S. Lu, Z. Qiu, Q. Sui, X. Zang, Z. Miao, M. Xu, Strong enhancement of trichloroethylene degradation in ferrous ion activated persulfate system by promoting ferric and ferrous ion cycles with hydroxylamine, Sep. Purif. Technol. (2015). doi:10.1016/j.seppur.2015.04.031.

[168] Y. Yang, J. Jiang, X. Lu, J. Ma, Y. Liu, Production of Sulfate Radical and Hydroxyl Radical by Reaction of Ozone with Peroxymonosulfate: A Novel Advanced Oxidation Process, Environ. Sci. Technol. 49 (2015) 7330–7339. doi:10.1021/es506362e.

[169] Y. Zhao, Y. Zhao, Q. Li, R. Zhou, X. Chen, Effect of common inorganic ions on aniline degradation in groundwater by activated persulfate with ferrous iron, Water Supply. 16 (2015) 667–674. doi:10.2166/ws.2015.174.

[170] H. Wang, W. Guo, B. Liu, Q. Wu, H. Luo, Q. Zhao, Q. Si, F. Sseguya, N. Ren, Edge-nitrogenated biochar for efficient peroxydisulfate activation: An electron transfer mechanism, Water Res. 160 (2019) 405–414. doi:10.1016/J.WATRES.2019.05.059.

[171] W. Da Oh, Z. Dong, T.T. Lim, Generation of sulfate radical through heterogeneous catalysis for organic contaminants removal: Current development, challenges and prospects, Appl. Catal. B Environ. 194 (2016) 169–201. doi:10.1016/J.APCATB.2016.04.003.

[172] P. Neta, R.E. Huie, A.B. Ross, Rate Constants for Reactions of Inorganic Radicals in Aqueous Solution, J. Phys. Chem. Ref. Data. 17 (1988) 1027–1284. doi:10.1063/1.555808.

[173] R. Luo, C. Liu, J. Li, J. Wang, X. Hu, X. Sun, J. Shen, W. Han, L. Wang, Nanostructured CoP: An efficient catalyst for degradation of organic pollutants by activating

peroxymonosulfate, J. Hazard. Mater. 329 (2017) 92–101. doi:10.1016/J.JHAZMAT.2017.01.032.

[174] J. Ma, Y. Yang, X. Jiang, Z. Xie, X. Li, C. Chen, H. Chen, Impacts of inorganic anions and natural organic matter on thermally activated persulfate oxidation of BTEX in water, Chemosphere. (2018). doi:10.1016/j.chemosphere.2017.09.148.

[175] S. Giannakis, K.-Y.A. Lin, F. Ghanbari, A review of the recent advances on the treatment of industrial wastewaters by Sulfate Radical-based Advanced Oxidation Processes (SR-AOPs), Chem. Eng. J. 406 (2021) 127083. doi:https://doi.org/10.1016/j.cej.2020.127083.

[176] R. Vahidi-Kolur, A. Yazdanbakhsh, S.A. Hosseini, A. Sheikhmohammadi, Photoreduction of atrazine from aqueous solution using sulfite/iodide/UV process, degradation, kinetics and by-products pathway, Sci. Rep. 14 (2024) 5217. doi:10.1038/s41598-024-55585-6.

[177] M. Zhou, T. You, Z. Yan, X. Zhu, M. Pi, X. Zeng, S. Wang, Y. Jia, Iodide and sulfite synergistically accelerate the photo-reduction and recovery of As(V) and As(III) in sulfite/iodide/UV process: Efficiency and mechanism, Water Res. 252 (2024) 121210. doi:10.1016/J.WATRES.2024.121210.

[178] X. Liu, T. Zhang, Y. Shao, Aqueous Bromate Reduction by UV Activation of Sulfite, CLEAN – Soil, Air, Water. 42 (2014) 1370–1375. doi:https://doi.org/10.1002/clen.201300646.

[179] F. Totoni Mofrad, A. Jonidi Jafari, M. Kermani, M. Farzadkia, A. Esrafili, 4-Chloro-2-methylphenoxyacetic acid photo-reduction with sulfite excitation under UV irradiation: Kinetics, energy consumption, operational variables and toxicology with Daphnia magna, Desalin. Water Treat. 317 (2024) 100276. doi:10.1016/J.DWT.2024.100276.

[180] G. Iosilevskii, D. Weihs, Speed limits on swimming of fishes and cetaceans, J. R. Soc. Interface. 5 (2007) 329–338. doi:10.1098/rsif.2007.1073.

[181] P. Koukouvinis, C. Bruecker, M. Gavaises, Unveiling the physical mechanism behind pistol shrimp cavitation, Sci. Rep. 7 (2017) 13994. doi:10.1038/s41598-017-14312-0.

[182] S.N. Patek, R.L. Caldwell, Extreme impact and cavitation forces of a biological hammer: strike forces of the peacock mantis shrimp Odontodactylus scyllarus, J. Exp. Biol. 208 (2005) 3655–3664. doi:10.1242/jeb.01831.

[183] L.C. Burrill, The phenomenon of cavitation1, Int. Shipbuild. Prog. 2 (1955) 503–511. doi:10.3233/ISP-1955-21501.

[184] E.A. Weitendorf, On the history of propeller cavitation and cavitation tunnels, in: Fourth Int. Symp. Cavitation, 2001.

[185] J. Carpenter, M. Badve, S. Rajoriya, S. George, V.K. Saharan, A.B. Pandit, Hydrodynamic cavitation: an emerging technology for the intensification of various chemical and physical processes in a chemical process industry, Rev. Chem. Eng. 33 (2017) 433–468. doi:doi:10.1515/revce-2016-0032.

[186] M. Gągol, A. Przyjazny, G. Boczkaj, Wastewater treatment by means of advanced oxidation processes based on cavitation – A review, Chem. Eng. J. 338 (2018) 599–627. doi:10.1016/j.cej.2018.01.049.

[187] G. Mancuso, M. Langone, G. Andreottola, A critical review of the current technologies in wastewater treatment plants by using hydrodynamic cavitation process: principles and applications, J. Environ. Heal. Sci. Eng. 18 (2020) 311–333. doi:10.1007/s40201-020-00444-5.

[188] A. Guzmán-Barraza, J.G. Ortega-Mendoza, P. Zaca-Morán, N.I. Toto-Arellano, C. Toxqui-Quitl, J.P. Padilla-Martinez, Optical cavitation in non-absorbent solutions using a continuous-wave laser via optical fiber, Opt. Laser Technol. 154 (2022) 108330. doi:10.1016/J.OPTLASTEC.2022.108330.

[189] Y.T. Shah, A.B. Pandit, V.S. Moholkar, Sources and Types of Cavitation BT - Cavitation Reaction Engineering, in: Y.T. Shah, A.B. Pandit, V.S. Moholkar (Eds.), Springer US, Boston, MA, 1999: pp. 1–14. doi:10.1007/978-1-4615-4787-7_1.

[190] D. Peters, Sonolytic degradation of volatile pollutants in natural ground water: conclusions from a model study, Ultrason. Sonochem. 8 (2001) 221–226. doi:10.1016/S1350-4177(01)00080-3.

[191] M. Dular, T. Griessler-Bulc, I. Gutierrez-Aguirre, E. Heath, T. Kosjek, A. Krivograd Klemenčič, M. Oder, M. Petkovšek, N. Rački, M. Ravnikar, A. Šarc, B. Širok, M. Zupanc, M. Žitnik, B. Kompare, Use of hydrodynamic cavitation in (waste)water treatment, Ultrason. Sonochem. 29 (2016) 577–588. doi:10.1016/J.ULTSONCH.2015.10.010.

[192] A. Patil, S. Baral, P. Dhanke, Hydrodynamic cavitation for process intensification of biodiesel synthesis- a review, Curr. Res. Green Sustain. Chem. 4 (2021) 100144. doi:10.1016/J.CRGSC.2021.100144.

[193] M.A. Kelkar, P.R. Gogate, A.B. Pandit, Intensification of esterification of acids for synthesis of biodiesel using acoustic and hydrodynamic cavitation, Ultrason. Sonochem. 15 (2008) 188–194. doi:10.1016/J.ULTSONCH.2007.04.003.

[194] J. Zhang, X. Qi, T. Jin, D. Fang, Y. Li, Z. Zhou, H. Wu, J. Wang, D. Fang, Hydrodynamic

cavitation synthesis of water-soluble CdSe quantum dots: Effect of venturi tube parameters on size distribution and fluorescence properties, with application in Fe3+ detection, Anal. Chim. Acta. 1348 (2025) 343828. doi:10.1016/J.ACA.2025.343828.

[195] P.R. Gogate, A.M. Kabadi, A review of applications of cavitation in biochemical engineering/biotechnology, Biochem. Eng. J. 44 (2009) 60–72. doi:10.1016/j.bej.2008.10.006.

[196] Z. Izadifar, P. Babyn, D. Chapman, Ultrasound Cavitation/Microbubble Detection and Medical Applications, J. Med. Biol. Eng. 39 (2019) 259–276. doi:10.1007/s40846-018-0391-0.

[197] C. C. Coussios, F. C. H., T.H. G., R.A. and Roy, Role of acoustic cavitation in the delivery and monitoring of cancer treatment by high-intensity focused ultrasound (HIFU), Int. J. Hyperth. 23 (2007) 105–120. doi:10.1080/02656730701194131.

[198] M. Sivakumar, S.Y. Tang, K.W. Tan, Cavitation technology – A greener processing technique for the generation of pharmaceutical nanoemulsions, Ultrason. Sonochem. 21 (2014) 2069–2083. doi:10.1016/J.ULTSONCH.2014.03.025.

[199] S.S. Arya, S. O., S. Sachin K., S. P. L, W. A., H. Ruly, J.C. Dos and Santos, Novel, Nonthermal, Energy Efficient, Industrially Scalable Hydrodynamic Cavitation – Applications in Food Processing, Food Rev. Int. 36 (2020) 668–691. doi:10.1080/87559129.2019.1669163.

[200] Z. Askarniya, X. Sun, Z. Wang, G. Boczkaj, Cavitation-based technologies for pretreatment and processing of food wastes: Major applications and mechanisms – A review, Chem. Eng. J. 454 (2023) 140388. doi:10.1016/J.CEJ.2022.140388.

[201] B. Avvaru, N. Venkateswaran, P. Uppara, S.B. Iyengar, S.S. Katti, Current knowledge and potential applications of cavitation technologies for the petroleum industry, Ultrason. Sonochem. 42 (2018) 493–507. doi:10.1016/J.ULTSONCH.2017.12.010.

[202] J.M. Greenly, J.W. Tester, Ultrasonic cavitation for disruption of microalgae, Bioresour. Technol. 184 (2015) 276–279. doi:10.1016/J.BIORTECH.2014.11.036.

[203] S.S. Save, A.B. Pandit, J.B. Joshi, Microbial cell disruption: role of cavitation, Chem. Eng. J. Biochem. Eng. J. 55 (1994) B67–B72. doi:10.1016/0923-0467(94)06062-2.

[204] J.G. Dalfré Filho, M.P. Assis, A.I.B. Genovez, Bacterial inactivation in artificially and naturally contaminated water using a cavitating jet apparatus, J. Hydro-Environment Res. 9 (2015) 259–267. doi:10.1016/J.JHER.2015.03.001.

[205] P. Li, Y. Song, S. Yu, Removal of Microcystis aeruginosa using hydrodynamic cavitation: Performance and mechanisms, Water Res. 62 (2014) 241–248.

doi:10.1016/J.WATRES.2014.05.052.

[206] I. Hua, R.H. Hochemer, M.R. Hoffmann, Sonochemical degradation of p-nitrophenol in a parallel-plate near-field acoustical processor, Environ. Sci. Technol. 29 (1995) 2790–2796.

[207] A. Bhatnagar, H.M. Cheung, Sonochemical Destruction of Chlorinated C1 and C2 Volatile Organic Compounds in Dilute Aqueous Solution, Environ. Sci. Technol. 28 (1994) 1481–1486. doi:10.1021/es00057a016.

[208] H.M. Hung, M.R. Hoffmann, Kinetics and Mechanism of the Sonolytic Degradation of Chlorinated Hydrocarbons: Frequency Effects, J. Phys. Chem. A. (1999). doi:10.1021/jp9845930.

[209] V. Desai, M.A. Shenoy, P.R. Gogate, Degradation of polypropylene using ultrasound-induced acoustic cavitation, Chem. Eng. J. 140 (2008) 483–487. doi:10.1016/J.CEJ.2007.11.030.

[210] M. Sivakumar, A.B. Pandit, Ultrasound enhanced degradation of Rhodamine B: Optimization with power density, in: Ultrason. Sonochem., 2001. doi:10.1016/S1350-4177(01)00082-7.

[211] J. Dewulf, H. Van Langenhove, A. De Visscher, S. Sabbe, Ultrasonic degradation of trichloroethylene and chlorobenzene at micromolar concentrations: kinetics and modelling, Ultrason. Sonochem. 8 (2001) 143–150. doi:10.1016/S1350-4177(00)00031-6.

[212] Y. Huang, Y. Wu, W. Huang, F. Yang, X.E. Ren, Degradation of chitosan by hydrodynamic cavitation, Polym. Degrad. Stab. 98 (2013) 37–43. doi:10.1016/J.POLYMDEGRADSTAB.2012.11.001.

[213] X. Wang, Y. Zhang, Degradation of alachlor in aqueous solution by using hydrodynamic cavitation, J. Hazard. Mater. 161 (2009) 202–207. doi:10.1016/J.JHAZMAT.2008.03.073.

[214] M. Zupanc, T. Kosjek, M. Petkovšek, M. Dular, B. Kompare, B. Širok, M. Stražar, E. Heath, Shear-induced hydrodynamic cavitation as a tool for pharmaceutical micropollutants removal from urban wastewater, Ultrason. Sonochem. 21 (2014) 1213–1221. doi:10.1016/j.ultsonch.2013.10.025.

[215] P.G. Suryawanshi, V.M. Bhandari, L.G. Sorokhaibam, J.P. Ruparelia, V. V Ranade, Solvent degradation studies using hydrodynamic cavitation, Environ. Prog. Sustain. Energy. 37 (2018) 295–304. doi:https://doi.org/10.1002/ep.12674.

[216] Z.-L. Wu, B. Ondruschka, P. Bräutigam, Degradation of Chlorocarbons Driven by Hydrodynamic Cavitation, Chem. Eng. Technol. 30 (2007) 642–648.

doi:https://doi.org/10.1002/ceat.200600288.

[217] B. Wang, T. Zeng, J. Shang, J. Tao, Y. Liu, T. Yang, H. Ren, G. Hu, Bubble dynamics model and its revelation of ultrasonic cavitation behavior in advanced oxidation processes: A review, J. Water Process Eng. 63 (2024) 105470. doi:10.1016/J.JWPE.2024.105470.

[218] Y.G. Adewuyi, Sonochemistry: Environmental Science and Engineering Applications, Ind. Eng. Chem. Res. 40 (2001) 4681–4715. doi:10.1021/ie010096l.

[219] X. Lu, W. Qiu, J. Peng, H. Xu, D. Wang, Y. Cao, W. Zhang, J. Ma, A Review on Additives-assisted Ultrasound for Organic Pollutants Degradation, J. Hazard. Mater. 403 (2021) 123915. doi:10.1016/J.JHAZMAT.2020.123915.

[220] L. Reggiane de Carvalho Costa, K. Guerra Pacheco Nunes, L. Amaral Féris, Ultrasound as an Advanced Oxidative Process: A Review on Treating Pharmaceutical Compounds, Chem. Eng. Technol. 44 (2021) 1744–1758. doi:https://doi.org/10.1002/ceat.202100090.

[221] D. Meroni, C.L. Bianchi, Ultrasound waves at the service of photocatalysis: From sonochemical synthesis to ultrasound-assisted and piezo-enhanced photocatalysis, Curr. Opin. Green Sustain. Chem. 36 (2022) 100639. doi:10.1016/J.COGSC.2022.100639.

[222] S.K. Gujar, P.R. Gogate, P. Kanthale, R. Pandey, S. Thakre, M. Agrawal, Combined oxidation processes based on ultrasound, hydrodynamic cavitation and chemical oxidants for treatment of real industrial wastewater from cellulosic fiber manufacturing sector, Sep. Purif. Technol. 257 (2021) 117888. doi:10.1016/J.SEPPUR.2020.117888.

[223] A. Abdelhay, M.A. Allawzi, B. Al-Khateeb, A. Albsoul, A.A. Othman, Optimization of the Performance of Ultrasonic Irradiation for the Treatment of Textile Wastewater: Synergetic Effect of US and Advanced Oxidation, Water, Air, Soil Pollut. 233 (2022) 210. doi:10.1007/s11270-022-05673-y.

[224] S. Chandak, P.K. Ghosh, P.R. Gogate, Treatment of real pharmaceutical wastewater using different processes based on ultrasound in combination with oxidants, Process Saf. Environ. Prot. 137 (2020) 149–157. doi:10.1016/j.psep.2020.02.025.

[225] M. Gągol, A. Przyjazny, G. Boczkaj, Effective method of treatment of industrial effluents under basic pH conditions using acoustic cavitation – A comprehensive comparison with hydrodynamic cavitation processes, Chem. Eng. Process. - Process Intensif. 128 (2018) 103–113. doi:10.1016/j.cep.2018.04.010.

[226] A. Dey, P.R. Gogate, Comparative study of different ultrasound based hybrid

oxidation approaches for treatment of real effluent from coke oven plant, J. Environ. Manage. 352 (2024) 120095. doi:10.1016/J.JENVMAN.2024.120095.

[227] N.J. Lakshmi, A.M. Iyer, P.R. Gogate, Treatment of wastewater containing ciprofloxacin using the hybrid treatment approach based on acoustic cavitation, Can. J. Chem. Eng. 102 (2024) 2403–2417. doi:https://doi.org/10.1002/cjce.25212.

[228] P.R. Gogate, A.B. Pandit, Engineering design methods for cavitation reactors II: Hydrodynamic cavitation, AIChE J. 46 (2000) 1641–1649. doi:10.1002/aic.690460815.

[229] B. Wang, Y. Liu, H. Zhang, W. Shi, M. Xiong, C. Gao, M. Cui, Hydrodynamic cavitation and its application in water treatment combined with ozonation: A review, J. Ind. Eng. Chem. 114 (2022) 33–51. doi:10.1016/J.JIEC.2022.07.031.

[230] P. Kanthale, R. Pandey, D. Thakur, S.K. Gujar, P.R. Gogate, S. Thakre, C.K. Dutta, Application of combined hydrodynamic cavitation and Fenton reagent for COD reduction of cellulosic fiber industry effluents, J. Water Process Eng. 56 (2023) 104500. doi:10.1016/J.JWPE.2023.104500.

[231] M.S. Kumar, S.H. Sonawane, B.A. Bhanvase, B. Bethi, Treatment of ternary dye wastewater by hydrodynamic cavitation combined with other advanced oxidation processes (AOP's), J. Water Process Eng. 23 (2018) 250–256. doi:10.1016/J.JWPE.2018.04.004.

[232] A.P. Bhat, P.R. Gogate, Cavitation-based pre-treatment of wastewater and waste sludge for improvement in the performance of biological processes: A review, J. Environ. Chem. Eng. 9 (2021) 104743. doi:10.1016/J.JECE.2020.104743.

[233] X. Sun, H. Xu, X. Xuan, S. Manickam, G. Boczkaj, B. Wang, Assessing the industrialization progress of hydrodynamic cavitation process intensification technology: a review, Curr. Opin. Chem. Eng. 45 (2024) 101037. doi:10.1016/J.COCHE.2024.101037.

[234] F. Hong, H. Tian, X. Yuan, S. Liu, Q. Peng, Y. Shi, L. Jin, L. Ye, J. Jia, D. Ying, S.R. Thomas, Y. Huang, CFD-assisted modeling of the hydrodynamic cavitation reactors for wastewater treatment — A review, J. Environ. Manage. 321 (2022) 115982. doi:10.1016/J.JENVMAN.2022.115982.

[235] X. Sun, X. Xuan, Y. Song, X. Jia, L. Ji, S. Zhao, J. Yong Yoon, S. Chen, J. Liu, G. Wang, Experimental and numerical studies on the cavitation in an advanced rotational hydrodynamic cavitation reactor for water treatment, Ultrason. Sonochem. 70 (2021) 105311. doi:10.1016/j.ultsonch.2020.105311.

[236] E. Cako, K.D. Gunasekaran, R.D. Cheshmeh Soltani, G. Boczkaj, Ultrafast

degradation of brilliant cresyl blue under hydrodynamic cavitation based advanced oxidation processes (AOPs), Water Resour. Ind. (2020). doi:10.1016/j.wri.2020.100134.

[237] P. Braeutigam, Z.-L. Wu, A. Stark, B. Ondruschka, Degradation of BTEX in Aqueous Solution by Hydrodynamic Cavitation, Chem. Eng. Technol. 32 (2009) 745–753. doi:10.1002/ceat.200800626.

[238] G. V. Buxton, C.L. Greenstock, W.P. Helman, A.B. Ross, Critical Review of rate constants for reactions of hydrated electrons, hydrogen atoms and hydroxyl radicals (·OH/·O ⁻ in Aqueous Solution, J. Phys. Chem. Ref. Data. 17 (1988) 513–886. doi:10.1063/1.555805.

[239] P.S. Rao, E. Hayon, Redox potentials of free radicals. IV. Superoxide and hydroperoxy radicals . O2- and . HO2, J. Phys. Chem. 79 (1975) 397–402. doi:10.1021/j100571a021.

[240] Y. Li, S. Ma, S. Xu, H. Fu, Z. Li, K. Li, K. Sheng, J. Du, X. Lu, X. Li, S. Liu, Novel magnetic biochar as an activator for peroxymonosulfate to degrade bisphenol A: Emphasizing the synergistic effect between graphitized structure and CoFe2O4, Chem. Eng. J. (2020) 124094. doi:10.1016/J.CEJ.2020.124094.

[241] F. Ghanbari, M. Moradi, Application of peroxymonosulfate and its activation methods for degradation of environmental organic pollutants: Review, Chem. Eng. J. 310 (2017) 41–62. doi:10.1016/J.CEJ.2016.10.064.

[242] D.T. Oyekunle, X. Zhou, A. Shahzad, Z. Chen, Review on carbonaceous materials as persulfate activators: structure–performance relationship, mechanism and future perspectives on water treatment, J. Mater. Chem. A. 9 (2021) 8012–8050. doi:10.1039/D1TA00033K.

[243] J. Fan, H. Qin, S. Jiang, Mn-doped g-C3N4 composite to activate peroxymonosulfate for acetaminophen degradation: The role of superoxide anion and singlet oxygen, Chem. Eng. J. 359 (2019) 723–732. doi:10.1016/J.CEJ.2018.11.165.

[244] Y. Wang, D. Cao, M. Liu, X. Zhao, Insights into heterogeneous catalytic activation of peroxymonosulfate by Pd/g-C3N4: The role of superoxide radical and singlet oxygen, Catal. Commun. 102 (2017) 85–88. doi:10.1016/J.CATCOM.2017.08.016.

[245] C.G. Joseph, Y.Y. Farm, Y.H. Taufiq-Yap, C.K. Pang, J.L.H. Nga, G. Li Puma, Ozonation treatment processes for the remediation of detergent wastewater: A comprehensive review, J. Environ. Chem. Eng. 9 (2021) 106099. doi:10.1016/J.JECE.2021.106099.

[246] Y. Nosaka, A.Y. Nosaka, Generation and Detection of Reactive Oxygen Species in

Photocatalysis, Chem. Rev. 117 (2017) 11302–11336. doi:10.1021/acs.chemrev.7b00161.

[247] H.E. Gsponer, C.M. Previtali, N.A. García, Kinetics of the photosensitized oxidation of polychlorophenols in alkaline aqueous solution, Toxicol. Environ. Chem. 16 (1987) 23–37. doi:10.1080/02772248709357245.

[248] E. Cako, Z. Wang, R. Castro-Muñoz, M.P. Rayaroth, G. Boczkaj, Cavitation based cleaner technologies for biodiesel production and processing of hydrocarbon streams: A perspective on key fundamentals, missing process data and economic feasibility – A review, Ultrason. Sonochem. 88 (2022) 106081. doi:https://doi.org/10.1016/j.ultsonch.2022.106081.

[249] Towarowa Giełda Energii. Wholesale prices of electricity in Poland from 2018 to July 2025. [cited 08, 2026]; Available from https://www.statista.com/statistics/1066654/poland-wholesale-electricity-prices/.

[250] L. Onga, N. Dulova, E. Kattel-Salusoo, Advanced Oxidation of Dexamethasone by Activated Peroxo Compounds in Water Matrices: A Comparative Study, Water. 17 (2025) 2303. doi:10.3390/w17152303.

[251] S.S. Sable, P.P. Ghute, P. Álvarez, F.J. Beltrán, F. Medina, S. Contreras, FeOOH and derived phases: Efficient heterogeneous catalysts for clofibric acid degradation by advanced oxidation processes (AOPs), Catal. Today. 240 (2015) 46–54. doi:10.1016/J.CATTOD.2014.03.050.

[252] Q. Sun, Y. Wang, L. Li, J. Bing, Y. Wang, H. Yan, Mechanism for enhanced degradation of clofibric acid in aqueous by catalytic ozonation over MnOx/SBA-15, J. Hazard. Mater. 286 (2015) 276–284. doi:10.1016/J.JHAZMAT.2014.12.050.

[253] X. Lu, Y. Shao, N. Gao, J. Chen, H. Deng, W. Chu, N. An, F. Peng, Investigation of clofibric acid removal by UV/persulfate and UV/chlorine processes: Kinetics and formation of disinfection byproducts during subsequent chlor(am)ination, Chem. Eng. J. 331 (2018) 364–371. doi:10.1016/J.CEJ.2017.08.117.

[254] H. Eibenberger, S. Steenken, P. O'Neill, D. Schulte-Frohlinde, Pulse radiolysis and electron spin resonance studies concerning the reaction of SO4. cntdot.-with alcohols and ethers in aqueous solution, J. Phys. Chem. 82 (1978) 749–750. doi: 10.1021/j100495a028.

[255] S. Wu, L. Shen, Y. Lin, K. Yin, C. Yang, Sulfite-based advanced oxidation and reduction processes for water treatment, Chem. Eng. J. 414 (2021) 128872. doi:10.1016/J.CEJ.2021.128872.